Evaluation of Yeast Display Fab Libraries Derived from Tumor Infiltrating B Cells

TECHNISCHE UNIVERSITÄT DARMSTADT

vom Fachbereich Chemie

der Technischen Universität Darmstadt

zur Erlangung des Grades

Doctor rerum naturalium

(Dr. rer. nat.)

Dissertation

von Ashi Sapir M. Sc.

Erstgutachter: Prof. Dr. Harald Kolmar

Zweitgutahter: Prof. Dr. Felix Hausch

Darmstadt 2019

Tag der Einreichung: März 2019

Tag der mündlichen Prüfung: Mai 2019

Die vorliegende Arbeit wurde unter der Leitung von Herrn Prof. Dr. Harald Kolmar am Clemens-Schöpf-Institut für Organische Chemie und Biochemie der Technischen Universität Darmstadt sowie bei Merck KGaA in Darmstadt von Januar 2016 bis Januar 2019 angefertigt.

Table of contents

1. Abstract

1.1. Zusammenfassung

Seit ihrer erstmaligen klinischen Zulassung für die Krebsbehandlung Ende der 1990er gelten monoklonale Antikörper (mAbs) als einer der erfolgreichsten und vielversprechendsten Behandlungsansätze in der Onkologie. mAbs, die gezielt auf tumorassoziierte Antigene (TAA) einwirken, und seit neuerem mAbs, welche die durch Checkpoints vermittelte Hemmung der T-Zell-Tumorantwort verhindern, haben sich als hinsichtlich der Tumorremission bei Krebspatienten wirksam erwiesen (Carter and Lazar, 2018). Dennoch gibt es auch in der Entwicklung von mAbs für die Krebsbehandlung Grenzen und viele mAbs kommen aufgrund der niedrigen Zulassungsrate nicht in der klinischen Praxis zur Anwendung (Nelson and Reichert, 2009; Workman et al., 2017). Nach mehr als 20 Jahren der Entwicklung gibt es noch immer relativ wenige tumorassoziierte Antigene (TAA) als Targets für die mAbs-Therapie, die für die klinische Therapie zugelassen sind. Daher müssen neue Ansätze und Strategien im Prozess der Selektion von mAbs gefunden werden, die zur Ermittlung neuer TAA bzw. besserer, neuartiger mAbs für die Krebstherapie führen können (Sánchez-Martín et al., 2015).

Zahlreiche Publikationen haben in den letzten Jahren gezeigt, dass das Vorliegen von tumorinfiltrierenden B-Zellen (TIL-B) in den Tumoren eines Patienten mit einem positiven Prognoseeffekt verbunden ist (Wouters and Nelson, 2018). Mehrere Veröffentlichungen deuten zudem darauf hin, dass TIL-B aus Patientengewebe eine reichhaltige Quelle für tumorbindende Antikörper sein können (Pavoni et al., 2007; Novinger, Ashikaga and Krag, 2015).

In der hier vorgestellten Studie wurden – soweit uns bekannt erstmalig – TIL-B-Antikörper-Repertoires von 8 Patienten mit kolorektalem Karzinom genutzt, um 2 Hefe-Fab-Oberflächendisplay-Bibliotheken (κ und λ) zu erstellen. Die Evaluierung der Bibliotheken anhand von Durchflusszytometrie-Screening im Hinblick auf eine Vielzahl von TAA- und Immun-Checkpoint-Molekülen führte zur Ermittlung mehrerer potenzieller Bindungspartner für diese Screeningtargets. Danach erfolgte anhand von Durchflusszytometrie eine Sortierung im Hinblick auf 4 Targets: CEACAM5, LRP6, LAG3 und OX40L. Dies erlaubte die Selektion spezifischer, aber niedrig-affiner humaner Antikörper für diese Targets. Die weitere Evaluierung der Bibliotheken umfasste einen neuartigen Ansatz: Dabei erfolgte ein phänotypisches Screening mithilfe einer Hefedisplay-Biopanning-Plattform gegen entsprechende aus kolorektalen Karzinomen abgeleitete Zelllinien (HCT 116, HT-29 und SW620). Eine hohe Anreicherung der Hefe-Fab-Oberflächendisplay-Bindungspartner an den aus kolorektalen Karzinomen abgeleiteten Zellen ließ sich innerhalb von nur 3 Runden Biopanning beobachten. Mithilfe des Biopanning-Verfahrens isolierte Antikörper (HCT 116, HT-29) zeigten eine selektive Bindung an ähnlichen Epitopen wie sie auf der Zelloberfläche von HCT116- und

HT-29-Zellen vorhanden sind, da diese Antikörper dieselbe schwere Kette aufwiesen, obwohl sie aus zwei unterschiedlichen Zelllinien selektiert wurden. Die unterschiedlichen leichten Ketten der isolierten Antikörper hatten nachweislich Einfluss auf ihre Affinität. Die weitere Charakterisierung eines der isolierten Antikörper (TILB-HCT116-B24) ergab einen EC50-Wert von 569 nM bei Bindung an HCT116. Ein Zellbindungsassay anhand von Fluoreszenzmikroskopie mit diesem Antikörper an HCT 116-Zellen und normalen Fibroblastenzellen aus dem Colon (CCD-18Co) belegte die spezifische Bindung an HCT 116-Zellen.

Soweit uns bekannt ist, ist dies die erste Studie, in der Next-Generation Sequencing (NGS) als Hochdurchsatz-Sequenzierung für die aus den TIL-B-Zellen der einzelnen Patienten abgeleiteten Klone im Hinblick auf die Fab-Hefeoberflächendisplay-Bibliotheken und die Klone aus der Biopanning-Anreicherung eingesetzt wurde. Diese NGS-Daten, die auf der klonalen Frequenzanalyse der schweren und leichten Kettensequenzen jedes Patienten basieren, können einen Hinweis auf die klonale Expansion von TIL-B geben, die im Tumor der Patienten auftritt. Zudem führte die Kombination von Hochdurchsatz-Sequenzierung und Hefe-Display-Biopanning-Screening zu einer ähnlich selektiven Anreicherung, wie wenn Biopanning der Hefe-Bibliothek gegen die aus kolorektalen Karzinomen abgeleiteten Zelllinien HCT 116 und HT-29 erfolgte. Hierbei fiel das Biopanning-Ergebnis gegen die aus kolorektalen Karzinomen abgeleitete SW620-Zelllinie anders aus: Es ergab andere Klone, was auf eine hochspezifische Selektion mithilfe des Biopanning-Prozesses schließen lässt.

So unterstützt die vorgestellte Studie die Hypothese, dass aus TIL-B abgeleitete Bibliotheken ein Antikörper-Repertoire enthalten, das vorzugsweise an Krebszellen bindet. Die Hefeoberflächendisplay-Biopanning-Technologie in Kombination mit Hochdurchsatz-Sequenzierung kann ein wirksames Hilfsmittel für die Ermittlung von Tumorantikörper-Therapeutika und möglicherweise für die Identifizierung neuartiger Tumor-Antigene darstellen.

1.2. Abstract

Since their first clinical approval for cancer therapy in the late−1990s, monoclonal antibodies (mAbs) are considered as one of the most successful and promising therapeutic approaches in oncology. mAbs, which target tumor-associated antigens (TAA) and more recently mAbs which prevent checkpoint-mediated inhibition of T cell responses against the tumor, proved to be affective for tumor remission in cancer patients (Carter & Lazar, 2018). However, the development of mAbs for cancer therapy still has it's limitations and many mAbs do not arrive to the clinic due to low approval rate (A. L. Nelson & Reichert, 2009; Workman, Draetta, Schellens, & Bernards, 2017). Over 20 years of development there are still relatively few tumor-associated antigens (TAA) for mAbs targeting in oncology that are approved for clinical therapy. This raises the need for the development of new approaches and strategies in the mAbs selection process that may result in finding new TAA and/or better novel mAbs for cancer therapy (Sánchez-Martín et al., 2015).

In recent years, it was shown in many reports that the presence of infiltrating B cells (TIL-B) in patient's tumors is associated with positive prognostic effect (Wouters & Nelson, 2018). Moreover, several reports indicate that TIL-B from patient's tissue can be a rich source of tumor-binding antibodies (Novinger, Ashikaga, & Krag, 2015; Pavoni et al., 2007)

In the presented study, to our knowledge for the first time, TIL-B antibody repertoires from 8 colon cancer patients were utilized to construct 2 yeast Fab surface display libraries (κ and λ). Evaluation of the libraries by flow cytometry screening to a variety of TAA and immune checkpoint molecules, revealed potential binders to these screened targets. Subsequent flow cytometry sorting to 4 targets: CEACAM5, LRP6, LAG3 and OX40L resulted in the selection of specific but low-affinity human antibodies to the targets. Further evaluation of the libraries involved a novel approach using phenotypic screening by a yeast display biopanning platform against corresponded colon cancer derived cell lines (HCT 116, HT-29 and SW620). High enrichment of yeast Fab surface display binders to the colon cancer derived cells was observed within only 3 rounds of biopanning. Isolated antibodies from the biopanning approach (HCT 116, HT-29) demonstrated a selective binding to similar epitopes present on the cell surface of HCT116 and HT-29 cells, as these antibodies were found to have the same heavy chain though they were selected on two different cell lines. The different light chains in the isolated antibodies were found to influence the antibodies affinity. Further characterization of one of the isolated antibodies (TILB-HCT116-B24) indicated an EC50 value of 569nM binding to HCT116. A cellular binding assay using fluorescence microscopy with this antibody to HCT 116 cells and normal colon fibroblast cells (CCD-18Co) showed specific binding to HCT 116 cells.

To our knowledge, this is the first study to use next-generation sequencing (NGS) to provide a high-throughput sequencing for the clones derived from each patients' TIL-B cells, for the Fab yeast surface display libraries and for the biopanning enrichment clones. This NGS data, based on clonal frequency analysis of

each patient's heavy and light chain sequences, may indicate the clonal expansion of the TIL-B that occurs in the patients' tumor. Moreover, combining high-throughput sequencing and yeast display biopanning screening, demonstrated similar selective enrichment occurred when biopanning the yeast library against colorectal derived cell lines HCT116 and HT-29. This was different from the biopanning against the metastatic colorectal derived SW620 cell line, which gave different clones, indicating high specific selection through the biopanning process.

Hence, the presented study supports the hypothesis that TIL-B derived libraries contain a repertoire of antibodies that can bind preferentially to cancer cells. The yeast surface display biopanning technology combined with high-throughput sequencing, could be effective tools for the discovery of antitumor antibody therapeutics and possibly for identifying novel tumor antigens.

2. Introduction

2.1. Role of B cells and antibodies in the immune system

The immune system is the host defense system of the human body which has a dual function: the first is distinguishing the cells, tissues and organs that are a part of the host body from foreign, “nonself,” antigens that might be present. The second is to attack and eliminate those “nonself” invaders, such as dangerous bacteria or viruses (Beck & Habicht, 1996). In addition, the immune system can recognize, and usually eliminate, “altered self” cells or tissues that have been changed by injury or mutation and even to eliminate an initial "tumor" from growing into a clinical cancer by a mechanism determined as cancer immunosurveillance (Dunn, Bruce, Ikeda, Old, & Schreiber, 2002).

The immune system can be divided into two arms of defense: the innate and the adaptive immune systems. The innate immune system includes the natural killer cells, mast cells, eosinophils, basophils that are leukocytes and the macrophages, neutrophils, and dendritic cells that are phagocytic cells. The innate immune system is the first line of defense against many common microorganisms, however, it is based on invariant receptors recognizing common features of pathogens and can be evaded or overcome by many pathogens. In addition, this early innate response does not lead to immunological memory. In contrast, the adaptive immune system has the ability to recognize pathogens specifically and to provide enhanced protection against reinfection, based on clonal selection of T-lymphocytes and B-lymphocytes which bear antigen-specific receptors. Each T and B lymphocyte carries cell-surface receptors of a single specificity, generated by random recombination of variable receptor gene segments and the pairing of different variable chains. The main distinctions between B- and T-lymphocyte receptors are that the immunoglobulin that serves as the T-cell antigen receptor has a single antigen-recognition site and is always a cell-surface molecule. In this case cells that differentiated to effector cells are able to destroy infected cells or activate other cells of the immune system. B-cell antigen receptors have two identical antigen-recognition sites and can be secreted when cells differentiate to effector cells, called plasma cells. The secreted B-cell antigen receptor is then called an antibody (Janeway, 2001).

B cells are generated and start to develop in the bone marrow where they differentiate from primitive stem cells to progenitor B cells. Then, they proceed through stages called V(D)J somatic recombination, which is marked by the sequential rearrangement of the heavy and light immunoglobulin gene segments to generate a diverse repertoire of antigen receptors. In the end of this process, once a light chain gene is assembled and a complete IgM isotype molecule is expressed on the cell surface, the cell is defined as an immature B cell. Immature B cells then undergo selection for self-tolerance and subsequently for the ability to survive in the peripheral lymphoid tissues. B cells that survive in the periphery undergo

further differentiation to become mature B cells that express IgD isotype in addition to IgM. These cells, also called naïve B cells until they encounter their specific antigen, recirculate through peripheral lymphoid tissues. In the germinal centers sites within of the lymph nodes or spleen the mature B cell activation occurs, by introduction of the antigen to the B cell receptor. This happens mostly by interaction with helper T cells and follicular dendritic cells (FDCs) cells. In the process of maturation, the B cells start to proliferate and coding sequences for the variable regions are modified yet again by somatic hypermutation aimed at achieving higher affinity. At this time also a class switch recombination to heavy chains constant domain isotypes, IgG, IgA or IgE is carried out by the enzyme activation-induced cytidine deaminase (AID) (Muramatsu et al., 2000). Finally, differentiation to Plasma B antibody secreting cells and to memory B cells occur. high-affinity B cells in the germinal center are selected on the basis of antigen engagement initiate the plasma cells differentiation, while subsequent helper T cells interaction completes their differentiation, In contrast, memory B cells preferentially emerge from a low affinity compartment (Suan, Sundling, & Brink, 2017)

2.1.1. Antibody structure and function

Antibodies are the secreted form of the B-cell receptor. An antibody is identical to the B-cell receptor of the cell that secretes it, except for a small portion of the C-terminus of the heavy-chain constant region. In the case of the B-cell receptor the C-terminus is a hydrophobic membrane-anchoring sequence, and in the case of antibody it is a hydrophilic sequence that allows secretion. The IgG is the class of immunoglobulin characterized by γ heavy chains and it is the most abundant class of immunoglobulin found in the plasma (Janeway, 2001). An antibody is a Y-shaped protein with a molecular mass of 150 kDa that consists of four polypeptide chains, two identical heavy chains (HC) with a molecular weight of 50 kDa each and two identical light chains (LC) of 25 kDa each (**Figure 1**). The heavy chains are linked via disulfide bonds and each side light chain is also linked via a disulfide bond with its correspond heavy chain. The polypeptide chains can be divided into functional domains. The N-terminus of the heavy chain consists of a variable domain (VH) contain three hypervariable regions, known as the complementary determining regions (CDR1, CDR2 and CDR3), which are flanked by four more conserved regions, known as framework regions (FR1,FR2,FR3 and FR4). The VH is linked to three constant domains (CH1, CH2 and CH2) in the C-terminus while CH1 and CH2 are linked to each other via a flexible hinge region. The light chain consists of a variable domain (VL) with same arrangement of CDRs and frameworks as the VH while here there is only one constant domain (CL) that can be discriminated by two different classes, lambda (λ) and kappa (κ). The two classes of CL have corresponding distinct gene loci and differentiation occurs at early stages in the bone marrow. This is in comparison to the IgG heavy chain's constant domain (γ) which, as mentioned, differentiate in the germinal center during B cell activation. During V(D)J somatic recombination the

diversity of variable regions encoded by combinatory design of the genetic locus of variable heavy and light chain consisting of germline encoded V for variable, D for diversity (VH only) and J for joining gene segments.

Digestion with the cysteine protease Papain (papaya proteinase I) cleaves an IgG molecule at the N-terminal side of the disulfide bonds in the hinge region and creates three fragments; two identical Fab fragments (Fragment antigen binding) and the Fragment crystallizable (Fc) (Fig 1B). These fragments can be determined by their functionality: each Fab fragment forms the antigen binding site and the FC portion has the ability to activate a number of immunological pathways. These include complement-dependent cytotoxicity (CDC) and antibody-dependent cellular cytotoxicity (ADCC). The Fc fragment contains the epitopes for the Fcγ receptor (FcγR) which is a protein found on the surface of immune cells that binds the Fc domain, and by that facilitates the cytotoxic or phagocytic activity of these cells.

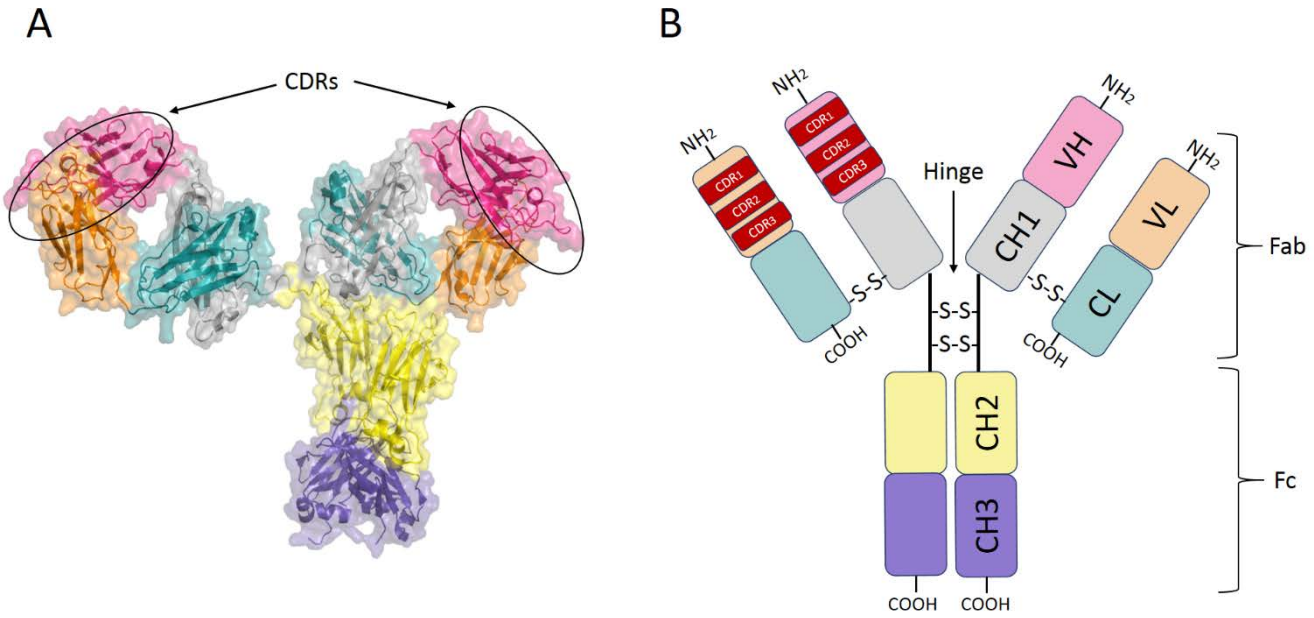

Figure 1: Antibody structure.

(A) Crystal structure of IgG1 (from PDB: 1hzh)**.** Surface and cartoon model generated by PyMOL v1.7.6.0 .**(B)** Schematic presentation. Same colors representing same segments in both presentations. Heavy chains segments: VH (Pink), CH1 (gray), CH2 (yellow) and CH3 (purple). Light chains segments: VL (light orange) and CL (deep teal). Heavy chain CH1 and CH2 are connected with a flexible region, denoted as hinge which contains two disulfide bonds(s-s) between the two heavy chains. The C-termini of CL and CH1 are also linked by a disulfide bond. Each variable domain contains three hypervariable regions, named complementary determining regions (CDRs) of VH and VL building up six loop structures to form the antigen binding site. The Fc is involved in effector site activation of a number of immunological pathways such as ADCC and CDC and by containing epitopes for the Fcγ receptor (FcγR).

2.2. Monoclonal antibodies in cancer therapy

It's been more than a century since the Nobel prize-awarded Paul Ehrlich had suggested that the immune system can prevent tumors growth and that antibodies are in a way "magic bullets" that identify their target and can function without harming the whole organism (Strebhardt & Ullrich, 2008). Currently oncologists see monoclonal (mAb) based cancer therapies as a vital component of state of the art cancer care (Weiner, 2015). In 1975, Köhler and Milstein issued a landmark publication outlining how to produce mAbs by fusion of isolated B cells from immunized animals with immortalized myeloma cells resulting in a hybrid cell called hybridoma (KÖHLER & MILSTEIN, 1975), a discovery that led to a Nobel Prize 10 years later. A year after (1986) Muromonab (Orthoclone OKT3), a very powerful immunosuppressive drug marketed by Cilag AG was the first monoclonal murine antibody to become available for therapy in humans. ORT/OKT3 is an IgG2a immunoglobulin produced by the hybridoma technique that recognizes, binds and blocks the CD3 complex of the T-cell receptor (Emmons & Hunsicker, 1987). But as a murine immunoglobulin it caused to significant immunological side effect in patients (Sgro, 1995). An appreciation of the consequences of an immune response to murine antibodies has led to the development of engineered mAb humanization techniques that carry a lower risk of immune reactions. The development of humanization approaches was pioneered by Winter and colleagues, where murine Fc and Fv framework regions were replaced by human germline amino acids (Riechmann, Clark, Waldmann, & Winter, 1988). Through this technology, lower immune responses to antibodies were observed. This technique led to the successful generation of Rituximab (Rituxan), a chimeric monoclonal antibody, targeting CD20 on B-cells for non-Hodgkin's lymphoma and Chronic lymphocytic leukemia which is the first monoclonal antibody to be approved for clinical use in the therapy of cancer (Grillo-López et al., 1999). Since then, strategies to generate fully human antibodies containing only human amino acid sequence derived antibody regions have been developed. Antigen specificity is nowadays being selected either in vivo by the use of genetically modified rodents or by antibody engineering processes as antibody libraries combined with screening tools such as fluorescence-activated cell sorting (FACS) (Hoogenboom, 2005; Lonberg, 2005, 2008).

Currently to the end of 2018, 31 mAbs have been approved for clinical use for cancer therapy (data from FDA). Those successful monoclonal antibody therapeutics have been based on a number of mechanisms of action (MoA). Immunoglobulin G (IgG) molecules that bind to target cancer cells can mediate antibody-dependent cellular cytotoxicity (ADCC) by immune effector cells or induce complement-dependent cytotoxicity (CDC). Some mAbs can mediate the direct signaling-induced death of cancer cells such as in the case of Trastuzumab that binds to HER2 or Rituximab that binds to EGFR. mAbs such as Bevacizumab that binds VEGF ligand can be used to inhibit angiogenesis. Antibodies as Ipilimumab that blocks CTL4 or Nivolumab that blocks PD1 or Avelumab that binds

PDL-1 can block inhibitory immune checkpoint molecules, thereby resulting in a stronger antitumor T cell responses .Radioimmunoconjugates as Ibritumomab tiuxetan deliver radioisotopes to the cancer cells, whereas antibody–drug conjugates as Brentuximab vedotin and Trastuzumab emtansine deliver highly potent toxic drugs to the cancer cells, while Moxetumomab pasudotox delivers an immunotoxin into the tumor.

mAb variable regions are also used to retarget immune effector cells towards cancer cells through the use of bispecific mAbs that recognize cancer cells with one arm and activating antigens on immune effector cells with the other arm, as Blinatumomab that binds to CD3 and CD19. Recent years approvals also include mAbs targeting new targets such as RNKL, GD2, SLAMF7, PDGFRα and CCR4 mostly with MoA of ADCC. A summary of all the approved monoclonal antibodies used for cancer therapy with their binding target and MoA are depicted in **Table 1**.

	Agent	Target(s)	Proposed MoA	Year approved
1	Rituximab (Rituxan, Mabthera)	CD20	Depletes target cells by ADCC, CDC and inducing apoptosis	1997
2	Tositumomab (Bexxar)			2002
3	Ofatumumab (Arzerra,)			2003
4	Obinutuzumab (Gazyva)			2009
5	Ibritumomab tiuxetan (Zevalin)	CD20	Radiation from 90Y induces cellular damage	2013
6	Brentuximab vedotin (Adcetris)	CD30	Antibody drug cinjugate	2011
7	Blinatumomab((Blincyto)	CD3 and CD19	Mediates formation of a T lymphocyte–tumour cell synapse that results in tumour cell lysis	2014
8	Daratumumab (Darzalex)	CD38	Depletes target cells by ADCC, CDC and inducing apoptosis	2015
9	Gemtuzumab ozogamicin (Mylotarg)	CD33	Antibody drug cinjugate	2017
10	Inotuzumab ozogamicin (Besponsa)	CD22	Antibody drug cinjugate	2017
11	Moxetumomab pasudotox	CD22	antibody immunotoxin	2018
12	Trastuzumab (Herceptin)	HER2	Depletes target cells by ADCC, CDC and inducing apoptosis	1998
13	Pertuzumab (Perjeta)			2012
14	Trastuzumab emtansine (Kadcyla)	HER2	Antibody drug cinjugate	2013
15	Cetuximab (Erbitux)	EGFR	Depletes target cells by ADCC, CDC and inducing apoptosis	2004
16	Necitumumab (Portrazza)			2015
17	Panitumumab (Vectibix)			2006
18	Bevacizumab (Avastin)	VEGF ligand	Binds and neutralizes ligand	2004
19	Ramucirumab (Cyramza)	VEGFR2	Binds and antagonizes receptor	2014
20	Ipilimumab (Yervoy)	CTLA-4	Binds and antagonizes receptor; augments T lymphocyte activation and proliferation	2011
21	Nivolumab (Opdivo)	PD-1	Binds and antagonizes receptor; augments T lymphocyte activation and proliferation	2014
22	Pembrolizumab (Keytruda)			2014
23	Cemiplimab (Libtayo)			2018
24	Atezolizumab (Tecentriq)	PD-L1	Binds and neutralizes ligand; releases inhibition of the immune response □	2016
25	Avelumab (Bavencio)			2017
26	Durvalumab (Imfinzi)			2017
27	Denosumab (Xgeva)	RANKL	Binds and neutralizes ligand; decreases bone resorption and increases mass and strength of some bones	2010
28	Dinutuximab (Unituxin)	GD2	Depletes target cells by ADCC, CDC and inducing apoptosis	2015
29	Elotuzumab (Empliciti)	SLAMF7	Activates NK cells through SLAMF7 pathway and Fc receptors; depletes target cells by ADCC	2015
30	Olaratumab (Lartruvo)	PDGFRα	Binds and antagonizes receptor; antitumour activity	2016
31	Mogamulizumab (Poteligeo)	CCR4	Depletes target cells by ADCC	2018

Table 1: Monoclonal antibodies approved for clinical use in cancer therapy.

List of the monoclonal antibodies approved for clinical use in cancer therapy with the target they bind, mechanism of action, and year of first approval. Currently there are 31 approved mAbs targeting 18 different targets with different MoA as described. Data adapted from (Carter & Lazar, 2018).

2.3. *In vitro* antibody selection by display technologies

In vitro antibody selection by display technologies is based on four key steps: Initially the generation (or cloning) of the antibody genotypic diversity. The sources of the antibody gene pools can be from B cell-receptor (BCR) gene repertoires after animal immunization with a specific antigen, naïve repertoires derived from peripheral lymphocytes of healthy individuals or synthetic antibody libraries. Most immunizations to date are done using transgenic rodents. Use of naïve repertoires or synthetic antibody libraries can theoretically yield antibodies against any given target. The second key step is linkage between the genotype and phenotype in order to be able to extract the genetic information of a selected binder; This is done by fusing the gene encoding the antibody binding fragments with a host (e.g. phage, yeast, bacteria) gene, causing the host to "display" by anchoring of antibody fragments (e.g. scFv/Fab) on the surface of the host while containing the antibody genes. The third key step is application of selective pressure e.g. high-throughput screening and selection using fluorescence activated cell sorting (FACS).The final key step is efficient amplification of the host (e.g. phage, yeast, bacteria) (Bradbury, Sidhu, Dübel, & McCafferty, 2011) .

The concept of display technology was pioneered by Smith in 1985 with the generation of a peptides phage display library (Scott & Smith, 1990; Smith, 1985). While antibody fragments display was first expressed in bacteria (Skerra & Plückthun, 1988), phage display antibody fragment library was first described by Winter group (McCafferty, Griffiths, Winter, & Chiswell, 1990). In 2018, Smith and winter were rewarded the Nobel Prize for their work. Since its development, phage display is the most established in vitro selection technology. To date 6 human antibodies have been discovered or developed by phage display that were approved for therapy with, Adalimumab being the first phage display derived antibody granted a marketing approval in 2002 (Frenzel, Schirrmann, & Hust, 2016) Another popular *in vitro* antibody selection display technology is the yeast display that was developed in 1997 by Boder and Wittrup and has become an attractive, eukaryotic alternative to phage display (Boder & Wittrup, 1997). In contrast to phage display, yeast can present post-translational modifications similar to mammalian systems which are not present in Escherichia coli bacteria that is used in phage display. Post-translational modifications with appropriate protein folding in the endoplasmic reticulum in the presence of chaperones allow more efficient display of functional library variants (Doerner, Rhiel, Zielonka, & Kolmar, 2014). For example, when antibody selection from an HIV-1 immune antibody library displayed on yeast was compared to selection from the same library displayed on phage, yeast display was shown to sample the immune antibody repertoire considerably better than phage display, selecting all the scFvs identified by phage display and twice as many novel antibodies. The conclusion from this work was that eukaryotic processing of the scFv is the biggest reason for the difference in selected clones from yeast and phage display (Bowley, Labrijn, Zwick, & Burton, 2007)

2.3.1. *In vitro* antibody selection by yeast display

First introduced by Boder and Wittrup, in vitro antibody selection by yeast display (YSD) is based on using the *Saccharomyces cerevisiae* yeast cells to present the antibody fragments on the cell surface (**Figure 2**). In this technology, antibody fragments (e.g. scFv/Fab) are fused to the a-agglutinin adhesion receptor of *Saccharomyces cerevisiae* which is localized on the yeast cell surface allowing the antibody repertoire to be screened and selected by fluorescence activated cell sorting (Boder & Wittrup, 1997). The A-agglutinin receptor is an adhesion molecule helping to stabilizes cell-cell interactions and promotes fusion between an "a" and α haploid cell to obtain a diploid cell in a process called yeast mating (Lu et al., 1995). This receptor is composed of the Aga1 and Aga2 proteins. While, Aga1 protein is secreted and binds covalently to b-glucan present in the extracellular matrix of the yeast cell wall,Aga2 protein binds to Aga1 protein through two disulfide bonds (Boder & Wittrup, 1997). In the YSD system, the HC fragments gene repertoire are genetically fused to the C-terminus of the Aga2 protein which is episomally encoded on a shuttle plasmid, while the Aga1 protein is chromosomally encoded in *Saccharomyces cerevisiae* yeast cells. Aga1 protein and the Aga2 protein fusion are expressed by induction of the galactose 1 promoter (GAL1) with galactose (Gera, Hussain, & Rao, 2013). The Aga2 protein-fusion can be flanked by epitope tags that can be used to assess the level of displayed antibodies.

YSD antibody libraries are constructed first by cloning the antibody genes into a yeast display vector. After yeast transformation and growth, antibody expression is induced by galactose medium and then yeast display the antibodies can be selected using fluorescence-activated cell sorting (FACS) with fluorescent ligands to enrich binders of the library. This is the major advantage of yeast display technology over phage display, as it allows defining specific parameters to select antibodies displayed on the yeast surface and enables high-throughput isolation of engineered clones from large libraries. Yeast displaying antibodies can be sorted by binding to a fluorescently-conjugated antigen and it is possible to separate clones quantitatively utilizing the different binding affinities of distinct clones. Unlike phage, yeast cells can display approximately $10^4 - 10^5$ fusion proteins on each yeast cell surface, and expression range can be evaluated by binding of epitope tags using fluorophore-labeled reagents (Doerner et al., 2014). In first years while comparing to phage display technology, the yeast display platform had limitation of the library size, due to the lower efficiency of yeast transformation (Boder, Raeeszadeh-Sarmazdeh, & Price, 2012). In 2010 efforts to overcome this problem led to the improvement of yeast transformation efficiency, allowing the construction of libraries with 10^8 to 10^9 transformants in a single working day (Benatuil, Perez, Belk, & Hsieh, 2010). Moreover, *saccharomyces cerevisiae* haploid yeast cells are capable of mating with haploid cells of the opposite mating type ("a" and α) to produce a stable diploid cell. This capability can be harnessed as an additional

option to greatly enhance diversity in yeast-based selection approaches. Since Fabs are composed of two distinct polypeptide chains HCs and LCs, it is possible to encode the two chains on different vectors in different yeast strains. The two chains can then be brought together in a single diploid yeast by mating, displaying Fab on the diploid surface cell. This yeast mating approach led to chain shuffled libraries with diversities up to 5 X 10^9 (Weaver-Feldhaus et al., 2004). The highest disadvantage of the YSD technology is the multivalent display of antibodies on yeast surface which causes the selection by FACS to be based on avidity parameters rather than affinity of the displayed clone (Boder et al., 2012; Sheehan & Marasco, 2015). This may cause selection of relatively low affinity antibodies.

Since the technology invention, scFv is the most frequent antibody format displayed on yeast surface while other formats such as Fab or single-chain Fab (scFab) were also described (Sheehan and Marasco, 2015; Böldicke, 2017). Yet, recently it has been suggested that Fab is the most efficient format to express functional antibodies by yeast surface display (Sivelle et al., 2018)

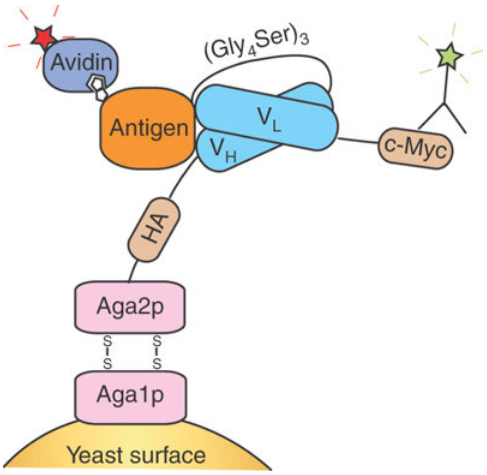

Figure 2: Yeast surface display.

Yeast surface display as described by Boder and Wittrup with scFv fusion protein. The scFv (cyan) is displayed as an Aga2 (pink) fusion protein on the surface of yeast. Expression can be detected by using fluorescent antibodies binding to the epitope tags (beige), and binding of the scFv to a biotinylated antigen (orange) can be detected using fluorescent avidin (blue). HA, hemagglutinin; VL, variable light chain; VH, variable heavy chain; (Gly4Ser)3, flexible peptide linker. Figure adapted from (Chao *et* al., 2006).

2.4. Phenotypic screening for antibody discovery, cell-based assay screening

Since the first approval about 20 years ago, most of the antibodies approved for clinical use in cancer therapy have been isolated using in vitro antibody selection combined with high throughput target-based screening. Although it is considered as one of the most promising strategies for the development of cancer therapies, target-based strategies are limited to targets that have been identified previously ("known" targets), while the number of tumor-specific molecules "known" for antibody targeting is limited. Currently all the 31 approved mAb antibodies approved for clinical use in cancer therapy are

directed against a limited number of 18 targets only as shown in table 1. Moreover, while applying target-based screening with “known” antigens, it first requires obtaining of a recombinant soluble extracellular domain (ECD) of the target, which is not always reachable. In cases were the antigen can be produced as a recombinant ECD, screening can result in selection of antibodies that will not bind effectively to the target expressed on the intact cell in it’s native conformation. This can be caused for example due to incorrect folding of the soluble recombinant protein, different posttranslational modifications of the recombinant protein or alteration of the target proteins due to additional tags on the recombinant protein (Stern et al., 2016).

The limitation of the selection process using recombinant ECD protein together with the currently limited number of tumor-specific targets renders the search for clinical antibodies to be more challenging and the target space increasingly competitive. Alternative strategies, such as phenotypic drug discovery or cell based screening where screening is performed on targets in their native conformation on intact cell, are gaining favor (Minter, Sandercock, & Rust, 2017) . These approaches can lead to the discovery of novel targets in the cancer therapy landscape. Although these strategies have not been widely used, Alemtuzumab, the first clinical approved humanized mAb, was discovered from a phenotypic screen. Immunization of rats with human T cells followed by hybridoma technology identified antibodies that specifically bound T cells. After humanization, the lead antibody was tested and found to effective for chronic lymphocytic leukemia (CLL) by mechanism of T cell depletion while the identification of the antigen as CD52 was made only later (Minter et al., 2017; Waldmann & Hale, 2005) . Phenotypic screening for an antibody targeting cancer can be performed not only following immunization. An example for this is the isolation of the BI-505 antibody using the FIRSTTM platform, where a naïve antibody phage library panned against intact ramos B lymphoma cells with an initial depletion step on membrane vesicles derived from Jurkat T leukemia cells. This attempt led to the isolation of an antibody that acts by induction of B lymphoma cells apoptosis named BI-505. Also, in this case, just after isolation of the antibody, the target was identified as intercellular adhesion molecule 1 (ICAM-1). Interestingly, ICAM-1 had never been reported to be involved in apoptosis in B lymphoma cells. Further characterization of BI-505 revealed that ICAM-1 are strongly expressed in multiple myeloma (MM) and currently the antibody is under phase II clinical trials (Fransson, Tornberg, Borrebaeck, Carlsson, & Frendéus, 2006; Gonzalez-Munoz, Minter, & Rust, 2016).

2.4.1. Yeast display biopanning screening

Phenotypic screening using hybridoma and phage display technologies have demonstrated the ability to yield successful antibodies targeting cancer antigens. Using the advantages mentioned before for yeast display (having the machinery of eukaryotic cells, presenting high copy of protein displayed with multivalent display) together with other characteristics such as low binding of the yeast cells to mammalian cells and the fact that yeast cells size typically is around ~5 μm allowing it to be observed easily under light microscopy without the need of fluorescent tagging, YSD technology can be promising when combined to mammalian cell-based screening for phenotypic selection of antibodies.

In 2005, a method for yeast display biopanning on mammalian cell monolayers was first introduced by Shusta (Xin & Shusta, 2005). Yeast displaying anti-fluorescein scFv mixed with large non-binders yeast cells were panned on fluoresceinated endothelial monolayer adherent cells. Just after three rounds of biopanning yeast displaying anti-fluorescein scFv were enriched and recovered from the background of irrelevant yeast cells. Later attempts in his lab led to successful isolation of antibodies that bind the plasma membranes of rat brain endothelial cells after 5 biopanning rounds of an naïve human scFv yeast library against confluent rat brain endothelial cells (RBE4 cell line) (Wang, Cho, & Shusta, 2007). Recently, also in the Shusta lab, biopanning of a naïve yeast antibody library against patient-derived Glioblastoma stem-like cells (GSC), led to isolation of clones with differential binding against multiple human normal, tumor, and GSC lines. One of the isolated human GSC-selective antibody was validated for use as a research tool for in vivo immunodiagnostics to visualize tumor xenografts (Zorniak et al., 2017). Other labs also implement the method, biopanning a naïve yeast antibody library against androgen-dependent prostate cancer cells led to isolation of high affinity and specific binders to those cells (Williams, Hajiran, Nayeem, & Sooter, 2014). Also anti-B7-H4-targeting scFv that reversed *in vitro* inhibition of CD3-stimulated T cells, which was isolated by biopanning a yeast display scFv library derived from patients with ovarian cancer against C30 ovarian cancer cell line (Dangaj et al., 2013). In 2013 the Shusta Lab published an optimized protocol for biopanning with an additional method for antibody characterization and antigen identification using cell lysate and yeast display (Tillotson, Cho, & Shusta, 2013). Illustration of the biopanning method steps are depicted in **Figure 3**.

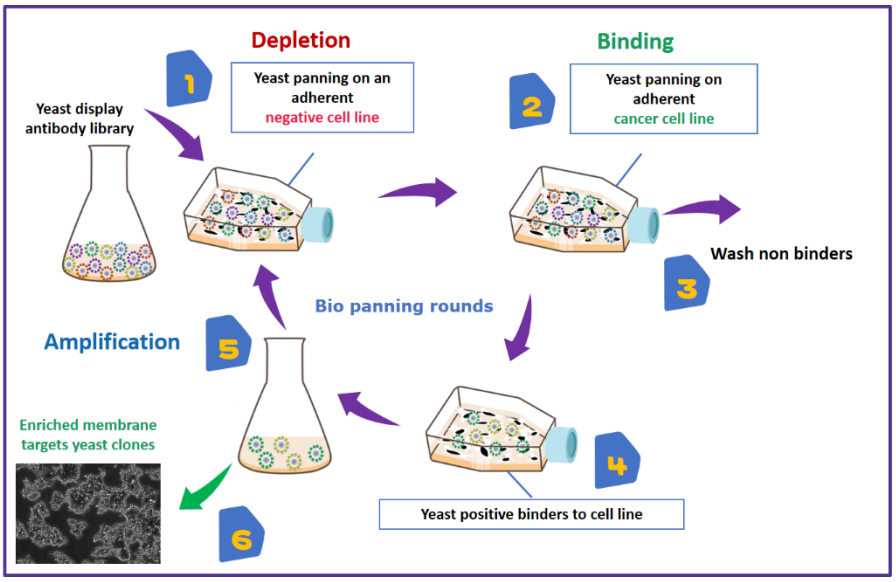

Figure 3: Yeast antibody surface display biopanning process.

(1) Yeast surface antibody display ,after induction, incubated on an adherent monolayer negative cell line in order to deplete "non-wanted" binders (optional step). **(2)** Yeast that do not bind the negative cell line are transferred and incubated on an adherent monolayer cancer cell line (positive cell line) **(3)** Non-binders are removed by washing. **(4)** Yeast-cell binders together with the mammalian adherent cells are removed. **(5)** Yeast cells are amplified and induced for the next biopanning round. **(6)** After several rounds of biopanning, enrichment can be observed by light microscopy.

2.5.Tumor infiltrating immune cells and tumor infiltrating B cells (TIL-B)

Although the phenomenon of infiltration of the immune cells into the tumor tissue is already known for over 150 years (Underwood, 1974) and the correlation between high density of infiltrated immune cells and better clinical outcome in breast cancer patients was documented in a clinical cohort as early as 1922 (Sistrunk & Maccarty, 1922), the research of the phenomenon in clinical and therapy aspects has only progressed in the last decade together with cancer immunotherapy research (Pagès et al., 2010). The immune cells that infiltrate into solid tumors are heterogeneous between tumor types and are very diverse from patient to patient in their occurrence, density and their location in the tumor tissue. All the immune cell types can infiltrate into the tumor including macrophages, dendritic cells, mast cells, natural killer (NK) cells. T and B lymphocytes that infiltrate to the tumor are defined as "Tumor infiltrating lymphocytes" (TILs) and these including memory, naïve and plasma B cells, effector T cells including various subsets of T cell: T helper cells, T helper 1 (TH1) cells,TH2 cells, TH17 cells, regulatory T (TReg) cells, T follicular helper (TFH) cells and cytotoxic T cells. These immune cells can be located in the core (the center) of the tumor, in the invasive margin or in the adjacent tertiary lymphoid structures (TLS) (Fridman, Pagès, Sautès-Fridman, & Galon, 2012). Among the infiltration the dominant cell population is usually T cells which are strongly associated with patient survival in a

wide variety of human cancers. Less is known about tumor infiltrating B cells and their role in the immune response to cancer is not fully understood (B. H. Nelson, 2010).

2.5.1. Tumor infiltrating B Cells (TIL-B)

Tumor infiltrating B cells with high density were observed in many cancer types as melanoma, breast cancer, non-small cell lung cancer (NSCLC), ovarian cancer, colorectal cancer and prostate cancer (Flynn, Somasundaram, Arnold, & Sims-Mourtada, 2017). As mentioned, their role within the tumor is not fully understood and conceivably complex. There are many factors which may influence TIL-B infiltration, as tumor type and stage, the location, subset and activation status of B cells and interaction with other immune cells present within the tumor microenvironment. A large number of studies and clinical trials tried to describe the positive and negative functions of B lymphocytes in a tumor environment, suggesting B cells can promote anti-tumor immunity by different functions such as: differentiate into plasma cells and function as antibody generators, antigen-presenting cells (APCs), producing stimulatory cytokines and chemokines for enhancement of T-cell responses or as direct killers. Additionally B cells can perform immunosuppressive functions by regulatory B cells that can act together with regulatory T cells (Shen et al., 2016). Recently, a review was published of 96 studies representing 19 cancers types with cohorts of 50 or more cases in which the prognostic value of TIL-B was assessed by immunohistochemistry and/or gene-expression analysis. The data indicated that 50.0% of the studies reported a positive prognostic effect for TIL-B within the tumor, whereas the remainder found a neutral (40.7%) or negative (9.3%) effect. Additionally, 21 studies showed that when the presence of TIL-B were analyzed by gene-expression, a large majority reported positive prognostic effect. (Wouters & Nelson, 2018).

2.5.2. TIL-B as an efficient source of highly specific immunoglobulins recognizing tumor membrane proteins

Early in the 1980s together with the hybridoma technology development, a first indication that tumor infiltrating B lymphocyte (TIL-B)-derived antibodies are able to secrete tumor-specific antibodies were obtained by production of human hybridomas derived from TIL-B of cancer patients (Sikora, Alderson, Ellis, Phillips, & Watson, 1983; Sikora, Alderson, Phillips, & Watson, 1982). Later, B cell expansion of TIL-B derived from patient tumor biopsies showed IgG reactivity with autologous tumor targets (Punt et al., 1994) and also B cell expansion of melanoma-derived TIL-B followed by cloning of the scFv antibody showed binding of the specific scFv with different melanoma cell lines (Zhang et al., 1995). Also subcutaneous transplantation of human lung cancer tissue with infiltrated B cells in immunodeficient mice resulted in obtaining secreted IgG derived from TIL-B that highly bound to membrane antigens of autologous cancer cells (Yasuda et al., 2002).

The occurrence of reactive antibodies to tumor specific antigens can be explained by the induction of the immune response in the tumor microenvironment. The elements that stimulate the immune response in the tumor microenvironment is the same as by infection diseases while in the last one a pathogen molecule is recognized by immune receptors present on the surface of lymphocytes, and in cancer the antigens are self-molecules that are created during oncogenesis (Dunn et al., 2002; Goodnow, Vinuesa, Randall, MacKay, & Brink, 2010). Those "self" tumor associated antigens may lose their immunological tolerance by many causes as tolerance defects, downregulation of regulatory T cells, inflammation in the tumor, overexpression of the tumor antigen at levels high enough to exceed the engaged TCR threshold required for CD4+ T cell activation, aberrant expression site of the tumor antigen or altered protein structure like neoepitope exposure mutation and different post-translational modifications. The antibodies that are generated against these antigens can be referred to as autoantibodies (Zaenker, Gray, & Ziman, 2016).

Tumor antigens that drain to the near local tumor-draining (sentinel) lymph node (SN) are introduced to naïve B cells in the lymph node germinal centers where they differentiate into memory B cells or plasma cells that now can circulate back and infiltrate into the tumor (Meeusen, Lim, & Mathivanan, 2017). This adaptive immune response can occur also in the Tertiary lymphoid structures (TLS) within the tumor stroma (Dieu-Nosjean, Goc, Giraldo, Sautès-Fridman, & Fridman, 2014). Recently, a study published by Novinger analyzing heavy and light chain immunoglobulin sequences, from breast cancer patient's infiltrating B cells and B cells present in the tumor-draining lymph node indicated they antibodies are functional and derived from the same clones. This study was the first to report a shared B cell lineage in two different locations in the same breast cancer patient. More than that, by constructing scFv phage display libraries from the patient's tumor infiltrating B cells, tumor-draining sentinel lymph node and peripheral blood followed by enrichment with panning on autologous tumor lysates, an increasing clonal relationship between tumor and lymph node in both the heavy and light chain populations could be detected. This indicates that the relationship shared between tumor and lymph node B cells in this patient may be characterized by selection for tumor-associated antigens. It was also found that replacement mutations were enriched over silent mutations in the CDR regions compared to the framework regions of light chains in the tumor and lymph node libraries, suggesting antigen-mediated selection. In addition, the study showed the after panning, the top 25% of all scFV clone binders to BT474 breast cancer cells were TIL-B and lymph node derived clones and not peripheral derived clones. Further binding analysis on tissues, indicated that multiple phage-displayed antibodies bound specifically to the tumor tissue and not to corresponding normal breast tissue from the same patient (Novinger et al., 2015).

In addition to Novinger's study indicated that phage antibody libraries derived from infiltrating B cells of patients with breast cancer can be a rich source of tumor-binding antibodies, previous reports

indicated isolation of antibodies from scFv phage display libraries derived from sentinel lymph node were binding common tumor targets, such as CEA and HER2 (Ayat et al., 2013a; Belimezi, Papanastassiou, Merkouri, Baxevanis, & Mamalaki, 2006) and antibodies binding to cancer cell lines have been isolated from libraries derived from TIL-B cells (Pavoni et al., 2007; Rothe et al., 2004) also Antibodies that bind ganglioside D3 in a tumor have been identified from libraries constructed from TIL-B cells in a medullary carcinoma (Kotlan et al., 2005)

2.4. Aim of this study

The presented work aims to generate yeast Fab display libraries representing the immunoglobins of B cells infiltrating into colon cancer tumors followed by evaluation of the libraries as a source for antibodies targeting cancer associated antigens. Using traditional yeast display technology and target-based screening by fluorescence-activated cell sorting (FACS) and by using emerging technologies as deep sequencing (NGS) and yeast display biopanning phenotypic screening on mammalian cancer cell lines, we will try to better understand the role of B cell infiltration into tumors. This research may lead to finding improved mAbs for therapy, finding new tumor-associated antigens that can be targeted for cancer therapy or reveal new mechanism of action to fight tumor growth.

3. Material

3.1. Tissues

Tissues were collected at Rambam Health Care Campus (Haifa, Israel) according to a protocol approved by the hospital "Helsinki" Committee, tissues were obtained from a patient with colon cancer at the time of surgical treatment

3.2. Bacterial strains, yeast strains and human cell lines

Bacterial strains

E. coli One Shot Mach1 chemically competent cells (#C862003, Life Technologies, Karlsruhe, Germany); Genotype: *lacZΔM15 hsdR lacX74 recA endA tonA*

Yeast strains

S. cerevisiae EBY100 (ATCC®, Manassas, VA, USA)

Genotype: MATa AGA1::GAL1-AGA1::URA3 ura3-52 trp1 leu2-delta200 his3-delta200 pep4::HIS3 prbd1.6R can1 GAL

S. cerevisiae BJ6454 (ATCC®, Manassas, VA, USA)

Genotype: MATalpha ura3-52 trp1 leu2-delta1 his3-delta200 pep4::HIS3 prb1-delta1.6R can1 GAL

Mammalian cell lines

All mammalian cell lines were cultivated at 37°C,5% or 10% CO_2. Cells were obtained from the American Type Culture Collection (ATCC®, Manassas, VA, USA), or companies as summarized in the following table (**Table 2**).

Table 2: List of mammalian cell lines.

Cell type and cell origin are listed for each cell line:

Cell line	Cell type	Origin
A431	human epidermoid carcinoma	ATCC® CRL 1555™
A549	human lung carcinoma	ATCC® CCL 185™
CHO-S1	Chinese hamster ovary	Life Technologies, Darmstadt, Germany (1119775)
CCD-18Co	human normal colon fibroblast	ATCC® CRL-1459™
HEK 293 EBNA	human embryonic kidney	ATCC® CRL-10852™
HT-29	Human colorectal adenocarcinoma	ATCC® HTB-38™
HCT 116	human colorectal carcinoma	ATCC® CCL-247™
MDA-MB-468	human breast adenocarcinoma (mammary gland)	ATCC® HTB 132™
MKN45	human gastric adenocarcinoma	DSMZ ACC 409
MCF7	human breast adenocarcinoma (mammary gland)	ATCC® HTB-22™
NCI-H1975	human lung adenocarcinoma	ATCC® CRL-5908™
NTERA-2 cl.D1	human testis carcinoma	ATCC® CRL-1973™
SK-BR-3	human breast adenocarcinoma (mammary gland)	ATCC® HTB-30™
SW620	human dukes' type C, colorectal adenocarcinoma	ATCC® CCL-227™

3.3.Plasmids

In the following **Figure 4** depicts the composition of the yeast used plasmids.

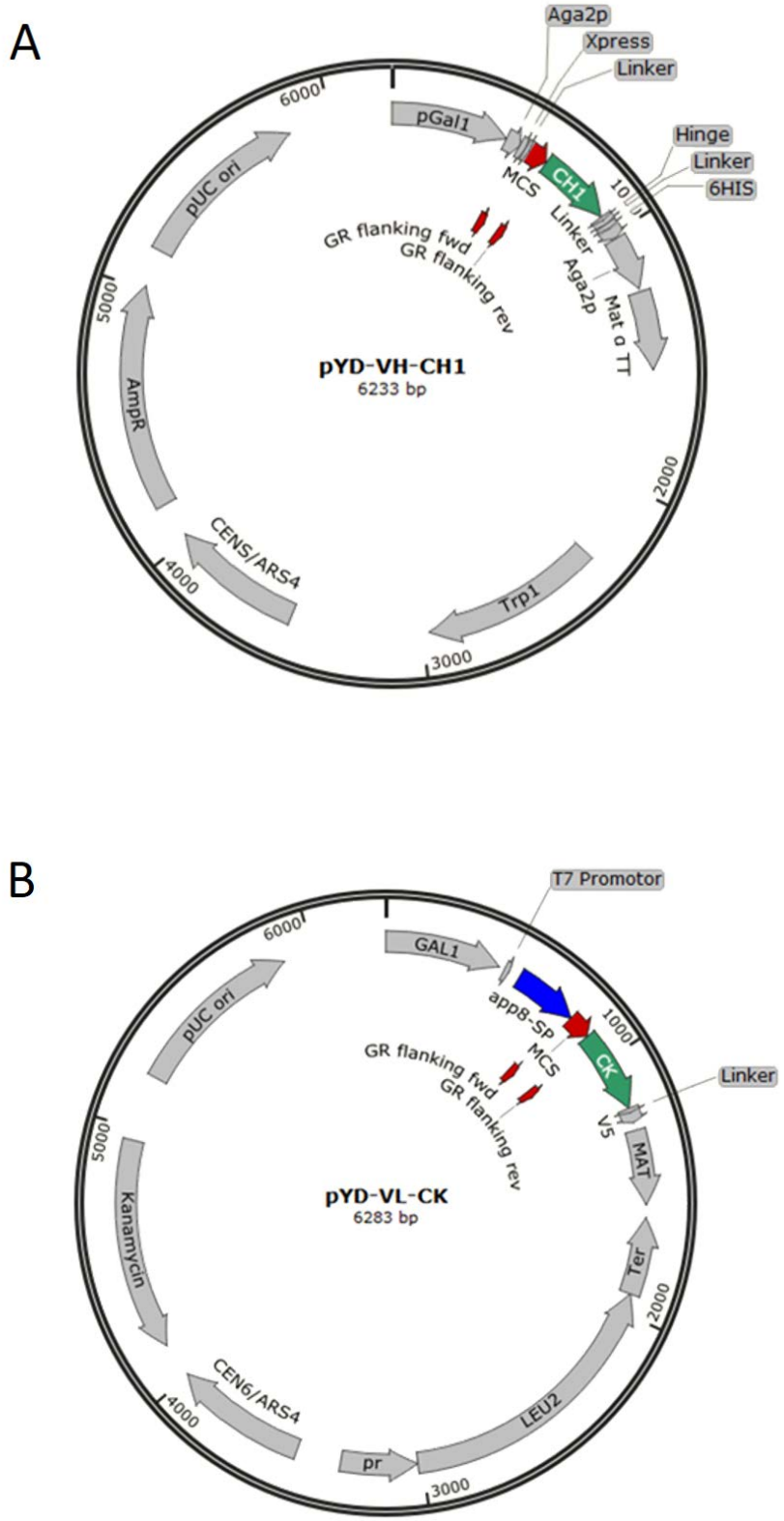

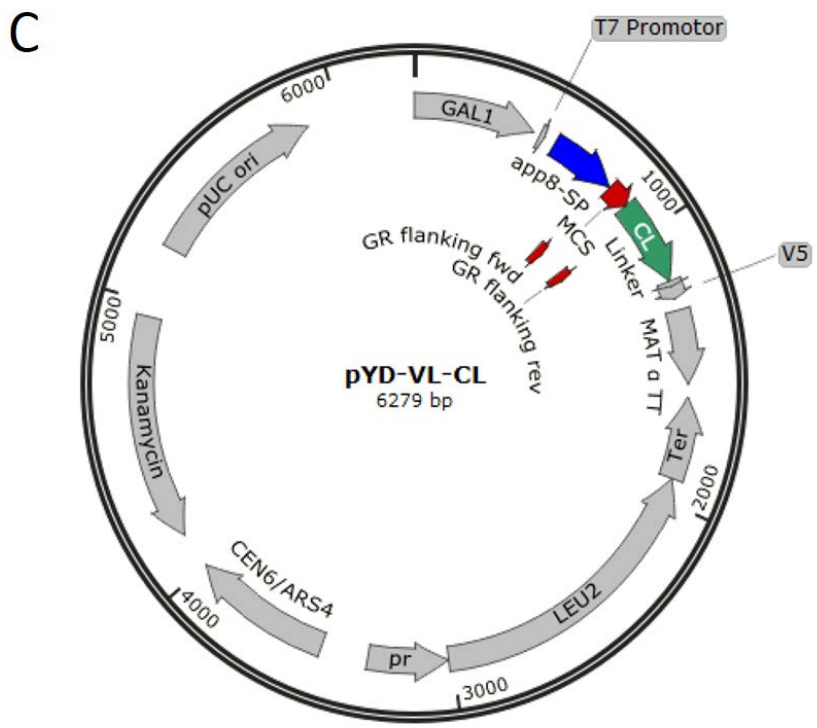

Figure 4: Schematic structure of plasmids used for library construction.

All plasmids **(A,B,C)** were used for the yeast library construction are derivatives of the pYD1 vector (Invitrogen/Life Technologies, Darmstadt, Germany).All of the plasmids contains the CEN6/ARS4: Yeast origin of replication. pUC ori: Bacterial origin of replication. pGal1: Gal1/10 promotor region. Mat α TT: MAT alpha transcription termination region. Plasmid for the heavy chain **(A)** contain signal peptide: AGA2 gene for soluble protein secretion. MCS with bases homologous to the flanking VH gene for gap reaper homologous recombination.CH1: Gene sequence of the CH1 domain of human IgG .Aga2p: Gene encoding for Aga2 protein of the a-agglutinin receptor. Trp1: Gene sequence for the phosphoribosylanthranilate isomerase (auxotrophic marker) and AmpR: Coding sequence for β-lactamase for ampicillin resistance. Plasmid for the light chain kappa **(B)** contain app8: Secretory leader for soluble protein secretion. MCS with bases homologous to the flanking VL kappa gene for gap reaper homologous recombination. CL: Coding gene for the constant domain of the human IgG light chain kappa. Leu2: Coding sequence for the β- isopropylmalate dehydrogenase (auxotrophic marker) and coding sequence for kanamycin resistance. Plasmid for the light chain lambda **(C)** contain app8: Secretory leader for soluble protein secretion. MCS with bases homologous to the flanking VL kappa gene for gap reaper homologous recombination. CL: Coding gene for the constant domain of the human IgG light chain lambda. Leu2: Coding sequence for the β- isopropylmalate dehydrogenase (auxotrophic marker) and coding sequence for kanamycin resistance. Arrows indicate the orientations of genetic elements. The plasmids maps were created with SnapGene Viewer ver. 4.2.6.

In the following **Figure 5** depicts the composition of the mammalian expression plasmids.

A

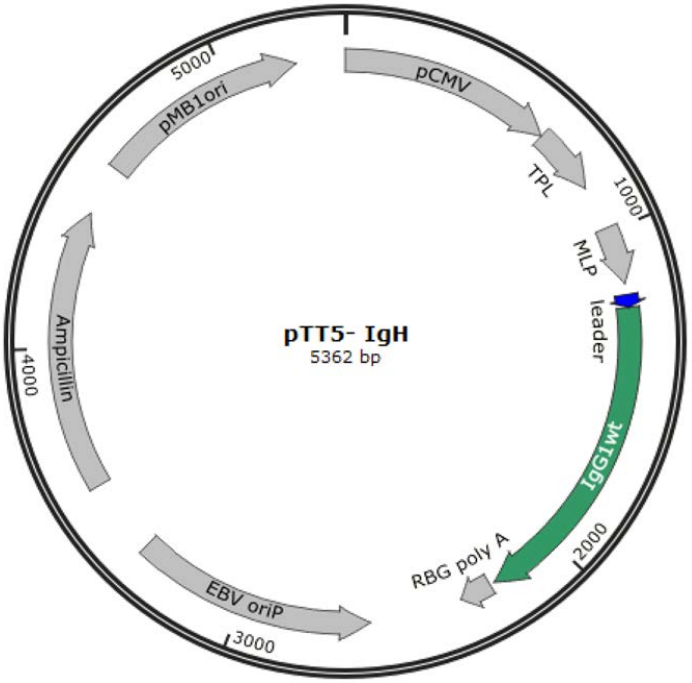

B

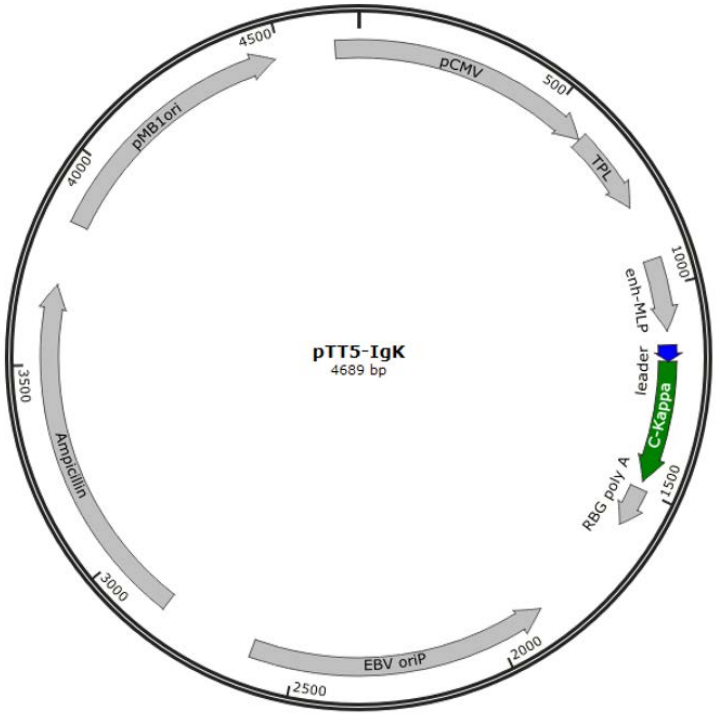

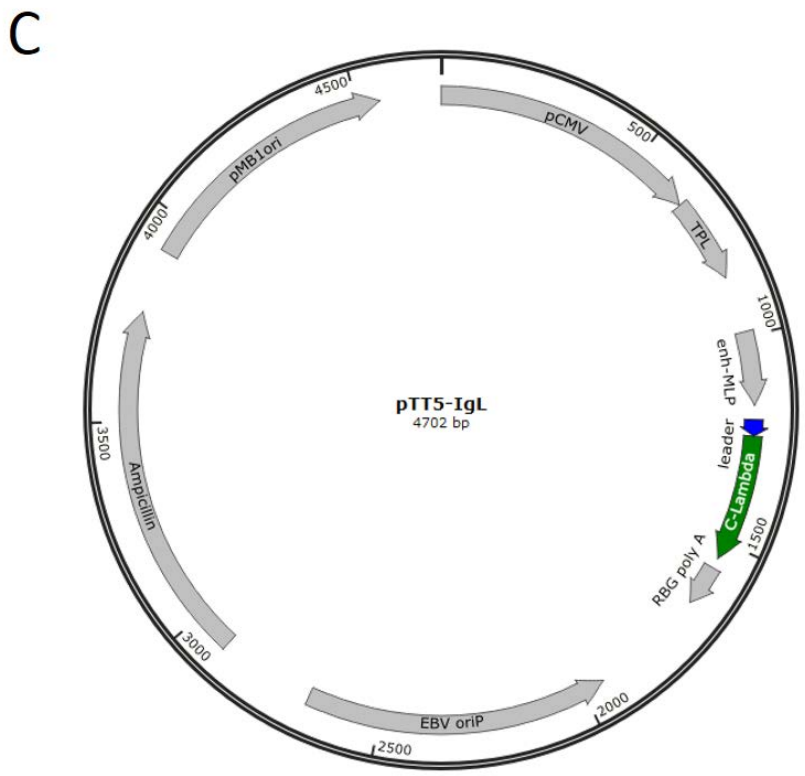

Figure 5: Schematic structure of plasmids used for subcloning.

All plasmids (**A,B,C**) were used for subcloning the variable region of heavy and light chain DNA from selected clones with the yeast expression vectors (pYD) into the mammalian expression vector as IgG1 antibody. Construction are derivatives of pTT5 mammalian expression vectors (Expresso® CMV system, Lucigen, Middleton, WI, USA) and designed with bases homologous to the flanking of the variable regions insertion. EBV oriP: Origin of replication in human cells. AmpR: Coding sequence for β-lactamase. pMB1 ori: Bacterial origin of replication. pCMV: Promotor region. TPL:Tripartite leader sequence. MLP: Adenoviral enhancer element. Signal peptide: Gene encodes the secretory leader and RGB polyA: rbGlob polyA for terminating transcription. Plasmid for the heavy chain (**A**) contain leader and gene sequence of the CH1:CH2:CH3 domain and hinge of human IgG1 with bases homologous to the flanking VH gene for homologous recombination. Plasmid for the light chain kappa (**B**) contain leader and. CK: Coding gene for the constant domain of the human IgG light chain kappa with bases homologous to the flanking VK gene for homologous recombination. Plasmid for the light chain lambda (**C**) contain leader and CL: Coding gene for the constant domain of the human IgG light chain kappa with bases homologous to the flanking VL gene for homologous recombination. Arrows indicate the orientations of genetic elements. The plasmids maps were created with SnapGene Viewer ver. 4.2.6.

3.4.Enzymes and proteins

AccuPrime™ Taq DNA Polymerase	Thermo Fisher Scientific, Carlsbad,USA
Recombinant Human 5T4 (His)	Merck, Darmstadt, Germany
Recombinant Human B7-H3-(2Ig) (Avi-His)	EMD,Billerica,MA,USA
Recombinant Human B7-H3-(4Ig) (Avi-His)	EMD,Billerica,MA,USA
Recombinant Human CD200 (His)	EMD,Billerica,MA,USA
Recombinant Human CEACAM1 (His)	Merck, Darmstadt, Germany
Recombinant Human CEACAM5 (His)	Merck, Darmstadt, Germany
Recombinant Human CEACAM6 (His)	Merck, Darmstadt, Germany
Recombinant Human C-Met (His)	Merck, Darmstadt, Germany
Recombinant Human CTLA4-Fc	EMD,Billerica,MA,USA
Recombinant Human DLK-1 (His)	Merck, Darmstadt, Germany
Recombinant Human EGFR (His)	EMD,Billerica,MA,USA
Recombinant Human GRP78 (His)	Merck, Darmstadt, Germany
Recombinant Human HER-2 (His)	EMD,Billerica,MA,USA
Recombinant Human LAG3 (His)	EMD,Billerica,MA,USA
Recombinant Human LRP6 (E3:E4) (His)	Merck, Darmstadt, Germany
Recombinant Human OX40L (His)	R&D Systems Inc,Minneapolis, MN,USA
Recombinant Human PD-1 (His)	Novoprotein Scientific,Summit, NJ ,USA
Recombinant Human PDL1 (His)	EMD,Billerica,MA,USA
Recombinant Human TEM1 (His)	R&D Systems Inc,Minneapolis, MN,USA
Recombinant Human TIM3 (His)	Novoprotein Scientific,Summit, NJ ,USA
Ribonuclease A from bovine pancreas	Sigma-Aldrich,St louise,MO,USA
Streptavidin - DyLight 633 conjugate	Thermo Fisher Scientific, Carlsbad,USA
Streptavidin Allophycocyanin (APC) conjugate	Biolegend,San Diego, CA,USA
Streptavidin-Phycoerythrin(PE) conjugate	Biolegend,San Diego, CA,USA
Taq Ready Mix (2x)	Hy-Labs,Rehovot,Israel
TrypLE™ Express Enzyme	Life Technologies,Grand Island,NY,USA

3.4.1. Antibodies

Reference antibodies

Cetuximab (Erbitux®)	Merck, Darmstadt, Germany
Anti- human CEACAM5	Merck, Darmstadt, Germany
Anti- human LAG-3	EMD,Billerica,MA,USA
Anti- human LRP6 (E3:E4)	Merck, Darmstadt, Germany
mouse anti human OX40L	R&D Systems Inc,Minneapolis, MN,USA

Detection antibodies for flow cytometry

Goat F(ab')2 Anti-Human Kappa-PE conjugate	Southern Biotech, Birmingham, AL,USA
Goat F(ab')2 Anti-Human Lambda-PE conjugate	Southern Biotech, Birmingham, AL,USA
Donkey F(ab')2 Anti-Human IgG, Fcγ fragment -Alexa Fluor® 488 conjugate	Jackson ImmunoResearch, Cambridgeshire, UK

Detection antibodies for Microscopy

Goat F(ab')2 Anti-Human IgG, Fcγ fragment -Alexa Fluor® 488 conjugate	JacksonImmunoResearch, Cambridgeshire, UK

3.4. Oligonucleotides

Oligonucleotides were obtained from Merck Sigma-Aldrich, Rehovot, Israel.

Primers for VH amplification (1stPCR):

MHVH1_f	CAGGTBCAGCTGGTGCAGTCTGG
MHVH1/7_f	CARRTSCAGCTGGTRCARTCTGG
MHVH2_f	CAGRTCACCTTGAAGGAGTCTGG
MHVH3_f1	SARGTGCAGCTGGTGGAGTCTGG
MHVH3_f2	GAGGTGCAGCTGKTGGAGWCYSG
MHVH4_f1	SARGTGCAGCTGGTGGAGTCTGG
MHVH4_f2	CAGSTGCAGCTRCAGSAGTSSGG
MHVH5_f	GARGTGCAGCTGGTGCAGTCTGG
MHVH6_f	CAGGTACAGCTGCAGCAGTCAGG
MHIgGCH1_r	GACCGATGGGCCCTTGGTGGA

Primers for VK amplification (1stPCR):

MHVK1_f1	GACATCCAGATGACCCAGTCTCC
MHVK1_f2	GMCATCCRGWTGACCCAGTCTCC
MHVK2_f	GATRTTGTGATGACYCAGWCTCC
MHVK3_f	GAAATWGTGWTGACRCAGTCTCC
MHVK4_f	GACATCGTGATGACCCAGTCTCC
MHVK5_f	GAAACGACACTCACGCAGTCTCC
MHVK6_f	GAWRTTGTGMTGACWCAGTCTCC
Kappa1stPCR_r	GACAGATGGTGCAGCCACAGT

Primers for VL amplification (1stPCR):

MHVL1_f1	CAGTCTGTGCTGACTCAGCCACC
MHVL1_f2	CAGTCTGTGYTGACGCAGCCGCC
MHVL2_f	CAGTCTGCCCTGACTCAGCCT
MHVL3_f1	TCCTATGWGCTGACWCAGCCACC
MHVL3_f2	TCTTCTGAGCTGACTCAGGACCC
MHVL4_f1	CTGCCTGTGCTGACTCAGCCC
MHVL4_f2	CAGCYTGTGCTGACTCAATCRYC
MHVL5_f	CAGSCTGTGCTGACTCAGCC
MHVL6_f	AATTTTATGCTGACTCAGCCCCA
MHVL7_8_f	CAGRCTGTGGTGACYCAGGAGCC
MHVL9_10_f	CAGSCWGKGCTGACTCAGCCACC
Lambda1stPCR_r	AGAGGASGGYGGGAACAGAGTGA(

Primers for addition of VH gap repair DNA flanking oligonucleotides (2nd PCR):

Xpress-Liker-MHVH1_f	GCAGGGGATCTGTACGACGATGACGATAAGGGTGGTGGTGGTTCTcaggtbcagctggtgcagtctgg
Xpress-LikerMHVH1/7_f	GCAGGGGATCTGTACGACGATGACGATAAGGGTGGTGGTGGTTCTcarrtscagctggtrcartctgg
Xpress-LikerMHVH2_f	GCAGGGGATCTGTACGACGATGACGATAAGGGTGGTGGTGGTTCTcagrtcaccttgaaggagtctgg
Xpress-LikerMHVH3_f1	GCAGGGGATCTGTACGACGATGACGATAAGGGTGGTGGTGGTTCTsargtgcagctggtggagtctgg
Xpress-LikerMHVH3_f2	GCAGGGGATCTGTACGACGATGACGATAAGGGTGGTGGTGGTTCTgaggtgcagctgktggagwcysg
Xpress-LikerMHVH4_f1	GCAGGGGATCTGTACGACGATGACGATAAGGGTGGTGGTGGTTCTsargtgcagctggtggagtctgg
Xpress-LikerMHVH4_f2	GCAGGGGATCTGTACGACGATGACGATAAGGGTGGTGGTGGTTCTcagstgcagctrcagsagtssgg
Xpress-LikerMHVH5_f	GCAGGGGATCTGTACGACGATGACGATAAGGGTGGTGGTGGTTCTgargtgcagctggtgcagtctgg
Xpress-LikerMHVH6_f	GCAGGGGATCTGTACGACGATGACGATAAGGGTGGTGGTGGTTCTcaggtacagctgcagcagtcagg
CH1-VHJ1_r	GGAGGAGGGTGCCAGGGGGAAGACCGATGGGCCCTTGGTACTAGctgaggagacggtgaccagggttcc
CH1-VHJ2_r	GGAGGAGGGTGCCAGGGGGAAGACCGATGGGCCCTTGGTACTAGctgaggagacggtgaccgtggtccc
CH1-VHJ3_r	GGAGGAGGGTGCCAGGGGGAAGACCGATGGGCCCTTGGTACTAGctgaggagacrgtgaccagggtscc
CH1-VHJ4_r	GGAGGAGGGTGCCAGGGGGAAGACCGATGGGCCCTTGGTACTAGctgaagagacggtgaccattgtccc

Primers for addition of VK gap repair DNA flanking oligonucleotides (2nd PCR):

APP8-MHVK1_f1	GCCAGCATTGCTGCTAAAGAAGAAGGGGTACAACTCGATAAAAGAgacatccagatgacccagtctcc
APP8-MHVK1_f2	GCCAGCATTGCTGCTAAAGAAGAAGGGGTACAACTCGATAAAAGAgmcatccrgwtgacccagtctcc
APP8-MHVK2_f	GCCAGCATTGCTGCTAAAGAAGAAGGGGTACAACTCGATAAAAGAgatrttgtgatgacycagwctcc
APP8-MHVK3_f	GCCAGCATTGCTGCTAAAGAAGAAGGGGTACAACTCGATAAAAGAgaaatwgtgwtgacrcagtctcc
APP8-MHVK4_f	GCCAGCATTGCTGCTAAAGAAGAAGGGGTACAACTCGATAAAAGAgacatcgtgatgacccagtctcc
APP8-MHVK5_f	GCCAGCATTGCTGCTAAAGAAGAAGGGGTACAACTCGATAAAAGAgaaacgacactcacgcagtctcc

APP8-MHVK6_f	GCCAGCATTGCTGCTAAAGAAGAAGGGGTACAACTCGATAAAAGAgawrttgtgmtgacwcagtctcc
Kappa2ndPCR_r	AGCTGTACCAGACTTCAATTGTTCGTCAGATGGTGGAAAAATGAAgacagatggtgcagccacagt

Primers for addition of VL gap repair DNA flanking oligonucleotides (2nd PCR):

APP8-MHVL1_f1	GCCAGCATTGCTGCTAAAGAAGAAGGGGTACAACTCGATAAAAGAcagtctgtgctgactcagccacc
APP8-MHVL1_f2	GCCAGCATTGCTGCTAAAGAAGAAGGGGTACAACTCGATAAAAGAcagtctgtgytgacgcagccgcc
APP8-MHVL2_f	GCCAGCATTGCTGCTAAAGAAGAAGGGGTACAACTCGATAAAAGAcagtctgccctgactcagcct
APP8-MHVL3_f1	GCCAGCATTGCTGCTAAAGAAGAAGGGGTACAACTCGATAAAAGAtcctatgwgctgacwcagccacc
APP8-MHVL3_f2	GCCAGCATTGCTGCTAAAGAAGAAGGGGTACAACTCGATAAAAGAtcttctgagctgactcaggaccc
APP8-MHVL4_f1	GCCAGCATTGCTGCTAAAGAAGAAGGGGTACAACTCGATAAAAGActgcctgtgctgactcagccc
APP8-MHVL4_f2	GCCAGCATTGCTGCTAAAGAAGAAGGGGTACAACTCGATAAAAGAcagcytgtgctgactcaatcryc
APP8- MHVL5_f	GCCAGCATTGCTGCTAAAGAAGAAGGGGTACAACTCGATAAAAGAcagsctgtgctgactcagcc
APP8- MHVL6_f	GCCAGCATTGCTGCTAAAGAAGAAGGGGTACAACTCGATAAAAGAaattttatgctgactcagcccca
App8-MHVL7_8_f	GCCAGCATTGCTGCTAAAGAAGAAGGGGTACAACTCGATAAAAGAcagrctgtggtgacycaggagcc
APP8-MHVL9_10_f	GCCAGCATTGCTGCTAAAGAAGAAGGGGTACAACTCGATAAAAGAcagscwgkgctgactcagccacc
Lambda2ndPCR_r	ACTGATGAGACACACCAGTGTGGCCTTGTTGGCTTGAAGCTCCTCagaggasggygggaacagagtgac

Primers for amplification of VH gap repair DNA flanking oligonucleotides (3rd PCR):

HC3rdPCR_f	GCAGGGGATCTGTACGACGATG
HC3rdPCR_r	GGAGGAGGGTGCCAGGGGGAAGAC

Primers for amplification of VK gap repair DNA flanking oligonucleotides (3rd PCR):

kappa3rdPCR_f	GCCAGCATTGCTGCTAAAGA
kappa3rdPCR_r	AGCTGTACCAGACTTCAATT

Primers for amplification of VL gap repair DNA flanking oligonucleotides (3rd PCR):

lambada3rdPCR_f	GCCAGCATTGCTGCTAAAGA
lambada3rdPCR_r	ACTGATGAGACACACCAGTG

Primers for sequencing:

pTT5_VH_r	TCTTGTCCACCTTGGTGTT

pTT5_VL_r	TCTCGACACCAGCCTTGAC
pTT5_VK_r	GCGTTATCAACTTTCCATT

3.5. Chemicals and supplements

Ampicillin sodium salt	Sigma-Aldrich,St louise,MO,USA
2-Mercaptoethanol	Sigma-Aldrich,St louise,MO,USA
Bovine serum albumin (BSA)	Equitech-Bio, Kerrville, USA
Calcium chloride (CaCl2)	Sigma-Aldrich,St louise,MO,USA
D-(+)- Galactose	Sigma-Aldrich,St louise,MO,USA
D-(+)Glucose	Sigma-Aldrich,St louise,MO,USA
Dako Fluorescence Mounting Medium	Agilent Technologies,Santa Clara,CA,
DDT in ddH2O	Sigma-Aldrich,St louise,MO,USA
Disodium hydrogen phosphate (Na2HPO4*2H2O)	Merck, Darmstadt, Germany
DO Supplement –Leu	Clontech,Mountain View,CA,USA
DO Supplement –Leu/–Trp	Clontech,Mountain View,CA,USA
DO Supplement –Trp	Clontech,Mountain View,CA,USA
Eagle Minimal Essential Medium (MEM)	Sigma-Aldrich,St louise,MO,USA
EDTA (ethylenediaminetetraacetic acid)	Sigma-Aldrich,St louise,MO,USA
Ethanol	Sigma-Aldrich,St louise,MO,USA
EX-CELL® 293 Serum-Free Medium	Sigma-Aldrich,St louise,MO,USA
EZ-Link NHS-PEG4-Biotin, No-Weigh Format	Thermo Fisher Scientific,Waltham,USA
Fibronectin bovine plasma	Sigma-Aldrich,St louise,MO,USA
Gel loading dye (6×)	New England Biolabs, Ipswich, MA, USA
Gibco® Dulbecco's modified eagle medium(DMEM)	Life Technologies, Darmstadt, Germany
Gibco® Fetal bovine serum (FBS)	Life Technologies, Darmstadt, Germany
Gibco® L-glutamine	Life Technologies, Darmstadt, Germany
Gibco® sodium pyruvate	Life Technologies, Darmstadt, Germany
Giboc® RPMI 1640 medium	Life Technologies, Darmstadt, Germany
Giboco® DMEM/F-12 (1:1)	Life Technologies, Darmstadt, Germany
Giboco® FreeStyle™ 293	Life Technologies, Darmstadt, Germany
Glycerol	Sigma-Aldrich,St louise,MO,USA
Glycine	Merck, Darmstadt, Germany
Guava instrument cleaning fluid (ICF)	Merck, Darmstadt, Germany
Hoechst 33342	Sigma-Aldrich,St louise,MO,USA
Hydrochloric acid smoking 37% (HCl)	Merck, Darmstadt, Germany

Kinetics buffer (X10)	Pall ForteBio LLC, Menlo Park, CA, USA
LB + ampicillin plates	Hy-Labs,Rehovot,Israel
LB Broth	Hy-Labs,Rehovot,Israel
Lithium acetate	Sigma-Aldrich,St louise,MO,USA
Magnesium sulfate heptahydrate (MgSO4)	Sigma-Aldrich,St louise,MO,USA
Minimal SD Agar Base	Clontech, Mountain View, CA, USA
Minimal SD-Base Gal/Raf	Clontech, Mountain View, CA, USA
Paraformaldehyde 16% aqueous solution	EMS,Hatfield,PA,USA
Pepton from casein	Merck, Darmstadt, Germany
Potassium chloride (KCl)	Sigma-Aldrich,St louise,MO,USA
Potassium dihydrogen phosphate (KH2PO4)	Sigma-Aldrich,St louise,MO,USA
Potassium di-hydrogen phosphate (KH2PO4)	Merck, Darmstadt, Germany
ProCHO 5 serum-free media	Lonza,Basel, Switzerland
ProCHO5 medium	Lonza, Basel, Switzerland
Quick-Load® 100 bp DNA Ladder	New England Biolabs, Ipswich, MA, USA
S.O.C. medium	NEB,Ipswich, MA,USA
Salmon sperm DNA	Thermo Fisher Scientific, Carlsbad,USA
SeaKem® LE Agarose	Lonza,Basel, Switzerland
Sodium chloride (NaCl)	Sigma-Aldrich,St louise,MO,USA
Sodium dehydrogen phosphate monohydrate(NaH2PO4 H2O)	Merck, Darmstadt, Germany
Sodium hydroxide (NaOH)	Merck, Darmstadt, Germany
Sodium phosphate dibasic (Na2HPO4 2H2O)	Merck, Darmstadt, Germany
Sorbitol	Merck, Darmstadt, Germany
TAEx50 buffer	Hy-Labs,Rehovot,Israel
Tris Base	Merck, Darmstadt, Germany
Yeast Nitrogen Base w/o Amino acids	Sigma-Aldrich,St louise,MO,USA
YPD agar plate	Hy-Labs,Rehovot,Israel
YPD broth	Hy-Labs,Rehovot,Israel

3.6. Cell culture media

Mammalian

A431, NTERA-2cl.D1, SK-BR-3	DMEM, 10% (v/v) FBS
SW620, CHO-S (adherent)	DMEM/F-12 (1:1), 10% (v/v) FBS
A549,MDA-MB-468,HT-29,HCT116, MKN45,MCF7, NCI-H1975	RPMI 1640, 10% (v/v) FBS, 2 mM L-glutamine, 1 mM sodium pyruvate
CCD-18Co	MEM Eagle, 10% (v/v) FBS, 2 mM L-glutamine
CHO-S	ProCHO5, 4 mM L-glutamine, Gibco® HT Supplement (1:50)
HEK 293 EBNA(growth)	EXcell-293
HEK 293 EBNA(expression)	FreeStyle 293,0.5% (v/v) FBS

Yeast (*S. cerevisiae*)

SD -Trp, SD -Leu, SD -Trp/-Leu	6.7 g/L Yeast Nitrogen Base w/o Amino acid, 20g/L D-(+)Glucose, 12.1 g/L NaH2PO4×H2O, 2.1 g/L Na2HPO4, one of the dropout supplements (0.74 g/L DO-mix -Trp, 0.69 g/L DO-mix -Leu, 0.64 g/L DO-mix -Trp/- Leu)
SG-Trp/-Leu + Pepton	37 g/L minimal SD-Base Gal/Raf, 8.56 g/L NaH2PO4×H2O, 20.6 g/L Na2HPO4, 0.64 g/L DO-mix -Trp/-Leu, 50 g/L Pepton from casein
SD -Trp plates, SD - Leu plates, SD -Trp/-Leu plates	46.7 g/L minimal SD agar base, one of the dropout supplements (0.74 g/L DO-mix -Trp, 0.69 g/L DO-mix -Leu, 0.64 g/L DO-mix - Trp/- Leu)

3.7. Solutions, media and buffer

Phosphate buffered saline (PBSx1)	140 mM NaCl, 3 mM KCl, 8 mM Na_2HPO_4 x $2H_2O$, 2 mM KH_2PO_4, pH
PBMCMA (biopanning washing buffer)	PBSx1, 0.9 mM CaCl2, 0.49 mM MgCl21 g/l BSA
Washing buffer (Yeast, flow cytometry analysis)	PBSx1, 0. 5% (w/v) BSA,2mM EDTA
Binding buffer (Mammalian, flow cytometry analysis)	PBSx1, 1% (w/v) BSA,2mM EDTA
LB- Ampicillin	LB Broth, 0.1%(v/v) Ampicillin
LB-glycerol	LB-Ampicillin,30%(v/v) glycerol
PA SpinTrap binding buffer	2g/L H_2NaO_4P,1.2g/L Na2HPO4 x 2H2O,
PA SpinTrap Elution buffer	0.1M Glycine/HCl pH 2.7
PA SpinTrap Neutralizing buffer	1M Tris/HCl pH 7
Yeast lysis buffer	20 nM NaOH, 5µg/ml Ribonuclease A
Yeast library freezing solution	15% (v/v) glycerol, SD -Trp/ SD -Leu/ SD -Trp/-Leu
Yeast transformation buffer	1 M sorbitol, in dH2O

3.8. Kits and laboratory materials

6/12 Well cell culture plate sterile	Greiner Bio-one, Frickenhausen, Germany
96 well polypropylene black microplates F-Bottom	Greiner Bio-one, Frickenhausen, Germany
Amicon® Ultra-15 and 0.5 ml centrifugal filter units 10k	Merck, Darmstadt, Germany
Erlenmeyer Flask- Baffled Base 2L, 1L, 500ml, 250ml, 125ml	TriForestLabware,Irvine, CA, USA
Falcon® 96-well Clear Round Bottom plates	Cornning,NY,USA
FortéBio tips (AHC,AMC,Streptavidin,	Pall ForteBio LLC, Menlo Park, CA, USA
Gene Pulser cuvette 0.2cm	Bio-Rad, Hercules, CA, USA
Ingenio® Electroporation Kit	Mirus Bio,Madison,WI,USA

MicroAmp™ Optical 96-Well Reaction Plate	Thermo Fisher Scientific,Waltham,USA
Nunc™ Cell Culture Treated Flasks with Filter Caps T-80	Thermo Fisher Scientific,Roskilde,Denmark
Petri dish 90mm	Hy-Labs,Rehovot,Israel
Protein A HP SpinTrap	GE Healthcare,Buckinghamshire,UK
Qiaquick pcr purification kit	Qiagen, Hilden, Germany
RNA ScreenTape kit	Agilent Technologies,Santa Clara,CA, USA
RNeasy® Midi kit	Qiagen, Hilden, Germany
SuperScript™ III Reverse Transcriptase	Thermo Fisher Scientific, Carlsbad,USA
TaqMan Gene Expression Assay (CD19,CD20,RPLP0)	Applied Biosystems ,Foster City,CA,USA

3.9. Equipment

Analytical balance New Classic MF MS3002S	Mettler Toledo, Giessen, Germany
Agilent 2200 TapeStation	Agilent Technologies,Santa Clara, USA
Analytical balance New Classic MF MS3002S	Mettler Toledo, Giessen, Germany
Applied Biosystems ViiA™ 7 Real-Time PCR System	Thermo Fisher Scientific, Waltham, MA ,USA
BD FACSAria™ III cell sorter	BD Biosciences,San Jose,CA,USA
Bio RS-24, Mini-rotator	Biosan,Riga, Latvia
CCD microscope camera Leica DFC3000 G	Leica,Wetzlar, Germany
Cell counter Vi-CELL® XR	Beckmann Coulter, Brea, CA, USA
Circulating Bath	PolyScience,Niles,IL,USA
Class II, Type A2 Biosafety Cabinets	Labconco Corporation,Kansas City, MO,USA
Electrophoresis chambers	Bio-Rad, Hercules, CA, USA
Elite Dry Bath Incubator	Major Science , Saratoga, CA, USA
Flow cytometer Guava easyCyte HT 2L	Merck, Darmstadt, Germany
FortéBio Octet RED	Pall ForteBio LLC, Menlo Park, CA, USA
Gene Pulser Xcell™ Electroporation Systems	Bio-Rad, Hercules, CA, USA
Heracell CO2 Incubator	Thermo Fisher Scientific, Waltham, MA ,USA
Heraeus Multifuge X3R	Thermo Fisher Scientific, Waltham, MA ,USA
Heraeus™ Fresco™ 17 Microcentrifuge	Thermo Fisher Scientific, Waltham, MA ,USA
Incubation shaker Multitron Standard	Infros HT, Bottmingen, Switzerland
Mini horizontal gel unit	Scie-Plas Ltd,Cambridge,UK
MiniBIS Pro - DNR Bio Imaging System	DNR,Neve Yamin,Israel
MultiSUB™ horizontal gel electrophoresis unit	Cleaver Scientific Ltd,Warwickshire,UK
NanoDrop™ 1000 Spectrophotometer	Thermo Fisher Scientific, Waltham, MA ,USA
NanoDrop™ 2000 Spectrophotometer	Thermo Fisher Scientific, Waltham, MA ,USA

Pannoramic MIDI II	3DHISTECH,Budapest,Hungary
Power supply PS500X DC	Hoefer,Holliston, MA,USA
Rotor-Stator TH Tissue Homogenizers	Omni International,Kennesaw,GA,USA
SterilGARD® III Advance Safety Cabinets	The Baker Company,Sanford, Maine,USA
Veriti™ 96-Well Thermal Cycler	Thermo Fisher Scientific, Waltham, MA ,USA

Further equipment comprised common laboratory instrumentation.

3.10. Software

Agilent 2200 TapeStation analysis ver A.01.09	Agilent Technologies,Santa Clara,CA, USA
Agilent 2200 TapeStation conroler ver A.01.09	Agilent Technologies,Santa Clara,CA, USA
BD FACSDIVA™ software ver 1.1.3	BD Biosciences,San Jose,CA,USA
cellSens Entry Imaging ver v4.7	Olympus,Tokyo,Japan
Clone Manager professional ver 9.51	Scientific & Educational Software ,Denver, CO, USA
FCS Express 6 ver 6.06.0014	De Novo Software,Glendale, CA,USA
FortéBio octet data acquisition ver. 8.0	Pall ForteBio LLC, Menlo Park, CA, USA
FortéBio octet data analysis ver. 8.0	Pall ForteBio LLC, Menlo Park, CA, USA
GraphPad Prism verV6.07	GraphPad Software, La Jolla, CA, USA
GuavaSoft ver 3.1	Merck, Darmstadt, Germany
Jalview ver 2.10.4	http://www.jalview.org
Leica application suite ver v4.7	Leica,Wetzlar, Germany
Mendeley Desktop ver.1.19.2	Mendeley Ltd,London,UK
Microsoft Office 2016	Microsoft Corp., Redmond, WA, USA
Panoramic Viewer ver 1.15.4	3DHISTECH,Budapest,Hungary
PyMOL ver.vl.1.7.6.0	Schrodinger LLC, San Diego, CA, USA
QuantStudio™ Real-Time PCR ver.1.3	Applied Biosystems ,Foster City,CA,USA
SALSA2	EMD,Billerica,MA,USA
SnapGene® Viewer ver. 4.2.6	GSL Biotech LLC, Chicago, IL, USA
Vi-CELL® XR ver. 2.04	Beckmann Coulter, Brea, CA, USA

4. Methods

4.1. Molecular biological methods

4.1.1. Total RNA isolation from patients' tissues

Total RNA was Isolated separately for each patient's tissue using the RNeasy® Midi kit (chapter 3.8) according to the manufacturer's instruction. Samples were taken out from storage in liquid nitrogen and immediately placed in a bucket with liquid nitrogen until weighting of the samples. The weighed tissues were placed in a suitably 15ml centrifuge tube followed by immediately adding of 6 ml lysis buffer (6ml buffer RLT+ 60µl β-Mercaptoethanol) and homogenized immediately using a conventional rotor–stator homogenizer (chapter 3.8) for 45 sec until the samples were uniformly homogeneous. The tissue lysates were centrifuged (4500xg, 10 min) and the lysate supernatants were transferred to a new 15 ml tube by pipetting. Subsequently, only the lysate supernatants were used. one volume of 70% ethanol was added to the homogenized lysates and were mixed immediately by shaking vigorously. The lysates of each sample were divided and applied on three RNeasy® Midi columns placed in a 15 ml centrifuge tube and were centrifuged (4500xg, 5 min). The flow-through were discarded. Followed by pipetting 2 ml buffer RW1 into the RNeasy® Midi columns. The columns were centrifuged (4500xg, 5 min) and the flow-through were discarded. 160 µl of DNase I incubation mix (20 µl + 140 µl buffer RDD) were directly added to the RNeasy® Midi columns silica-gel membrane and were placed on the benchtop for 15 min at 25°C.Then, 2 ml of buffer RW1 were added into the RNeasy® Midi columns and placed on the benchtop for 5 min at 25°C. The columns were centrifuged (4500xg, 2 min) and the flow-through were discarded. For washing, 2.5 ml of buffer RPE were added to RNeasy® Midi columns. The columns were centrifuged (4500xg, 2 min) and the flow-through were discarded. This step was repeated 2 times. For elution the RNeasy® Midi columns were transferred to new 15 ml tubes and 150 µl of RNase-free water were added directly onto the RNeasy® Midi columns silica-gel membrane and placed on the benchtop for 1 min at 25°C. The elution steps were repeated once as describe above. RNA concentration was photometrically determined (cf. chapter 4.1.2).

4.1.2. Determination of DNA/RNA concentration

The nucleic acid concentration in aqueous solutions was measured by a UV spectrophotometer, Nanodrop ND1000 (chapter 3.9) applying 1.5 µl of sample. The underlying physical principals are the law of Lambert-Beer and the absorption of aromatic nucleobases within the DNA/RNA at the wavelength 260 nm. The ratios A_{260}/A_{280} and A_{260}/A_{230} can be used as a quality criterion for the purity of the DNA/RNA.

For DNA ratios should be around 1.8 and 2.0-2.2, respectively. For RNA ratios should be around 2 and 2.0-2.2, respectively.

4.1.3. Determination of RNA integrity number

The determination of quality of the total RNA isolated from the patient's tissues were measured using the 2200 TapeStation system electrophoresis bioanalyzer (chapter 3.9) using the RNA ScreenTape kit according to the manufacturer's instruction by applying 1 µl of RNA from each sample. The RNA integrity number equivalent (RINe) provides an independent quality score for total RNA was analyzed by the Agilent 2200 TapeStation Software (chapter 3.10) .

4.1.4. Polymerase chain reaction

DNA can be exponentially and specifically amplified by the polymerase chain reaction (PCR) employing DNA flanking, complementary oligonucleotides or primers (Mullis et al., 1986).

PCRs for library contraction

For each patient heavy and light chain variable region amplification (1st PCR), 2 µl of cDNA template (cf. chapter 4.1.5) were mixed with 5 µl AccuPrime™ reaction mix, 0.2 µM forward and reverse primers(chapter 3.5) 0.5 µl 2.5 U/µl AccuPrime™ Pfx DNA Polymerase (chapter 3.4), and dH_2O in a final volume of 50 µl. After initial denaturation at 95°C for 60 sec, 30 cycles of amplification were performed for each 15 sec at 95°C for denaturation, 30 sec at 55°C for annealing, and 45 sec at 68°C for extension followed by a final extension for 10 min at 68°C.DNA was recover and purified from gel (cf. chapter 4.1.7). For addition of gap repair DNA flanking oligonucleotides (2nd PCR) was performed, 2 µl of 1st PCR DNA clean-up product were mixed with 5 µl AccuPrime™ reaction mix, 0.2 µM forward and reverse primers (chapter 3.5), 0.5 µl 2.5 U/µl AccuPrime™ Pfx DNA Polymerase, and dH2O in a final volume of 50 µl. After initial denaturation at 95°C for 60 sec, 30 cycles of amplification were performed for each 15 sec at 95°C for denaturation, 30 sec at 55°C for annealing, and 45 sec at 68°C for extension followed by a final extension for 10 min at 68°C. For amplification of 2nd PCR products in sufficient amount for Gap Repair (3rd PCR), 6 µl of 2st PCR DNA clean-up product were mixed with 10 µl AccuPrime™ reaction mix, 0.2 µM forward and reverse primer (chapter 3.5), 0.5 µl 2.5 U/µl AccuPrime™ Pfx DNA Polymerase, and dH2O in a final volume of 100 µl. After initial denaturation at 95°C for 60 sec, 30 cycles of amplification were performed for each 15 sec at 95°C for denaturation, 30 sec at 55°C for annealing, and 45 sec at 68°C for extension followed by a final extension for 10 min at 68°C. DNA was recover and purified from gel (cf. chapter 4.1.7)

PCRs for subcloning

In order to subcloning the variable region of heavy and light chain DNA from selected clones with the yeast expression vectors (pYD) into the mammalian expression vector (pTT5). 2 µl of yeast lysis (cf. chapter 4.2.3) were mixed with 5 µl AccuPrime™ reaction mix, 0.2 µM forward and reverse primer, 0.5 µl 2.5 U/µl AccuPrime™ Pfx DNA Polymerase, and dH2O in a final volume of 50 µl. After initial denaturation at 95°C for 60 sec, 30 cycles of amplification were performed for each 15 sec at 95°C for denaturation, 30 sec at 55°C for annealing, and 45 sec at 68°C for extension followed by a final extension for 10 min at 68°C.

Colony PCRs

To verify the insertion for the mammalian expression vector (pTT5) after transformation (cf. chapter 4.2.1) colony PCR were performed using Taq Ready Mix (chapter 3.4). Small amount of colony was mixed with 10 µl Taq Ready Mix (2X), 0.1 µM forward and reverse primer and dH2O in a final volume of 50 µl. After initial denaturation at 95°C for 60 sec, 33 cycles of amplification were performed for each 15 sec at 95°C for denaturation, 30 sec at 58°C for annealing, and 45 sec at 68°C for extension followed by a final extension for 10 min at 68°C.

4.1.5. Reverse transcriptase to synthesize first-strand cDNA

cDNA was synthesized from each patient's isolated total RNA using SuperScript™ III Reverse Transcriptase kit (chapter 3.9) according to the manufacturer's instruction. Briefly, 4 µg of total RNA template were mixed with 200 ng/µl random hexamers primer, 4 µl of 10 mM dNTP Mix and sterile distilled dH_2O in a final volume of 40 µl. The mixture was heated to 65°C for 5 min and incubated on ice for at least 1 min. Followed by brief centrifugation and mixing with, 2 µl 10X First-Strand Buffer, 1 µl 0.1 M DTT, 1 µl 40 U/µl RNaseOUT™ Recombinant RNase Inhibitor, 2 µl 200 U/µl SuperScript™ III RT. The mix was incubated at 25°C for 5 min followed by incubation at 50°C for 50 minutes for cDNA synthesis, and 15 min at 70°C for inactivation.

4.1.6. Real time PCR for quantitative gene expression analysis

Expression of CD19 and CD20 genes in the cDNA templates synthesized from patient's RNA (cf. chapter 4.1.5) was performed using the Applied Biosystems TaqMan Gene Expression Assay (chapter 3.9) according to the manufacturer's instruction with the ViiA 7 Real-Time PCR System (chapter 3.10). Briefly, cDNA templets from the patients were diluted 1:2 with DEPC water. For each reaction 5 µl master mix (enzyme),0.5µl assay mix (TaqMan probe and primers) and 4.5µl were mixed in a well of MicroAmp® optical 96-well reaction plate (chapter 3.9). The samples were analyzed using the QuantStudio™ Real-Time PCR Software (chapter 3.11) applying the comparative cT assay.

4.1.7. Purification of DNA and gel extraction

DNA fragments were purified after PCR amplification or from agarose gel bands excised with a clean scalpel. PCR amplifications were cleaned and purified using the QIAquick PCR Purification kit (chapter 3.9) according to the manufacturer's instructions. The recovery of DNA from agarose gel was done by using the Zymoclean Gel DNA Recovery kit (chapter 3.9) according to the manufacturer's instructions. DNA was eluted in 30 µl dH_2O. DNA concentration was photometrically determined (cf. chapter 4.1.3).

4.1.8. Gel electrophoresis

With the help of agarose gel electrophoreses, linear DNA fragments can be separated in an electric field based on their length. In general, 1-2% (w/v) agarose gels were prepared in TAE buffer (X1) (chapter 3.6) supplemented with SeaKem® LE Agarose (chapter 3.6). DNA premixed with 6x loading dye were loaded on gels along with 10 µl Quick-Load® 100 bp DNA Ladder (0.1-15 kbp) for determination of size and isolating of separated DNA (chapter 3.6) . Fragments on gels were run for 45 min at 100 V. DNA bands were visualized by UV light using the DNR Bio Imaging System, MiniBIS Pro (chapter 3.10).

4.1.9. Sanger DNA sequencing

Isolated plasmid DNA (15 µl with 50-100 ng/µl) or alternatively yeast clones were transferred to HyLabs (Rehovot, Israel) and sequenced using primers listed in (chapter 3.5).

4.1.10. Next-generation sequencing

Yeast clones were transferred to Dr. Thomas Clarke, EMD Merck (Billerica, USA) the clones VH and VL were sequenced and analyzed using the Illumina MiSeq System.

4.2. Microbiological methods

4.2.1. Transformation and cloning in *E. coli*

Transformation and cloning were carried out with One Shot® Mach1™-T1R Chemically Competent E. coli (chapter 3.2) by heat shock. The genes of interest (heavy or light chain variable region) were amplified using specifically designed primers which are flanked with additional 15-20 base pairs of non-annealing 5'-tail (chapter 3.5) that carries the homology to the insertion site in the specific pTT5 mammalian expression plasmid. The linearized plasmids pTT5 IgH/pTT5 IgK/ pTT5 IgK provided by Lucigen Corporation (chapter 3.3) were transformed together with the PCR amplicon (cf. chapter 4.1.4) into the competent E.coli strain while the recombination occurred in vivo. 25 ng PTT5 plasmid and 1 µl of purified PCR amplicon were incubated with 10 µl One Shot® Mach1™-T1R Chemically Competent E. coli, which were thawed on ice, for 30 min. Heat-shock was performed for 30 sec at 42°C

followed by incubation on ice for 2 min. Then, transformed cells were shaken in 175 µl S.O.C. medium for 1 h at 225 rpm and 37°C followed by plating on LB-A selective agar (chapter 3.6) and incubation overnight at 37°C.

4.2.2. Extraction of pure plasmid DNA from bacterial cultures

The pTT5 plasmids with the insertion of the selected clones after colony PCR verification (cf. chapter 4.2.1) were extracted and purified using the AccuPrep® Plasmid Mini Extraction kit (chapter 3.9) according to the manufacturer's instructions. DNA was eluted in 50 µl dH2O. DNA concentration was photometrically determined (cf. chapter 4.1.3).

4.2.3. Lysis of the yeast cells

In order to isolate the heavy and the light chain variable regions from each selected clone by PCR (cf. chapter 4.1.4), crude lysate of the cytoplasmic fluids were done. The lysates contained, among other, the heavy and light yeast expression vector. These lysates were used as template for the PCRs for the isolation of the variable regions of the antibodies for cloning into specific pTT5 mammalian expression plasmid. Large glob of cells from freshly growing yeast on an agar plate were mixed with 50 µl lysis buffer (chapter 3.7), incubated for 2 min at 100°C and centrifuged (21000xg, 2 min, RT). The lysate supernatants were collected by pipetting.

4.2.4. Generation and transformation of competent S. cerevisiae

Electrocompetent *S. cerevisiae* cells were prepared for the electroporation with pYD derived plasmids that enable covalent cell surface display of heterodimeric antibody Fab fragments. Fresh electrocompetent cells were prepared prior to electroporation (Benatuil et al., 2010). Briefly, one colony of *S. cerevisiae* BJ5464 or EBY100 yeast cells from YPD agar plate were grown in YPD medium to stationary phase overnight at 30 °C, 250 rpm and an aliquot of cells was used for inoculation of 400 ml YPD at an initiate 0.3 OD600 ($3x10^6$ cells per ml). An absorbance value of 1 at 600 nm corresponded to approximately 1×10^7 cells per ml, measured with the Vi-CELL XR cell counter (chapter 3.9). Cells were cultivated at 30 °C ,225 rpm until 1.5 OD600. The culture was chilled on ice for 15 min and cells were harvested by centrifugation (1600×g, 5 min, 4 °C). The cell pellets were washed three times in 30 ml ice cold dH2O following by resuspension in 50ml 1M sorbitol/1M CaCl2 solution (chapter 3.4) following by centrifugation (1600×g, 5 min, 4 °C), twice. The cell pellets were suspended with 50ml cold 1 M sorbitol solution (chapter 3.5) following by centrifugation (1600×g, 5 min, 4 °C). The cell pellets than were resuspend with 1 M sorbitol solution in concentration of $16.25x10^8$ cells per ml. Aliquots with 0.4 ml cell suspension were prepared in 1.5 ml tubes and stored at ice until transformation. The transformations were done immediately after preparation of the electrocompetent cells. For each patient's gap repair transformations of vHC or vLC fragments one aliquot of competent yeast cells were used. Cells were washed

once with 1ml of 1 M sorbitol solution followed by centrifugation (4100×rpm,1min,4°C). The pellets were resuspended with 400 µl 1 M sorbitol solution to give approximately 1.6×10^9 cells/ml and with 2 µg respective linearized plasmid HC or LC (chapter 3.3) and 6 µg of respective vHC or vLC DNA fragments. The suspensions were mixed by pipetting and transferred to a pre-chilled cuvette. Cells were electroporated with 1.5 kV, 25 µF and 200 Ω (time constants ranged from 3-4.5 ms). Directly after electroporation, cells were diluted with 1 ml of ice-cold 1.0 M sorbitol. For expansion each of the transformed cells were inoculated with appropriate 300 ml selective SD media for 48hr at 30°C,225 rpm. The cells were harvested (1600×g, 10 min, RT) and re-inoculated in appropriate 300 ml selective SD media (chapter 3.7) for 5 hr at 30°C,225 rpm. Cells then were harvested (1600×g, 10 min, RT) and resuspend in selective SD solution with final 15% glycerol (chapter 3.7) in concentration of $1x10^9$cells per ml. For transfection efficiency and library size evaluation, same appropriate dilution of cells was plated onto selective respective SD and YPD plates after transformation and after inoculation and were allowed to grow for 72 h at 30 °C. Cells were count and transfection efficiency and library size evaluation were calculated respectively.

4.2.5. Construction of Fab libraries by mating of *S. cerevisiae* cells

In order to construct the Fab yeast displayed libraries, yeast mating was performed. After construction of heavy and light chain plasmids encoding regions VH-CH1 and VL-CL, respectively, via homologous recombination in haploid EBY100 (VH-CH1) and BJ5464 (VL-CL) yeast strains. The haploid yeast cells were combined into diploid cells that display functional Fabs on their surface after mating. For Fab library generation, $1x\ 10^9$ of each 8 patients' (VH-CH1) EBY100 transformed yeast cells (MATα strain) were thawed and mixed into 400 ml SD-TRP selective media and were inoculated for 12 hr at 30 °C ,225 rpm. Respectively, $1x\ 10^9$ of each 8 patients' (VL-CL) kappa or lambda BJ5464 transformed yeast cells (MATa strain) were thawed and mixed into 400 ml SD-LEU selective media (chapter 3.7) and were inoculated for 12 hr at 30 °C ,225 rpm. $1 x\ 10^9$ of each culture were mixed together, (VH-CH1) EBY100 with (VL-CL) kappa or lambda BJ5464. Cells then were harvested (1600×g, 5 min, RT) and the pellet was resuspended in 300 µl YPD broth. The mixed cells were then spotted (50µl) in the center of a prewarmed 30 °C YPD plate. The plates were incubated at 30 °C for 19 hr. The yeast colonies were scrapped off from the plates into tube contained selective SD-Trp/-Leu media (chapter 3.7). Mated cells then of both libraries kappa and lambda were transferred to 1.4 L of SD -Trp/-Leu medium at concentration of $2.5 x\ 10^6$ cells per ml and cultivated for 48 h 25 30 °C and 225 rpm. Immediately after mating and after inoculation cells were taken for serial dilution for plating onto SD -Trp/- Leu SD- Trp and SD -Leu (chapter 3.7). Cells were allowed to grow for 72 h at 30 °C to and library size was calculated by the number of independent clones that were grown. Mating efficiency were calculated by relatively by subtraction of clone numbers that were grown on the control plates.

4.2.6. Cultivation, induction of Fab surface expression and storage of *S. cerevisiae* cells

Cultivation of S. cerevisiae yeast cells were performed for propagation as well as to induce cell surface display of antibody fragments on yeast cell surface. Propagation of cells carrying pYD-VH-CH1 and/or pYD-VL-CK, pYD-VL-CL constructs was done in minimal SD media, supplemented with drop out supplements to confirm auxotrophic phenotypes and to select transformants towards their episomally encoded marker genes (chapter 3.3)

For this, cells from plate, glycerol stoke, flow cytometry sorting or bio-panning were transferred into selective SD medium. Expansion of the culture was carried out for 24-72 h at 30 °C and 225 rpm until stationary phase was reached (OD600 of approximately 4-6). For induction and expression of antibody fragments, cells of a stationary phase SD culture were harvested and transferred to SG-Trp-Leu+50 gr/ml peptone medium (chapter 3.7) to an initiate OD600 of 1, followed by cultivation for 48 h at 20 °C and 225 rpm. Culture volumes typically varied between 10-50 ml. For storage of single clone yeast cells, cells of stationary SD cultures were centrifuged and resuspended in selective SD solution with final 15% glycerol (chapter 3.7) at 4-6 × 10^8 cells/ml. Aliquots with 1.5 ml cell suspension were prepared in 2 ml cryogenic vials and stored at -70 °C.

4.2.7. Flow cytometry binding assays using yeast surface display

Flow cytometric binding analysis was carried out at a Guava easyCyte HT cytometer or BD FACSARIA III cytometer (chapter 3.9) using corresponding software Guava ExpressPro or BD FACSDIVA™ software respectively (chapter 3.10). Flow cytometry was performed for evaluation of different recombinant cancer associated antigens binding and surface presentation of antibody Fab fragments of the yeast cells from the libraries. Briefly, cells were induced for Fab expression in 10 ml SG-Trp-Leu+50 gr/ml peptone medium (chapter 3.7) in 50 ml filtered tube at 20 °C for 48 hr. 5x10^6 cells were taken into 2 ml tube and washed with 1 ml of cold D-PBS + 0.5 % BSA (chapter 3.7) followed with centrifugation (4500×rpm,3 min,4°C). The pellets were resuspended with 50 µl DPBS with the respective concertation of biotinylated antigen, followed by incubation with rotation on RT for 20 min and on ice for 10 min. Then cells were washed with 1 ml of cold D-PBS + 0.5 % BSA (chapter 3.4) followed with centrifugation (4500×rpm,3 min,4°C). The pellets were resuspended with 50 µl with 5 µg/ml anti LC Kappa or lambda PE conjugated and 4 µg/ml SA APC conjugated (chapter 3.4.1) fluorescents markers. Followed by incubation with rotation on RT for 20 min and on ice for 10 min. Then cells were washed with 1 ml of cold D-PBS + 0.5 % BSA (chapter 3.7) followed with centrifugation (4500×rpm,3 min,4°C) twice . The cells were then resuspended with 0.5 ml DPBS and were taken for the FACS analysis. For control, yeast cells were labeled without the biotinylated antigen.

For high-throughput screening of individual clones, individual clones were grown with streaking on SD-Trp/-Leu selective plates. Each individual clone was transferred to 96 deep well plate (chapter 3.8) filled

with 0.9 ml SG-Trp-Leu+50 gr/ml peptone medium. The plate was incubated for 48 hr at 20 °C ,450 rpm with 80 % humidity. Then, 100 µl of yeast cells were transferred from the deep well plats into u-bottom well plates. The plates were centrifuged (3000×g,3 min) supernatant were removed by inversion of the plate. The plates were washed with 150 µl per well of cold D-PBS + 0.5 % BSA. Followed by centrifugation (3000×g,3 min) and the supernatants were removed by inversion of the plate. The pellets in each well was resuspended with 50 µl DPBS with the respective concertation of biotinylated antigen, followed by incubation on ice for 30 min. Then, the plates were centrifuged (3000×g,3 min) supernatant were removed by inversion of the plate. The plate washed with 150 µl per well of cold D-PBS + 0.5 % BSA, followed by centrifugation (3000×g,3 min) and the supernatant were removed by inversion of the plate. The pellets on each well were resuspended with 50 µl DPBS and anti LC Kappa or lambda PE conjugated and 4 µg/ml SA APC conjugated fluorescents markers. Followed by incubation on ice for 30 min. Then, the plates were centrifuged (3000×g,3 min) supernatant were removed by inversion of the plate and the plates washed with 150 µl per well of cold D-PBS + 0.5 % BSA. Followed by centrifugation (3000×g,3 min) and the supernatant were removed by inversion of the plate. The cells then resuspend with 150 µl per well DPBS and were taken for the GUAVA analysis. For control individual yeast clones were labeled without the biotinylated antigen.

4.4.Cell biological methods

4.2.8. Flow cytometry sorting for isolating high binders using yeast surface display

In order to sort high yeast binders from the libraries to different recombinant cancer associated antigens. Flow cytometric sorting assay was carried out at the FACS Aria III (chapter 3.9) using corresponding Diva softer (chapter 3.10). The binding of the yeast cells expressed Fab on their surface preformed as described in chapter 4.27 with exception of all the process performed under sterile condition and the amount of yeast cells for binding and sorting were between 100-250 $x10^6$ cells. After binding were performed the pellet resuspend with 1.5-3 ml respectively and were taken for the FACS Aria III for sorting. The sort was performed in 2 steps, the gated population with the top PE and APC fluorescent cells respectively were sorted. Immediately after the sort, re-sort was performed while again the gated population with the top PE and APC fluorescent cells respectively were sorted. After the re-sort the sorted cells were transferred into 50 ml filtered tube containing 5 ml SD/Trp-Leu for inculcation 24-72 h at 30 °C and 320 rpm until stationary phase was reached. In addition, appropriate diluted amount of yeast cells was plated on a selective SD-Trp/-Leu selective agar plate for clone streaking. Incubate at 30 0C, 320 rpm.

4.2.9. Bio-Panning on cancer derived cell lines using yeast surface display

In order to isolate high yeast binders from the libraries, targeting the surface displayed antigens on cancer derived cell lines, biopanning assay was carried out. Briefly, adherent cell line cultures were prepared in T80 flasks. In the first bio-panning round, 4 flasks from each cell line were seeded with

$5x10^6$ cells per flask in the appropriate growth medium (chapter 3.6) and incubated for 3 days at 37 °C with 5% CO2 until more than 80% confluency were reached. The flasks where washed twice with washing buffer (PBSCMA) (chapter 3.6) to remove all unattached cancer cells immediately before adding the yeast cells.

$2x10^9$ yeast cells of the kappa library were induced for Fab expression in 200 ml SG-Trp-Leu+50 gr/ml peptone medium (chapter 3.6) in 2L filtered tube at 20 °C for 48 hr. The yeast cells were reached a total number of ~ $20x10^9$ cells. The cells were washed with washing buffer (PBSCMA) (chapter 3.4) followed with centrifugation (2500×g,3 min). The pellets were resuspended with 40 ml washing buffer and 10 ml ($5x10^9$ cells) were transfer to each flask with the attached negative derived cell line culture (depletion). The overlaid yeast cells, were incubated for 2 hr at 20 °C. Then the unbonded yeast cells were removed and transferred respectively to 4 flasks with the specific cancer cell line culture(positive binding). Followed by incubation for 2 hr at 20 °C. After incubation the cells that didn't bind were discarded and the flasks were washed 3 times with washing buffer and 3 times with DPBS. After washing, pictures of the cancer derived cells and the yeast binders were taken using the CCD microscope camera Leica DFC3000 G (chapter 3.9) and the corresponding software Leica application suite software (chapter 3.10).The cancer derived cells and the yeast binders were removed from the flasks using 2.5 ml of 0.48 mM EDTA per flask. Cells were washed out with SD/Trp-Leu medium, centrifuged (2500×g,3 min) and the pellet were transferred into 50 ml filtered tube in 5 ml SD/Trp-Leu medium for inculcation 24-72 h at 30 °C and 320 rpm until stationary phase of the yeast cells were reached. In the next bio-panning rounds only 1 flask was used for the bio-panning rounds containing $1x10^9$ yeast cells per flask. In the 4^{th} round only $1x10^8$ yeast cells were used.

4.4.1. Cultivation of mammalian cells

All mammalian cell lines (chapter 3.2) were cultivated in tissue culture flasks of appropriate sizes (chapter 3.8), T80 or alternatively Erlenmeyer flask using the recommended media formulations (chapter 3.6) under sterile conditions at 37°C, 5% or 10% CO_2 under humidified atmosphere. Cells were certified mycoplasma-free and never exceeded passage 25.

Adherent cells were detached by 2.5ml TrypLE™ Express Enzyme (chapter 3.4) for 2-3 min at 37°C after washing with DPBS+1%BSA to remove residual serum components for cell analysis or with appropriate medium for cultivation. Cell number and viability of detached adherent cells or unprocessed suspension cells were measured by the cell counting device Vi-CELL® XR (chapter 3.9) by calculating the average of 50 images of trypan blue treated cells. For analysis, after cell pelleting (250xg, 10 min, RT), supernatants were

discarded, and cells were diluted in DPBS+1%BSA yielding appropriate cell numbers (dependent on cell line). Cell lines were testified mycoplasma free and cell culture conditions were standardized.

4.4.2. Transfection of mammalian cells and antibody expression

Antibodies were expressed by transient co-transfection of antibody chains in HEK293-EBNA cells (chapter 3.2) by electroporation using the Ingenio Electroporation kit (chapter 3.6 and 3.8) according to the manufacturer's instruction. Briefly, HEK293-EBNA cells were cultivated with starting concentration of 0.6x 10^6/ml cells in growth medium in Erlenmeyer flasks at 37°C, 5% CO_2 and 125 rpm orbital shaking for 2 days. Then, cells were counted and 40x10^6 viable cells per transfection were taken. Cells were pelleted (800xrpm,5min) washed with DPBS and pelleted again (800xrpm,5min). The pellet was resuspended with 0.25 ml Ingenio electroporation buffer per transfection and were transferred to 1.8 ml tube for each transaction. For small scale expression, 5 µg DNA (plasmid ratio: 1:1 HC:LC) and 15 µg UltraPure™ Salmon Sperm DNA Solution were added as a carrier. The suspensions were mixed by pipetting and transferred to 4mm cuvette. Cells were electroporated with 1 pulse 250V and 25msec. Immediately after electroporation 1 ml of FreeStyle 293 expression medium +0.5%FBS were added to the cuvette and cells were transferred to 20ml expression medium +0.5%FBS respectively to final concentration of 2.0x10^6 cells/ml. Then the transfected cells were incubated 37°C, 5% CO2 and 125 rpm orbital shaking for 4 hours then the temperature were reduced to 32°C for 5 days. Supernatants were harvested 5 days post transfection by centrifugation (1600xrpm, 5 min) and sterile filtration through 0.22 µm Steriflip devices.

4.4.3. Flow cytometry for cellular binding assay

Flow cytometric cellular binding analysis for the reformatted to IgG Abs was carried out at a BD FACSARIA III cytometer (chapter 3.9) using corresponding software BD FACSDIVA™ (chapter 3.10). Adherent human cell lines were detached at 70-80% confluency with TrypLE™ Express Enzymeand suspension cells were directly subjected to assays (chapter 3.4). Cells were counted with the ViCELL® XR (chapter 3.10). For the determination of antibody binding to cellular targets by flow cytometry, 1x10^6 viable cells were washed with DPBS +1% BSA pelleted at 2500xrpm (4°C, 3 min) and incubated with the appropriate concentration of crude or purified Abs (50-2000 nM) for 1 hr on ice. After washing with 1 ml DPBS +1% BSA pelleted at 2500xrpm (4°C, 3 min), antibody binding was detected via Alexa flour 488 conjugated $F(ab')_2$ donkey anti-human Fcγ specific pAb (chapter 3.4.1) after washing with DPBS +1% BSA pelleted at 2500xrpm (4°C, 3 min) cells were resuspended in 0.4 ml DPBS and analyzed in the cytometer . All incubation steps were carried out in DPBS +1% BSA buffer (chapter 3.7). For geometric mean fluorescence intensity (MFI) values, background autofluorescence values of cells treated with medium only were subtracted. For EC50 value analysis,

MFI values were plotted versus logarithm of mAb concentration and fitted by a 4PL model using GraphPad Prism 6 (chapter 3.10).

4.4.4. Fluorescence microscope for cellular binding imaging on slides

Cellular binding on cells attached to slides for the reformatted to IgG Abs and the imaging was carried out with the Olympus BX43 upright fluorescence microscope together with the Olympus DP74 color camera for fluorescence (chapter 3.9) using corresponding software cellSens Entry (chapter 3.10). Adherent human cell lines were detached at 70-80% confluency with TrypLE™ Express Enzymeand suspension cells were directly subjected to assays (chapter 3.4). Cells were counted with the ViCELL® XR (chapter 3.9). For the determination of antibody binding to cellular targets by fluorescence microscope imaging. $0.25\text{-}0.5 x 10^6$ cells were seeded on preincubated 20 µg/ml fibronectin round coverslip per well with the appropriate medium in 6 well plate (chapter 3.8) for 24 hr to 70-80% confluency. Medium were removed, and wells were washed with DPBS. Cells were then incubated for 1 hr on ice with the respective Ab (50-500 nM). Then, cells were washed with DPBS +1% BSA. After washing, 0.5 ml paraformaldehyde (4%) were added to each well for 20 min incubation at RT. After incubation, paraformaldehyde was aspirated, and cells were washed immediately with DPBS +1% BSA twice. Then, 0.5 ml of 0.1M glycine were added to each well for 10 min incubation at RT. After incubation, glycine was aspirated, and cells were washed immediately with DPBS +1% BSA twice the cells. For blocking, cells were incubated with 1 ml DPBS+3%BSA per well for 1 hr at RT and washed once with 1 ml DPBS +1% BSA. Antibody binding was detected via Alexa flour 488conjugated $F(ab')_2$ goat anti-human Fcγ specific pAb, and nuclei were stained with 0.5 µg /ml Hoechst stain solution (chapter 3.5), cells were incubated with mixed of the solutions for 40 min at RT at dark. After incubation cells were washed twice with DPBS and coverslips with the cells were attached to microscope slide with one drop of mounting medium per each coverslip. The slides were kept O.N at dark box till drying. Binding and cell nuclei staining were observed in the fluorescence microscope and imaging were taken.

4.3. Biochemical and Biophysical methods

4.3.1. Tissue procurement and tissue immunohistochemistry

Tissues were collected at Rambam Health Care Campus (Haifa, Israel) according to a protocol approved by the hospital “Helsinki” Committee, tissues were obtained from a patient with colon cancer at the time of surgical treatment. Small portion of the tissue were formalin-fixed, and the rest were flash frozen and stored until used at liquid nitrogen. For selecting tissues with high density of infiltrating B cells, formalin-fixed tissues first stained with hematoxylin and eosin for demonstrating the presence of lymphocytes within tumor tissue. Then the tissues presented high lymphocyte were stained with mouse anti-CD20 for selecting the tissues presenting high B cell density. The staining preformed at Rambam

Health Care Campus by Dr. Yaniv Zohar. The sections were scanned using the Pannoramic MIDI II i automatic digital slide scanner (chapter 3.9) at the Technion Biomedical Core Facility, Haifa, Israel.

4.3.2. Determination of protein concentration

Protein concentration were photometrically determined either by absorption at 280 nm (A_{280}) according to the law of Lambert-Beer's, by applying the UV spectrophotometer Nanodrop ND2000 (cf. chapter 3.9) while the concentration was calculated to the respective molecular weight (in kDa) and molar extinction coefficient (M-1 cm-1) of the protein

4.3.3. Protein biotinylation

Biotinylation was performed with the EZ-LinkTM NHS-PEG4-Biotin, No-Weigh Format Kit (chapter 3.8) according to the manufacturer's instructions. Incubating 0.5-1 mg protein with a 20-fold molar excess of EZ-LinkTM NHS-PEG4-Biotin reagent in PBS. Residual reagent was removed by ZebaTM Desalt Spin columns (chapter 3.8).

4.3.4. Protein A affinity purification

For purification of antibodies from supernatants of small-scale productions (25 ml, chapter 4.4.2) purification was carried out with Protein A HP SpinTrap columns (chapter 3.8) according to manufacturer's instructions using recommended buffers binding buffer, elution buffer and neutralization buffer (chapter 3.7) as well as centrifugation (100xg, 30 sec per step) after the supernatants were concentrated in a centrifuge using the Amicon® Ultra-15 centrifugal filter device with 10,000 molecular weight cut-off (MWCO; 4000xg, ~30 min) (chapter 3.8) (4000xg,RT) until reaching volume of 600 µl. Briefly, Protein A HP SpinTrap columns were equilibrated with binding buffer and 600 µl supernatants were applied on the columns followed by incubation 4 min in RT while gently mixing. Followed by two washing steps with binding buffer. Elution was carried out with 400 µl elution buffer in tubes containing 30 µl neutralization buffer in 2 steps. Eluates were concentrated and dialyzed with DPBS using Amicon® Ultra-15 centrifugal filter device with 10,000 molecular weight cut-off (MWCO; 3000xg, ~20 min) 3 times.

4.3.5. Biolayer interferometry

Biosensor experiments using biolayer interferometry were performed on an Octet Red96 platform using Octet Data Acquisition and Analysis software (cf. chapter 3.9 and 3.10) at 30°C using 1000 rpm orbital sensor agitation in a volume of 200 µl in black 96-well microplates. The physical principal of biolayer interferometry is based on the optical detection of changes within the layer thickness on biosensor tips by association and dissociation of molecules resulting in a shift in the interference pattern of reflected light. White light is thereby directed through the biosensor and is reflected once by a reference layer within the biosensor tip and secondly by the tip surface . (Rich & Myszka, 2007)

For determining the concentration of produced reformatted IgG antibodies, Dip and Read™ Anti-hIgG Fc Capture biosensor (chapter 3.8) were used. Biosensors were equilibrated in 10mM Glycine and kinetics buffer (chapter 3.8) and in the medium or buffer, in which the mAb is present, for 30 sec. Then, loading of mAbs is evaluated for 300 sec at 1000 rpm. Based on standard curves of mAbs of known concentration in the respective medium, the concentration can be calculated. For this, binding rates were calculated with the analysis software based on four parameter fitting (4PL unweighted) using the initial slope the "R equilibrium" after 300 sec.

4.3.6. Determination of mAbs binding to antigens ECD

Dip and Read™ Anti-hIgG Fc Capture biosensor were equilibrated 5 sec in 10 mM Glycine followed by 5 sec in kinetics buffer 5 times. Then, 5 µg/ml antibodies diluted in kinetics buffer were immobilized on biosensor tips for 300 sec, a baseline was recorded for 60 sec in kinetics buffer (KB) followed by stepwise association and dissociation of the analyte (serial dilution in KB) for 600 sec and 900 sec, respectively. Buffer controls were subtracted as background and binding parameters were calculated assuming a 1:1 Langmuir binding model performing global fitting algorithm provided by the Octet data analysis software.

4.3.7. Determination of mAbs binding to biotinylated antigens ECD

For evaluating binding of mAbs with the avidity affect, streptavidin biosensors were equilibrated with kinetics buffer for 300 sec. Then, 5 µg/ml biotinylated antigen ECD were captured on the streptavidin biosensor tips for 900 sec, a baseline was recorded for 60 sec in kinetics buffer (KB) followed by stepwise association and dissociation of mAbs (200nM) in kinetics buffer for 600 sec and 900 sec, respectively. As controls, the non-related isotype control mAb were implemented to exclude unspecific binding.

5. Results

5.1. Construction of yeast display antibody libraries derived from tumor infiltrating B cells of colon cancer patients

In the recent years several publications reported on constructions of tumor infiltrating B cells derived libraries, most of which are phage display libraries (Novinger et al., 2015). In this work, for the first time to our knowledge, we construct yeast display libraries from infiltrating B cells antibodies repertoire. In order to construct the libraries, RNA from tumor tissues of 8 colon cancer patients was extracted. RNA was then subjected to cDNA synthesis by RT PCR. Hypervariable V(D)J antibody regions amplification was done by PCR from cDNA templates using site-specific primers. Yeast display antibody (Fab) libraries were created utilizing the hypervariable V(D)J antibody region DNA amplification by yeast transfection and mating. A standardized protocol for collection of tissue samples procurement was developed together with pathologists from the Rambam Health Care Campus that allows the cancer tissue from a single patient to be used both as a source of high-quality RNA and also as tissue for subsequent histological analysis.

5.1.1. Selection of colon cancer tissues from patients demonstrating high B cells infiltration

Previous publications related high density of lymphocyte infiltration to the tumor with better survival (Wouters & Nelson, 2018). Therefore, in this work only tissues with high B cell infiltration were used as a source for the construction of libraries. From 40 formalin-fixed tissue specimens of colon cancer patients, which were obtained during surgical treatment at the Rambam Health Care Campus, only 8 demonstrated high immunohistochemistry staining by anti-CD20 marker. These tissues were selected as source of infiltrated B cells for libraries construction. Scans of the formalin-fixed histological sections of the 8 colon cancer patients with high B cell infiltration to the tumor are depicted in **Figure 6**. Patient demographic and clinical data of the selected tissues show diversity in gender, age, colon section and tumor grade, as summarized in **Table 3**.

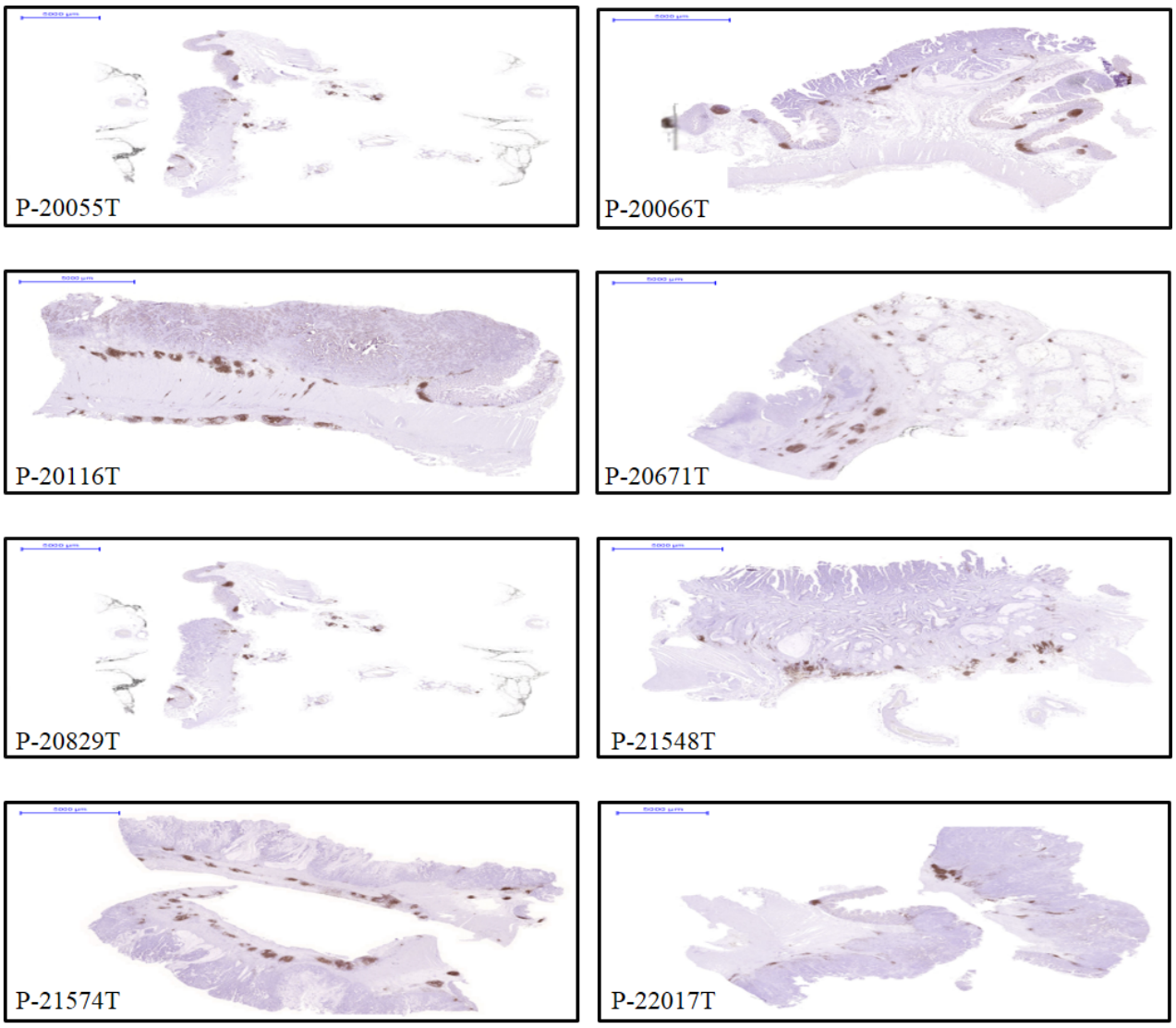

Figure 6: Anti-CD20 Immunohistochemistry staining of patients' tissue specimens with high tumor infiltrating B cells.

Formalin-fixed histological sections of the 8 colon cancer patients with high B cell infiltration to the tumor. The sections were immunohistochemistry stained with mouse anti-CD20 (Brown). Patient's reference number is represented in the left bottom corner of each image. Sections were scanned using a Panoramic MIDI digital slide scanner. Visualizations were performed using the Panoramic Viewer software. Scale bar = 5000 μm.

Patient ref Number	Age	Gender	Primary Tumor(T) [stage]	Colon section	Intertumoral Lymphocyte Response	CD20 Staining	Freezing time after surgery [min.]
P-20055T	75	F	T2	Transverse colon or right colic flexure	+	+	35
P-20066T	50	M	T1	Right flexure	+	+	22
P-20116T	85	F	T1	Sigmoid colon	+	+	40
P-20671T	63	F	T3	Cecum	+	+	35
P-20829T	76	M	T3	Cecum	+	+	40
P-21548T	89	F	T3	Ascending colon	+	+	34
P-21574T	69	M	T2	Descending colon or transverse colon	+	+	37
P-22017T	67	M	T2	Cecum	+	+	28
P-21955T	52	F	T3	Ascending colon	-	-	35

Table 3: Patients' demographic and clinical data of the compatible selected tissues.

P-21955T tissue section was used as a control tissue, as it showed no tumor B cell infiltration. All samples were snap frozen with liquid nitrogen within one hour post surgical treatment.

5.1.2. RNA isolation from tissues

RNA degradation is the main concern when performing extraction of mRNA from tumor specimens which were removed during surgical procedure. Several reports indicate that up to one hour post surgery is an adequate time to maintain non-degraded mRNA(Grizzle, Bell, & Sexton, 2011). In this work a standardized protocol for collection of tissue samples was developed together with pathologists from the Rambam Health Care Campus. Hence, successful maintaining was achieved, including rapid tissue acquisition to prevent RNA degradation (**Table 3**), together with acquisition of separate tumor pieces for subsequent histological analysis. Tissues were stored in liquid nitrogen until RNA isolation. To isolate RNA, tissues were thoroughly homogenized with a conventional rotor–stator homogenizer and further purified with a QIAGEN RNeasy Midi kit. The total RNA yields obtained from each patient's tissue are summarized in **Table 4.** The weights of tissue specimens of all patients were adequate for good total RNA yields. Absorbance ratios 260/280 and 260/230 of all extracted total RNA yields indicated relatively high purity of total RNA in all samples (Matlock, 2015). RNA yields were adequate for subsequent processing.

Patient ref number	Weight (mg)	Absorbance ratios 260/280	260/230	Total RNA (ng/µl)	Total Volume (µl)	RNA Yield (µg)
P-20055T	102	2.04	2.23	425	430	183
P-20066T	54	2.06	2.16	550	440	242
P-20116T	161	2.07	2.26	550	430	237
P-20671T	121	2.05	2.25	450	400	180
P-20829T	70	2.02	2.25	400	430	172
P-21548T	64	2.03	2.23	425	430	183
P-21574T	94	2.05	2.31	220	430	95
P-22017T	47	2.03	2.24	325	430	140
P-21955T	153	2.07	2.27	1582	400	632

Table 4: Specimen weights, yield and purity of the total RNA obtained from patients' tissues.

Total RNA yields obtained from each patient's tissue. Tissues were thoroughly homogenized with a conventional rotor–stator homogenizer and further purified with a QIAGEN RNeasy Midi kit. Weights of each patient's tissue were taken for better RNA isolation efficiency. Absorbance ratios 260/280 and 260/230 of all extracted total RNA yields indicated relatively high purity of total RNA in all samples (Matlock, 2015). RNA yields were adequate for subsequent processing.

5.1.3. Extracted total RNA quality, RNA Integrity Number (RIN) score

As the source of RNA in this work are tissues taken from patients during surgical treatment. Since RNA degradation may occur during the acquisition process it is important to ensure the quality of the extracted RNA and further the expression of the representing B cells repertoire genes (Grizzlea, Bella, & Sextonb, 2012). The integrity of RNA molecules is of paramount importance for experiments that try to reflect the snapshot of gene expression at the moment of RNA extraction. The RNA integrity number equivalent (RIN^e) provides an independent quality score for total RNA (Schroeder et al., 2006). The RIN^e score of each patient's isolated RNA was analyzed by the Agilent 2200 TapeStation. The RIN^e score for each patient together with a gel-like image of the analysis are depicted in **Figure 7**. The data analysis confirms that all the extracted RNA samples from patients partially degraded during the acquisition process (RIN^e score 4.6-7.9) but no substantial degradation with a low RIN^e score were observed. As a control, RNA was extracted from a Raji cell line and revealed a score of 8.4 RIN^e, with a score above 8 considered good RNA quality.

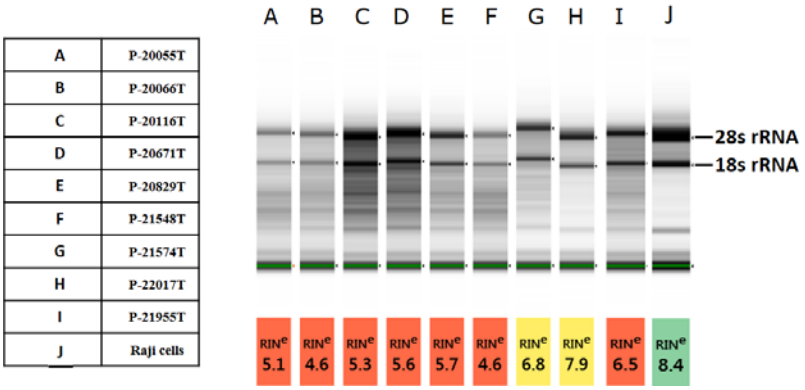

Figure 7: Analysis of total RNA integrity gel-like image.

Gel-like image of total RNA integrity, by the Agilent 2200 TapeStation, showed partial degradation in RNA extractions of all patients. Many degradation products appear between the two ribosomal bands and below the 18S band (line A-I). The control Raji cell RNA extraction sample showed high-quality total RNA with the 18S and 28S subunits as two distinct bands.

5.1.4. cDNA synthesis by RT PCR and real-time PCR for CD19 and CD20 gene expression

In order to amplify hypervariable V(D)J antibody regions site-specific primers by PCR were use. cDNA templates for each patient's tissue RNA were synthesized using the Invitrogen SuperScript™ III Reverse Transcriptase kit. Due to the partial RNA degradation during the acquisition process (chapter 5.1.3), expression levels of B cell marker genes were analyzed by real time PCR applying the comparative cT assay (Livak & Schmittgen, 2001) to verify adequate expression for further hypervariable V(D)J antibody regions amplification. cDNA from all patients and from the control sample (low B cells infiltration) were analyzed for gene expression of the B cells markers CD19 and CD20 and the house keeping RPLP0 gene was used as control gene for overall gene expression. In comparative cT assay in real time PCR, the cT values are inverse to the amount of target nucleic acid and correlate with the number of target copies in the sample. Lower cT values, typically below 29 cycles, indicate high amounts of the target sequence. Higher cT values, above 38 cycles, mean lower amounts of the target nucleic acid. As depicted in **Figure 8** there is a correlation between gene expression of CD19 and CD20 and the cT values which indicate high amount of the gene expression. The control sample showed the lowest expression of CD19 and CD20, as expected. Expression of the housekeeping gene RPLP0 was very high in all patients' cDNA (~ cT 15), as expected. Interestingly, there was no correlation found between expression of the B cells markers (CD19 and CD20) genes and the RPLP0. The correlation between the cT values and the RIN^e scores of all patient's samples are depicted in **Figure 9**. The graph shows a negative correlation between the RIN^e scores and the cT values (when one is low the other is high, and the other way around), which indicates a decrease in the expression of the housekeeping gene as a result of the RNA degradation. However, as there is no correlation between the RPLP0 expression with the CD19 and CD20 expression, it may indicate less RNA degradation of the B cells that infiltrated into the tumor relatively to the surrounding tumor tissue itself.

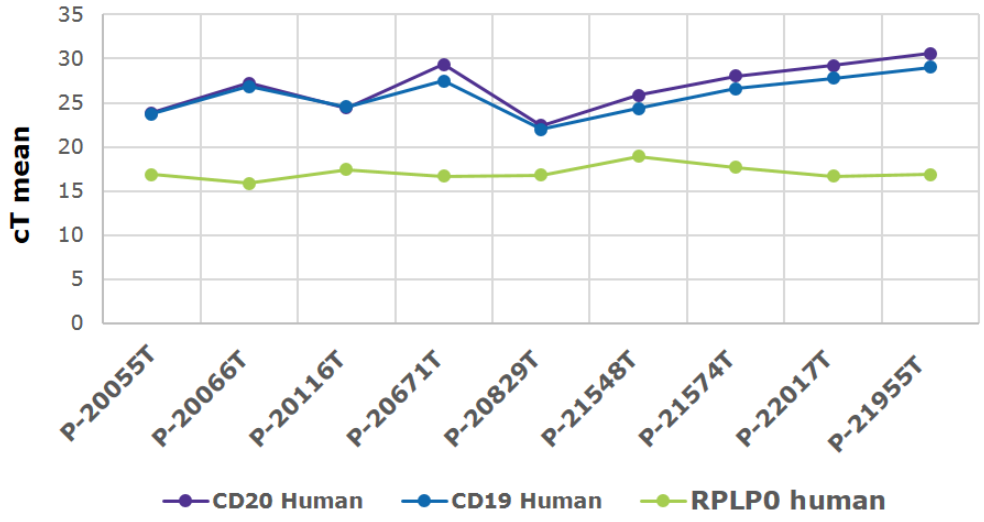

Figure 8: Real time PCR cT mean of B cells and the housekeeping RPLP0 marker genes.

cT mean from the comparative cT real time PCR assay of CD19, CD20 and the housekeeping gene RPLP0 expression of each patient's cDNA. No correlation between the expression of CD19 and CD20 genes to the RPLP0 gene is observed. CD19 and CD20 cT values indicate high gene expression. The control sample shows the lowest expression of CD19 and CD20, as expected.

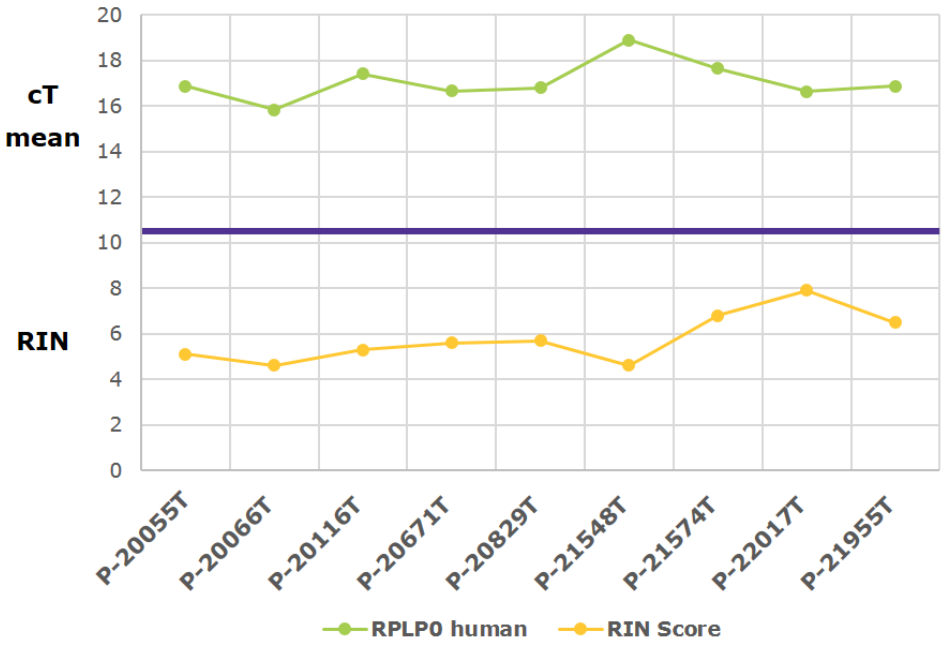

Figure 9: RIN^e score value Vs cT mean of RPLP0 gene.

A correlation between the cT value and the RINe score of each patient's sample. The graphs show a "mirror" picture: when the RINe score is low the cT value is high. This may indicate a decrease in the expression of the housekeeping gene, as a result of the RNA degradation.

5.1.5. Hypervariable V(D)J antibody region amplification by PCR

Using amplification of antibodies hypervariable region from peripheral lymphocytes of healthy individuals in order to create antibody libraries with Naïve repertoires is an established method in the recent years (Hust & Dübel, 2010). Here, tumor infiltrating B cells were derived from the patients as a source for the antibody gene pool. Amplification of VH and VL was conducted in a nested PCR approach using AccuPrime™ Taq DNA Polymerase. Antibody gene repertoire was amplified in three steps. In the first step, VH and VL were amplified using a set of subfamilies framework 1 forward primers and IgG1, kappa and lambda constant domain reverse primers. The second PCR reaction was performed to incorporate 5′ and 3′ overhangs for gap repair cloning into the pYD derived plasmids. In the third step, amplification of the second PCR was performed in order to obtain enough DNA material for the gap repair cloning reaction. Imaging of the first PCR products separated on agarose gel are depicted in **Figure 10**. Amplification of most VH and VL (kappa and lambda) subfamilies from all patients can be observed, excluding rare subfamilies that showed low amplification in all patients.

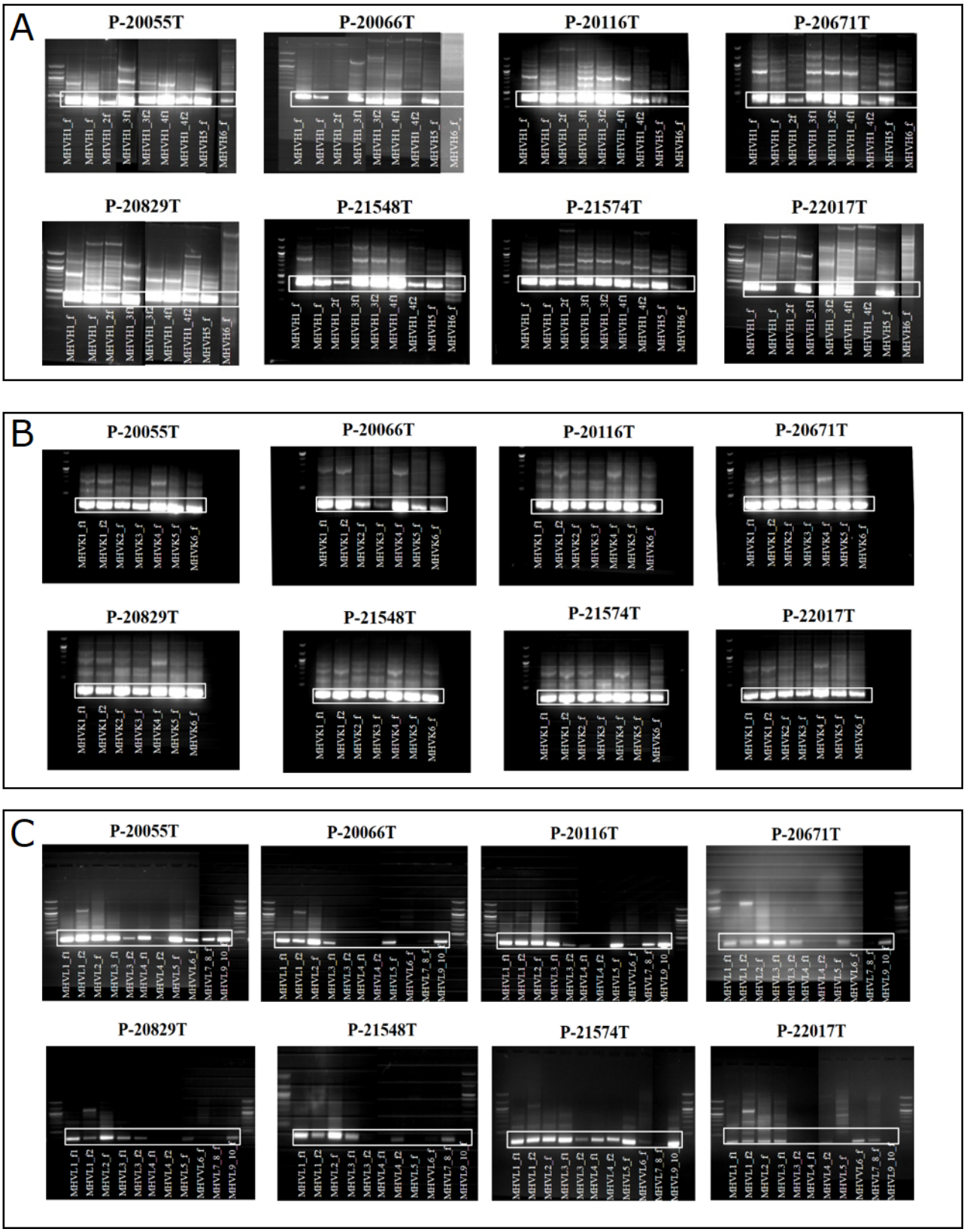

Figure 10: Agarose gel electrophoresis of first PCR VH and VL subfamilies amplification.

(A) Agarose gel electrophoresis of VH subfamilies - first PCR amplification. **(B)** Agarose gel electrophoresis of VL kappa subfamilies - first PCR amplification. **(C)** Agarose gel electrophoresis of VL lambda subfamilies - first PCR amplification. Each gel represents a patient with the reference number. Each line represents amplification with a specific subfamily primer. In general, it can be observed that most of VH and VL subfamilies were amplified, excluding rare subfamilies that showed low amplification in all patients.

5.1.6. Antibody yeast display libraries generation

Generation of the yeast display (YSD) antibody libraries in this work was based on the a-agglutinin system, initially developed by Boder and Wittrup (Boder & Wittrup, 1997). Modified pYD1 yeast surface display vectors were used: vectors for heavy chain (pYD1-VH-CH1) and light chain expression (pYD1-VL-CK or pYD1-VL-CL) were used for surface expression of Fab1-fragments, both under control of a galactose-inducible GAL1 promoter (chapter 3.3). A linkage to the yeast cell wall was conducted by a genetic fusion of Aga2p to the C-terminus of the CH1 domain, allowing for the covalent surface display of the following N-terminal fusion protein: Xpresstag-(G4S)–VH–CH1- (G4S)–His-(G4S)3-Aga2p. The light chain expression vector encoded an aMFpp8 leader sequence for soluble light chain secretion (Rakestraw, Sazinsky, Piatesi, Antipov, & Wittrup, 2009). In order to generate YSD libraries for each patient, gap repair cloning by homologous recombination in two yeast strains was employed (Bessa, Pereira, Moreira, Johansson, & Queirós, 2012). PCR products and linearized YSD plasmids from each out of 8 patients were used for generation of 24 yeast libraries (8 HC, 8 LC kappa and 8 LC lambda) (Benatuil et al., 2010). Heavy and light-chain diversities were introduced into the different haploid yeast strains, heavy chain to EBY100 (MATa) and light chain to BJ5464 (MATα), with opposite mating types, and then combined into diploid cells by yeast mating (Weaver-Feldhaus et al., 2004). **Figure 11** schematically illustrates the yeast surface display expression system of the antibody Fab fragment display on the surface of diploid *Saccharomyces cerevisiae* cells after yeast mating. Patients' libraries sizes were calculated by plating of serial dilutions, using the respective auxotrophic markers selective agar plates (-Trp or -Leu). The size of the libraries and the percentage of transfected cells is summarized in **Table 5**. For yeast mating all 8 patients' HC libraries were mixed as were also the LC kappa libraries and LC lambda libraries. These combined libraries were used for yeast mating, resulting in final library sizes of approximately 4.1×10^8 unique clones for the HC-LC kappa library (TIL-B kappa) and approximately 2.5×10^8 unique clones for the HC-LC Lambda library (TIL-B lambda).

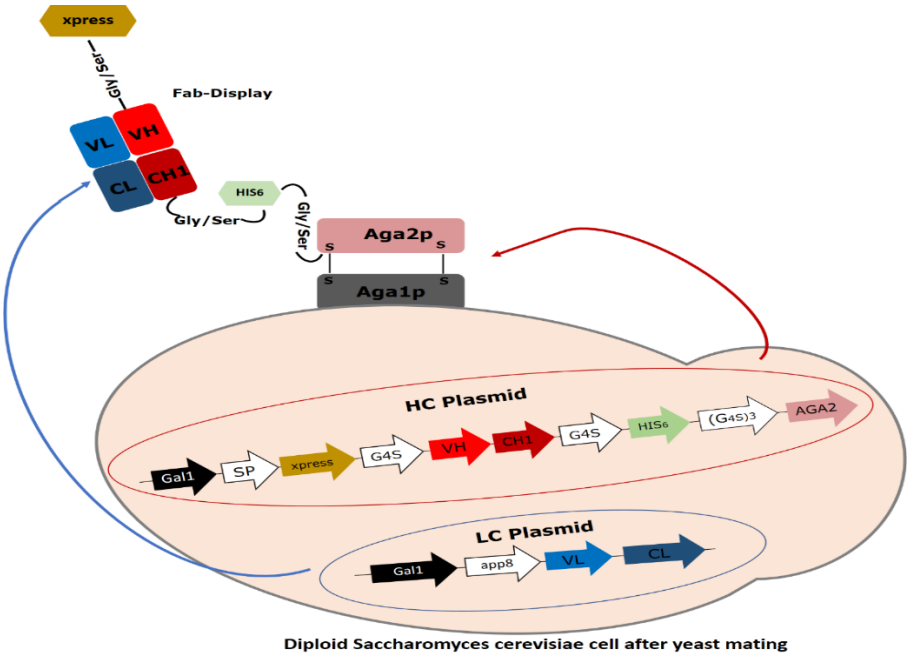

Figure 11: Schematic illustration of the yeast surface display expression system of the antibody Fab fragment display on the surface of diploid *Saccharomyces cerevisiae* cells after yeast mating.

As a result of yeast mating, diploid cells were generated, where a surface-anchored heavy chain assembles with the secreted light chain to form a Fab fragment. Fab fragments are expressed on the yeast surface as Aga2p fusions with a C-terminal His-tag and N-terminal Xpress-tag for optional detection of Fab presentation. The two single copy plasmids encode for the antibody heavy chain and the antibody light chain which contain the TRP or LEU auxotrophic markers for selection in yeast, respectively. Aga1p is chromosomally encoded by AGA1 in yeast. The heavy chain of the Fab fragment is C-terminally fused to the a-agglutinin yeast adhesion receptor protein Aga2p which assembles with the co-expressed light chain as well as with the Aga1p via two disulfide bonds. Aga1p in turn is covalently linked to β-glucan of the extracellular yeast cell matrix and anchors the heavy and light chain assembly to the cell wall. Expression of Aga1p as well as plasmid encoded proteins are under control of the inducible galactose 1 promotors.

Patient ref number	Heavy chain		Light chain kappa		Light chain Lambda	
	% transfected cells	Library size	% transfected Cells	Library size	%transfected cells	Library size
P-20055T	9.2 %	$5.1x10^7$	1.2%	$3.9x10^7$	2.9%	$4.8X10^7$
P-20066T	5.2 %	$3.6x10^7$	3%	$3x10^7$	2.5%	$3.6X10^7$
P-20116T	6.1 %	$4.7x10^7$	3.9%	$2.4x10^7$	1.9%	$5.6X10^7$
P-20671T	2.8 %	$2x10^7$	3.7%	$1.5x10^7$	3%	$5.4X10^7$
P-20829T	5.8 %	$3.5x10^7$	4%	$5.2x10^7$	2.9%	$5.1X10^7$
P-21548T	7.5 %	$2.3x10^7$	5.9%	$5.8x10^7$	1.6%	$5.3X10^7$
P-21574T	8.5 %	$2.2x10^7$	5.4%	$1.4x10^7$	2.9%	$4.3X10^7$
P-22017T	11.5 %	$3x10^7$	4.9%	$2x10^7$	2.1%	$4X10^7$

Table 5: Patients' library sizes and percentage of transfected cells.

Patients' libraries sizes were calculated by plating of serial dilutions using the respective auxotrophic markers selective agar plates SD /-TRP for the HC libraries and SD/-LEU for the LC libraries. All libraries resulted in final library sizes of 1.4-5.6x 10^7. Percentage of transfected cells were calculated relatively to the plating of serial dilutions using non-selective YPD agar plates.

5.2. Yeast display libraries screening for cancer associated antigens and immune checkpoints by flow cytometry

After the constriction of the two tumor infiltrating B cells patients derived YSD antibody libraries were completed (TIL-B kappa and lambda), the aim of this work was to evaluate the libraries for binding to the conventional researched cancer associated antigens and immune checkpoints. Hence, a panel of an extracellular domain of human cancer associated antigens and immune checkpoints were biotinylated with EZ-Link NHS-PEG4-Biotin (Chapter 4.3.3) in order to screen the YSD libraries by flow cytometry. Bivariate screening by flow cytometry was performed, including monitoring the binding of biotinylated ECD antigens to the antibody Fab fragments on cells by streptavidin Allophycocyanin (APC) conjugate marker and monitoring the display levels of antibody Fab fragments on cells by labeled PE antibodies directed against the constant region of the displayed light chain. For the screening of associated cancer antigens and immune checkpoints targeting antibodies, screening was performed using an antigen concentration of 1μM in order to observe potential high-affinity binders that will selected during flow cytometry sorting selection. Approximately 1×10^6 cells after induction were used for each antigen analysis. Total mean fluorescence intensity (MFI) of the APC marker from the gated population compared to the MFI obtained from yeast-cells labeled without the antigen (background) were chosen to predict potential high-affinity binders to some of the antigens in the tested antigen panel. Total MFI obtained from different cancer

associated antigens that were bound to the antibody Fab fragments on cells of the kappa and the lambda libraries are depicted in **Figure 12**. The data indicated that all antigen cancer associated antigens which were tested have some binders to the antibody Fab fragments on cells in both libraries (apart from TEM1 in the kappa library). In the kappa library h-5T4 and h-LRP6 had strongest total MFI, while in the lambda library h-LRP6 and h-CEACAM5 had strongest total MFI. The total MFI obtained from immune checkpoints that were bound to the antibody Fab fragments on cells of the kappa and the lambda libraries are depicted in **Figure 13**. The data indicated, that most of the immune checkpoints, unlike the antigen cancer associated antigens, which were tested had no binders to the antibody Fab fragments on cells in both libraries. In the kappa library only h-LAG-3, h-OX40L, h-TIM3 and h-CTL4 had total MFI above the background, while in the lambda library only h-OX40L and h-TIM3 had significant total MFI above the background. A display of antibody Fab fragments was observed in both libraries (data not shown).

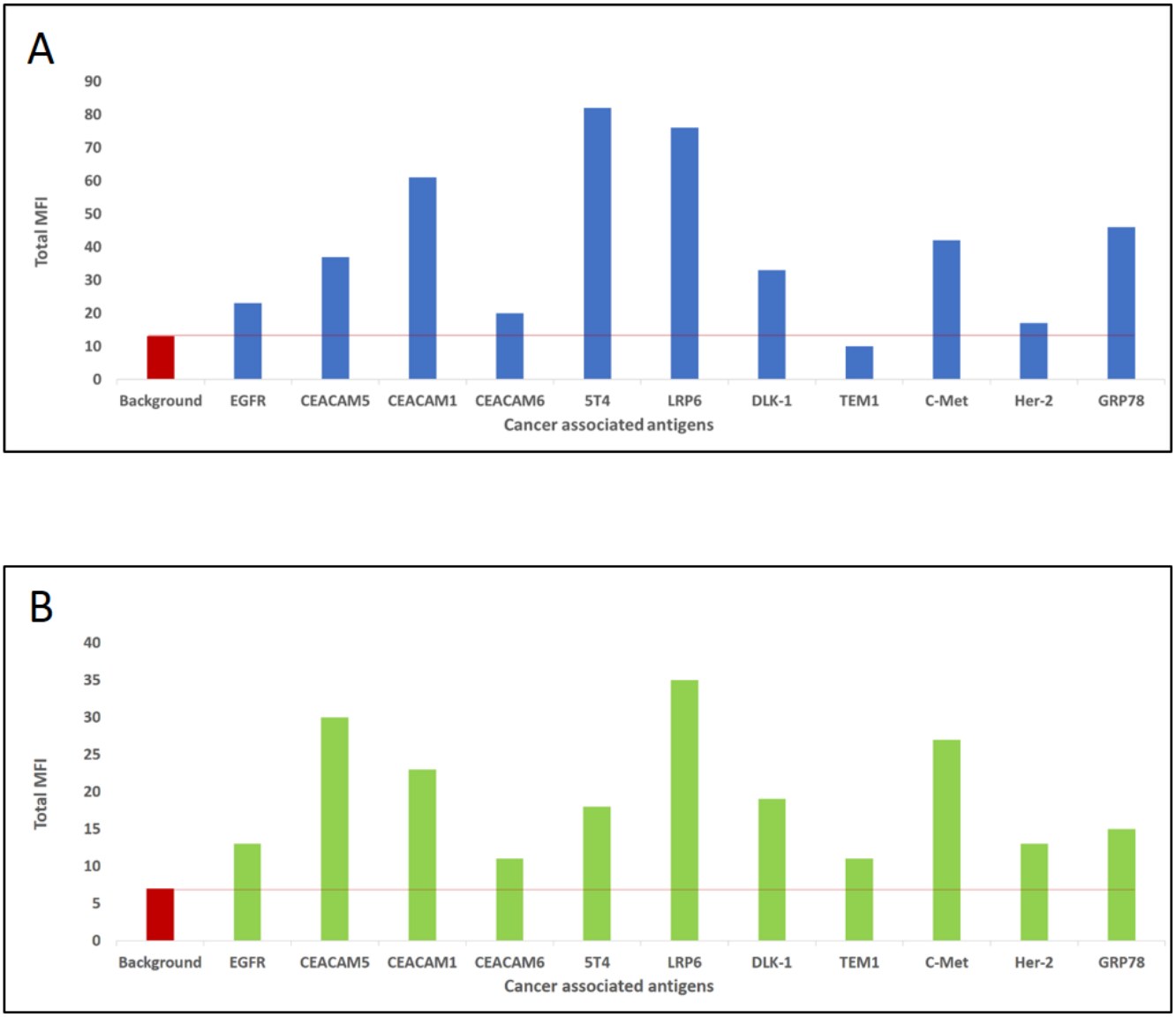

Figure 12: Screening of the TIL-B kappa and lambda yeast Fab fragments libraries for cancer associated antigens binders by flow cytometry.

(A) Total MFI obtained from different cancer associated antigens that were bound to the antibody Fab fragments on yeast-cells of the TIL-B kappa library. **(B)** Total MFI obtained from cancer associated antigens that were bound to the antibody Fab fragments on yeast-cells of the TIL-B lambda library. The red line indicates the background level of the total MFI that was obtained from cells labeled with a SA-APC marker without the biotinylated antigen.

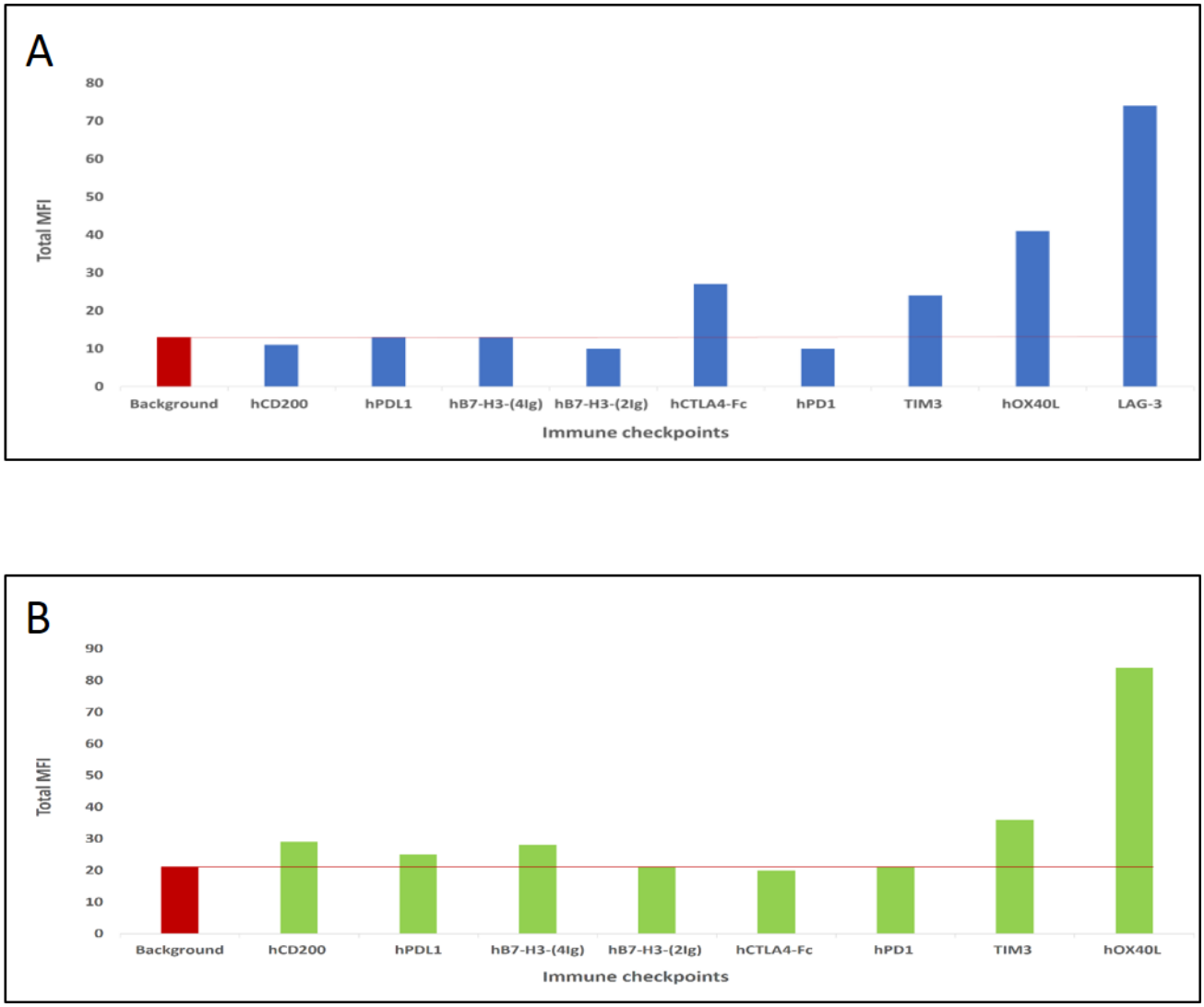

Figure 13: Screening of the TIL-B kappa and lambda yeast Fab fragments libraries for immune checkpoints binders by flow cytometry.

(A) Total MFI obtained from different immune checkpoints that were bound to the antibody Fab fragments on yeast-cells of the TIL-B kappa library. **(B)** Total MFI obtained from immune checkpoints that were bound to the antibody Fab fragments on yeast-cells of the TIL-B lambda library. The red line indicates the background level of the total MFI that was obtained from cells labeled with a SA-APC marker without the biotinylated antigen.

5.3. Selection of cancer associated antigens and immune checkpoints targeting antibodies by FACS.

Previous studies have well established the process of screening antibody repertoires from immunized transgenic rats harboring human variable antibody regions against a cancer related antigen by fluorescence-activated cell sorting (FACS) of yeast Fab displayed immune libraries (Schröter et al., 2018). In this work, to our knowledge, we were first to attempt to isolate binders to associated antigens and immune checkpoints from YSD libraries constructed based on antibody repertoires from patients' tumor infiltrating B cell repertoire. Based on screening both libraries (kappa and lambda) with a panel of cancer associated antigens and immune checkpoints (cf. chapter 5.2) two cancer associated antigens were selected, h-LRP6 and h-CEACAM5, as well two immune checkpoint targets, h-OX40L and LAG3, for the process of FACS selection. Those targets showed relatively high total MFI in the first screening for binders. This was an interesting finding, as LRP6 and CEACAM5 are considered colon cancer associated antigens (Heine et al., 2011; Rismani et al., 2017) while the libraries B cells source had been derived from colon cancer patients.

5.3.1. Selection of h-OX40L targeting antibodies by FACS sorting

The TIL-B lambda library was chosen for the sorting selection of h-OX40L targeting antibodies, based on the first screening analysis which showed that h-OX40L had relatively high total MFI binding to Fab fragments displayed on the yeast-cells surface (cf. chapter 5.2). Bivariate sorting selections by FACS were performed. Binding of the h-OX40L to the Fab fragments displayed on the yeast surface was detected by the red laser (640 nm) by the second staining step using streptavidin APC or streptavidin DyLight 633 conjugates and the display levels of antibody Fab fragments on cells were detected by the blue laser (488 nm) by incubation of cells with anti-human lambda light chain-specific goat F(ab′)2 R-PE conjugate. For that, the human h-OX40L amino acids (Gln51-Leu183) were labeled with EZ-Link NHS-PEG4-Biotin (chapter 3.5). N-Hydroxysuccinimide (NHS) esters react efficiently with primary amino groups (-NH2) by nucleophilic attack, forming an amide bond and releasing the NHS. The h-OX40L protein was labelled in the primary amine in the side chain of lysine (K) residues and the N-terminus of each polypeptide. For the sorting section the TIL-B lambda library was induced for Fab fragment surface display with SG–Trp–Leu + peptone medium at 20ºC for 48 hr. Post induction 1.5 x 10^8 cells were incubated with an initial concentration of 1µM biotinylated h-OX40L followed by incubation of the cells with SA-APC and the goat F(ab')2 anti-human lambda-R-PE (3.4.1). Cells were subjected to FACS **(Figure 14)**. The bivariate dot plot showed that 6.9% (MFI-336) of the library cells were positive to h-OX40L and 37.8% (MFI-875) of the library cells were positive to the display antibody Fab fragment on surface cells. Top 1.2% of cells positive to h-OX40L and the Fab display were sorted. A subsequent re-sort was performed immediately with the sorted cells for better selection of high affinity binders. In the re-sort the bivariate dot plot showed that 46% (MFI-500) of the library cells were positive to h-OX40L and 67.5% (MFI-823) of the library cells were positive to the display antibody Fab

fragment on surface cells. Here, top 25.4% of cells positive to h-OX40L and the Fab display were sorted. Then the sorted cells were re-grown in SD–Trp–Leu and utilized for inoculation of SG–Trp–Leu + peptone medium for induction of the Fab fragment between all subsequent sorting rounds. In the second round of sorting, antigen concentration was reduced to 0.5 µM biotinylated h-OX40L and $1x10^8$ cells were taken for the sorting. The bivariate dot plot showed an increase in the amount of the library cells that were positive to h-OX40L up to 13.9% (MFI-385) and as well an increase in the display antibody Fab fragments on surface cells, up to 48% (MFI-998). Top 1.5% of cells positive to h-OX40L and to the Fab display were sorted. In the subsequent re-sort the bivariate dot plot showed that 54% (MFI-539) of the library cells were positive to h-OX40L and 72% (MFI-822) were positive to the display of antibody Fab fragment on surface cells. Here, top 14.4% of positive cells to h-OX40L and Fab display were sorted. After the second sorting, binding analysis of yeast-cells labeled with only SA-APC and anti-lambda R-PE indicated for yeast-cells that unspecific enriched for binding to the APC marker during the sorting rounds with 5.5% yeast-cells (**Figure 15**). Hence, in order to eliminate the unspecific binders to the APC marker, antigen concentration that was reduced to 0.25 µM biotinylated h-OX40L was followed this time with SA-PE and not SA-APC detection for the third sorting. Top 3.4% of positive cells to h-OX40L were sorted. In the fourth subsequent round sorting, antigen concentration and number of cells were the same as third sorting. The bivariate dot plot showed for increasing of the library cells that were positive to h-OX40L up to 48% (MFI-710) and as well increasing in the display antibody Fab fragment on surface cells up to 57.6% (MFI-1141). Top 6.1% of positive cells to h-OX40L and Fab display were sorted. In the subsequent re-sort the bivariate dot plot showed for 78.9% (MFI-893) of the library sorted cells were positive to h-OX40L and 80.9% (MFI-1060) cells were positive to display of antibody Fab fragment on surface cells. Here, Top 22.2% of positive cells to h-OX40L and Fab display were sorted. In the last subsequent round sorting the detection marker used was SA-DyLight 633 for final polishing of the enriched unspecific yeast-cell binders to the APC marker which showed of 6% **(Figure 15).** Antigen concentration and number of cells were the same as the third sorting. The bivariate dot plot showed of 25.4% (MFI-344) of the library cells that were positive to h-OX40L and 53.2 % (MFI-1065) were positive to the display of antibody Fab fragment on surface cells. Top 2.6% of positive cells to h-OX40L and Fab display were sorted. In the subsequent re-sort the bivariate dot plot showed for 58.2% (MFI-575) of the library cells were positive to h-OX40L and 72.4% (MFI-1007) cells were positive to display of antibody Fab fragment on surface cells. Here, Top 23.1% of positive cells to h-OX40L and Fab display were sorted. After five rounds of FACS sorting, final binding analysis showed 28.9% of positive yeast-cells binders to h-OX40L (**Figure 14**) with 1.2% of unspecific binders **(Figure 15)**. Single cells were plated on SD–Trp–Leu agar plates, and yeast-cell clones were subjected to binding analysis by the Guava easyCyte HT cytometer and further sequencing procedure (single colony sequencing service at Hay labs) to identify and select clones for sub cloning and expression of full-length IgG.

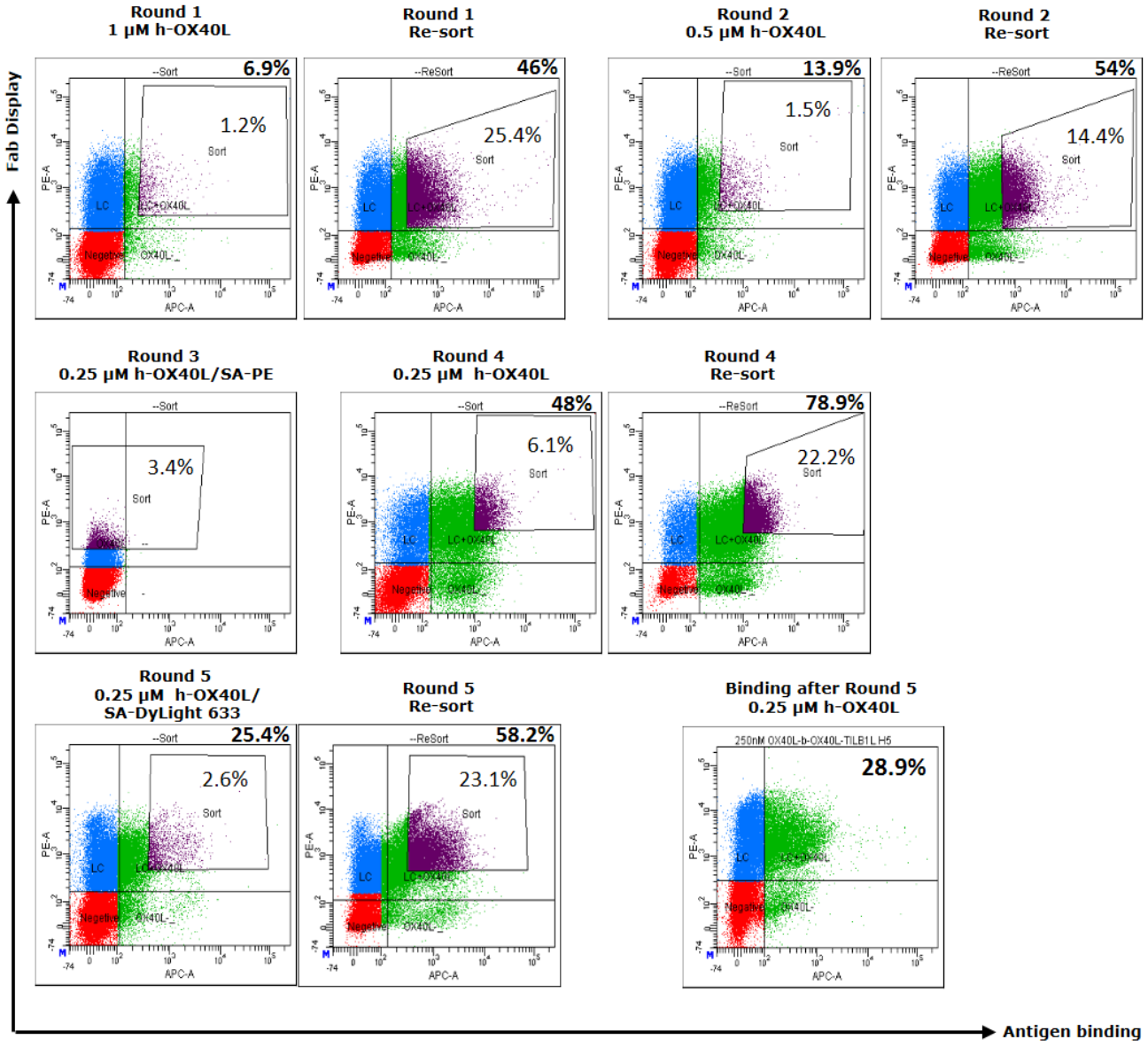

Figure 14: FACS sorting selection process of the TIL-B lambda library to h- OX40L yeast-cell binders.

FACS sorting selection process of the TIL-B lambda library. Each round was immediately followed with a re-sort for better yeast cell selection. Bivariate plots show yeast-cells labelled with biotinylated h-OX40L, SA-APC and anti-lambda R-PE for detection of surface expression display of Fab fragments during round I and II. In round III plots represent yeast-cells labelled with biotinylated h-OX40L, SA-PE for elimination of unspecific APC yeast-cell binders. In round IV biotinylated h-OX40L yeast-cells were labelled back with SA-APC. In round V sorting was performed using SA-DyLigh 633 for another round of elimination of unspecific yeast-cells binders to APC. The percentage of yeast-cells taken for each sorting round are presented in each sort gate. The percentage of the enriched yeast-cells that were positive to h-OX40L in each sorting round are presented in the right top of the dot plot images. Final analysis of the outcome of round V sorting showed 28.9% of positive yeast-cells binders to h-OX40L.

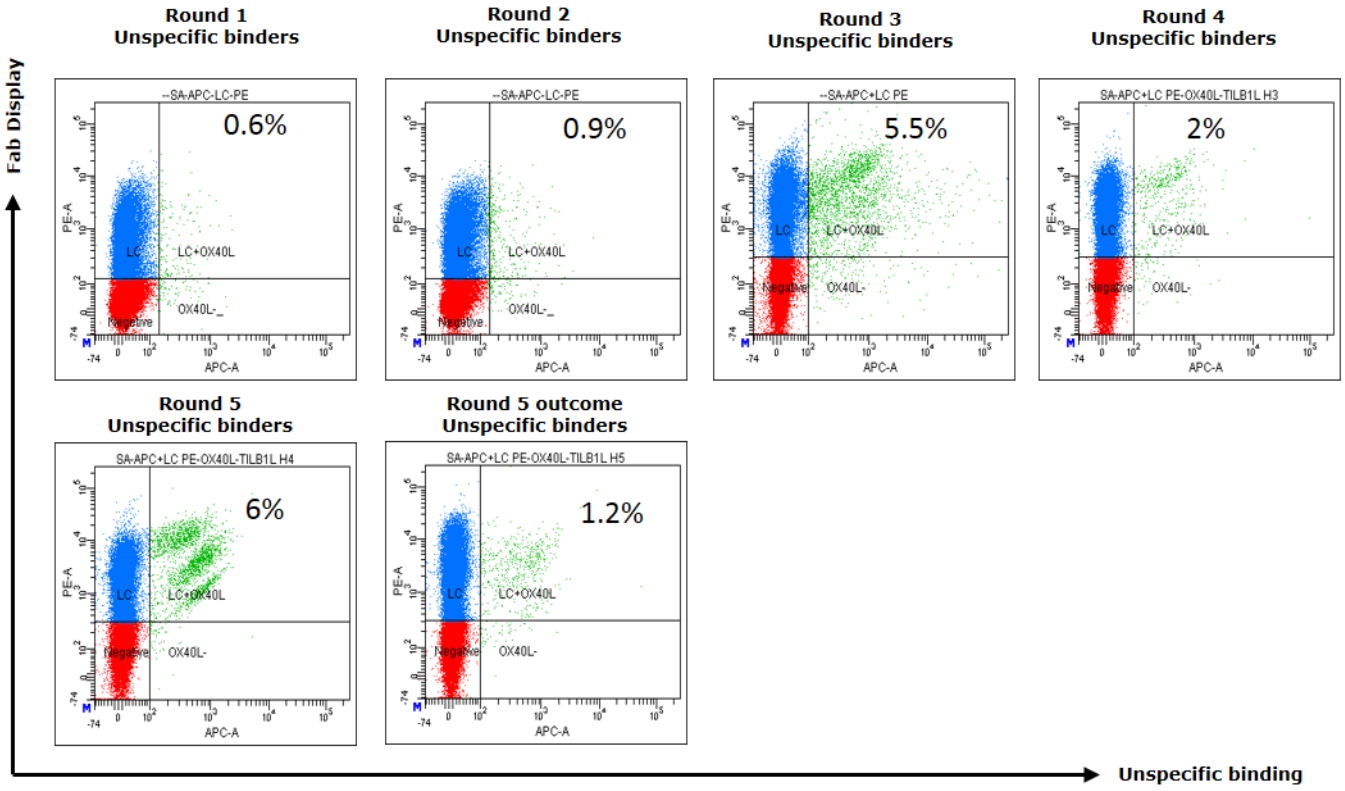

Figure 15: Unspecific binding to APC marker during FACS sorting selection process of the TIL-B lambda library to h- OX40L yeast-cell binders.

Bivariate plots of yeast-cells labeled without biotinylated h-OX40L and only with SA-APC and anti-lambda R-PE for detection of surface expression display of Fab fragment. The analysis indicated for yeast-cells that unspecific enriched for binding to the APC marker during the sorting rounds. Round III and V were performed for elimination of those binders (**Figure 14**). Analysis of the outcome of round V showed unspecific binding of 1.2% yeast-cells.

5.3.2. Selection of h-LRP6 targeting antibodies by FACS sorting

*Parts of the work in this chapter were done by Svea Becker as part of her Master thesis.

The TIL-B kappa library was chosen for the sorting selection of h-LRP6 targeting antibodies, based on the first screening analysis, which showed that h-LRP6 had relatively high total MFI binding to Fab fragments displayed on the yeast surface (cf. chapter 5.2). Bivariate sorting selections by FACS were performed the same as described with the h-OX40L sorting (chapter 5.3.1). The human h-LRP6, extracellular homologous regions domains E3-E4 was labelled with EZ-Link NHS-PEG4-Biotin same as described before (chapter 5.3.1). For the sorting section the TIL-B kappa library was induced for Fab fragment surface display with a SG–Trp–Leu + peptone medium at 20ºC for 48 hr. Post induction, 1.5 x 10^8 cells were incubated with initial concentration of 1µM biotinylated h-LRP6 followed by incubation of the cells with SA-APC and the goat F(ab')2 anti-human lambda-R-PE (chapter 3.4.1). Cells were subjected to FACS sorting (**Figure 16**). The bivariate dot plot showed that 7.3% (MFI-562) of the library cells were positive to h-LRP6 and 34% (MFI-2189) were positive to the display of antibody Fab fragment on surface cells. Top 1.4% of positive cells to h-

LRP6 and Fab display were sorted. A subsequent re-sort was performed immediately with the sorted cells for better selection of high affinity binders. In the re-sort the bivariate dot plot showed that 12.5% (MFI-480) of the library cells were positive to h-LRP6 and 46.4% (MFI-1718) were positive to the display of antibody Fab fragment on surface cells. Here, Top 6.8% of positive cells to h-LRP6 and Fab display were sorted. Sorted cells were re-grown in SD–Trp–Leu and utilized for the inoculation of SG–Trp–Leu + peptone medium for induction of Fab fragment between all subsequent sorting rounds. In the second sorting round, antigen concentration was reduced to 0.5 µM biotinylated h-LRP6 and $1x10^8$ cells were incubated. The bivariate dot plot showed reducing of the library cells that were positive to h-LRP6 up to 3% (MFI-385) with 0.5 µM antigen but increasing in the display antibody Fab fragment on surface cells up to 47.6% (MFI-2233). Top 1.9% of positive cells to h-LRP6 and Fab display were sorted. In the subsequent re-sort the bivariate dot plot showed that 49.2% (MFI-524) of the library cells were positive to h-LRP6 and 70.6% (MFI-2225) cells were positive to display of antibody Fab fragment on surface cells. Here, Top 13.8% of positive cells to h-LRP6 and Fab display were sorted. In the third sorting round, antigen concentration was reduced to 0.25 µM biotinylated h-LRP6 and again $1x10^8$ cells were incubated. The bivariate dot plot showed increasing of the library cells that were positive to h-LRP6 up to 41.2% (MFI-1003) with 0.25 µM antigen but reducing in display antibody Fab fragment on surface cells up to 40.6% (MFI-1685). Top 7.2% of positive cells to h-LRP6 and Fab display were sorted. In the subsequent re-sort the bivariate dot plot showed that 78.7% (MFI-1213) of the library cells were positive to h-LRP6 and 81% (MFI-1572) cells were positive to display of antibody Fab fragment on surface cells. Here, Top 23.7% of positive cells to h-LRP6 and Fab display were sorted. In the fourth sorting round, antigen concentration was reduced to 0.1 µM biotinylated h-LRP6 and again $1x10^8$ cells were incubated. The bivariate dot plot showed reducing of the library cells that were positive to h-LRP6 up to 25.9% (MFI-1494) with 0.1 µM antigen and as well reducing in the display antibody Fab fragment on surface cells up to 36.7% (MFI-1680). Top 2.1% of positive cells to h-LRP6 and Fab display were sorted. In the subsequent re-sort the bivariate dot plot showed that 66.5% (MFI-1313) of the library cells were positive to h-LRP6 and 75% (MFI-1572) were positive to display of antibody Fab fragment on surface cells. Here, Top 13.4% of positive cells to h-LRP6 and Fab display were sorted. After the second sorting, a binding analysis, which yeast-cells labeled without biotinylated h-LRP6 and only with SA-APC and anti-lambda R-PE, were indicated for yeast-cells that unspecific enriched for binding to the APC marker during the sorting rounds up to 42.2% (**Figure 17**).Hence, In the last sorting round, order to eliminate the unspecific binders to the APC marker, the detection marker replaced to SA-DyLight 633 for final polishing. The antigen concentration and number of cells were the same as forth sorting. The bivariate dot plot showed that 16.7% (MFI-1347) of the library cells were positive to h-LRP6 and 59.4 % (MFI-3065) of the library cells were positive display of antibody Fab fragment on surface cells. Top 1.5% of positive cells to h-LRP6 and Fab display were sorted. In the subsequent re-sort the bivariate dot plot showed that 55.4% (MFI-1694) of the library cells were positive to h-LRP6 and 76% (MFI-1007) of the library cells were positive display of antibody Fab fragment on surface cells. Here, top 16.3.1% of positive cells to h-LRP6 and Fab display were

sorted. After five rounds of FACS sorting, a final binding analysis showed 51.1% of positive yeast-cells binders to h-LRP6 (**Figure 16**) with 10% of unspecific binders (**Figure 17**). Single yeast cells were plated on SD–Trp–Leu agar plates, and yeast-cell clones were subjected to binding analysis by FACS and further sequencing procedure (single colony sequencing service at Hay labs) to identify and select clones for sub cloning and expression of full-length IgG molecules.

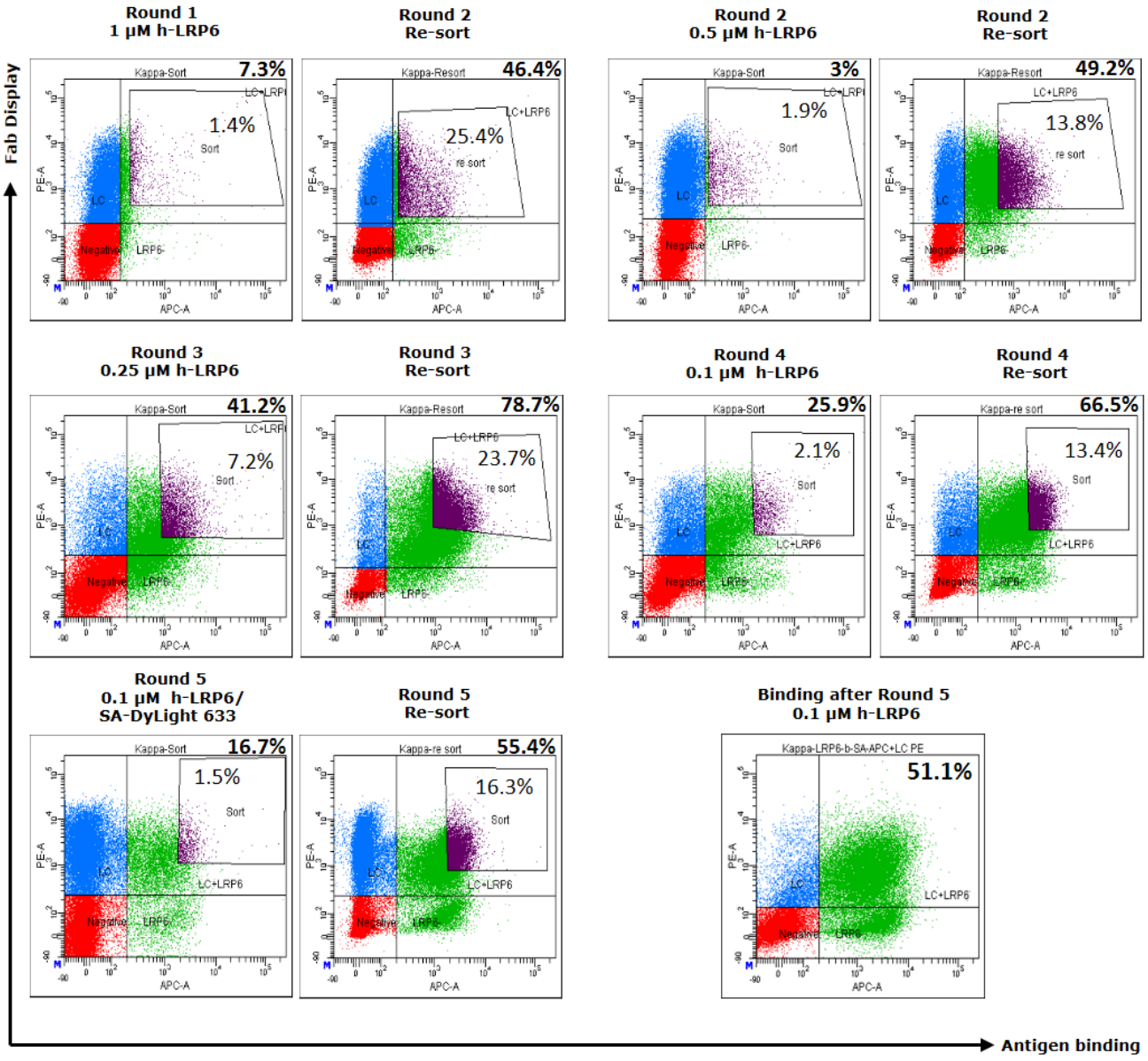

Figure 16: FACS sorting selection process of the TIL-B kappa library to h-LRP6 yeast-cell binders.

FACS sorting selection process of the TIL-B kappa library. Each round was immediately followed with a re-sort for better yeast cell selection. Bivariate plots show yeast-cells labelled with biotinylated h-LRP6, SA-APC and anti-lambda R-PE for detection of surface expression display of Fab fragment during round I-IV. In Round V sorting were performed using SA-DyLigh 633 for elimination of unspecific yeast-cells binders to APC marker. The percentage of yeast-cells were taken for each sorting round are presented in each sort gate. The percentage of the enriched yeast-cells that were positive to h-LRP6 in each sorting round are presented in the right top of the dot plot images. Final analysis of the outcome of round V sorting showed 51.1% of positive yeast-cells binders to h-LRP6.

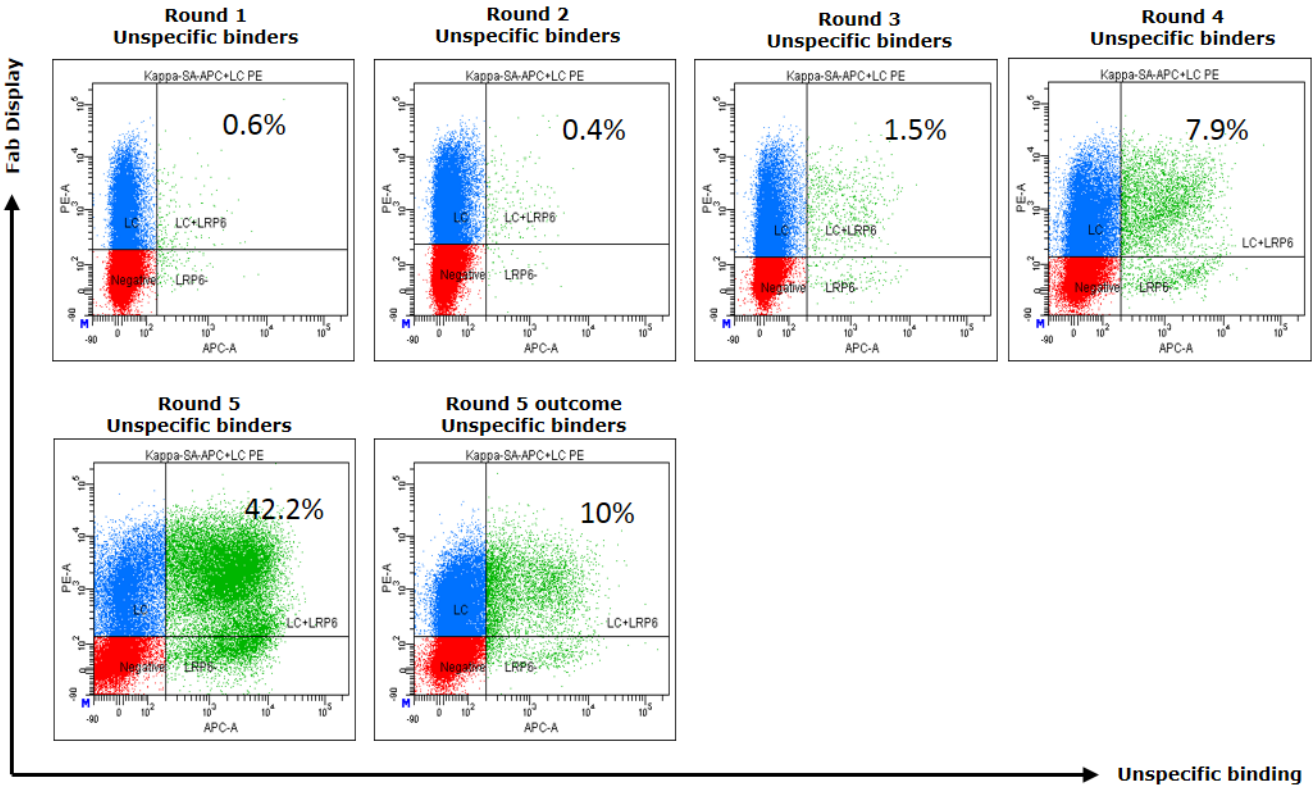

Figure 17: Unspecific binding to APC marker during FACS sorting selection process of the TIL-B kappa library to h-LRP6 yeast-cell binders.

Bivariate plots of yeast-cells labeled without biotinylated h-LRP6 and only with SA-APC and anti-lambda R-PE for detection of surface expression display of Fab fragment. The analysis indicated for yeast-cells that unspecific enriched for binding to the APC marker during the sorting rounds. Round V were performed for elimination of those binders (**Figure 16**). Final analysis of the outcome of round V showed unspecific binding of 1.2% yeast-cells.

5.3.3. Selection of h-LAG3 targeting antibodies by FACS sorting

The TIL-B kappa library was chosen for the sorting selection of h-LAG3 targeting antibodies, based on the first screening analysis, which showed that h-LAG3 had relatively high total MFI binding to Fab fragments displayed on the yeast surface (chapter 5.2). Bivariate sorting selections by FACS were performed the same as described in previous sorting (chapter 5.3.1). The human LAG3 (Leu23-Leu450) was labeled with EZ-Link NHS-PEG4-Biotin as described before (chapter 5.3.1). For the sorting section the TIL-B kappa library was induced for Fab fragment surface display with a SG–Trp–Leu + peptone medium at 20ºC for 48 hr. Post induction 1.5 x 10^8 cells were incubated with initial concentration of 1µM biotinylated h-LAG3 followed by incubation of the cells with SA-APC and the goat F(ab')2 anti-Human lambda-R-PE (3.4.1). Cells were subjected to FACS sorting (**Figure 18**). The bivariate dot plot showed that 1.1% (MFI-4639) of the library cells were positive to h-LAG3 and 26.8% (MFI-2433) were positive to the display of antibody Fab fragment on surface cells. Top 0.5% of positive cells to h-LAG3 and Fab display were sorted. A subsequent re-sort was performed immediately with the sorted cells for better selection of high affinity binders. In the re-sort the bivariate dot plot showed that 34.2% (MFI-1116) of the library cells were positive to h-LAG3 and 48.1%

(MFI-823) were positive to the display of antibody Fab fragment on surface cells. Here, Top 14.8% of positive cells to h-LAG3 and Fab display were sorted. Sorted cells were re-grown in SD–Trp–Leu and utilized for the inoculation of a SG–Trp–Leu + peptone medium for induction of Fab fragment between all subsequent sorting rounds. In the second sorting round, antigen concentration was reduced to 0.25 µM biotinylated h-LAG3 and $1x10^8$ cells were incubated. . The bivariate dot plot showed reducing of the library cells that were positive to h-LAG3 up to 4.8% (MFI-1029) with 0.25 µM antigen and increasing in the display antibody Fab fragment on surface cells up to 51.2% (MFI-2957). Top 3.3% of positive cells to h-LAG3 and Fab display were sorted. In the subsequent re-sort the bivariate dot plot showed that 27.8% (MFI-378) of the library cells were positive to h-LAG3 and 62.1% (MFI-2379) cells were positive to display of antibody Fab fragment on surface cells. Here, Top 8.9% of positive cells to h-LAG3 and Fab display were sorted. In the third sorting round, antigen concentration and number of cells that were taken for incubation were the same. The bivariate dot plot showed increasing of the library cells that were positive to h-LAG3 up to 10.7% (MFI-1072) with 0.25 µM antigen, as well as in display antibody Fab fragment on surface cells up to 58.7% (MFI-3425). Top 4.4% of positive cells to h-LAG3 and Fab display were sorted. In the subsequent re-sort the bivariate dot plot showed that 58.2% (MFI-649) of the library cells were positive to h-LAG3 and 79.8% (MFI-3025) cells were positive to display of antibody Fab fragment on surface cells. Here, Top 7.8% of positive cells to h-LAG3 and Fab display were sorted. After three rounds of FACS sorting, a final binding analysis showed 67.4% of positive yeast-cells binders to h-LAG3 (**Figure 18**) with 7.9% of unspecific binders (**Figure 19**). Single cells were plated on SD–Trp–Leu agar plates, and yeast-cell clones were subjected to binding analysis by FACS and further sequencing procedure (single colony sequencing service at Hay labs) to identify and select clones for sub cloning and expression of full-length IgG.

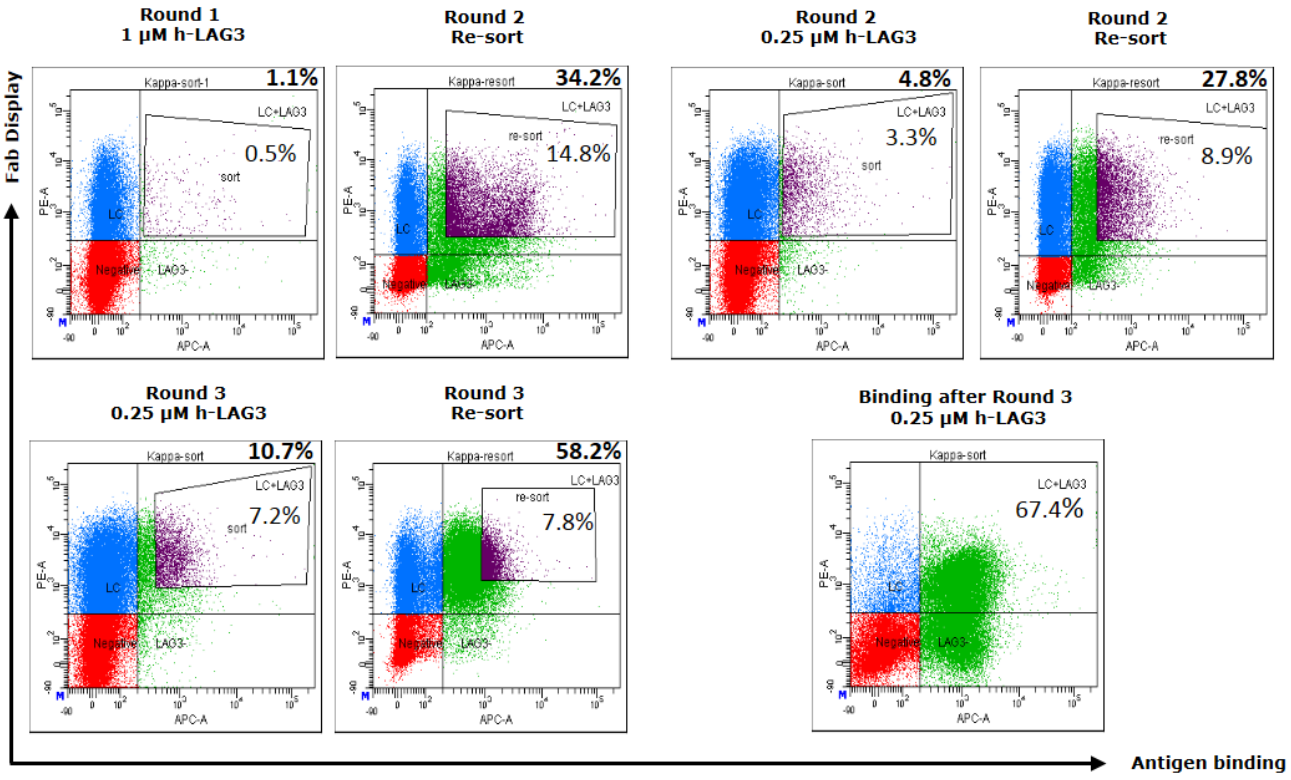

Figure 18: FACS sorting selection process of the TIL-B kappa library to h-LAG3 yeast-cell binders.

FACS sorting selection process of the TIL-B kappa library. Each round was immediately followed with a re-sort for better yeast cell selection. Bivariate plots show yeast-cells labelled with biotinylated h-LAG3, SA-APC and anti-lambda R-PE for detection of surface expression display of Fab fragment. The percentage of yeast-cells were taken for each sorting round are presented in each sort gate. The percentage of enriched yeast-cells that were positive to h-LAG3 in each sorting round are presented in the right top of the dot plot images. Final analysis of the outcome of round III sorting showed 67.4% of positive yeast-cells binders to h-LAG3.

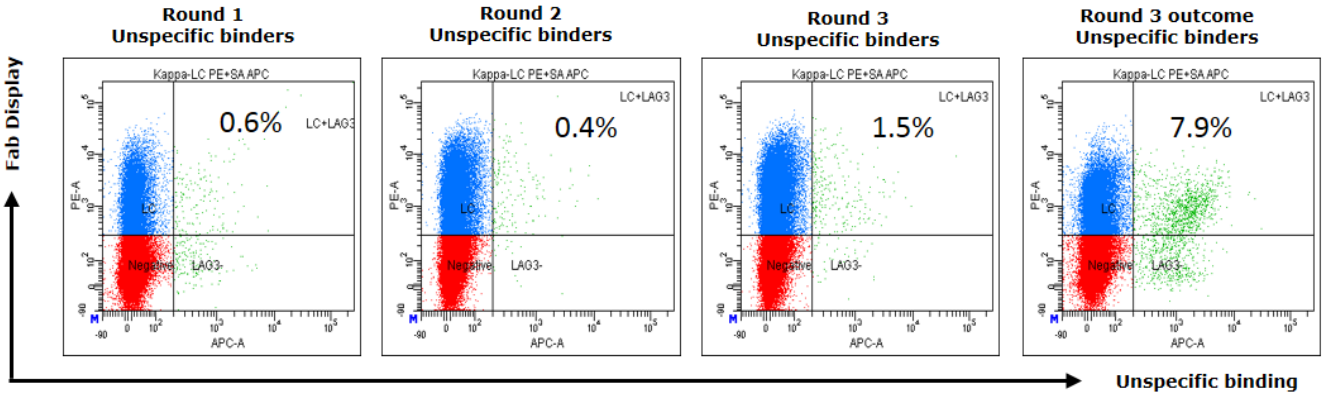

Figure 19: Unspecific binding to APC marker during FACS sorting selection process of the TIL-B kappa library to h-LAG3 yeast-cell binders.

Bivariate plots of yeast-cells labeled without biotinylated h-LAG3 and only with SA-APC and anti-lambda R-PE for detection of surface expression display of Fab fragment. The analysis indicated for yeast-cells that unspecific enriched for binding to the APC marker during the sorting rounds. Final analysis of the outcome of round III unspecific binding indicated for 7.9% yeast-cells.

5.3.4. Selection of h-CEACAM5 targeting antibodies by cell biopanning and FACS sorting

In order to improve selectivity of antibodies from the TIL-B library, this time for the h-CEACAM5 cancer associated antigen, selection of h-CEACAM5 targeting antibodies was performed with a combination of two selection processes, cell biopanning and FACS sorting. Yeast display biopanning cell-based screening of antibody libraries was previously described to successfully identify antibodies targeting cell surface antigens (Tillotson et al., 2013). The CEACAM5 antigen showed relatively high total MFI binding to a Fab fragment display on the yeast surface in the first screening analysis (chapter 5.2). Here, unlike in the previous selection approach only by FACS sorting, the selection was started with cell biopanning selection. Here the amount of the TIL-B library yeast-cells that were taken for the first-round panning were one-fold grater (~10^9), compared to the FACS sorting approach when the yeast-cells taken for the first run are limited (~10^8). The human gastric cancer derived cells line MKN-45 were chosen to be panned on. The MKN-45 cell line was previously shown to have high expression of CEACAM5 on the cell surface (Alonso-Camino, Sánchez-Martín, Compte, Sanz, & Álvarez-Vallina, 2009), which was also found in our internal experiments (data not shown). For depletion of non CEACAM5 binders, CEACAM5 CRISPR-Cas9 knockout MKN45 cells that were constructed at our labs (ITL) were used. Hence, depletion was conducted on cells that are identical to the selection strain, with the elimination of the target itself. The Fab fragment display induced TIL-B lambda yeast library (4 x10^9) were panned first against the confluent CEACAM5 CRISPR-Cas9 knockout MKN45 cells for 2 hr at RT and then immediately after the washing step the non-binders yeast-cells were panned against the confluent MKN-45 cells. After panning yeast-cells were washed and removed using EDTA. Panned cells were re-grown in an SD–Trp–Leu medium and utilized for the inoculation of the SG–Trp–Leu + peptone medium to induce a Fab fragment between all subsequent biopanning rounds. After five rounds of binding, washing, clone recovery and amplification there was clear enrichment in the number of yeast cells Fab display binding to the MKN45 cells, as compared to the panning on the depletion cells. This is shown in the light microscopy images of each biopanning round (**Figure 20**).

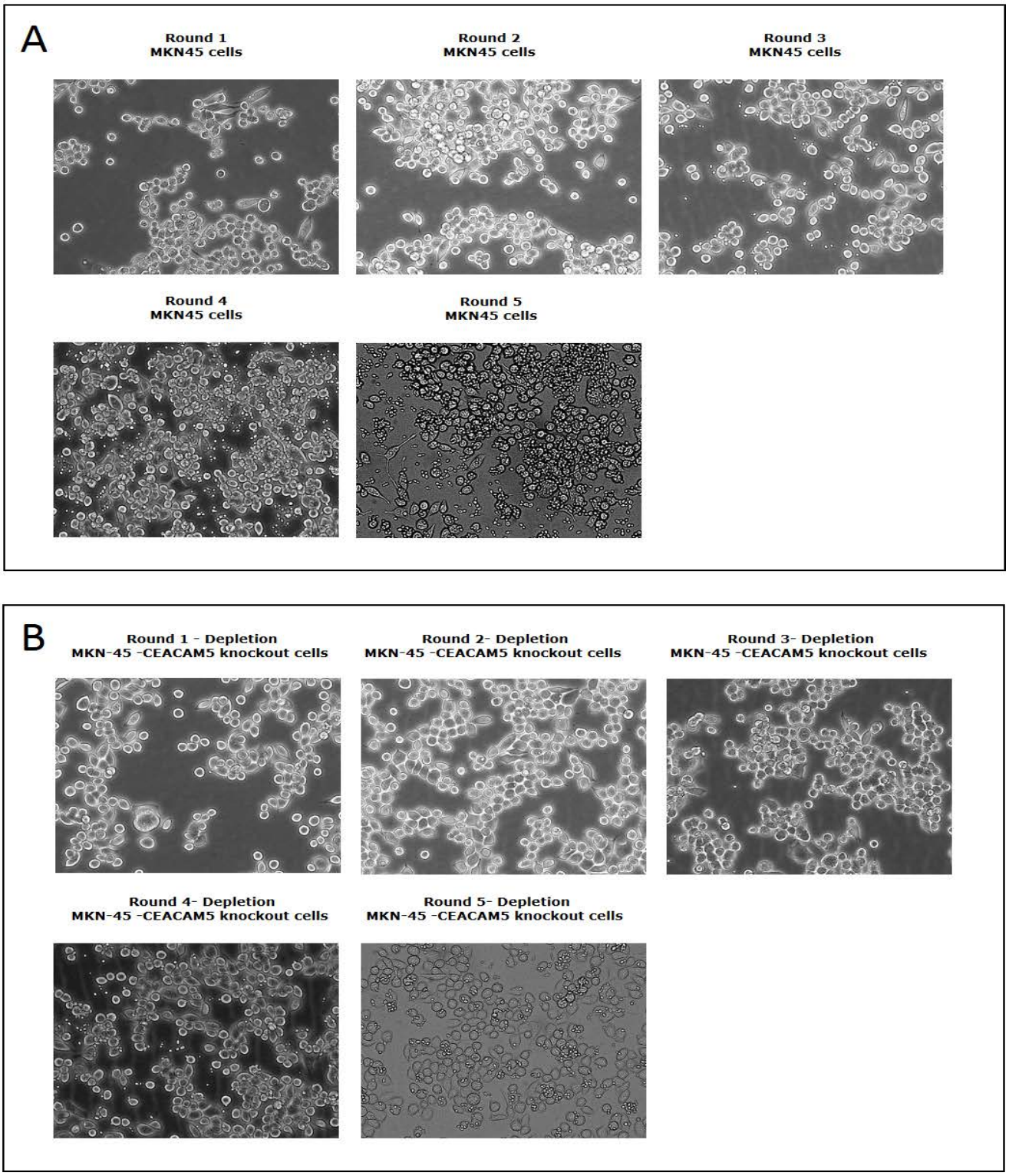

Figure 20: TIL-B lambda library biopanning rounds on MKN5 cell line and depletion rounds on CEACAM5 CRISPR-Cas9 knockout MKN45 cells.

(A) Light microscopic analysis of enrichment of the TIL-B lambda library yeast cells after each round against a confluent MKN-45 monolayer. **(B)** TIL-B lambda library yeast-cells after each round of depletion against a confluent CEACAM5 CRISPR-Cas9 knockout MKN45 cells monolayer. Scale bar, 100 µm. Yeast cells are the small objects (~5 µm) residing on the monolayer cells.

To validate the binding of the TIL-B lambda library yeast-surface display to h-CEACAM5 expressed on the surface of MKN-45 cells during biopanning rounds, the yeast-cell outputs of each round were

screened in a FACS binding analysis. The human CEACAM5 extra cellular domain was labeled with EZ-Link NHS-PEG4-Biotin, as described before (chapter 5.3.1). A bivariate binding analysis by flow cytometry was performed, as described previously (chapter 5.3.1). Then, screening was performed using an antigen concentration of 0.5µM. Approximately 1×10^6 cells were subjected to the flow cytometry analysis 48 hr post induction with a SG–Trp–Leu + peptone medium at 20ºC. The bivariate dot plot (**Figure 21**) shows an increase in positive yeast-cell binders to h-CEACAM5 from 0.6% in the initial biopanning round to 4.6% in the fourth biopanning round. The analysis in round five showed a slight reduction in the positive yeast- cells binders but with increased mean fluorescence intensity from the positive yeast cells binders.

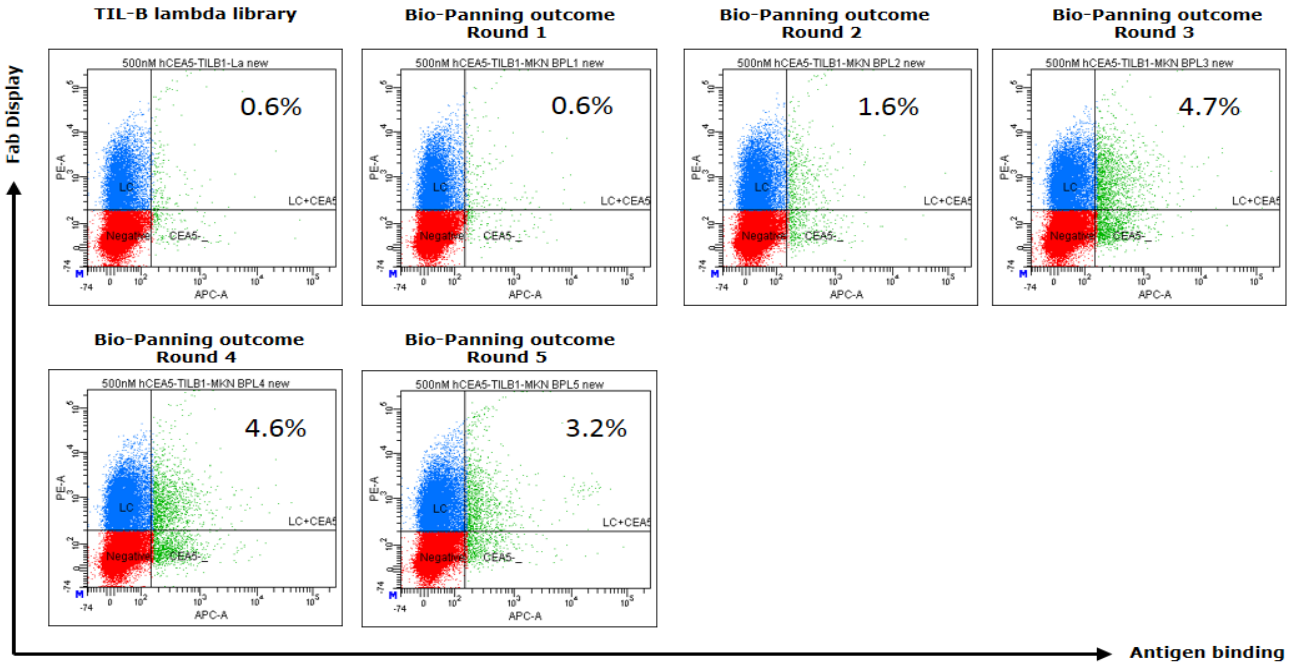

Figure 21: FACS binding screening of the yeast-cells outcome of the biopanning rounds.

Yeast-cells from each biopanning round induced for a Fab fragment display and incubated with 0.5µM biotinylated h-CEACAM5. Bivariate plots of yeast-cells labelled with SA-APC for h-CEACAM5 binders and anti-lambda R-PE for detection of surface expression display of a Fab fragment show enrichment of yeast- cells from the TIL-B lambda library to h-CEACAM5, up to 4.6 % in round IV. Round V showed slight reduction in the positive yeast- cells binders but with an increase in the mean fluorescence intensity from the positive yeast cells binders.

After the biopanning selection, while the selection was done to h-CEACAM5 that expressed on MKN-45 cell line, yeast-cells outcome from the fifth biopanning round were subjected to FACS selection using the biotinylated h-CEACAM5 in order to isolate high affinity binders. For the sorting section the yeast-cells were induced for Fab fragment surface display with a SG–Trp–Leu + peptone medium at 20ºC for 48 hr. Post induction 1.5 x 10^8 cells were incubated with initial concentration of 0.5µM biotinylated h-CEACAM5 followed by incubation of the cells with SA-APC and the Goat F(ab')2 Anti-Human lambda-R-PE (chapter 3.4.1). Cells were subjected to FACS (**Figure 22**). The bivariate dot plot showed that 8.6% (MFI-503) of the library cells were positive to h-CEACAM5 and 27.8% (MFI-2433) cells were positive to display of antibody Fab fragment on surface cells. Top 2.9% of positive cells to h-CEACAM5 and Fab display were sorted. A

subsequent re-sort performed immediately with the sorted cells for better selection of high affinity binders. In the re-sort the bivariate dot plot showed that 38.1% (MFI-399) of the library cells were positive to h-CEACAM5 and 62.5% (MFI-700) cells were positive to display of antibody Fab fragment on surface cells. Here, Top 19.3% of positive cells to h-CEACAM5 and Fab display were sorted. Sorted cells were re-grown in SD–Trp–Leu and utilized for the inoculation of SG–Trp–Leu + peptone medium for induction of Fab fragment between all subsequent sorting rounds. In the second subsequent round sorting, antigen concentration was reduced to 0.25 µM biotinylated h-CEACAM5 and $1x10^8$ cells were incubated. The bivariate dot plot showed increasing of the library cells that were positive to h-CEACAM5 up to 10.3% (MFI-450) with 0.25 µM antigen and increasing in the display antibody Fab fragment on surface cells up to 49.9% (MFI-1115). Top 5.2% of positive cells to h-CEACAM5 and Fab display were sorted. In the subsequent re-sort the bivariate dot plot showed that 15.6% (MFI-593) of the library cells were positive to h-CEACAM5 and 63.9% (MFI-2379) cells were positive to display of antibody Fab fragment on surface cells. Here, Top 7% of positive cells to h-CEACAM5 and Fab display were sorted. In the third sorting round, antigen concentration and number of cells taken for incubation were the same as previous round. The bivariate dot plot showed slight reducing of the library cells that were positive to h-CEACAM5 up to 9.7% (MFI-343) with 0.25 µM antigen but increasing in display antibody Fab fragment on surface cells up to 54.2% (MFI-1053). Top 4.4% of positive cells to h-CEACAM5 and Fab display were sorted. In the subsequent re-sort the bivariate dot plot showed that 27.3% (MFI-326) of the library cells were positive to h-CEACAM5 and 71.7% (MFI-597) cells were positive to display of antibody Fab fragment on surface cells. Here, Top 5.2% of positive cells to h-CEACAM5 and Fab display were sorted. In the fourth subsequent round sorting, antigen concentration and number of cells taken for incubation were the same as previous round. The bivariate dot plot showed slight increasing of the library cells that were positive to h-CEACAM5 up to 10.2% (MFI-514) with 0.25 µM antigen, but slight reducing in display antibody Fab fragment on surface cells up to 52.9% (MFI-975). Top 0.7% of positive cells to h-CEACAM5 and Fab display were sorted. In the subsequent re-sort the bivariate dot plot showed that 14.8% (MFI-724) of the library cells were positive to h-CEACAM5 and 59.5% (MFI-597) cells were positive to display of antibody Fab fragment on surface cells. Here, Top 1.2% of positive cells to h-CEACAM5 and Fab display were sorted. After four rounds of FACS sorting, a final binding analysis showed 12.1% of positive yeast-cells binders to h-CEACAM5 (**Figure 22**). Single cells were plated on SD–Trp–Leu agar plates, and yeast-cell clones were subjected to yeast-cell clones binding analysis by FACS and further sequencing procedure (single colony sequencing service at Hay labs) to identify and select clones for sub cloning and expression of full-length IgG.

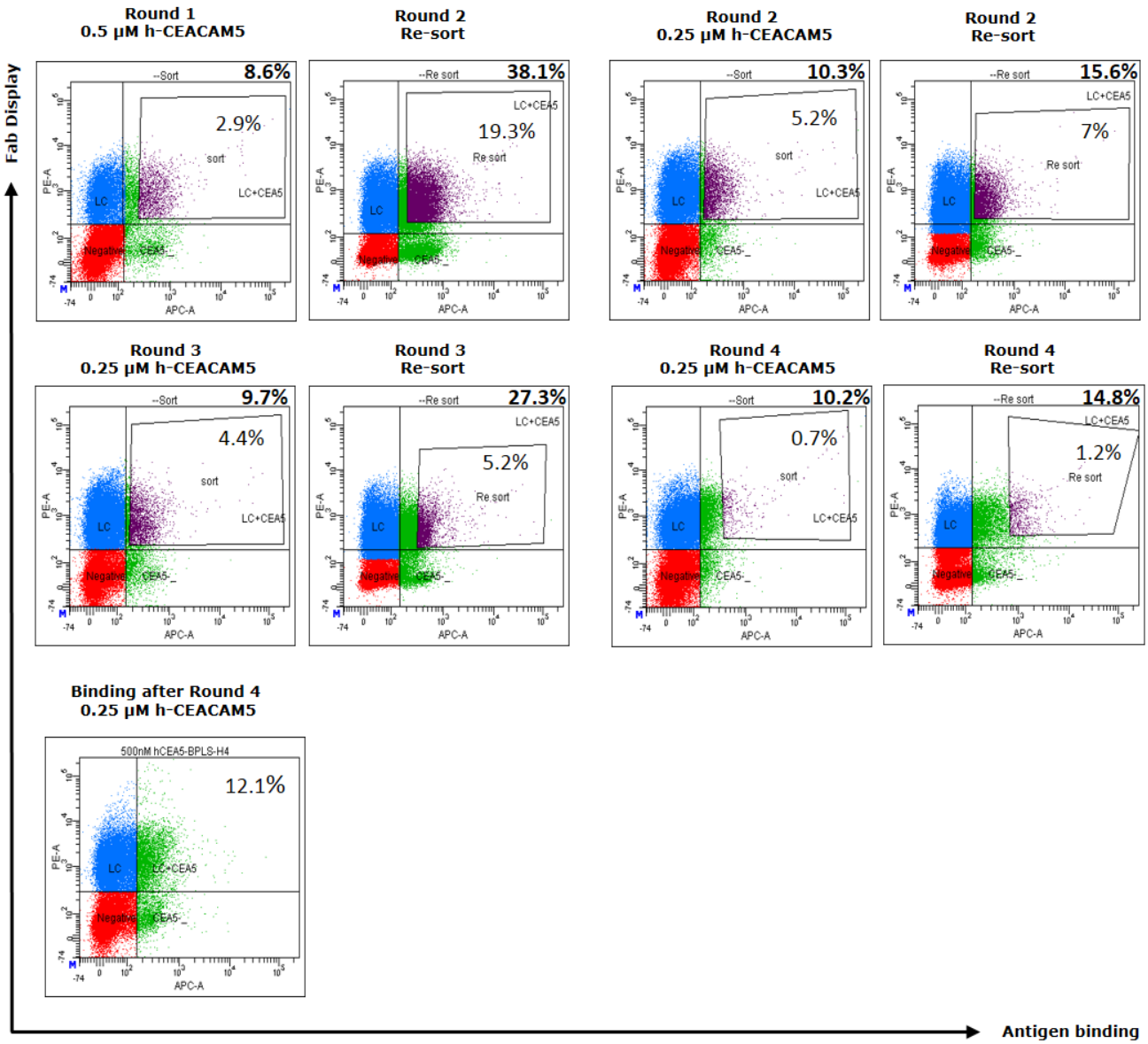

Figure 22: FACS sorting selection process of the biopanning on MKN-45 cell line outcome to h-CEACAM5 yeast-cell binders.

FACS sorting selection process of the yeast-cells biopanning on MKN-45 cell line outcome to h-CEACAM5. Each round immediately followed with a re-sort for better selection. Bivariate plots show yeast-cells labelled with biotinylated h-CEACAM5, SA-APC and anti-lambda R-PE for detection of surface expression display of Fab fragment. The Percentage of yeast-cells were taken for each sorting round are presented in each sort gate. The percentage of enriched yeast-cells that were positive to h-CEACAM5 in each sorting round are presented in the right top of the dot plot images. Final analysis of the outcome of round IV sorting showed 12.1% of positive yeast-cells binders to h-CEACAM5.

5.4. Evaluation of sorted individual yeast-cells clones: binding analysis, sequencing, formatting as IgG antibody, expression and purification

After the selection sorting process with the different TIL-B kappa library to antibodies targeting h-LRP6 and h-LAG3 and the TIL-B lambda library to antibodies targeting the h-OX40L and h-CEACAM5, single cells from the last-round sort were plated on SD–Trp–Leu agar plates and individual yeast-cell clones were picked for single yeast-cell clones binding analysis by Guava easyCyte HT cytometer or by flow cytometry binding analysis, in order to evaluate high single yeast-cell clones that bind to the antigens. Single yeast-cell clones

were induced for a Fab fragment surface display with a SG–Trp–Leu + peptone medium at 20ºC for 48 hr. The same labeling procedure, as described previously (chapter 5.2), was applied here. Then the cells were incubated with initial concentration of 0.1-0.2 µM biotinylated antigen. After individual clones were confirmed for binding to the antigen, the single clones were analyzed by sequencing their variable region frameworks and complementary determining region (CDR) diversities within the heavy and light-chain and then analyzed by Salsa analysis (Merck). Then a clustering strategy was applied, where sequences with ≥ 90% identical CDR residues were allocated to the same cluster for identification of unique clones. Functionality of the heavy and the light chain for correct expression was tasted and the heavy or the light chain were removed from subsequent analyses if the third complementarity determining region (CDR3) was of indeterminate length, stop codons were present, or the amino acid translation was out of frame. Unique clones' VH and VL regions of IgG molecules that showed specific binding to the antigen were subcloned into pTT5 plasmids (chapter 3.3). Ligation-free subcloning of VH or VL gene regions was performed by lysis and by PCR application from the yeast cell individual clones into pTT5 plasmid to generate pTT5-IgG-HC and pTT5-IgG-CL constructs, using the Expresso CMV system (chapter 3.3). This method is based on the system described previously (Bubeck, Winkler, & Bautsch, 1993) employing linearized acceptor vectors and target genes that were PCR amplified using primers containing 18 bp overlaps with the vector ends. Chemically competent One Shot Mach1™-T1R *E. coli* cells were co-transformed with both a linearized vector and amplified inserts, to allow fusion of the PCR product to the vector via homologous recombination. After sequence verification of cloned constructs, HEK293-EBNA cells were transiently transfected with expression vectors (chapter 4.4.2). Five days post transfection, antibody containing supernatants were harvested and purified by a protein A HP SpinTrap column (chapter 3.8). Purified IgG antibodies were analyzed for binding to the antigen with BLI analysis (chapter 4.3.5).

5.4.1. Evaluation of sorted individual yeast-cells clones targeting h-OX40L

After the selection sorting process of the TIL-B Lambda library with the h-OX40L immune checkpoint (cf. chapter 5.3.1), single cells from the fifth-round sort were plated on SD–Trp–Leu agar plates. Ninety-five single yeast-cell clones were picked for the single yeast-cell clones binding analysis by Guava easyCyte HT cytometer, in order to evaluate high single yeast-cell clones that bind to the h-OX40L. The 95-single yeast-cell clones were induced and labelled, as described previously (chapter 5.3.1), and then the cells were incubated with an initial concentration of 0.1µM biotinylated h-OX40L and subjected to an analysis in the Guava easyCyte HT cytometer. **Figure 23** depicts the mean fluorescence intensity (MFI) of the APC marker from the 95 yeast-cell clones that bound to the h-OX40L obtained by the Guava easyCyte HT cytometer binding analysis. All 95 yeast-cells clones had MFI above the background MFI level (yeast-cells labelled without biotinylated h-OX40L) and above the pool that the yeast-cells clones had been isolated from.

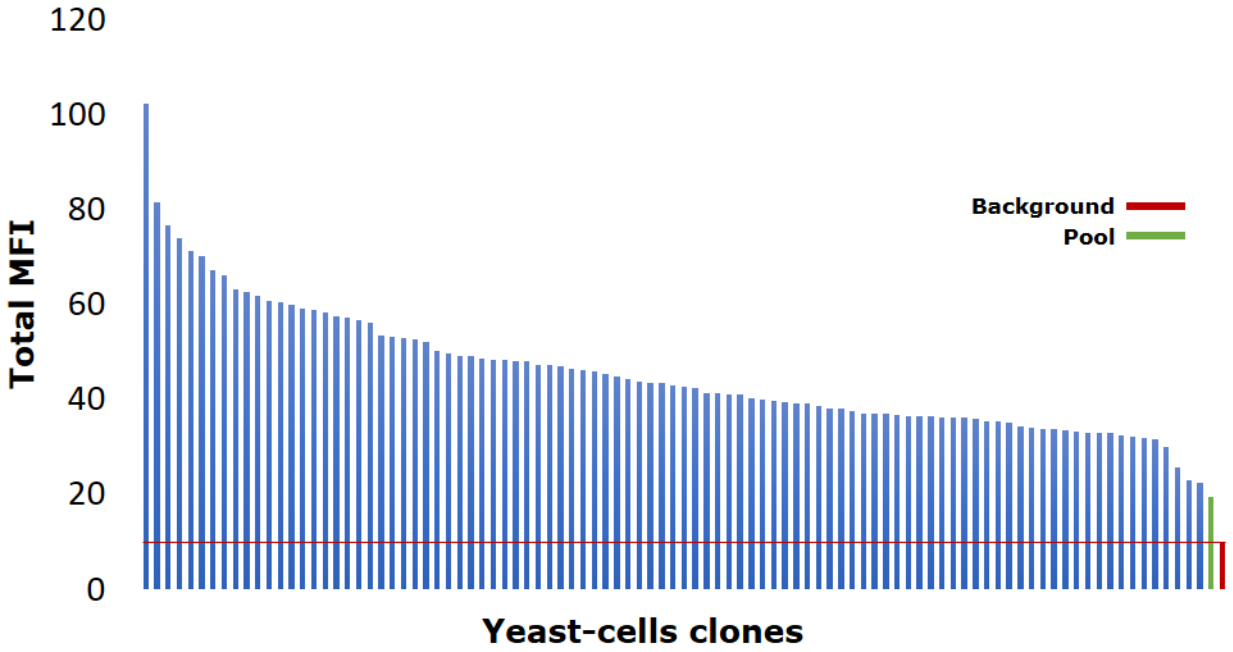

Figure 23: Binding analysis of single yeast-cell clones to h-OX40L by the Guava easyCyte HT cytometer.

Binding enrichment of individual yeast-cells clones from the TIL-B lambda library to h-OX40L. Bars represent the total MFI obtained from the biotinylated h-OX40L that were bound to the antibody Fab fragments, followed by the SA-APC marker, from the individual clones. All yeast-cells clones had higher MFI signal than the background level of the total MFI obtained from the yeast -cell clones labeled with a SA-APC marker without biotinylated h-OX40L, and from the pool that the yeast-cell clones had been isolated from.

As all yeast-cell clones bound to the h-OX40L, all single clones were sequenced and clustered as described previously (chapter 5.4). **Table 6** summarizes the unique clones that were identified by an ID name of a representative clone from all the clustered clones, the number of repeats in clustered and clone germline diversity of the heavy (VDJ) and light (VJ) gene segments with their identity percentage from the germline. Thirteen unique heavy and light chain combinations were identified and represented as unique functional clones.

Clone ID	repeats	VH-region identity (%)	VH gene	DH gene	JH gene	VL-region identity (%)	VL gene	VJ gene
A01	4	96	IGHV6-1*01	IGHD6-19*01	IGHJ3*02	92	IGLV1-51*01	IGLJ2*01
A02	26	90	IGHV1-3*01	IGHD5-12*01	IGHJ6*01	99	IGLV6-57*01	IGLJ2*01
A03	31	90	IGHV3-30*03	IGHD3-22*01	IGHJ6*02	90	IGLV1-44*01	IGLJ3*02
A06	1	100	IGHV6-1*01	IGHD5-24*01	IGHJ3*01	95	IGLV2-23*02	IGLJ2*01
A09	9	97	IGHV4-39*07	IGHD3-10*01	IGHJ6*02	93	IGLV1-40*01	IGLJ3*02
A10	1	95	IGHV6-1*01	IGHD3-10*01	IGHJ3*01	87	IGLV1-40*01	IGLJ3*02
A16	1	96	IGHV6-1*01	IGHD3-10*01	IGHJ6*02	91	IGLV3-19*01	IGLJ3*02
B07	3	91	IGHV1-3*01	IGHD5-12*01	IGHJ6*01	94	IGLV1-44*01	IGLJ3*02
B13	1	95	IGHV3-11*01	IGHD1-26*01	IGHJ6*02	95	IGLV3-21*02	IGLJ3*02
B17	1	87	IGHV4-31*03	IGHD5-24*01	IGHJ6*02	85	IGLV1-44*01	IGLJ3*02
D10	1	93	IGHV6-1*01		IGHJ4*02	88	IGLV2-14*01	IGLJ2*01
D12	1	92	IGHV3-30*04	IGHD6-19*01	IGHJ2*01	76	IGLV1-47*01	IGLJ2*01
D19	1	87	IGHV6-1*01	IGHD3-22*01	IGHJ6*02	99	IGLV6-57*01	IGLJ3*02

Table 6: Isolated unique binders to h-OX40L with their germline diversity.

Summary of the sequence clustering analysis for the individual yeast-cell clones that bind to h-OX40L.Clone ID name is a yeast clone number representative for the cluster. After clustering, 13 clones out of 95 were identified as unique. The 13 clustered sequences were verified for functional expression for both heavy and light chain to generate the functional Fab fragment. Repeats of clones in each cluster and germline diversity of the heavy (VDJ) and light (VJ) gene segments with their identity percentage from the germline are presented.

The 13 unique clones of VH an VL regions of IgG molecules that showed specific binding to the h-OX40L were subcloned into pTT5 plasmids, as described previously (chapter 5.4). After expression and purification, as described before (chapter 5.4), purified IgG1 antibodies were analyzed for binding to the antigen with BLI analysis (chapter 5.5.1).

5.4.2. Evaluation of sorted individual yeast-cells clones targeting h-LRP6

After the selection sorting process of the TIL-B kappa library with the h-LRP6 E3:E4 domain (cf. chapter 5.4.2), single cells from the fifth-round sort were plated on SD–Trp–Leu agar plates. This time, because an aggressive sorting strategy was applied during the sorting process, only 20 single yeast-cell clones were picked for single yeast-cell clones binding analysis. Here, because the unspecific binding analysis (**Figure 17**) in the last sorting round showed that 10% of the yeast- cells bound unpacifically, an unspecific binding analysis by FACS was performed, as described before (chapter 5.3.1), for each individual clone in order to

eliminate unspecific binder clones for further analysis. Exemplary histograms of relative fluorescence intensities are depicted in **Figure 24**. Only 2 clones exhibited strong binding to the SA-APC marker (A10 and A16) and were excluded from further analysis.

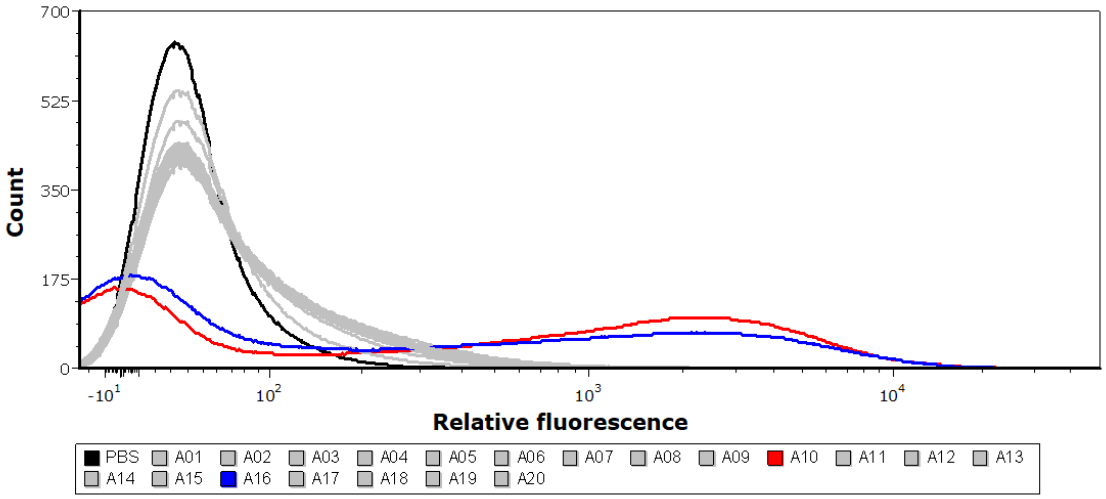

Figure 24: Unspecific binding analysis of single yeast-cell clones sorted for h-LRP6 binders.

Twenty individual clones picked from the final h-LRP6 sorting round were incubated without the biotinylated h-LRP6 but only with the SA-APC marker followed by flow cytometry. The analysis revealed 2 clones that bound strongly to the SA-APC marker (A10 and A16).

The 18 remaining yeast-cell clones were identified with specific binding to the h-LRP6. The single clones were sequenced and clustered, as described previously (Chapter 5.4). The cluster analysis revealed two unique clones. **Table 7** includes the ID name of a representative clone from the clustered clones, the number of repeats in clustered, and clone germline diversity of the heavy (VDJ) and light (VJ) gene segments with their identity percentage from the germline.

Clone ID	repeats	VH-region identity (%)	VH gene	DH gene	JH gene	VL-region identity (%)	VL gene	VJ gene
A01	17	95	IGHV3-48*01	IGHD3-22*01	IGHJ6*03	75	IGKV1-27*01	IGKJ5*01
A15	1	90	IGHV3-23*04	IGHD3-3*01	IGHJ6*02	94	IGKV2-30*01	IGKJ2*01

Table 7: Isolated unique binders to h-LRP6 with their germline diversity.

Summary of the sequence clustering analysis for the individual yeast-cell clones that bind to h-LRP6. Clone ID name is a yeast clone number representative for the cluster. After clustering, 2 clones out of 18 were identified as unique. The 2 clustered sequences were verified for functional expression for both heavy and light chains to generate a functional Fab fragment. Repeats of clones in each clustered and germline diversity of the heavy (VDJ) and light (VJ) gene segments with their identity percentage from the germline are presented.

To confirm specific binding to the h-LRP6 ligand, the 2-unique single yeast-cell clones were induced and labelled, as described previously (chapter 5.3.1). Cells were incubated with initial concentration of 0.25µM biotinylated h-LRP6 and subjected to flow cytometer for binding analysis, as described before (chapter 5.3.1). Exemplary histograms of relative fluorescence intensities are depicted in **Figure 25**. The 2 clones (A01 and A15) exhibited significant binding to the h-LRP6 antigen.

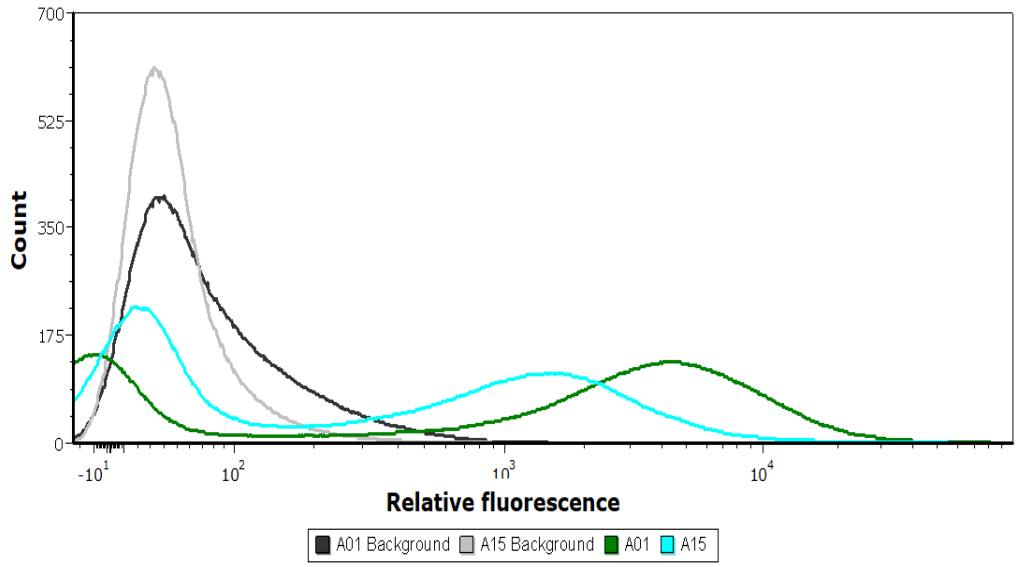

Figure 25: Binding analysis of individual yeast-cell clones sorted to h-LRP6 binding.

The two individual clones picked from the final h-LRP6 sorting round V were incubated with biotinylated h-LRP6 and labelled by the SA-APC marker, followed by flow cytometry. The analysis indicated significant binding of the unique yeast-cells clones to the h-LRP6 antigen.

The two unique clones of VH and VL regions of IgG molecules that showed specific binding to the h-OX40L were subcloned into pTT5 plasmids, as described previously (chapter 5.4). After expression and purification, as described before (chapter 5.4), purified IgG1 antibodies were analyzed for binding to the antigen with BLI analysis (chapter 5.5.2).

5.4.3. Evaluation of sorted individual yeast-cells clones targeting h-LAG3

After the selection sorting process of the TIL-B kappa library with the h-LAG3 immune checkpoint. (chapter 5.4.3), single yeast-cells from the third-round sort were plated on SD–Trp–Leu agar plates. Ninety-four single yeast-cell clones were picked for single yeast-cell clones binding analysis by Guava easyCyte HT cytometer, in order to evaluate high single yeast-cell clones that bind to the h-LAG3. The 94-single yeast-cell clones were induced and labeled as described previously (chapter 5.3.1),and then cells were incubated with initial concentration of 0.2µM biotinylated h-LAG3 and subjected to Guava easyCyte HT cytometer. **Figure 26** depicts the mean fluorescence intensity (MFI) of the APC marker indicated from the 94 yeast-cell clones that bind to the h-LAG3 obtained by the Guava easyCyte HT cytometer binding analysis. All 94 yeast-cells clones

had MFI above the background MFI level (yeast-cells labeled without biotinylated h-LAG3). Sixty-three yeast-cells clones had total MFI above the pool that the yeast-cells clones had been isolated from.

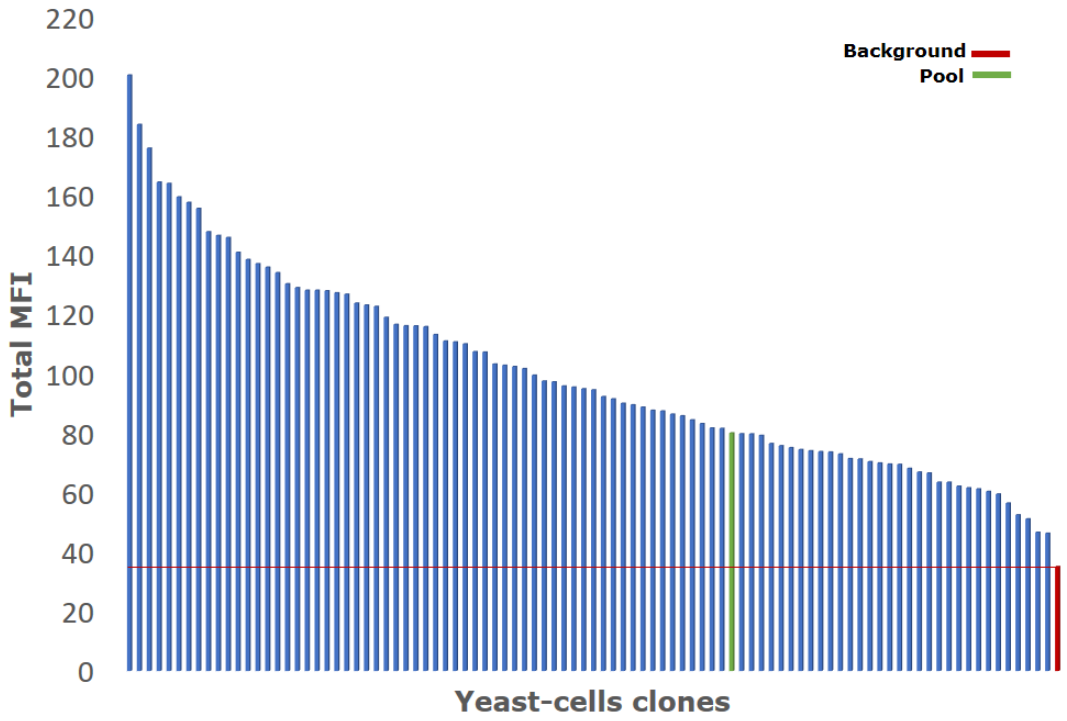

Figure 26: Binding analysis of single clones to h-LAG3 by Guava easyCyte HT cytometer.

Binding enrichment of individual yeast-cell clones from the TIL-B kappa library to h-LAG3. Bars represent the MFI obtained from the biotinylated h-LAG-3 followed by the SA-APC marker that were bind to the antibody Fab fragments on the individual clones. All yeast-cells clone indicated for high MFI signal than the background level of total MFI that obtained from yeast-cells labeled with SA-APC marker without biotinylated h-LAG-3. Sixty-three yeast-cell clones indicated for high total MFI than the pool yeast-cell clones were isolated from.

As all yeast-cell clones bound to the h-LAG3, all the single clones were sequenced and clustered as described previously (chapter 5.4). **Table 8** summarizes the 18 unique clones that were identified by an ID name of a representative clone from all the clustered clones, the number of repeats in clustered and clone germline diversity of the heavy (VDJ) and light (VJ) gene segments with their identity percentage from the germline.

Clone ID	repeats	VH-region identity (%)	VH gene	DH gene	JH gene	VL-region identity (%)	VL gene	VJ gene
A04	5	92	IGHV3-30*03	IGHD4-17*01	IGHJ4*02	95	IGKV2-30*01	IGKJ1*01
A12	11	90	IGHV3-9*01	IGHD5-24*01	IGHJ6*02	90	IGKV3-20*01	IGKJ2*01
A13	3	95	IGHV3-30-3*01	IGHD3-3*01	IGHJ6*02	92	IGKV1-27*01	IGKJ2*01
A17	2	91	IGHV3-23*04	IGHD3-3*01	IGHJ6*02	89	IGKV4-1*01	IGKJ2*01
A22	1	92	IGHV4-61*02	IGHD5-12*01	IGHJ4*02	89	IGKV4-1*01	IGKJ2*01
A23	9	92	IGHV3-23*04	IGHD5-18*01	IGHJ1*01	88	IGKV3-15*01	IGKJ4*01
B06	1	93	IGHV3-33*05	IGHD3-22*01	IGHJ3*02	88	IGKV2-28*01	IGKJ5*01
B23	1	90	IGHV5-51*03	IGHD3-22*01	IGHJ6*01	82	IGKV2-28*01	IGKJ5*01
B24	1	96	IGHV3-30*18	IGHD3-3*01	IGHJ6*02	84	IGKV1-12*01	IGKJ4*02
C02	1	83	IGHV1-2*02	IGHD6-19*01	IGHJ5*02	92	IGKV1-8*01	IGKJ1*01
C06	1	85	IGHV4-59*01		IGHJ6*03	95	IGKV2-28*01	IGKJ5*01
C09	35	84	IGHV3-21*01	IGHD4-17*01	IGHJ3*01	87	IGKV3-11*01	IGKJ5*01
C17	2	91	IGHV3-30*03	IGHD4-17*01	IGHJ1*01	88	IGKV3-20*01	IGKJ2*01
D01	1	91	IGHV3-48*01	IGHD3-22*01	IGHJ6*02	91	IGKV1-9*01	IGKJ2*02
D03	1	95	IGHV3-64*05	IGHD3-22*01	IGHJ3*01	91	IGKV1-39*01	IGKJ2*01
D05	1	88	IGHV4-34*01	IGHD3-22*01	IGHJ3*01	94	IGKV1-9*01	IGKJ4*01
D10	1	95	IGHV6-1*01		IGHJ4*02	91	IGKV3-20*01	IGKJ4*01
D19	1	93	IGHV3-53*01	IGHD3-22*01	IGHJ3*02	95	IGKV2-30*01	IGKJ1*01

Table 8: Isolated unique binders to h-LAG3 with their germline diversity.

Summary of the sequence clustering analysis for the individual yeast-cell clones that bind to h-LAG3. Clone ID name is a yeast clone number representative for the cluster. After clustering, 18 clones out of 95 were identified as unique. The 18 clustered sequences were verified for functional expression for both heavy and light chains to generate functional Fab fragment. Repeats of clones in each clustered and germline diversity of the heavy (VDJ) and light (VJ) gene segments with their identity percentage from the germline are presented.

The 18 unique clones VH an VL regions of IgG molecules that showed specific binding to the h-LAG3 were subcloned into pTT5 plasmids , as described previously (chapter 5.4). After expression and purification, as described before (chapter 5.4), purified IgG1 antibodies were analyzed for binding to the antigen with BLI analysis (cf. Chapter 5.5.3).

5.4.4. Evaluation of sorted individual yeast-cells targeting h-CEACAM5

After the selection sorting process with the TIL-B Lambda library with the h-CEACAM5 ECD (chapter 5.4.4), single yeast-cells from the fourth-round sort were plated on SD–Trp–Leu agar plates. This time, because the selection was started with biopanning on MKN45 cell line followed by selection by FACS sorting strategy, only 10 single yeast-cells clones were picked. The single clones were sequenced and clustered as described previously (chapter 5.4). **Table 9** summarized the two unique clones that were identified by an ID name of a representative clone from all the clustered clones, the number of repeats in clustered and clone germline diversity of the heavy (VDJ) and light (VJ) gene segments with their identity percentage from the germline

Clone ID	repeats	VH-region identity (%)	VH gene	DH gene	JH gene	VL-region identity (%)	VL gene	VJ gene
A01	7	88	IGHV3-7*01	IGHD1-14*01	IGHJ4*02	87	IGLV3-19*01	IGLJ5*01
A03	3	89	IGHV3-30*03	IGHD2-15*01	IGHJ4*02	93	IGLV7-46*01	IGLJ3*02

Table 9: Isolated unique binders to h-CEACAM5 with their germline diversity.

Summary of the sequence clustering analysis for the individual yeast-cell clones that bind to h-CEACAM5. Clone ID name is a yeast clone number representative for the cluster. After clustering, 13 clones out of 95 were identified as unique. The 2 clustered sequences were verified for functional expression for both heavy and light chains to generate functional Fab fragment. Repeats of clones in each clustered and germline diversity of the heavy (VDJ) and light (VJ) gene segments with their identity percentage from the germline are presented.

To confirmed specific binding to the h-CEACAM5 ECD, the 2-unique single yeast-cell clones were induced and labeled as described previously **(chapter 5.3.1)**, cells were incubated with initial concentration of 0.25µM biotinylated h-CEACAM5 and subjected to flow cytometer for binding analysis. Exemplary histograms for relative fluorescence intensities are depicted in **Figure 27**. Clone A01 exhibited significant differential binding to h-CEACAM5 compared to clone A03.

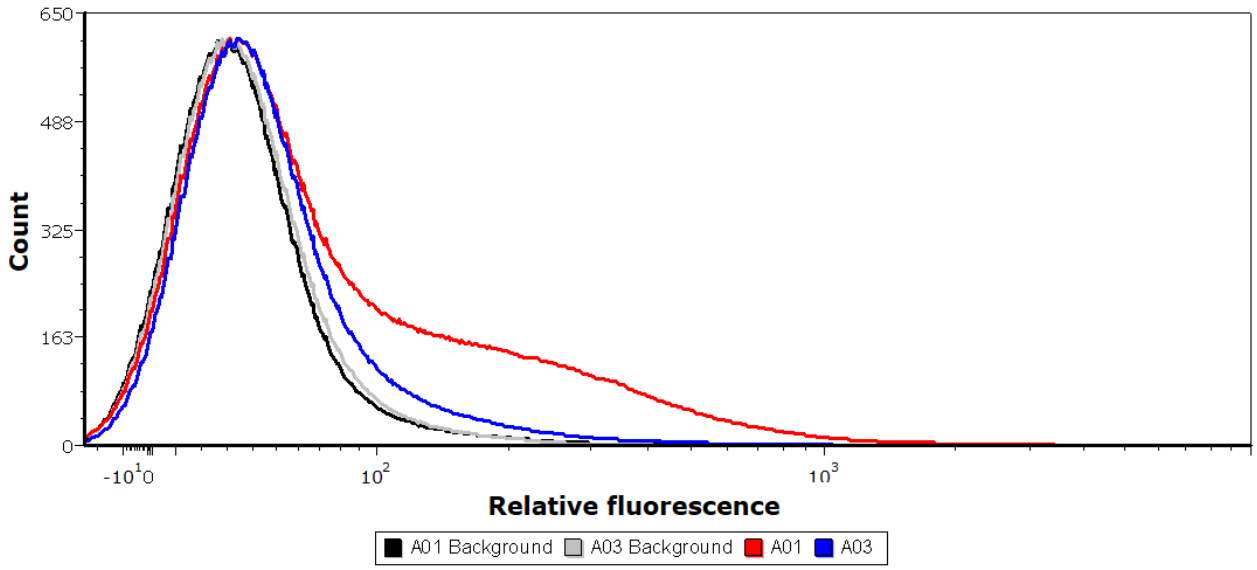

Figure 27:Binding analysis of individual yeast-cell clones sorted to h-CEACAM5 binding.

The two individual clones picked from the final h-CEACAM5 sorting round IV were incubated with the biotinylated h-CEACAM5 and labeled by the SA-APC marker followed by flow cytometry. The relative MFI indicate for significant binding of the unique yeast-cells clones A01 than to clone A03 to the h-CEACAM5 antigen.

A01 unique clone VH and VL regions of IgG molecules that showed stronger specific binding to the h-CEACAM5 antigen were subcloned into pTT5 plasmids, as described previously (chapter 5.4). After expression and purification, as described before (chapter 5.4), purified IgG1 antibodies were analyzed for binding to the antigen with BLI analysis (chapter 5.4.4).

5.5.Evaluation of re-formatted full-length IgG1 selected mAbs by BLI

After the selected yeast-clones VH and VL regions sequences were re-formatted into full-length IgG1 by subcloning into pTT5 mammalian expression vectors and were expressed in the HEK293-EBNA cells, the secreted full-length IgG1 antibodies were evaluated for affinity and specificity to the antigen which they were selected for. For that, biolayer interferometry (BLI) measurements were performed (cf. chapter 4.3.5) utilizing anti human Fc (AHC) biosensor tips and the relevant recombinant antigen protein. Antibodies were first captured on the AHC biosensor tips. Afterwards, in the association step, binding to the relevant antigen can be measured by incubation of biosensors in relatively high concentration (200 nM) of the relevant antigen, to ensure also binding of low affinity antibodies. It should be noted that the lowest limit of detection for this biophysical method of kinetic measurements is 1 µM (Estep et al., 2013). Hence, in order to measure specificity to the antigen of antibodies with affinity lower than 1 µM, BLI measurements were performed utilizing streptavidin (SA) biosensor tips. For that, the biotinylated antigen was immobilized on the SA biosensors followed by incubation of the biosensors with the relevant antibody in the association step. In this orientation of the BLI measurement

the binding rate of the antibodies increased by avidity due the bivalent Fab fragments in the full-length IgG1 antibodies that bind to the immobilized biotinylated antigen (Tobias & Kumaraswamy, 2013).

5.5.1. Evaluation of re-formatted full-length IgG1 h-OX40L targeting antibodies

*Parts of the work in this chapter were done by Svea Becker as part of her Master thesis.

After sequence verification of the cloned constructs of the heavy and light chain, only 10 clones were confirmed with correct sequence for transient transfection to the HEK293-EBNA cells. Five days post transfection antibodies were harvested and purified by protein A HP SpinTrap column (chapter 4.3.4) according to the manufacturer's instructions. To evaluate their kinetic parameters the antibodies were analyzed by biolayer interferometry (BLI) to assess the binding after reformatting to full-length IgG1. Briefly, antibodies were immobilized on anti-human Fc (AHC) biosensor tips and association as well as dissociation of the h-OX40L were monitored. Exemplary sensorgrams of the analysis of all reformatted antibodies are depicted in **Figure 28**. The data indicate a wavelength shift in nm for all antibodies when captured by the AHC biosensors. No shifts in the association step with the h-OX40L were detected. That means that the antibodies may lose their ability to bind the h-OX40L after the reformatting process to full-length IgG1 or the antibodies are low affinity antibodies with affinity below the assay limit of detection.

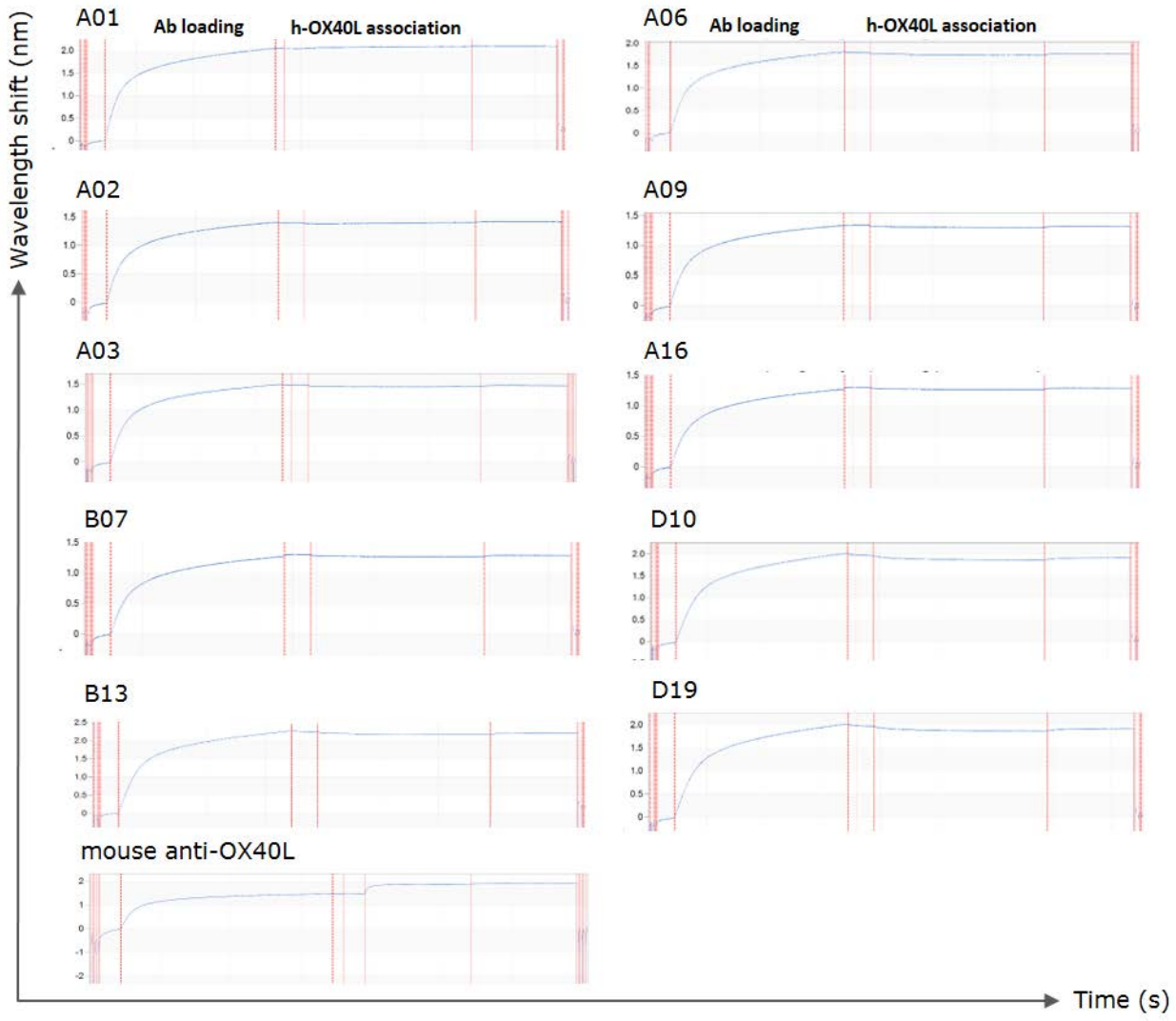

Figure 28: Binding analysis of h-OX40L to reformatted full-length IgG1 mAbs by BLI.

Antibodies were immobilized on AHC biosensors (mAb loading). Then, association of the h-OX40L (200nM) was monitored. There was no interference pattern shift observed for none of the antibodies in the association steps, indicating low affinity antibodies or non-binders antibodies. The mouse anti-OX40L used as a control bound to the h-OX40L recombinant protein.

To determine whether the antibodies are low affinity antibodies or non-binders antibodies, BLI binding analysis using the streptavidin biosensors was applied. In brief, biotinylated h-OX40L was captured on streptavidin biosensor tips. Then, antibodies were associated (200 nM). Exemplary sensorgrams of the analysis are depicted in **Figure 29**. The wavelength shifts of the association of the antibodies with the biotinylated h-OX40L indicate specific binding. The control mouse anti-OX40L bound to the h-OX40L with a high nm shift, while the non-related isotype antibody (anti-CEACAM5) did not bind to the h-OX40L. The data confirmed specific binding of the antibodies but with low affinity.

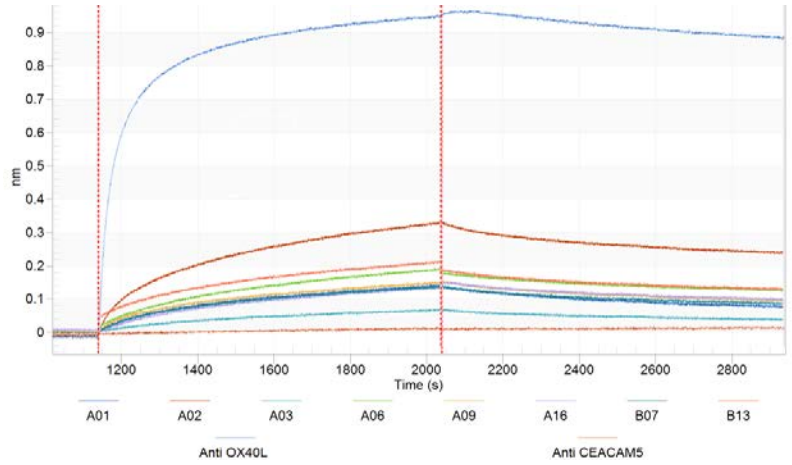

Figure 29: Binding analysis of h-OX40L to reformatted full-length IgG1 mAbs by BLI using SA biosensors.

Biotinylated h-OX40L were immobilized on streptavidin biosensors. Then, association of the different antibodies was monitored. Exemplary sensorgrams of the association steps show an interference pattern shift that indicates specificity of the antibodies to the h-OX40L. The control mouse anti-OX40L bound to the h-OX40L with a high nm shift, while the non-related isotype antibody (anti-CEACAM5) did not bind to the h-OX40L. The data confirmed specific binding of the antibodies but with low affinity.

5.5.2. Evaluation of re-formatted full-length IgG1 h-LRP6 targeting antibodies

After sequence verification of the cloned constructs of the heavy and light chain, the 2 unique clones were confirmed with correct sequence for transient transfection to the HEK293-EBNA cells. Five days post transfection antibodies were harvested and purified by protein A HP SpinTrap column (chapter 4.34) according to manufacturer's instructions. To evaluate their kinetic parameters antibodies were analyzed by biolayer interferometry (BLI) to assess the binding after reformatting to full-length IgG1. Briefly, antibodies were immobilized on anti-human Fc (AHC) biosensor tips and association as well as dissociation of the h-LRP6 E3:E4 domain were monitored. Exemplary sensorgrams of the analysis of all reformatted antibodies are depicted in **Figure 30**. The data indicate a wavelength shift in nm for all antibodies when capture to the AHC biosensors. No shifts in the association step with the h-LRP6 were detected. That means that the antibodies may lose their ability to bind the h-LRP6 after the reformatting process to full-length IgG1 or the antibodies are low affinity antibodies with affinity below the assay limit of detection.

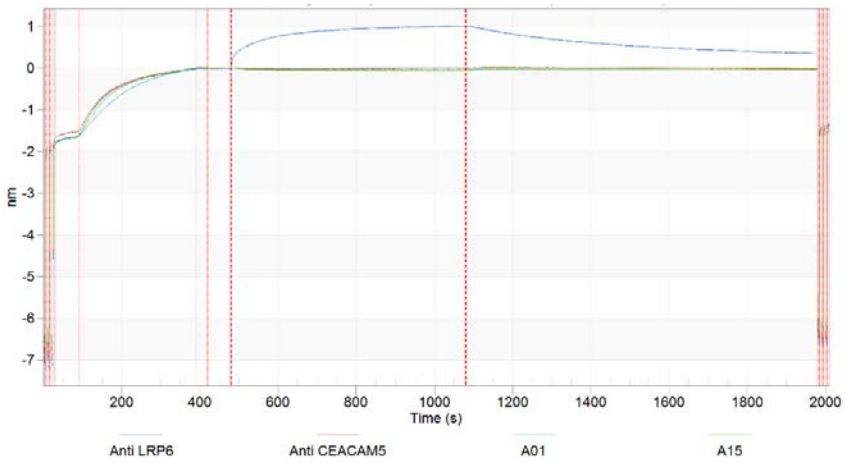

Figure 30: Binding analysis of h-LRP6 to reformatted full-length IgG1 mAbs by BLI.

Antibodies were immobilized on AHC biosensors (mAb loading). Then, association of the h-LRP6 (200nM) was monitored. There was no interference pattern shift observed for none of the antibodies in the association steps, indicating low affinity antibodies or non-binders antibodies. The anti-LRP6 mAb used as a control bound to the h-LRP6 recombinant protein.

To determine whether the antibodies are low affinity antibodies or non-binders antibodies, BLI binding analysis using the streptavidin biosensors was applied. In brief, biotinylated h-LRP6 was captured on streptavidin biosensor tips. Then, antibodies were associated (200 nM). Exemplary sensorgrams of the analysis are depicted in **Figure 31**. The wavelength shifts of the association of the antibodies with the biotinylated h-OX40L indicate specific binding. The control anti- h-LRP6 mAb bound to the h-LRP6 with a high nm shift, while the non-related isotype antibody (anti-CEACAM5) did not bind to the h-LRP6. The data confirmed specific binding of the antibodies but with low affinity.

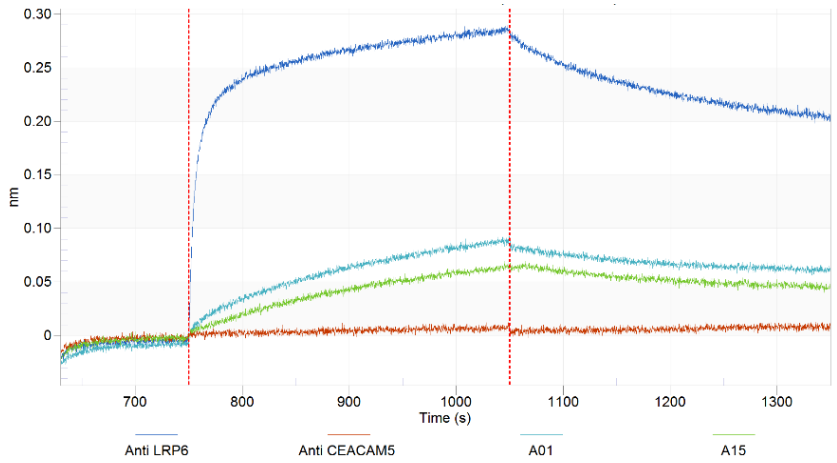

Figure 31: Binding analysis of h-LRP6 to reformatted full-length IgG1 antibodies by BLI using SA biosensors.

Biotinylated h-LRP6 were immobilized on streptavidin biosensors. Then, association of the different antibodies was monitored. Exemplary sensorgrams of the association steps show an interference pattern shift that indicates specificity of the antibodies to the h-LRP6. The control anti-LRP6 mAb bound to the h-LRP6 with a high nm shift, while the non-related isotype antibody (anti-CEACAM5) did not bind to the h-LRP6. The data confirmed specific binding of the antibodies but with low affinity.

5.5.3. Evaluation of re-formatted full-length IgG1 h-LAG3 targeting antibodies

After sequence verification of the cloned constructs of the heavy and light chain, only 10 clones were confirmed with correct sequence for transient transfection to the HEK293-EBNA cells. Five days post transfection antibodies were harvested and purified by protein A HP SpinTrap column (chapter 4.3.4) according to the manufacturer's instructions. To evaluate their kinetic parameters the antibodies were analyzed by biolayer interferometry (BLI) to assess the binding after reformatting to full-length IgG1. Briefly, antibodies were immobilized on anti-human Fc (AHC) biosensor tips and association as well as dissociation of the h-LAG3 were monitored. Exemplary sensorgrams of the analysis of all reformatted antibodies are depicted in **Figure 32**. The data indicate a wavelength shift in nm for all antibodies when captured by the AHC biosensors. No shifts in the association step with the h-LAG3 were detected. That means that the antibodies may lose their ability to bind the h-LAG3 after the reformatting process to full-length IgG1 or the antibodies are low affinity antibodies with affinity below the assay limit of detection.

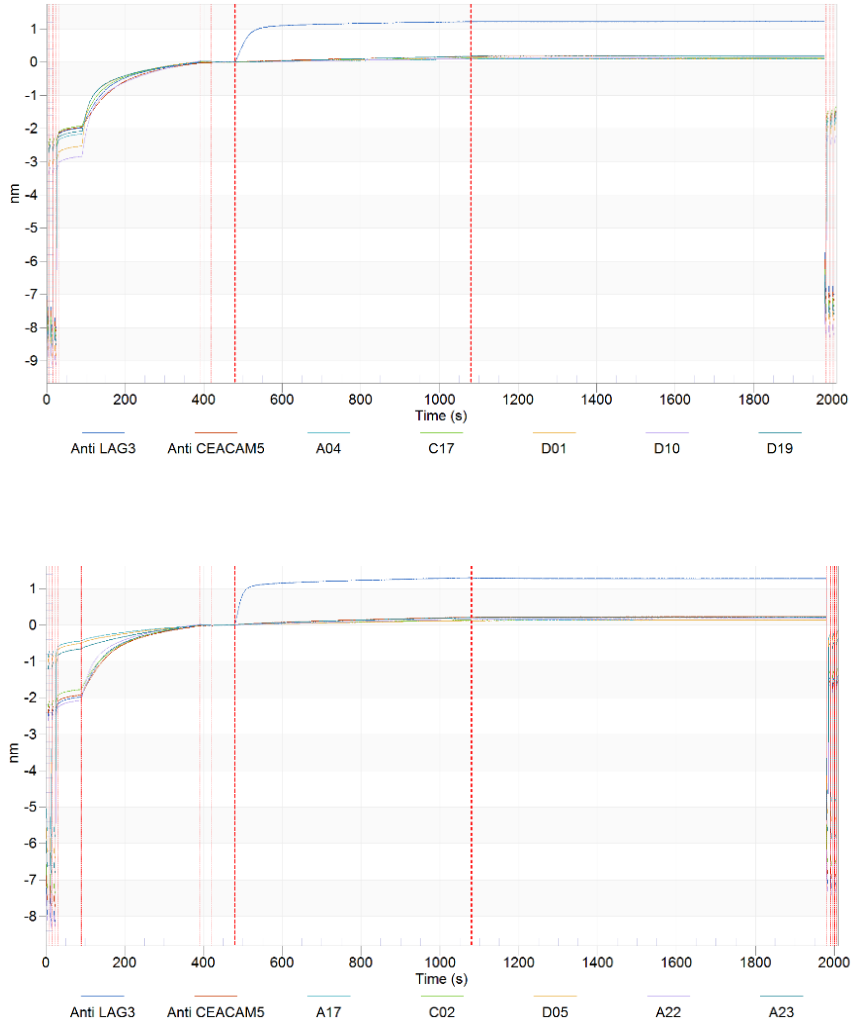

Figure 32: Binding analysis of h-LAG3 to reformatted full-length IgG1 antibodies by BLI.

Antibodies were immobilized on AHC biosensors (mAb loading). Then, association of the h-LAG3 (200nM) was monitored. There was no interference pattern shift observed for none of the antibodies in the association steps, indicating low affinity antibodies or non-binders antibodies. The anti-LAG3 mAb used as a control bound to the h-LAG3 recombinant protein.

To determine whether the antibodies are low affinity antibodies or non-binders antibodies, BLI binding analysis using the streptavidin biosensors was applied. In brief, biotinylated h-LAG3 was captured on streptavidin biosensor tips. Then, antibodies were associated (200 nM). Exemplary sensorgrams of the analysis are depicted in **Figure 33**. The wavelength shifts of the association of the antibodies with the biotinylated h-LAG3 indicate specific binding. The control anti-LAG3 bound to the h-LAG3 with a high nm shift, while the non-related isotype antibody (anti-CEACAM5) did not bind to the h-LAG3. The data confirmed specific binding of the antibodies but with low affinity.

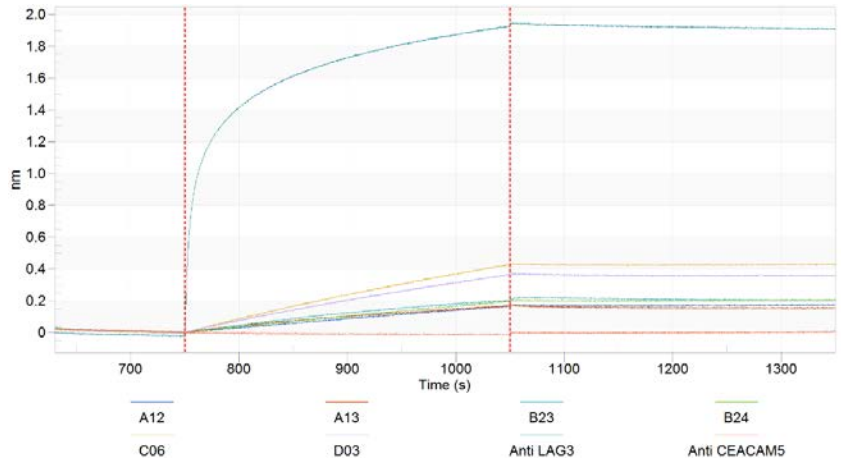

Figure 33: Binding analysis of h-LAG3 to reformatted full-length IgG1 antibodies by BLI using SA biosensors.

Biotinylated h-LAG3 were immobilized on streptavidin biosensors. Then, association of the different antibodies was monitored. Exemplary sensorgrams of the association steps show an interference pattern shift that indicates specificity of the antibodies to the h-LAG3. The control anti-LAG3 mAb bound to the h-LAG3 with a high nm shift, while the non-related isotype antibody (anti-CEACAM5) did not bind to the h-LAG3. The data confirmed specific binding of the antibodies but with low affinity.

5.5.4. Evaluation of re-formatted full-length IgG1 h-CEACAM5 targeting antibodies

After sequence verification of the cloned constructs of the heavy and light chain. The 2 unique clones were confirmed with correct sequence for transient transfection to the HEK293-EBNA cells. Five days post transfection antibodies were harvested and purified by protein A HP SpinTrap column (chapter 4.3.4) according to the manufacturer's instructions. To evaluate their kinetic parameters the antibodies were analyzed by biolayer interferometry (BLI) to assess the binding after reformatting to full-length IgG1. Briefly, antibodies were immobilized on anti-human Fc (AHC) biosensor tips and association as well as dissociation of the h-CEACAM5 were monitored. Exemplary sensorgrams of the analysis of all reformatted antibodies are depicted in **Figure 34**. The data indicate a wavelength shift in nm for all antibodies when captured by the AHC biosensors. No shifts in the association step with the h-CEACAM5 were detected. That means that the antibodies may lose their ability to bind the h-CEACAM5 after the reformatting process to full-length IgG1 or the antibodies are low affinity antibodies with affinity below the assay limit of detection.

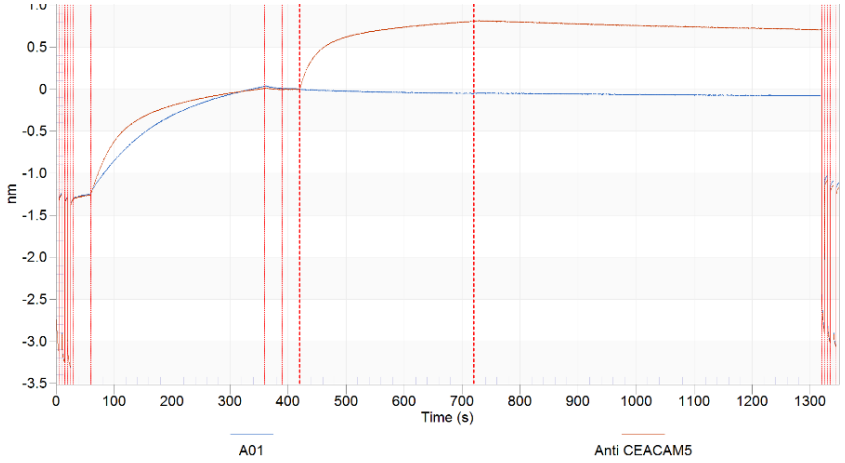

Figure 34: Binding analysis of h-CEACAM5 to reformatted full-length IgG1 antibodies by BLI.

Antibodies were immobilized on AHC biosensors (mAb loading). Then, association of the h-CEACAM5 (200nM) was monitored. There was no interference pattern shift observed for none of the antibodies in the association steps, indicating low affinity antibodies or non-binders antibodies. The anti-CEACAM5 mAb used as a control bound to the h-CEACAM5 recombinant protein.

To determine whether the antibodies are low affinity antibodies or non-binders antibodies, BLI binding analysis using the streptavidin biosensors was applied. In brief, biotinylated h-CEACAM5 was captured on streptavidin biosensor tips. Then, antibodies were associated (200 nM). Exemplary sensorgrams of the analysis are depicted in **Figure 35**. The wavelength shifts of the association of the antibodies with the biotinylated h-CEACAM5 indicate specific binding. The control anti-CEACAM5 mAb bound to the h-CEACAM5 with a high nm shift, while the non-related isotype antibody (anti-LRP6) did not bind to the h-CEACAM5. The data confirmed specific binding of the antibodies but with low affinity.

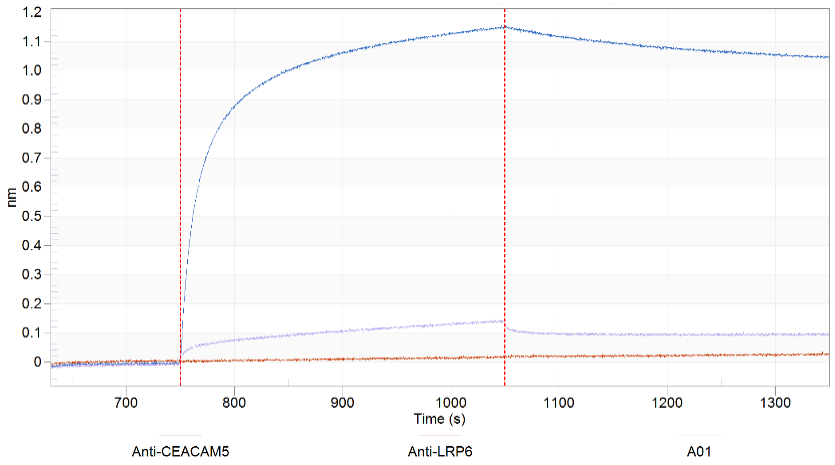

Figure 35: Binding analysis of h-CEACAM5 to reformatted full-length IgG1 antibodies by BLI using SA biosensors.

Biotinylated h-CEACAM5 were immobilized on streptavidin biosensors. Then, association of the different antibodies was monitored. Exemplary sensorgrams of the association steps show an interference pattern shift that indicates specificity of the antibodies to the h-CEACAM5. The control anti-CEACAM5 mAb bound to the h-CEACAM5 with a high nm shift, while the non-related isotype antibody (anti-LRP6) did not bind to the h-lrp6. The data confirmed specific binding of the antibodies but with low affinity.

5.6. Selection of colon cancer cells targeting antibodies using yeast biopanning of the yeast display antibody libraries derived from tumor infiltrating B cells of colon cancer patients

The approach to select antibodies from the yeast display antibody libraries derived from tumor infiltrating B cells of colon cancer patients (TIL-B) targeting the cancer associated antigens (LRP6 and CEACAM5) and immune chokepoint (OX40L and LAG3) revealed specific but low affinity full-length IgG1 antibodies. Here, the aim was to evaluate the TIL-B libraries for selection of binders to “unknown” targets on colon cancer cell lines by performing biopanning selection on live cells. Yeast display biopanning cell-based screening of antibody libraries was described previously to successfully identify antibodies targeting cell surface antigens (Tillotson et al., 2013). Here, biopanning with the TIL-B kappa library against 3 different colon cancer cell lines was performed, while normal colon fibroblast cells were used as negative cells for depletion of non-related cancer target binders. The cell lines selected for the screening were: HCT 116 (colorectal carcinoma derived), HT-29 (colorectal adenocarcinoma derived) and SW620 (colorectal adenocarcinoma derived from a metastatic lymph node site), as the libraries had been derived from tumor infiltrating B cells of colon cancer patients. A normal CCD-18Co colon fibroblast cell line was used as negative cells for depletion.

5.6.1. Biopanning of the TIL-B kappa library against HCT 116 cell line

For the biopanning selection of the TIL-B kappa library against HCT 116 cell line surface targets, the Fab fragment display of the library was induced with a SG–Trp–Leu + peptone medium at 20ºC for 48 hr. Post induction, $4x10^9$ yeast-cells were panned against the confluent HCT 116 cells. After the panning yeast-cells were washed and removed using EDTA. Panned cells were re-grown in a SD–Trp–Leu and utilized for the inoculation of a SG–Trp–Leu + peptone medium for induction of the Fab fragment between all subsequent biopanning rounds (chapter 4.2.9). In the second biopanning round yeast-cells were panned first against the confluent CCD-18CO normal colon fibroblast cell line for 2 hours at RT and then the non-binders to the CCD-18CO yeast-cells were immediately panned against the confluent HCT 116 cells. After three rounds of binding, washing, clone recovery and amplification there was a clear enrichment in the number of yeast cells Fab display binding to the HCT 116 cells, observed under the light microscopy imaging (**Figure 36A**). While panning on the depletion cells only few yeast-cell binders were observed (**Figure 36B**).

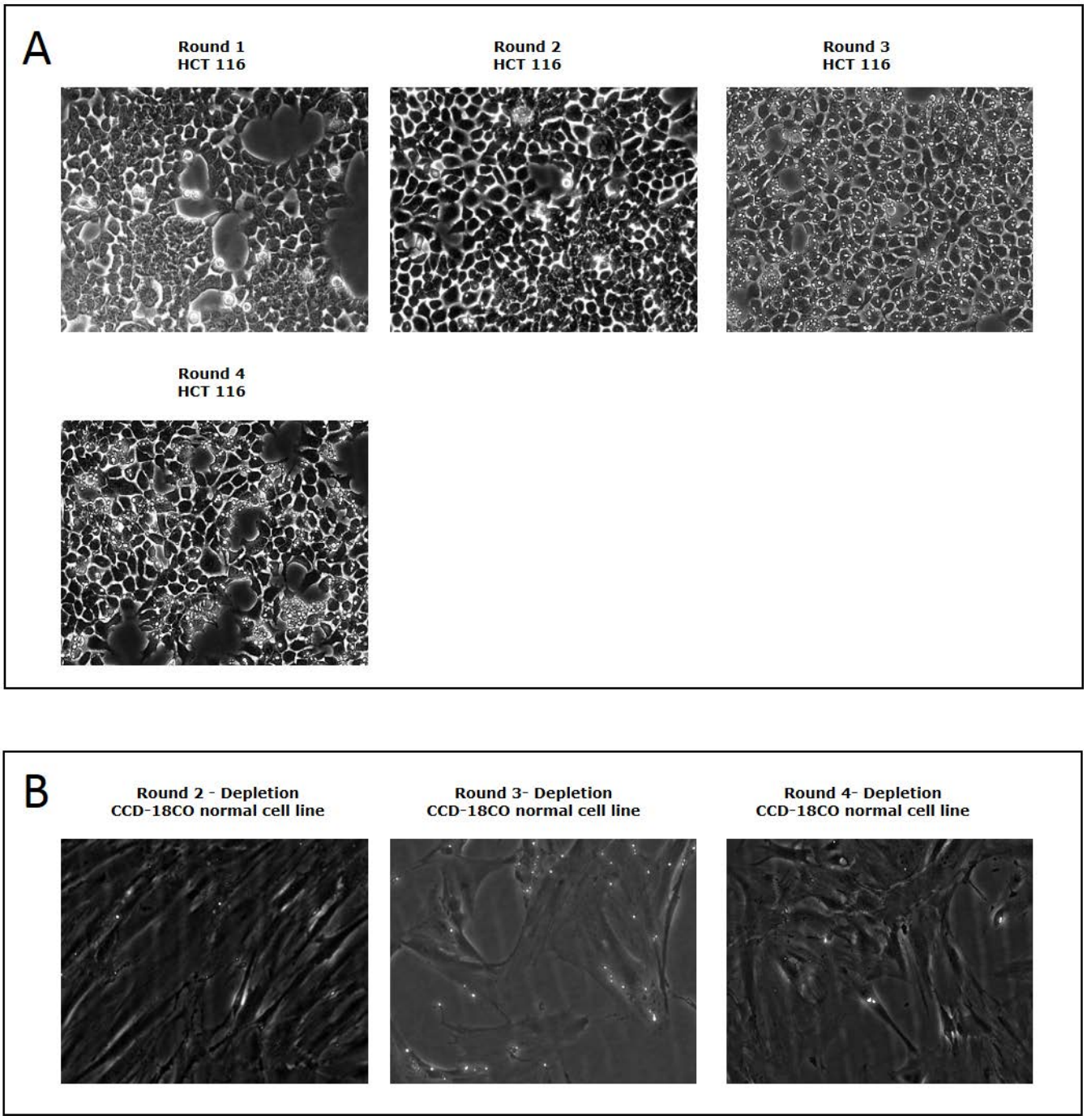

Figure 36: **TIL-B kappa library biopanning rounds against HCT 116 cell line and depletion rounds on normal colon CCD-18CO cell line (B).**

(A) Light microscopic imagining of enrichment of the TIL-B kappa library yeast cells after each round of biopanning against a confluent HCT 116 monolayer. **(B)** TIL-B kappa library yeast-cells after each round of depletion against a confluent CCD-18CO cells monolayer. Scale bar, 100 μm. Yeast are the small objects (~5 μm) residing on the monolayer cells. Enrichment can be observed after three rounds, while few binders can be observed on the normal CCD-18CO colon cells used for depletion.

5.6.2. Biopanning of the TIL-B kappa library against HT-29 cell line

For the biopanning selection of the TIL-B kappa library against HT-29 cell line surface targets, the Fab fragment display of the library was induced with a SG–Trp–Leu + peptone medium at 20ºC for 48 hr. Post induction, $4x10^9$ yeast-cells were panned against the confluent HT-29 cells. After the panning yeast-cells were washed and removed using EDTA. Panned cells were re-grown in a SD–Trp–Leu and utilized for the inoculation of a SG–Trp–Leu + peptone medium for induction of the Fab fragment between all subsequent biopanning rounds (chapter 4.2.9). In the second biopanning round yeast-cells were panned first against the confluent CCD-18CO normal colon fibroblast cell line for 2 hours at RT and then the non-binders to the CCD-18CO yeast-cells were immediately panned against the confluent HT-29 cells. After three rounds of binding, washing, clone recovery and amplification there was a clear enrichment in the number of yeast cells Fab display binding to the HT-29 cells, observed under the light microscopy imaging (**Figure 37A**). While panning on the depletion cells only few yeast-cell binders were observed (**Figure 37B**).

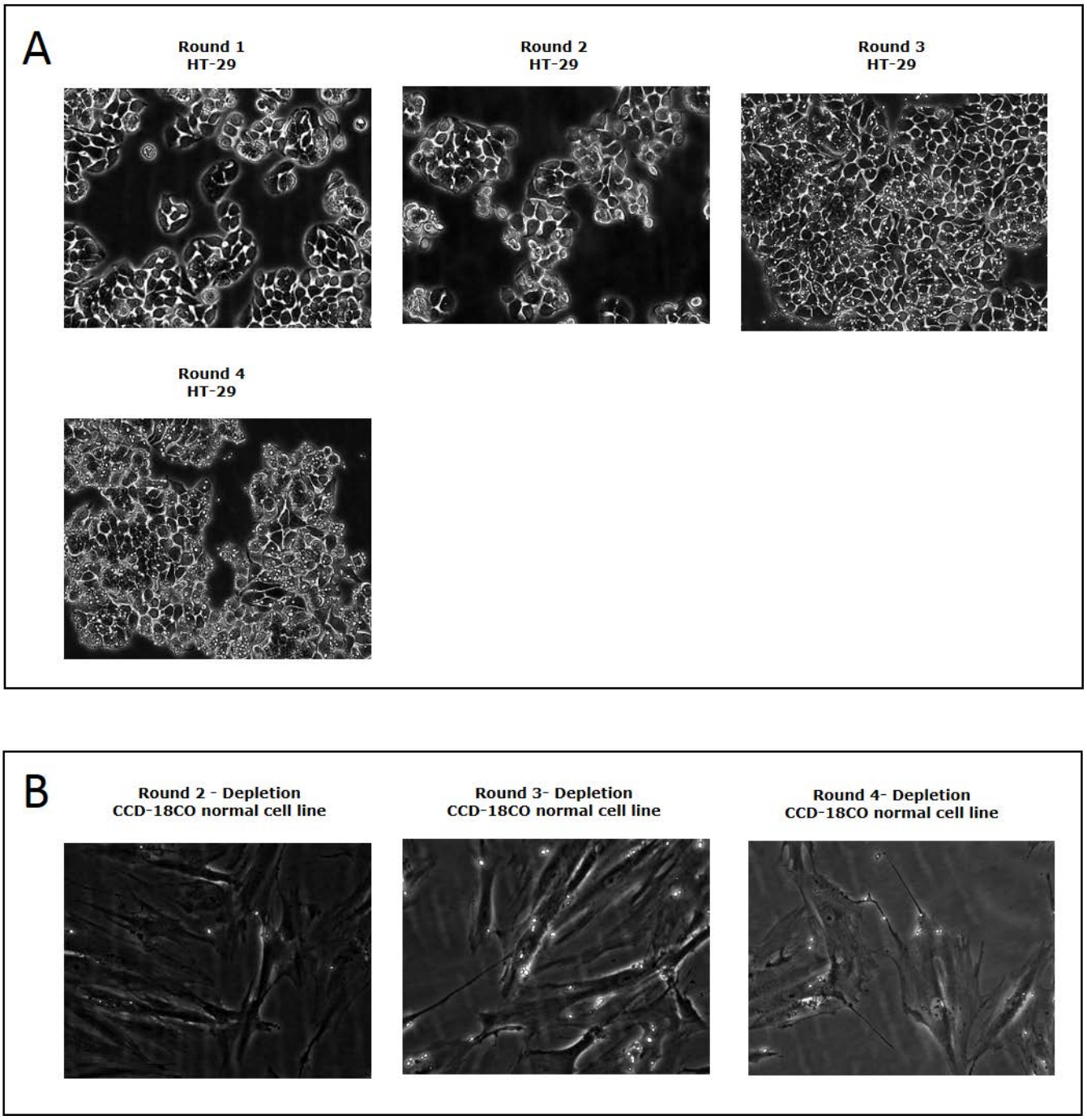

Figure 37: TIL-B kappa library biopanning rounds against HT-29 cell line and depletion rounds on colon normal CCD-18CO cell line.

(A) Light microscopic imagining of enrichment of the TIL-B kappa library yeast cells after each round of biopanning against a confluent HT-29 monolayer. **(B)** TIL-B kappa library yeast-cells after each round of depletion against a confluent CCD-18CO cells monolayer. Scale bar, 100 µm. Yeast are the small objects (~5 µm) residing on the monolayer cells. Enrichment can be observed after three rounds, while few binders can be observed on the normal CCD-18CO colon cells used for depletion.

5.6.3. Biopanning of the TIL-B kappa library against SW620 cell line

For the biopanning selection of the TIL-B kappa library against SW620 cell line surface targets, the Fab fragment display of the library was induced with a SG–Trp–Leu + peptone medium at 20ºC for 48 hr. Post induction, $4x10^9$ yeast-cells were panned against the confluent SW620 cells. After the panning yeast-cells were washed and removed using EDTA. Panned cells were re-grown in a SD–Trp–Leu and utilized for the inoculation of a SG–Trp–Leu + peptone medium for induction of the Fab fragment between all subsequent biopanning rounds (chapter 4.2.9). In the second biopanning round yeast-cells were panned first against the confluent CCD-18CO normal colon fibroblast cell line for 2 hours at RT and then the non-binders to the CCD-18CO yeast-cells were immediately panned against the confluent SW620 cells. After three rounds of binding, washing, clone recovery and amplification there was a clear enrichment in the number of yeast cells Fab display binding to the SW620cells, observed under the light microscopy imaging (**Figure 37A**). While panning on the depletion cells only few yeast-cell binders were observed (**Figure 37B**).

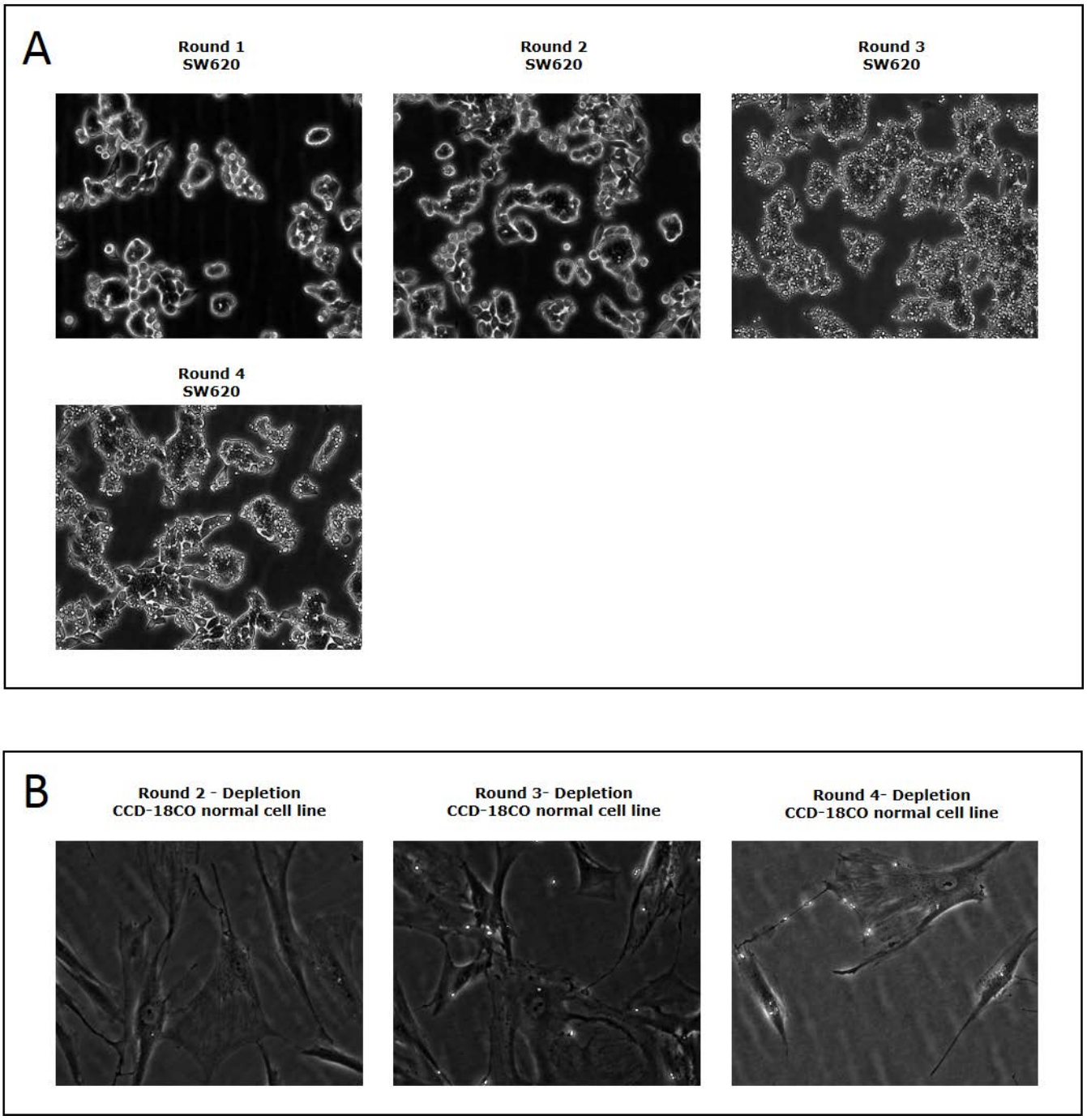

Figure 38: TIL-B kappa library biopanning rounds against SW620 cell line and depletion rounds on colon normal CCD-18CO cell line.

(A) Light microscopic imagining of enrichment of the TIL-B kappa library yeast cells after each round of biopanning against a confluent SW620 monolayer. **(B)** TIL-B kappa library yeast-cells after each round of depletion against a confluent CCD-18CO cells monolayer. Scale bar, 100 µm. Yeast are the small objects (~5 µm) residing on the monolayer cells. Enrichment can be observed after three rounds, while few binders can be observed on the normal CCD-18CO colon cells used for depletion.

5.7. Binding analysis of the enriched biopanning yeast-cells to panel of cancer and normal cell line

After rapid enrichment during three biopanning rounds, evaluation of the colon cancer cell-enriched Fab-displaying yeast-cell pools from the fourth final biopanning round against the three-colon cancer cell line HCT 116, HT-29 and SW620 were performed. To assess the binding profile of the 3 enriched pools, each was evaluated by binding analysis of the yeast-cell Fab display to 10 distinct cell lines representing the colon cancer cell lines which the yeast-cells were panned on, other cancer type cell lines, the normal colon fibroblast cell line (CCD-18CO) and the Chinese hamster ovary derived cell line (CHO-S1) as non-cancer cell lines. The yeast-cell binding analysis was performed with the goal of verifying selective enrichment to colon cancer cell lines and to rule out enrichment to the non-cancer cell lines.

5.7.1. Binding analysis of the enriched biopanning yeast-cells against the HCT 116 cell line

To evaluate the binding profile of the enriched yeast-cell pool that was panned against the HCT 116 cell line, the yeast-cell pool from the forth biopanning round was induced with a SG–Trp–Leu + peptone medium at 20ºC for 48 hr for a Fab fragment display. Post induction, 1 x 10^7 yeast-cells were incubated on each confluent cell line in a 12 well-plate. After 2 hr the incubated yeast-cells were washed, and non-binders yeast-cells were removed. Light microscopy was then used to assess the binding capacity of the Fab displayed HCT 116 binders enriched yeast-cell pool to each cell line and given a qualitative score from 0 to 4 (*no binding* to *high binding*). The light microscopy images of each cell line are depicted in **Figure 39**. The imaging data confirmed that the Fab displayed HCT 116 binders enriched yeast-cell pool demonstrated high selectivity to the colon cancer derived cell line (HCT 116 and HT-29), lower but also high selectivity was also observed to the gastric adenocarcinoma derived cell line (MKN-45). No binding to the non-cancer cell lines, including the normal colon fibroblast cell line (CCD-18CO) and the Chinese hamster ovary derived cell line (CHO-S1), was observed.

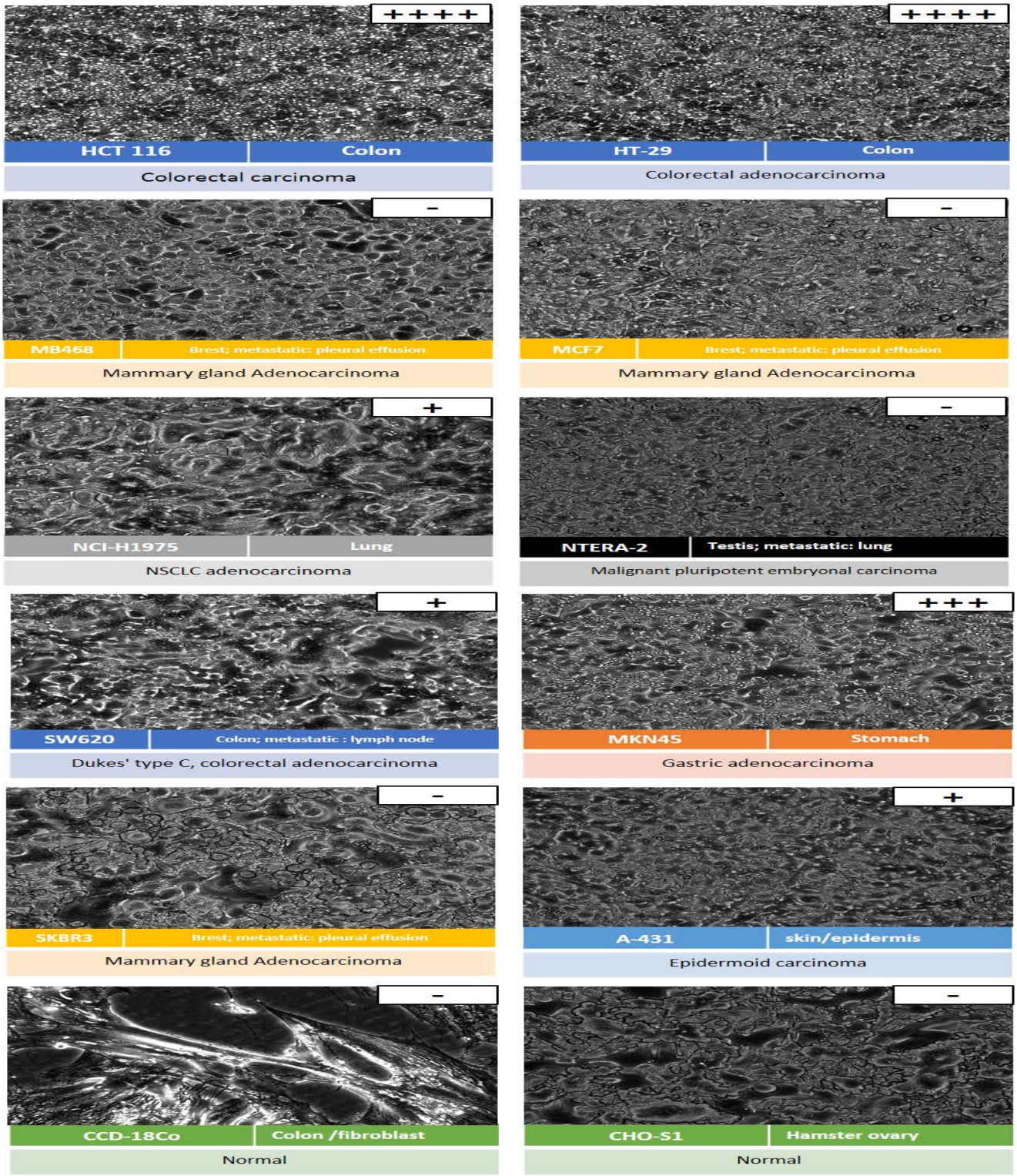

Figure 39: Binding analysis of the enriched biopanning yeast-cells against HCT 116 cell line to panel of cancer and normal cell line.

Light microscopic imagining binding profile of Fab displayed HCT 116 binders enriched yeast-cell pool to 12 distinct cell lines. Qualitative scoring of Fab displayed HCT 116 binders enriched yeast-cell pool binding with various intensity, from 0 (no observed binding) to 4 (significant yeast binding). High binding to the colon cancer derived cell line observed while no-binding observed to the non-cancer cell lines. Scale bar, 100 µm. Yeast are the small objects (~5 µm) residing on the monolayer cells.

5.7.2. Binding analysis of the enriched biopanning yeast-cells against HT-29 cell line

To evaluate the binding profile of the enriched yeast-cell pool that was panned against the HT-29 cell line, the yeast-cell pool from the forth biopanning round was induced with a SG–Trp–Leu + peptone medium at 20ºC for 48 hr for a Fab fragment display. Post induction, 1 x 10^7 yeast-cells were incubated on each confluent cell line in a 12 well-plate. After 2 hr the incubated yeast-cells were washed, and non-binders yeast-cells were removed. Light microscopy was then used to assess the binding capacity of the Fab displayed HT-29 binders enriched yeast-cell pool to each cell line and given a qualitative score from 0 to 4 (*no binding* to *high binding*). The light microscopy images of each cell line are depicted in **Figure 40**. The imaging data confirmed that the Fab displayed HT-29 binders enriched yeast-cell pool demonstrated high selectivity to the colon cancer derived cell line (HCT 116 and HT-29) lower but also high selectivity was observed also to the gastric adenocarcinoma derived cells line (MKN-45) and the metastatic colorectal derived cell line (SW620). No binding to the non-cancer cell lines, including the normal colon fibroblast cell line (CCD-18CO) and the Chinese hamster ovary derived cell line (CHO-S1), was observed.

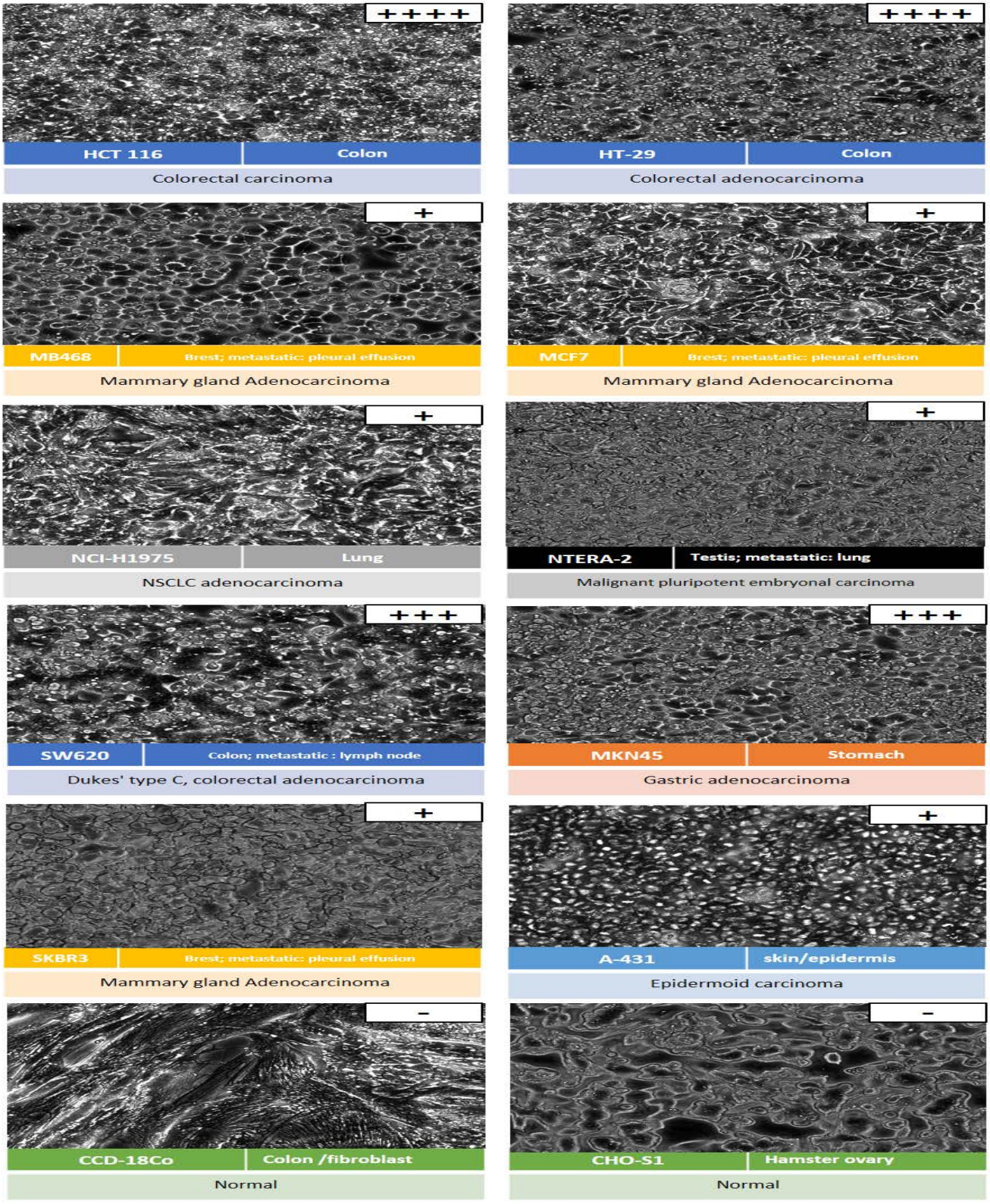

Figure 40: Binding analysis of the enriched biopanning yeast-cells against HT-29 cell line to panel of cancer and normal cell line.

Light microscopic imagining binding profile of Fab displayed HCT 116 binders enriched yeast-cell pool to 12 distinct cell lines. Qualitative scoring of Fab displayed HT-29 binders enriched yeast-cell pool binding with various intensity, from 0 (no observed binding) to 4 (significant yeast binding). High binding to the colon cancer derived cell line observed while no-binding observed to the non-cancer cell lines. Scale bar, 100 µm. Yeast are the small objects (~5 µm) residing on the monolayer cells.

5.7.3. Binding analysis of the enriched biopanning yeast-cells against SW620 cell line

To evaluate the binding profile of the enriched yeast-cell pool that was panned against the SW620 cell line, the yeast-cell pool from the forth biopanning round was induced with a SG–Trp–Leu + peptone medium at 20ºC for 48 hr for a Fab fragment display. Post induction, 1 x 10^7 yeast-cells were incubated on each confluent cell line in a 12 well-plate. After 2 hr the incubated yeast-cells were washed, and non-binders yeast-cells were removed. Light microscopy was then used to assess the binding capacity of the Fab displayed SW620 binders enriched yeast-cell pool to each cell line and given a qualitative score from 0 to 4 (*no binding* to *high binding*). The light microscopy images of each cell line are depicted in **Figure 41**. The imaging data confirmed that the Fab displayed SW620 binders enriched yeast-cell pool demonstrated high selectivity to the metastatic colorectal adenocarcinoma derived. Here different profile binding was observed to the other cell line, as high selectivity was observed to the metastatic mammary gland adenocarcinoma derived cells lines (MCF7, MB468, SKBR3), binding to the colorectal derived cells and to the gastric derived cells was also observed but with lower intensity No binding to the non-cancer cell lines, including the normal colon fibroblast cell line (CCD-18CO) and the Chinese hamster ovary derived cell line (CHO-S1), was observed.

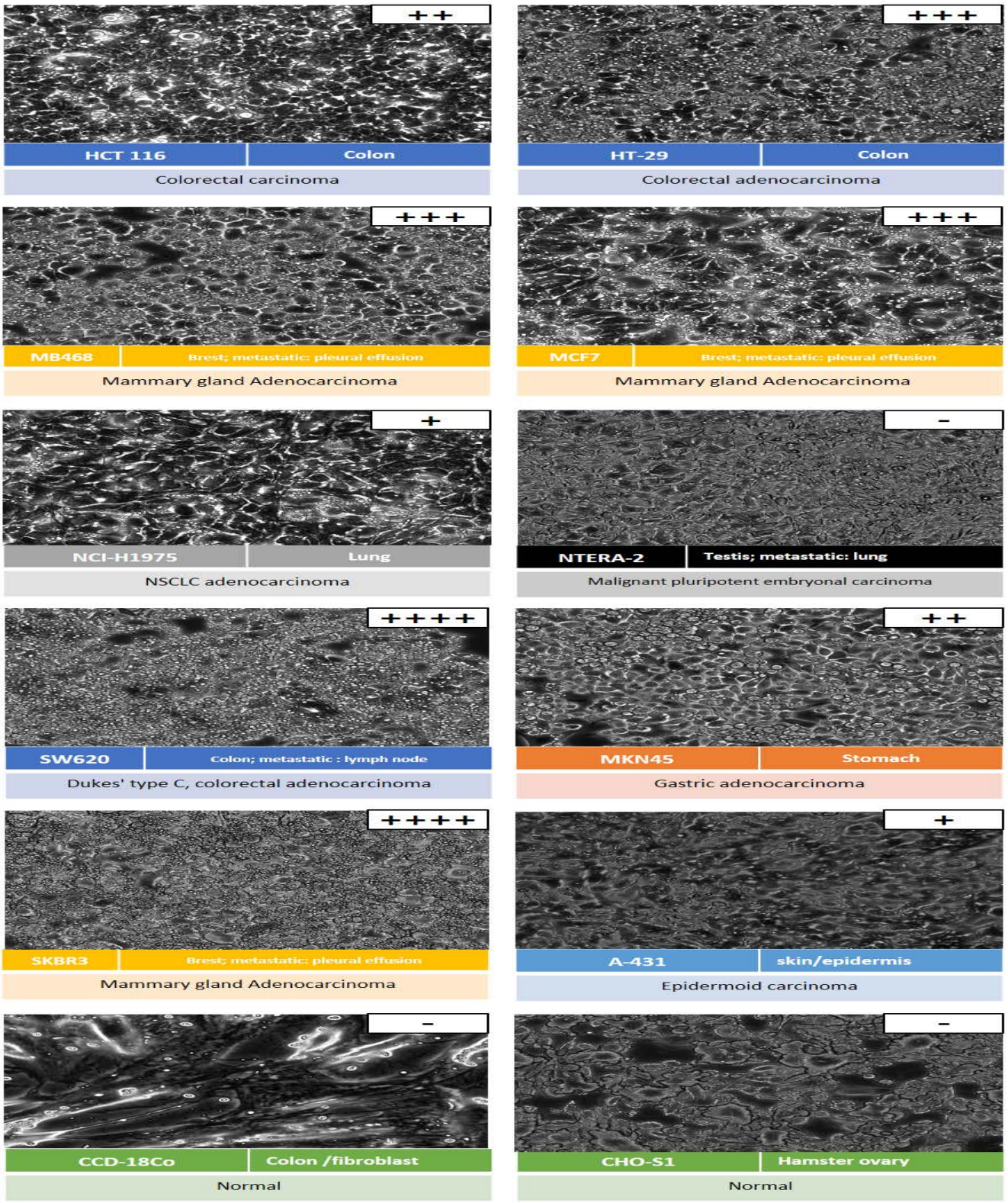

Figure 41: Binding analysis of the enriched biopanning yeast-cells against SW620 cell line to panel of cancer and normal cell line.

Light microscopic imagining binding profile of Fab displayed HCT 116 binders enriched yeast-cell pool to 12 distinct cell lines. Qualitative scoring of Fab displayed SW620 binders enriched yeast-cell pool binding with various intensity, from 0 (no observed binding) to 4 (significant yeast binding). High binding to the colon cancer derived cell line observed while no-binding observed to the non-cancer cell lines. Scale bar, 100 µm. Yeast are the small objects (~5 µm) residing on the monolayer cells.

5.8. Evaluation of biopanning enriched individual Fab display yeast-clones

After the assessment of selective enrichment of Fab display yeast-cells from the TIL-B kappa library to antigens expressed specifically on the colorectal cancer derived cell line through the biopanning process (cf. chapter 5.6.1-3), further evaluation of individual yeast cells clones was performed on the enriched clones that panned against the colorectal cancer derived cell lines only (HCT 116 and HT-29). For that, single cells from the forth (last) biopanning round were plated on SD–Trp–Leu agar plates and individual yeast-cell clones were picked. From each biopanning approach (HCT 116 and HT-29) 48 single clones from the 4^{th} round were analyzed by sequencing their variable region frameworks and complementary determining region (CDR) diversities within the heavy and light-chain and then analyzed by Salsa analysis (Merck). Then a clustering strategy was applied, where sequences with ≥ 90% identical CDR residues were allocated to the same cluster for identification of unique clones. Functionality of the heavy and the light chain for correct expression was tasted and the heavy or light chain were removed from subsequent analyses if the third complementarity determining region (CDR3) was of indeterminate length, stop codons were present, or the amino acid translation was out of frame. The analysis identified 13 unique yeast clones from the enriched HCT 116 cell line binder yeast-cell clones and 10 unique yeast clones from the enriched HT-29 cell line binder yeast-cell clones. Interestingly, 3 unique yeast clones were isolated from the two biopanning approaches (HCT 116 and HT-29) identified as the same clones. **Table 10** summarizes the unique clones that were identified by their ID name, germline diversity of the heavy (VDJ) and light (VJ) gene segments with their identity percentage from the germline.

Clone ID	VH-region identity (%)	VH gene	DH gene	JH gene	VL-region identity (%)	VL gene	VJ gene
TILB-HCT116/HT29 A06	91	IGHV3-15*01	IGHD2-15*01	IGHJ4*02	91	IGKV4-1*01	IGKJ2*01
TILB-HCT116/HT29 A17	89	IGHV3-15*07	IGHD2-15*01	IGHJ4*02	87	IGKV1-33*01	IGKJ1*01
TILB-HCT116/HT/29 B24	90	IGHV3-15*07	IGHD2-15*01	IGHJ4*02	90	IGKV3-20*01	IGKJ1*01
TILB-HCT116 A02	90	IGHV3-15*07	IGHD2-15*01	IGHJ4*02	97	IGKV3-11*01	IGKJ3*01
TILB-HCT116 A03	94	IGHV3-15*01	IGHD2-15*01	IGHJ4*02	87	IGKV3/OR2-268*02	IGKJ2*01
TILB-HCT116 A04	93	IGHV3-15*01	IGHD2-15*01	IGHJ4*02	94	IGKV4-1*01	IGKJ2*01
TILB-HCT116 A05	90	IGHV3-15*07	IGHD2-15*01	IGHJ4*02	96	IGKV3-15*01	IGKJ2*01
TILB-HCT116 A07	94	IGHV3-15*07	IGHD2-15*01	IGHJ4*02	85	IGKV1-6*01	IGKJ1*01
TILB-HCT116 A11	91	IGHV3-15*01	IGHD2-15*01	IGHJ4*02	91	IGKV1-39*01	IGKJ2*01
TILB-HCT116 A14	80	IGHV1-3*01	IGHD1-26*01	IGHJ4*02	92	IGKV3-20*01	IGKJ1*01
TILB-HCT116 B06	90	IGHV3-15*01	IGHD2-15*01	IGHJ4*02	88	IGKV3-20*01	IGKJ5*01
TILB-HCT116 B08	93	IGHV3-15*07	IGHD2-15*01	IGHJ4*02	82	IGKV1-39*01	IGKJ4*01
TILB-HCT116 B10	93	IGHV3-33*01	IGHD3-22*01	IGHJ6*03	96	IGKV2-30*02	IGKJ2*01
TILB-HT29 A05	84	IGHV3-23*01	IGHD4-23*01	IGHJ5*02	90	IGKV2-30*01	IGKJ2*01
TILB-HT29 A08	88	IGHV3-15*07	IGHD2-15*01	IGHJ4*02	92	IGKV1-5*01	IGKJ4*01
TILB-HT29 A14	91	IGHV1-3*01	IGHD2-2*01	IGHJ6*02	80	IGKV1-12*01	IGKJ4*01
TILB-HT29 A16	92	IGHV3-15*01	IGHD6-13*01	IGHJ4*02	97	IGKV4-1*01	IGKJ1*01
TILB-HT29 A20	95	IGHV1-3*01	IGHD3-10*01	IGHJ5*02	85	IGKV4-1*01	IGKJ2*01
TILB-HT29 B04	78	IGHV1-2*02		IGHJ4*03	97	IGKV4-1*01	IGKJ4*01
TILB-HT29 B24	92	IGHV1-3*01	IGHD2-2*01	IGHJ6*02	96	IGKV1-39*01	IGKJ2*02

Table 10: Isolated unique clones with their germline diversity from biopanning against HCT116 and HT-29 cell lines.

Summary of the sequence clustering analysis for the individual yeast-cell clones that bind to HCT 116 and HT-29 cell lines. Clone ID name represent the cell line which the clones were panned against. Clones TILB-HCT116/HT29 A06 A17 B24 found to be same clones that minded from the HCT 116 and HT-29 biopanning. After clustering, 20 clones from 96 were identified as unique. The 20 clustered sequences were verified for functional expression for both heavy and light chain to generate functional Fab fragment. Germline diversity of the heavy (VDJ) and light (VJ) gene segments with their identity percentage from the germline are presented.

5.8.1. Binding analysis to different cancer and normal cell liens

To evaluate specific binding of the unique clones to antigens expressed on colorectal cancer cells and not to the normal colon cell line, binding analysis of all the unique yeast-cell clones was performed. To assess the binding profile of the 20-unique yeast-clones, each was evaluated by analysis of binding of the yeast-

cell Fab display to the colorectal carcinoma derived cell line (HCT 116), the mammary gland metastatic adenocarcinoma derived cell line (MCF7), the normal colon fibroblast cell line (CCD-18CO) and the Chinese hamster ovary derived cell line (CHO-S1) as non-cancer cell lines. For that, the yeast-cell unique clones were induced with a SG–Trp–Leu + peptone medium at 20ºC for 48 hr to obtain a Fab fragment display. Post induction, 1 x 10^7 yeast-cells were incubated on each confluent cell line in a 12 well-plate. After 2 hr incubation yeast-cells were washed and non-binders yeast-cells were removed. Light microscopy was then used to assess the binding capacity of the Fab display of the unique clones to each cell line by giving a qualitative score for binding or no binding to the monolayer cell lines. A representative example of 3 unique yeast-cells binding profiles are depicted using light microscopy imaging in **Figure 42**. Clone A01 and A02 images represent unique clones with specific binding to the HCT 116 cells and no binding observed to the MCF7 cell line or to the non-cancer cell lines, CCD-18Co and CHO-S1. The clone A03 image represents a unique clone with unspecific binding, as there was binding both to the CCD-18Co and CHO-S1 cells. **Table 11** summarizes the binding profile of all 20 unique clones based on the light microscopy imaging. Twelve clones from the 20 unique clones showed specific binding to the HCT-116 cell line and were used for further evaluation.

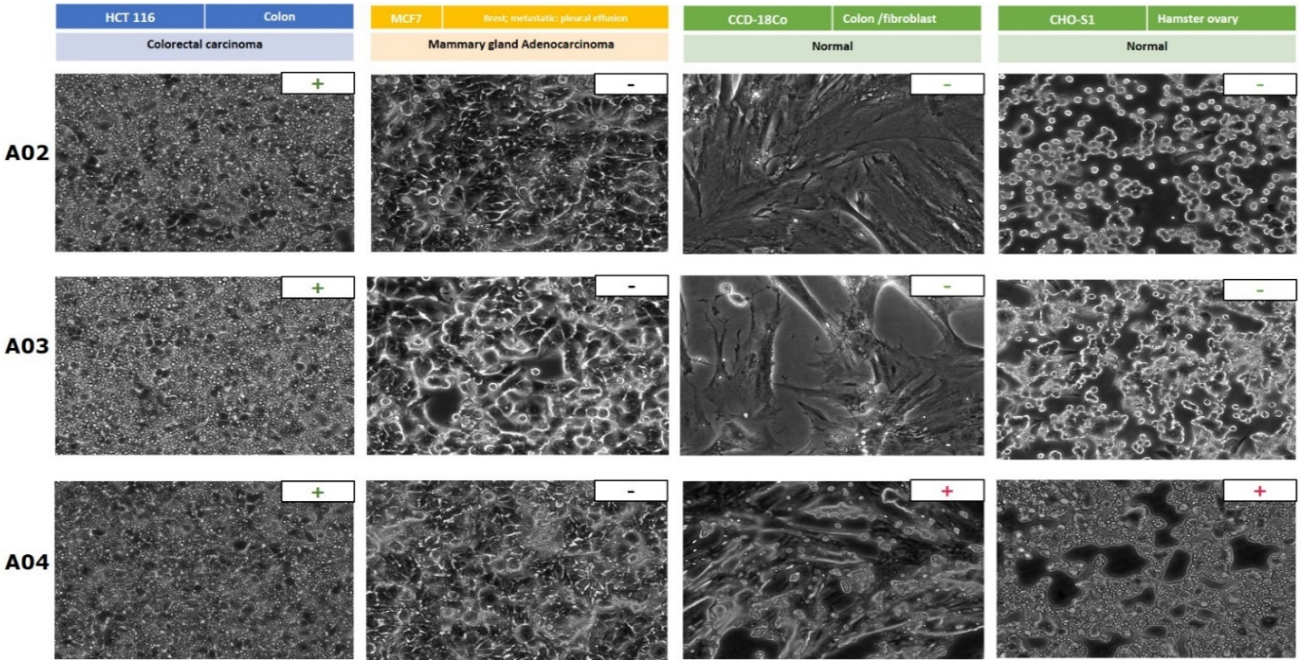

Figure 42: Example of TILB-HCT116/HT29 unique yeast-cell binding profile on the light microscopy imaging.

Light microscopic images representing examples of 3 unique yeast-cell binding profiles. Clones A01 and A02 images represent unique clones with specific binding to the HCT 116 cells and no binding observed to the MCF7 cell line or to the non-cancer CCD-18Co and CHO-S1 cell lines. The clone A03 image represents a unique clone with unspecific binding, as binding was observed both to the CCD-18Co and CHO-S1 cells. Scale bar, 100 µm. Yeast are the small objects (~5 µm) residing on the monolayer cells.

Clone ref number	HCT116	MCF7	CCD-18CO	CHO-S1
TILB-HCT116 A06	+	-	-	-
TILB-HCT116 A17	+	-	-	-
TILB-HCT116 B24	+	-	-	-
TILB-HCT116 A02	+	-	-	-
TILB-HCT116 A03	+	-	-	-
TILB-HCT116 A04	+	-	-	+
TILB-HCT116 A05	+	-	-	-
TILB-HCT116 A07	+	-	-	-
TILB-HCT116 A11	+	-	-	-
TILB-HCT116 A14	+	-	-	-
TILB-HCT116 B06	+	-	-	-
TILB-HCT116 B08	+	-	-	-
TILB-HCT116 B10	+	-	+	+
TILB-HT29 A05	+	-	+	+
TILB-HT29 A08	+	-	-	-
TILB-HT29 A14	+	+	+	+
TILB-HT29 A16	+	+	+	-
TILB-HT29 A20	+	+	+	+
TILB-HT29 B04	+	+	+	-
TILB-HT29 B24	+	+	+	+

Table 11: Binding profile summary of TILB-HCT116/HT29 unique yeast-cells.

Binding profile of all 20 unique clones based on the light microscopy imaging (example in **Figure 42**). Twelve clones from the 20 unique clones showed specific binding to the HCT-116 cell line and were used for further evaluation.

5.8.2. Cellular binding of re-formatted full-length IgG1 colorectal derived cells targeting antibodies

The 12 VH an VL regions of the unique clones of IgG molecules that showed specific binding to the HCT 116 cell line were subcloned into pTT5 plasmids. After sequence verification of the cloned constructs of the heavy and light chain, the 12 clones were confirmed by a correct sequence for transient transfection to the HEK293-EBNA cells. Five days post transfection, antibodies were harvested and purified with a protein A HP SpinTrap column, as described before (chapter 5.4). Then, crude harvests were quantified by BLI. To evaluate the binding of the unique clones after reformatting to full-length IgG1, binding analysis to HCT 116 cells was performed using flow cytometry. Therefore, 1 x 10^6 HCT 116 cells were incubated together with 200 nM of the antibodies followed by labelling with secondary Alexa Fluor 488 -conjugated antibody and flow cytometry (chapter 4.4.3). Unstained cells or cells only treated with secondary Alexa Fluor 488 -conjugated antibody served as controls to reveal the amount of cellular autofluorescence. Exemplary histograms of relative mean fluorescence intensities are depicted in **Figure 43**. Half of the antibodies exhibited fluorescence intensities same as the background level after reformatting to full-length IgG1 (A). This can be explained by low affinity antibodies

or by losing the binding during the reformatting process. While, the other half of the antibodies exhibited positive mean fluorescence intensities and binding of the antibodies to the HCT 116 cells(B).

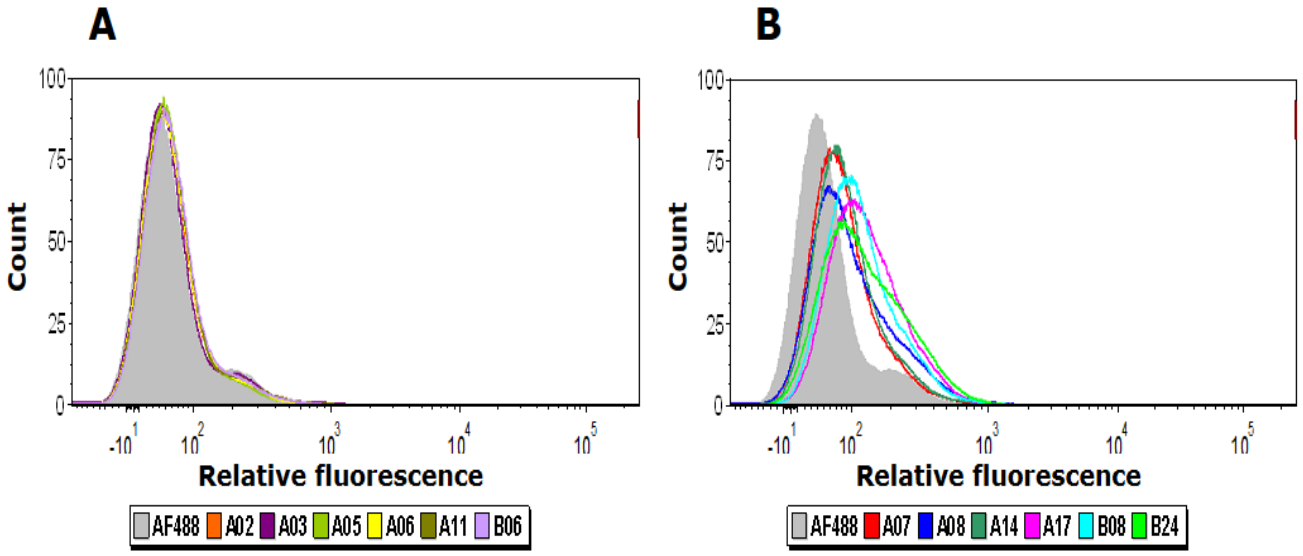

Figure 43: Cellular binding of unique mAbs to HCT116 cell line.

HCT116 cell lines were incubated with 200 nM antibodies (crude harvest) and binding was revealed with anti-human Fc antibody-Alexa Fluor 488 conjugate via flow cytometry (5,000 counts). **(A)** Six antibodies displayed fluorescence intensities same as the background level (gray) after reformatting to full-length IgG1. **(B)** The remaining 6 of the antibodies exhibited positive mean fluorescence intensities by binding to the HCT 116 cells.

5.8.3. Multiple sequence alignment for the heavy and light variable regions of the unique clones

As some of the selected unique clones after reformatting to full-length IgG1were demonstrated to bind to the HCT 116 cell line, while the other half was not found to bind (cf. chapter 5.8.2), further evaluation at the level of the heavy and light variable regions sequences of the unique clones was performed. For that, multiple sequence alignment of all unique heavy and light chain variable region sequences was performed. The alignment analysis (**Figure 44**) indicated high similarity between heavy chain variable region sequences: most of the variance occurred in the framework region one (FR1) and complementarity determining region one (CDR1), while the CDR3 region was identical across all clones excluding clone A24. In the light chain variable region sequences an opposite finding was observed as low similarity between the clones was identified with all frameworks and CDR sequences. Moreover, very low similarity was observed between CDR3's of the light chain sequences. Hence, as some of the clones were demonstrated binding and some not, and all clones (excluding A24) shared almost the same HC sequences, this may indicate the same target specificity determined by the heavy chain variable region. Changes in the affinity binding levels between the different unique clones were therefore determined by their light chain variable region.

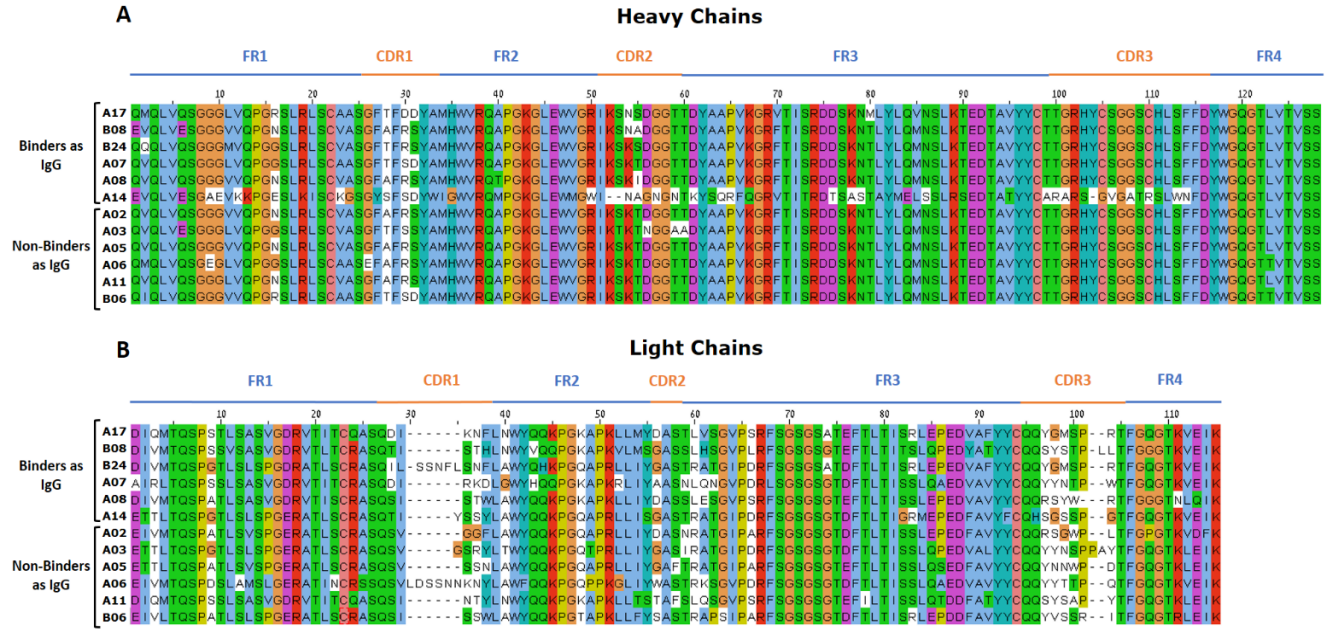

Figure 44: Multiple sequence alignment for the heavy and light variable regions of TIL-B HCT116 unique clones.

(A) Multiple sequence alignment of the heavy chain of the unique isolated TILB-HCT116 clones. **(B)** Multiple sequence alignment of the light chain of the unique isolated TILB-HCT116 clones. The analysis shows that all clones (excluding A24) share almost the same HC sequences, while between the LC sequences variation can be observed. This may indicate the same target specificity determined by the heavy chain variable region. Changes in the affinity binding levels between the different unique clones were therefore determined by their light chain variable region.

5.8.4. Cellular binding of re-formatted full-length IgG1 purified colorectal derived cells targeting clone TILB-HCT116-B24 by flow cytometry

For further evaluation, clone TILB-HCT116 B24 that showed binding to the HCT 116 cell line as full-length IgG1 crude harvest mAb was chosen (cf. chapter 5.8.2). This clone was purified by a protein A HP SpinTrap column (chapter 4.3.4) and subjected to cellular binding analysis with the HCT 116 cells by flow cytometry (chapter 4.4.3). A two-fold serial dilution of the mAb (2000 nM-0.98 nM) was applied for binding to HCT 116 cells. Exemplary histograms of relative mean fluorescence intensities are depicted in **Figure 45**. The TILB-HCT116-B24 mAb exhibited cellular binding to HCT 116 cells with an EC50 value of 569 nM.

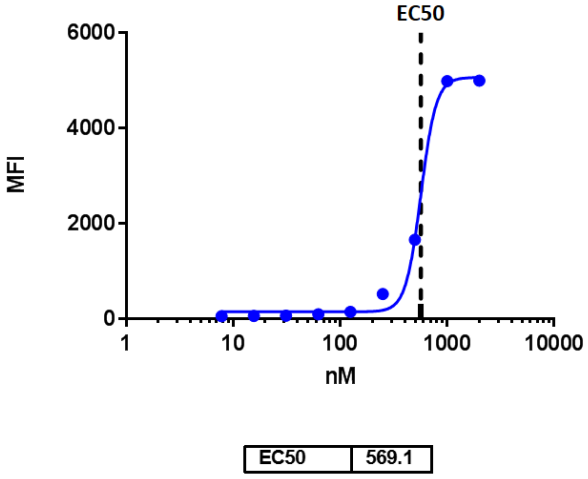

Figure 45: Cellular binding of clone TILB-HCT116-B24 mAb to the HCT116 cell line.

HCT 116 cell lines were incubated with a two-fold serial dilution (2000 nM-0.98 nM) of purified full-length IgG1 TILB-HCT116-B24 mAb. Binding was revealed with anti-human Fc antibody-Alexa Fluor 488 conjugate via flow cytometry (10,000 counts). MFI values were plotted against the logarithm of antibody concentration. The TILB-HCT116-B24 mAb exhibited cellular binding to HCT 116 cells with an EC50 value of 569 nM.

5.8.5. Cellular binding of re-formatted full-length IgG1 purified colorectal cancer derived cells targeting clone TILB-HCT116-B24 by fluorescence microscopy

After the binding analysis using TILB-HCT116-B24 mAb indicated binding to HCT 116 cells by flow cytometry, the aim was to confirm specific binding to the colorectal carcinoma derived cells and not to normal fibroblast colon derived cells. Cellular binding assay using fluorescence microscopy was performed (chapter 4.4.4). For that, HCT 116 cells and the CCD-18Co normal colon fibroblast cells, were incubated on coverslips together with the TILB-HCT 116-B24 mAb (500 nM). TILB-HCT116-A06 mAb that did not exhibit binding to HCT 116 cells was used as isotype control antibody. As HCT 116 cells and the CCD-18Co cells are both known as surface epidermal growth factor receptor (EGFR) expressed cells, the human-murine chimeric IgG1 cetuximab which is a therapeutic mAb for colorectal cancer and binds to domain III of the EGFR ECD (Li et al, 2005), was used here as a positive control antibody (50 nM). The antibody binding was followed by addition of a secondary antibody fragment, the anti-human Fc AlexaFluor488 conjugate. Cell nuclei were stained with Hoechst stain solution. Detection was carried out by fluorescence microscopy. The fluorescence microscopy images obtained for each cell line are depicted in **Figure 46**. Labeling the cells only with the anti-human Fc-AlexaFluor488 conjugate and the Hoechst stain solution was used as setup for the fluorescence background, so that the cell nuclei (blue) can be observed. As expected, the cetuximab mAb bound to EGFR expressed in both HCT 116 and CCD-18Co cells. The imaging data confirmed that TILB-HCT116-B24 mAb bind specifically to HCT 116 colorectal cancer derived cells but not to the CCD-18Co normal colon fibroblast cells. TILB-HCT116-A06 that served as an isotype control non-binder antibody, as expected, was not found to bind to both cells.

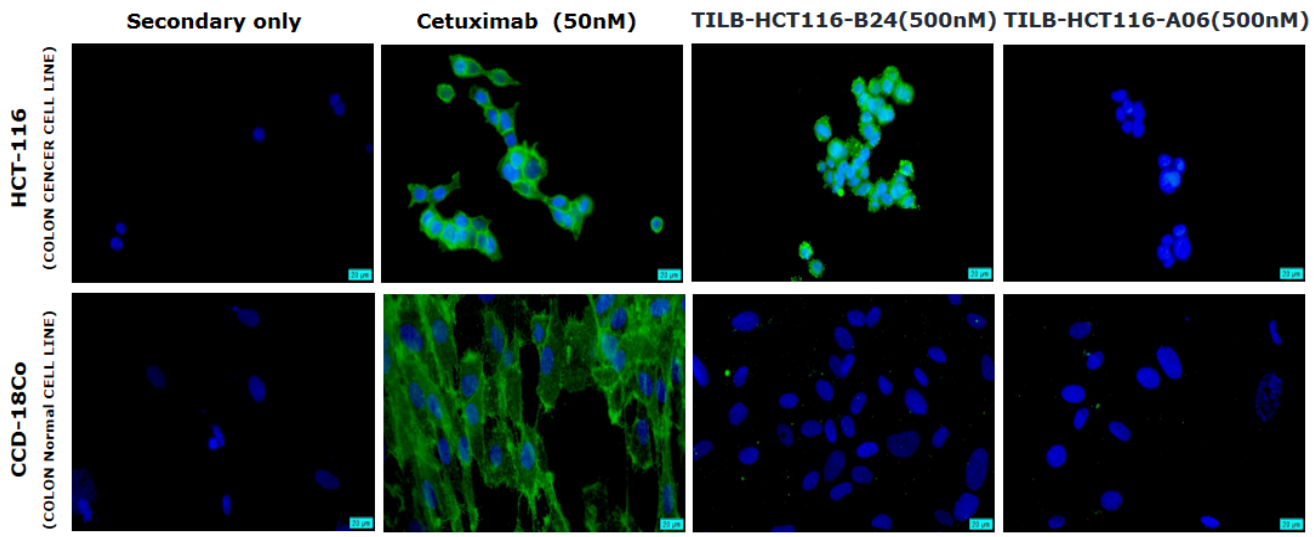

Figure 46: Cellular binding of TILB-HCT116-B24 to HCT 116 cells by fluorescence microscopy.

HCT 116 and CCD-18Co cells were plated on coverslips and incubated with 500 nM TILB-HCT116-B24, 500 nM TILB-HCT116-A06 (isotype control antibody) and 50 nM cetuximab mAb (positive control). Subsequently labeling with the anti-human Fc-Alexa Fluor488 conjugate was performed (green). Cell nuclei were stained with Hoechst stain solution (blue). Detection was carried out by fluorescence microscopy. Scale bar: 20 µm. TILB-HCT116-B24 showed specific binding to the HCT 116 cells while there was no binding observed for the CCD-18Co cells.

5.8.6. Binding analysis of TILB-HCT116-B24 mAb to different TAA by BLI

In order to evaluate if the isolated mAb, TILB-HCT116-B24, binds to one of the TAA which expressed on the surface of HCT 116 cells, the 4 ECD recombinant proteins: h-EGFR, h-CEACAM5, h-5T4 and h-LRP6 (E3:E4) were tested for binding to TILB-HCT-116-B24 mAb by biolayer interferometry (BLI). Briefly, TILB-HCT-116-B24 mAb was immobilized on anti-human Fc (AHC) biosensor tips and association as well as dissociation of the different ECD proteins were monitored. Reference antibodies to the corresponding ECD protein were tested in the same condition. Exemplary sensorgrams of the analysis are depicted in **Figure 47**. The data indicate a wavelength shift in nm of all antibodies captured by the AHC biosensors. A shift of the reference antibodies was observed in the association step with all the corresponding ECD proteins (**Figure 47A**). For TILB-HCT-116-B24 mAb, no wavelength shift was detected in the association step with h-CEACAM5 and h-5T4. A small shift was detected with h- EGFR and h-LRP6, although this shift was confirmed to be non-specific to the antibodies (data not shown) (**Figure 47B**).

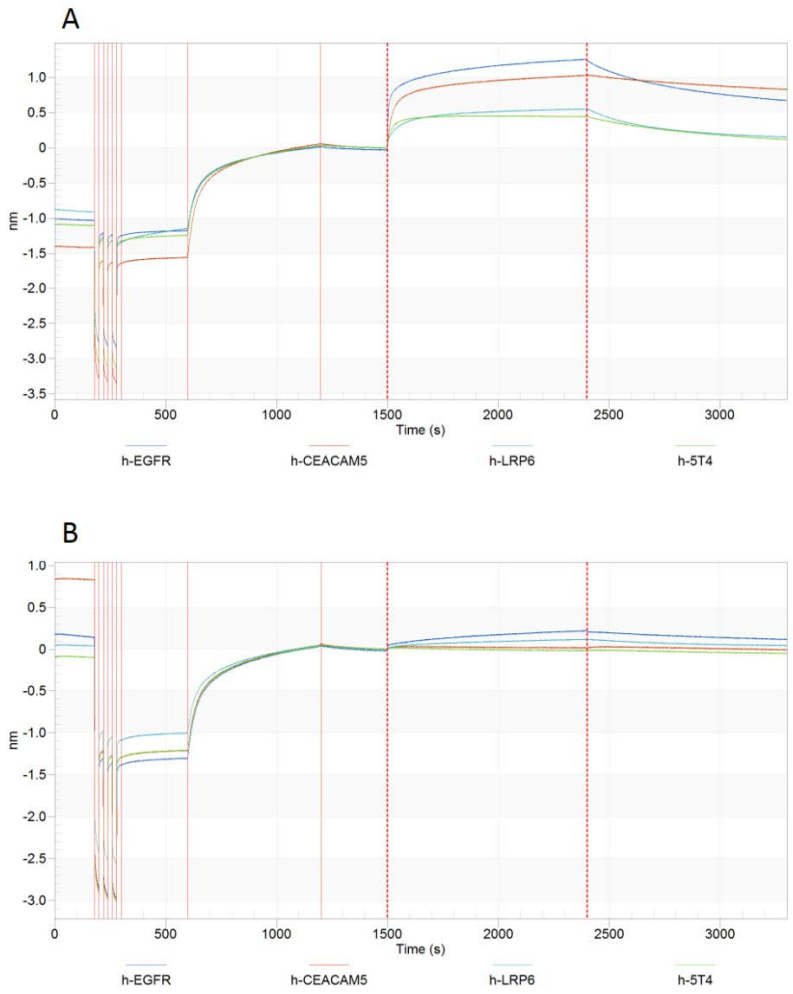

Figure 47:Binding analysis of TILB-HCT116-B24 mAb to different TAA by BLI.

(A) Reference antibodies were immobilized on AHC biosensors (Ab loading). Then, association and dissociation of the different corresponding TAA (200nM) were monitored. For all antibodies association steps an interference pattern shift was observed. **(B)** When TILB-HCT116-B24 mAb was immobilized on AHC biosensors, no wavelength shift was detected in the association step with h-CEACAM5 and h-5T4. A small shift was detected with h- EGFR and h-LRP6, although this shift was confirmed to be non-specific to the antibodies (data not shown).

5.9.NGS analysis of patient libraries (HV, VK, VL)

An NGS analysis was performed based on paired-end reads for the variable region frameworks and complementary determining region (CDR) diversities within the heavy and light-chain of yeast-cells clones of patient libraries (HV, VK, VL). The raw sequencing data was subjected to data quality control and filtering which indicated that sequence quality was very high which allowed for a reliable overlap of the forward and reverse reads (data not shown). Next, data was searched against the IMGT database to find the best match of germline V(D)J genes and to delineate the CDR sequences for each antibody variable domain sequence. After filtering, sequences with aligned V genes that did not contain a stop codon were considered functional sequences and defined as the total read. The V segments that were identical were combined into equivalence clusters and defined as unique. The number of the total reads, the unique sequences and their percentage in the total reads are summarized in **Table 12** for each VH, VK

and VL patient library. This NGS data indicate small diversity of V segments in all patient libraries. Analysis of top ten distribution frequencies NGS reads according to V gene families (VH, VK, VL) and CDR3 for each individual patient sample are depicted in **Figure 48** (only V gene families are presented). The analysis indicated high frequencies of the top sequence in most of the patients' sequences.

Patient ref number	VH Total	VH Unique	% VH Unique	VK Total	VK Unique	% VK Unique	VL Total	VL Unique	% VL Unique
P-20055T	34189	9152	**3%**	6092	22249	**4%**	43347	8778	**2%**
P-20066T	43038	12211	**3%**	4880	24772	**5%**	51836	9249	**2%**
P-20116T	29626	3407	**1%**	6287	18257	**3%**	50783	12134	**2%**
P-20671T	37307	3363	**1%**	3308	14351	**4%**	53003	13634	**3%**
P-20829T	97325	5150	**5%**	5329	14094	**3%**	51523	9451	**2%**
P-21548T	16934	7365	**4%**	2944	5525	**2%**	50828	15114	**3%**
P-21574T	11798	10095	**9%**	4708	14581	**3%**	47460	5919	**1%**
P-22017T	15364	10206	**7%**	2143	9681	**5%**	96564	12623	**1%**

Table 12: Summary of NGS result for the Patients' libraries V gene sequence reads.

The number of total V genes reads (VH, VL and Vk), unique sequences and their percentage in the total reads obtained from the NGS analysis. The NGS data indicate small diversity of V segments in all patients' libraries

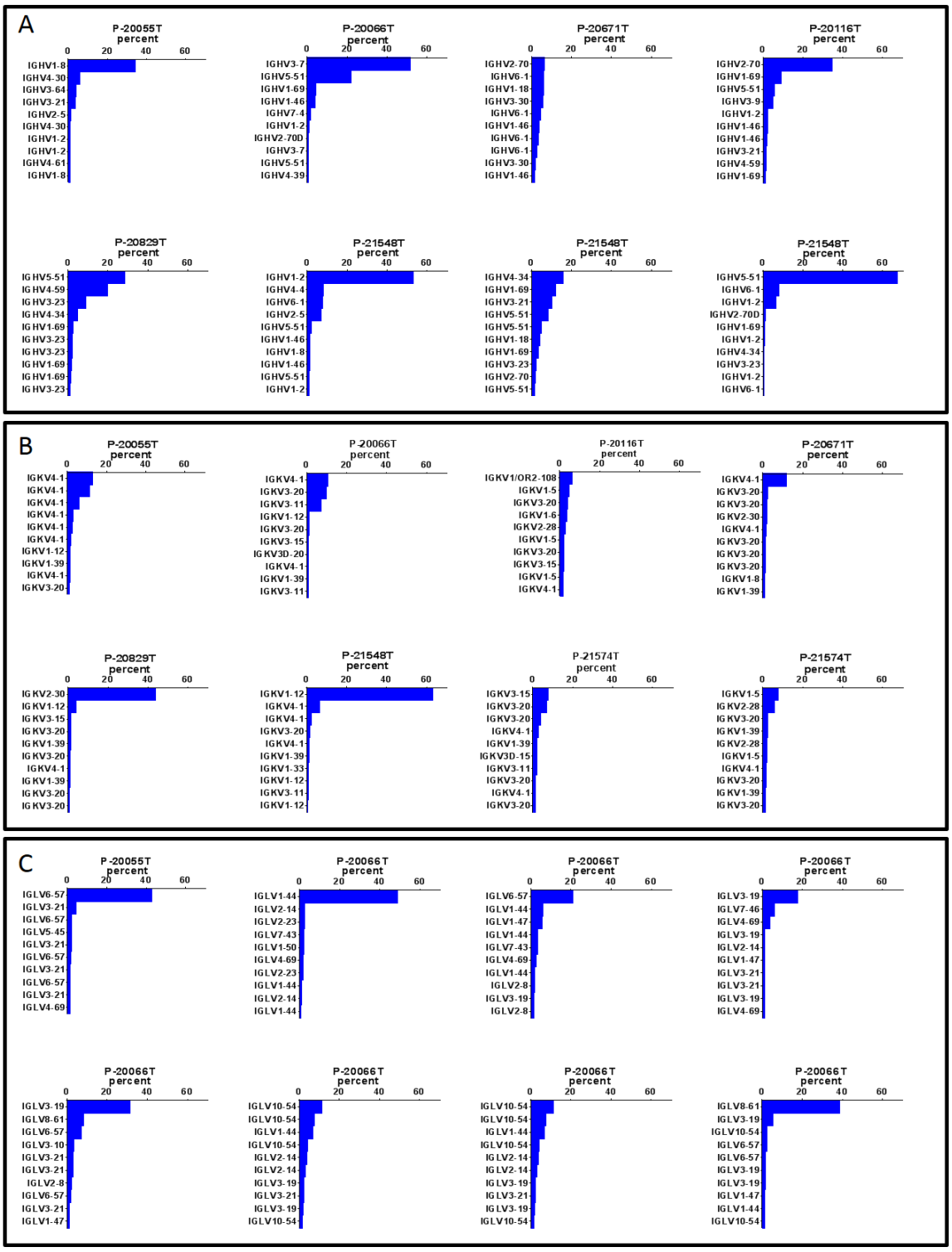

Figure 48: Summary of the NGS results for the patients' libraries top ten distribution frequencies reads.

Analysis of top ten distribution frequencies according to V gene families. **(A)**VH, **(B)**VK, **(C)**VL for each individual patient sample NGS reads. The NGS analysis indicates high frequencies of top sequences in most of the patients' sequences.

5.9.1. NGS analysis for mated libraries (TIL-B κ and TIL-B λ)

The NGS analysis was performed based on paired-end reads for the variable region frameworks and complementary determining region (CDR) diversities within the heavy and light-chain of yeast-cells clones of the mated libraries TIL-B κ and TIL-B λ (**Appendix, Figure 53 and 54**), same as described before (chapter 5.9). The number of total reads, unique sequences and unique sequences with a total read count greater than 1 are summarized in **Table 13** for each VH, VK and VL of the mated libraries. This NGS data show more diversity of the unique sequences reads, as a result of the patients' libraries mixing before the yeast mating.

Library	Total reads	Unique	Unique gt1
TIL-B λ VH	1205657	19302	8143
TIL-B λ VL	1873336	27642	13490
TIL-B κ VH	1980034	33517	13724
TIL-B κ VK	2666160	51933	29192

Table 13: Summary of NGS result for the mated libraries V gene sequence reads.

The number of total V genes reads (VH, VL and Vk), unique sequences from the NGS analysis. The number of unique chains with a total read count greater than 1 is shown as Unique gt1.

An overlap analysis of the two mated libraries showed high correlation of the HV sequence reads between the TIL-B κ and TIL-B λ libraries (**Figure 49**). This data confirms high mating efficiency, as most of the HV sequences reads were found present in both libraries. Moreover, the analysis of the VH gene family distribution of the 2 libraries showed similar distribution of the VH gene families in both libraries (**Figure 50**)

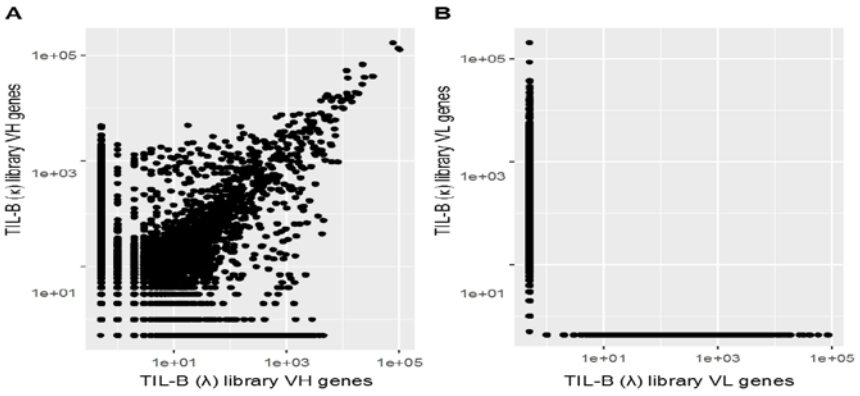

Figure 49: Overlap between V genes of mated TIL-B κ and TIL-B λ libraries.

Overlap graphs between the 2 mated libraries TIL-B κ and TIL-B λ of V gene sequences reads. **(A)** An overlap between VH genes sequence reads showing very high correlation. **(B)** An overlap between VK and VL; no correlation was observed as expected.

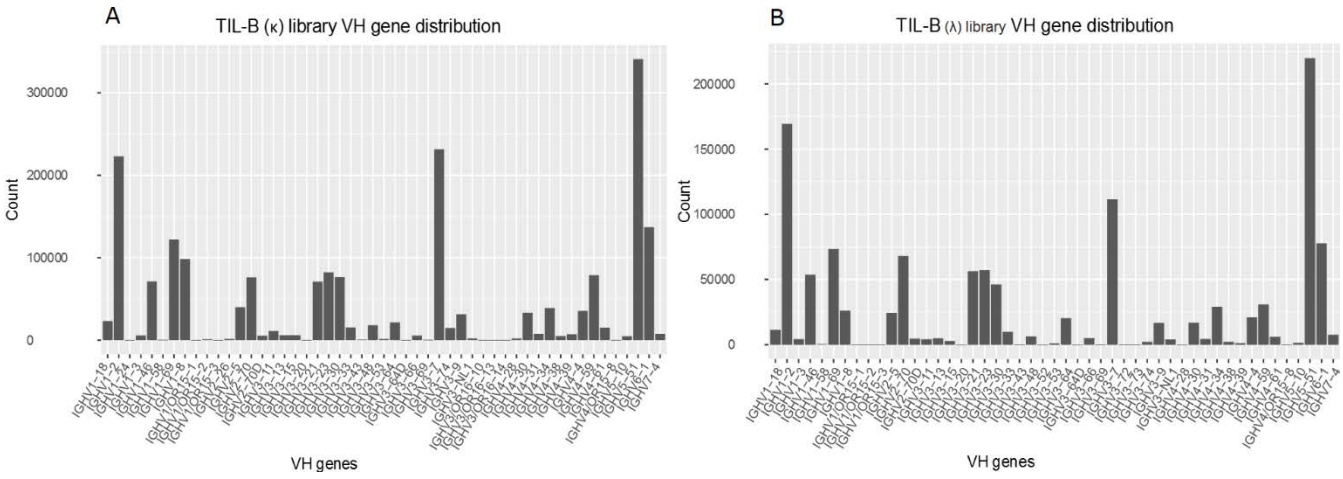

Figure 50: NGS analysis of the VH gene family distribution of mated TIL-B κ and TIL-B λ libraries.

(A) Analysis of the VH gene family distribution of the mated TIL-B κ library. **(B)** Analysis of the VH gene family distribution of the mated TIL-B λ library. Similar distribution of the VH gene families can be observed in both libraries.

5.10. NGS analysis for the enriched biopanning yeast-cells

The next NGS analysis was performed in order to assess the biopanning selection process, for better understanding the clone enrichment profile after the biopanning rounds and to evaluate the ability of mining the yeast libraries for potential cell-binding antibodies by cell biopanning. The NGS analysis included the variable region frameworks and complementary determining region (CDR) diversities within the heavy and light-chain of yeast-cells clones of the last biopanning round against the three cell lines (HCT 116, HT-29 and SW620). The raw sequencing data was subjected to data quality control and filtering which indicated that sequence quality was very high which allowed for reliable overlap of the forward and reverse reads (data not shown). Next, data was searched against the IMGT database to find the best match of germline V(D)J genes and to delineate the CDR sequences for each antibody variable domain sequence. The frequency of each germline gene usage was calculated, and a statistical analysis was done to characterize the CDR3 sequence profile for a given sample, as well as to identify the top enriched CDR3 sequences and sequence clusters in a sample (**Appendix, Figures 55-57**).

5.11. Unique V gene segment and CDR3 combination analysis

In order to analyse the clone enrichment through the biopanning process and to assess the number of the unique clones after the forth biopanning round, the latter was compared to the initial library for all three approaches (HCT 116, HT-29 and SW620). An analysis of the number of unique V gene segments and CDR3 combinations was performed. The total diversity of the variable domain of the heavy chain and the light chain kappa together with the number of chains with a total read count greater than 1 are summarized in **Table 14**. The NGS data analysis confirmed enriched diversity of the clones, as compared to the initial library (**Table 13**) by 1-fold (from ~ 10^4 to ~10^3). Moreover, this NGS analysis revealed that the strategy to pick up 48 clones after the final biopanning round which resulted with identification of 10 unique clones is about 1% of the clones' diversity.

Pool	VH	VK	VHgt1	VKgt1
TILB-HCT116	3018	1737	777	894
TILB-HT29	3231	2291	982	1198
TILB-SW620	1892	2102	676	1080

Table 14: Number of unique V gene segments and CDR3 combinations.

The number of unique V gene segments and CDR3 combinations obtained from the NGS analysis. The number of chains with a total read count greater than 1 is shown as VHgt1, VKgt1 and VLgt1. The diversity after the biopanning enrichment is significantly lower than the initial library diversity.

5.12. Overlap between unique clones from biopanning against HCT 116, HT-29 and SW620

Next, the overlap between the three biopanning outcome sequence reads (TILB-HCT116, TILB-HT29 and TILB-SW620) was examined. The unique sequences were defined by their V gene segments and CDR3 combination sequences. The overlap analysis between the VH unique sequences of the different biopanning approaches is depicted in **Figure 51**. Interestingly, the data indicated a strong correlation between the enriched unique VH clones that panned against the HCT 116 cell line and the HT-29 cell line. One is the colorectal carcinoma derived cell line and the other one is the colorectal adenocarcinoma cell line, respectively. A lower correlation was observed within the VK clone overlaps (**Figure 52**). These results may confirm that the enrichment of clones during the biopanning process is specific to the target expressed uniquely on those colorectal cancer derived cells. A significantly lower correlation was observed comparing the clones panned against the HCT-116 and the HT-29 cell lines to the SW620 colorectal adenocarcinoma metastatic derived cells, which observation supports the claim of the enrichment to specific targets expressed on the different cancer type cells through the biopanning process.

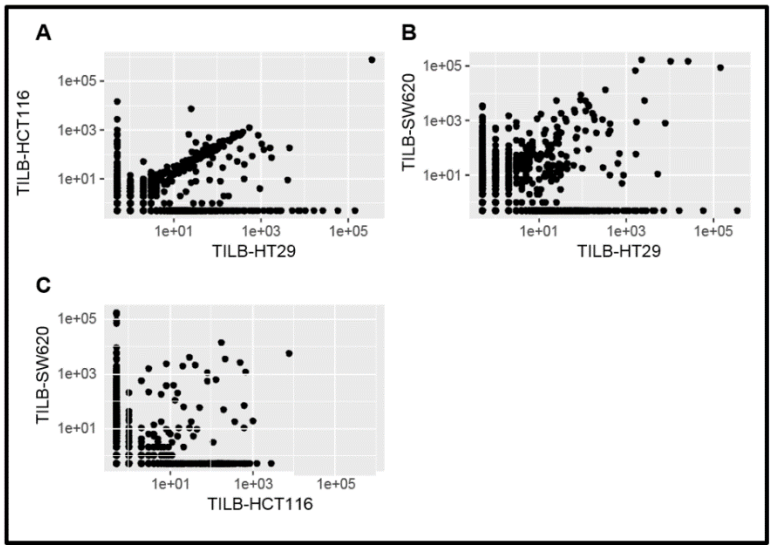

Figure 51: Overlap between unique clones from biopanning against HCT 116, HT-29 and SW620.

Overlap graphs between the three biopanning outcome VH gene segments and the CDR3 combination unique sequences of TILB-HCT116, TILB-HT29 and TILB-SW620. **(A)** The overlap between TILB-HCT116 and TILB-HT29 indicates very high correlation between the enriched clones. **(B)** The overlap between TILB-HT29 and TILB-SW620 indicates some correlation between the enriched clones. **(C)** The overlap between TILB-HCT116 and TILB-SW620 indicates low correlation between the enriched clones. The data may be indicative of enrichment to specific targets expressed on the different cancer type cells through the biopanning process.

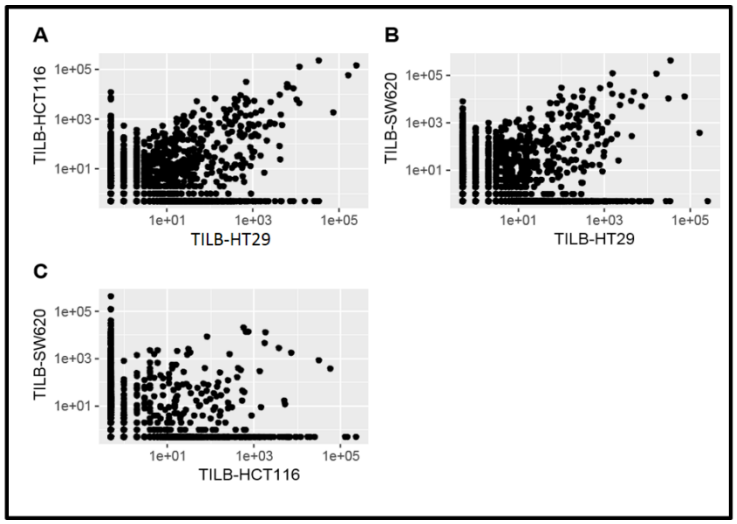

Figure 52: Overlap between unique clones from biopanning against HCT 116, HT-29 and SW620.

Overlap graphs between the three biopanning outcome VK gene segments and the CDR3 combination unique sequences of TILB-HCT116, TILB-HT29 and TILB-SW620. **(A)** The overlap between TILB-HCT116 and TILB-HT29 indicates some correlation between the enriched clones. **(B)** The overlap between TILB-HT29 and TILB-SW620 indicates some correlation between the enriched clones. **(C)** The overlap between TILB-HCT116 and TILB-SW620 indicates low correlation between the enriched clones.

5.13. V gene distribution, CDR3 length distribution, V gene and CDR3 combination top sequences

A further analysis of the V gene distribution, the CDR3 length distribution, as well as the V gene and CDR3 combination top sequences was performed for the three biopanning outcome sequences (TILB-HCT116, TILB-HT29 and TILB-SW620). The analyses are depicted in the appendix (**Figure 55-57**). The data confirmed very high selective enrichment within the heavy chain. In the TILB-HCT116 enriched pool there was selection during the biopanning of the IGHV3-15 VH gene with the CDR3 amino acid sequence: TTGRHYCSGGSCHLSFFDY with 92.6 % from all sequences reads. In the TILB-HT29 the same family gene with the CDR3 amino acid was selected with 25.9% from all sequence reads. For the TILB-SW620 enriched pool a different profile of enrichment was observed, as here most VH gene frequencies were IGHV1-18 and IGHV3-15,21,23 and 48. For the VL genes a wider distribution within the enriched clones was observed in all pools. For the TILB-HCT116 most of the VL gene frequencies were IGKV1-33, IGKV3-15, IGKV3-20, IGKV4-1. For the TILB-HT29 most of the VL gene frequencies were the same as for the TILB-HCT116, i.e. IGKV3-15, IGKV3-20, IGKV4-1. A different enrichment profile was observed for the TILB-SW620, as most of the VL gene frequencies were IGKV1-12, IGKV3-11, IGKV3-20, IGKV3-15 and IGKV4-1. This data also indicated that the enrichment of clones during the biopanning process is specific for a target expressed uniquely on the colorectal cancer derived cells (HCT116 and HT-29), as a different enrichment V genes distribution profile was observed from the SW620 enriched clones.

5.14. Frequency of V gene and CDR3 combination of selected clones

Finally, the frequency of the V gene and the CDR3 combinations of the selected clones was analyzed. The V genes of the heavy and the light chains with the combination of the CDR3 amino acid sequence, with their frequency within the NGS reads of the last biopanning round pools, TILB-HCT116 and TILB-HT29, are summarized in **Table 15**. The data indicate the same VH gene and CDR3 combination in 11 from the 12 selected unique clones that were identified as the IGHV3-15 VH gene and with the CDR3 amino acid sequence TTGRHYCSGGSCHLSFFDY. The results are consistent with the fact that this clone was identified as 96% of all the reads within the TILB-HCT116 pool and 50% of all the reads within the TILB-HT29 pool. The VL gene and the CDR3 combination for the selected clones appeared in both pools but with lower frequency than VH and with high distribution between clones. The data here again indicate selective enrichment in the biopanning process for a specific target that expressed uniquely on the derived colorectal cancer cell lines with specificity determined by the heavy chain domain.

Clone ID	VH gene	VH CDR3 AA	Frequency TILB-HCT116	Frequency TILB-HT29	VL gene	VL CDR3 AA	Frequency TILB-HCT116	Frequency TILB-HT29
TILB-HCT116/HT29 A06	IGHV3-15	TTGRHYCSGGSCHLSFFDY	92.6%	49.9%	IGKV4-1	QQYYTTPQT	16.3%	28.4%
TILB-HCT116/HT29 A17	IGHV3-15	TTGRHYCSGGSCHLSFFDY	92.6%	49.9%	IGKV1-33	QQYGMSPRT	14.5%	1.3%
TILB-HCT116/HT/29 B24	IGHV3-15	TTGRHYCSGGSCHLSFFDY	92.6%	49.9%	IGKV3-20	QQYGMSPRT	6.5%	18.3%
TILB-HCT116 A02	IGHV3-15	TTGRHYCSGGSCHLSFFDY	92.6%	49.9%	IGKV3-11	QQRSGWPLT	<0.5%	<0.5%
TILB-HCT116 A03	IGHV3-15	TTGRHYCSGGSCHLSFFDY	92.6%	49.9%	IGKV3/OR2-268	QQYYNSPPAYT	<0.5%	<0.5%
TILB-HCT116 A05	IGHV3-15	TTGRHYCSGGSCHLSFFDY	92.6%	49.9%	IGKV3-15	QQYNNWPDT	25.9%	3.8%
TILB-HCT116 A07	IGHV3-15	TTGRHYCSGGSCHLSFFDY	92.6%	49.9%	IGKV1-6	QQYYNTPWT	1%	<0.5%
TILB-HCT116 A11	IGHV3-15	TTGRHYCSGGSCHLSFFDY	92.6%	49.9%	IGKV1-39	QQSYSAPYT	0.6%	<0.5%
TILB-HCT116 A14	IGHV1-3	ARARSGVGATRSLWNFDY	0.9%	0.7%	IGKV3-20	QHSGSSPGT	<0.5%	<0.5%
TILB-HCT116 B06	IGHV3-15	TTGRHYCSGGSCHLSFFDY	92.6%	49.9%	IGKV3-20	QQYVSSRIT	<0.5%	<0.5%
TILB-HCT116 B08	IGHV3-15	TTGRHYCSGGSCHLSFFDY	92.6%	49.9%	IGKV1-39	QQSYSTPLLT	<0.5%	<0.5%
TILB-HT29 A08	IGHV3-15	TTGRHYCSGGSCHLSFFDY	92.6%	49.9%	IGKV1-5	QQRSYWRT	<0.5%	1.3%

Table 15: Frequency of the V gene and the CDR3 combination of the biopanning selected clones.

Frequency of V gene and CDR3 combination of selected clones were analyzed. V genes of the heavy and the light chains with the combination of the CDR3 amino acid sequence, with their frequency in the NGS analysis of the biopanning outcome pools, TILB-HCT116 and TILB-HT29, are summarized.

6. Discussion

6.1. Generating Fab YSD libraries derived from colon cancer patients' tumor infiltrating B cells

From the first FDA approval of the monoclonal antibody (Mab) Rituximab, targeting CD20 in non-Hodgkin's lymphoma patients about 20 years ago, until recent years approval of monoclonal antibodies that act by blocking checkpoint molecules such as PD-1, PD-L1 and CTLA-4, which enhance the immune system to fight against cancer cells. Monoclonal antibodies have been considered as breakthrough therapies in oncology. Still, cancer therapy by monoclonal antibodies has its limitations, and there is much space for better therapeutics to come. Historically, the success rate of monoclonal antibodies from Phase I clinical studies to clinical approval is low and can be estimated at 10 to 15% without considering many failures in preclinical studies (A. L. Nelson & Reichert, 2009; Workman et al., 2017). Currently there are relatively few tumor-associated antigens for antibody targeting in oncology that are approved for clinical therapy. This could be a result of lack in technologies enabling antigen profiling in intact tumors, to identify tumor markers targetable with antibodies, which raises the need for new strategies that may be used to overcome these limitations (Sánchez-Martín et al., 2015). In addition, a better understanding of the antitumor immune responses in cancer patients can be an important key for advancing the field of monoclonal antibodies in cancer therapy. This may result in better mAbs, successful targeting of new tumor-associated antigens and even finding novel mechanisms of action. This study aims to investigate part of the antitumor immune responses by generating yeast display libraries representing the immunoglobins of B cells infiltrating to the tumor of colon cancer patients. At a later stage, screening by traditional and emerging technologies such as deep sequencing (NGS) and phenotypic screening by yeast display biopanning, may lead to revealing new antibodies and targets for cancer therapy.

Previous reports indicate that tumor infiltrating B cells from patient's tissue can be a rich source of tumor-binding antibodies. (Novinger et al., 2015; Pavoni et al., 2007). These studies isolated the antibodies from a TIL B phage display library derived from the patients' tumors. To our knowledge, our work is the first study to construct YSD Fab libraries derived from colon cancer patients with high density of B cells infiltration (**cf. Figure 6**). The 8-patients showed diversity in gender, age, colon section and tumor grade (**cf. Table 3**). A standardized protocol developed with the hospital personnel insured snap freezing of the tissues less than an hour post surgery, to maintain mRNA integrity(Grizzlea et al., 2012). The RNAs isolated separately from each tissue, were adequate for continuous processes in terms of RNA quantity, purity and quality (**cf. Table 4, Figure 7**). cDNA was prepared, and the quality of the RNA and PCR was assessed by analyzing two known B-cell expressed genes (CD19 and CD20) (**cf. Figure 8 and 9**). Heavy and light chain hypervariable regions (VH,VL) were PCR amplified successfully from cDNA using VH and VL kappa and lambda primers and gel purified (**cf. Figure 10 ,11 and 12**). Sequences for these were adapted from

previously described methods (Hust & Dübel, 2010). A strategy to select the class-switched B cell population was applied by designing a reverse primer for VH amplification starting at IgG constant regions. A second PCR reaction was performed to flank 5′ and 3′ overhangs for gap repair cloning and amplification of DNA amount was carried out in a third PCR. After purification of the VH,VL kappa and lambda products and digestion of the corresponded YSD plasmids, cloning was carried out by gap repair according to Benatuil et. al.(Benatuil et al., 2010) to generate successfully heavy and light chain (kappa and lambda) libraries for each of the 8 patients. Library size was calculated to be approximately 1.4 to 5.6 x 10^7 clones for each VH and VL libraries with good transfection efficiency (**cf. Table 5**). All 8 VH libraries that were transformed into haploid EBY100 strain yeast and were united to one pool. The same pooling was carried out for the VL libraries (kappa and lambda) that were transformed into a haploid BJ5464 strain. Functional Fab YSD libraries were obtained after fusion of haploid cells EBY100 and BJ5464 by yeast mating, according to a previously described method (Weaver-Feldhaus et al., 2004) resulting in final library sizes of approximately 4.1×10^8 clones for the HC-LC kappa library (TIL-B kappa) and approximately 2.5×10^8 clones for the HC-LC Lambda library (TIL-B lambda).

6.1.1. Deep sequencing analysis of TIL-B derived libraries

TIL-B phage antibody display libraries have been analyzed in previous studies by isolation of around 10^2 clones in combination with Sanger sequencing (Coronella et al., 2002; Novinger et al., 2015). To our knowledge, this is the first study to use next-generation sequencing (NGS) to provide a high-throughput sequencing of clones derived from patients' TIL-B cells, allowing for far greater insights into library diversity by providing up to ~10^6 sequences reads per library. Comprehensive NGS analysis was run based on paired-end reads for each of the 8 patients libraries (HV, VL κ, VL λ) and for the mated Fab displayed TIL-B kappa and TIL-B lambda libraries. After filtering, sequences with aligned V genes that did not contain a stop codon were considered functional sequences and defined as total reads. V segments that were identical were combined into equivalence clusters and defined as unique. Interestingly, looking at the number of V unique segments percentage out of the total reads, revealed a narrow diversity of V segments in all patients' libraries (**cf. Table 12**) that could be due to a small number of the initial source of infiltrating B cells in the tumor. This is consistent with a previous study with phage display libraries, comparing sequencing of VH CDR3 of synthetic libraries and donor-derived libraries with high and low number of donors, using the Illumina platform (That also have been used in this study). That study revealed that the synthetic libraries had many more unique clones compared with donor-derived libraries. In the donor libraries, the higher amount of donors lead to the higher amount of unique clones. (Ravn et al., 2013).

In this study, we analyzed the top ten distribution frequencies according to V genes and CDR3 for each individual patient sample. This revealed V gene sequences that were present in high copy number at high percentages from all sequences (**cf. Figure 48**). In some patients there are V genes and CDR3 that are present in more than 40% of all sequences, and these are observed for HC and LC (κ & λ). Although, amplification biases during antibody library construction and during the NGS platform should always been considered (Fantini et al., 2017), this distribution with dominant V genes over all unique genes that occurred in all patients could suggest clonal expansion within the infiltrated B cells source rater then a bias. This case, of high frequency of a single sequence as V gene or CDR3 fits to libraries after selection, as shown in previous studies (Ravn et al., 2013).

Mated libraries TIL-B kappa and TIL-B lambda were also analyzed by NGS. As expected, both libraries presented more diversity as result of the patients' libraries mixing before the yeast mating **(cf. Appendix Figure 53 and 54**). Interestingly, the V gene distribution after 2 distinct yeast mattings of the HC library once with the LCκ and once with the LC λ, resulted in quite similar patterns of distribution **(cf. Figure 50**). This can be seen also in the strong linear correlation between the 2 HC V genes overlap plot **(cf. Figure 49)**, indicating also for high efficiency of the mating process.

6.2. Evaluation of the YSD TIL-B libraries with target-based screening and selection

Although previous studies have demonstrated successful isolation of tumor infiltrating B derived antibodies binding to autologous tumor targets on cancer cells (Novinger et al., 2015; Pavoni et al., 2007), only one study reported isolation of a ScFv anti-GD3 antibody fragment from phage display tumor infiltrating B cells derived library based on target-based screening to GD3 ganglioside (Kotlan et al., 2014) . Additionally, two studies demonstrated target-based screening of phage display libraries derived from invaded lymph nodes of a breast cancer patient, resulting in isolation of antibodies targeting Her-2 and CEA (Ayat et al., 2013b; Belimezi et al., 2006). In this study, comprehensive target-based screening of two yeast Fab display TIL-B derived libraries (κ& λ) against a broad panel of defined tumor associated antigens (TAA) and immune checkpoint proteins was performed. Biotinylated recombinant soluble targets were incubated with the Fab displayed yeast cells, followed by staining with streptavidin allophycocyanin (APC) conjugate and were subjected to flow cytometry for binding evaluation. The tumor associated antigens panel were selected based on antigens that are overexpressed in colon cancer, such as EGFR (Harari, 2004), CEACAM5,6,1 (Heine et al., 2011), LRP6 (Rismani et al., 2017), DLK-1 (Yanai et al., 2010), C-MET (Su Jin Lee et al., 2018) and 5T4 (Starzynska et al., 1994). The panel included also HER-2 that has low expression in colon cancer (Nathanson et al., 2003) and other antigens as TEM1 that displays elevated expression during tumor angiogenesis (Carson-Walter et al., 2001) or membrane GRP78 that is overexpressed under stress conditions of the tumor microenvironment (Ni, Zhang, & Lee, 2011). The panel of immune checkpoint molecules included

targets that are expressed on T cells such as PD-1, LAG3, CTL-4 and TIM3 and ones that are expressed on antigen-presenting cells and tumors such as PDL-1,CD200,OX40L and B7-H3 (Pardoll, 2012). Interestingly, the screening of both TIL-B libraries kappa and lambda indicated Fab displayed yeast-cell binders to all tumor associated antigens resulting in total MFI above the background level (**cf. Figure 12**). Significant total MFI was observed from binders to 5T4 and LRP6 antigens in the TIL-B kappa library while in the TIL-B lambda library the most significant total MFI was observed with CEACAM5 and LRP6. These results align with the reported relatively high overexpression of 5T4, LRP6 and CEACAM5 in colon cancer. Conversely, screening for Her-2, which is known for its low expression in colon cancer, resulted in low total MFI in both libraries. Screening both libraries with immune checkpoint antigen targets resulted in in total MFI close to the background (**cf. Figure 13**). Here, significant total MFI was observed only from binders to OX40L and LAG-3 when screening the TIL-B kappa library. In the TIL-B lambda library most significant total MFI were observed from OX40L (LAG-3 was not screened). These are interesting observations, as LAG-3 is an immune checkpoint that is expressed on tumor infiltrating immune cells and was found to be significantly associated with a better disease-free survival (Soo Jung Lee et al., 2018). OX40L expression is upregulated in response to antigen presentation on multiple antigen-presenting cells (Webb, Hirschfield, & Lane, 2016).

Based on the screening results, the two cancer associated antigens LRP6 and CEACAM5, as well the two immune checkpoints proteins OX40L and LAG3 were chosen for further high-throughput selection by fluorescence-activated cell sorting applying a multiparameter screening strategy based on antigen binding and Fab display levels, to isolate human mAbs from the YSD TIL-B derived libraries. This YSD selection strategy has been reported in previous studies for isolation of high affinity mAbs to RTK , CEACAM5 and 6, where it was based on immune repertoires of transgenic rodents after immunization with the targeted antigen (Krah et al., 2017; Schröter et al., 2018). For all targets, enrichment was achieved during the sorting rounds. When monitoring binding of YSD clones during sorting rounds without adding the biotinylated antigen but only the SA-APC marker, enrichment of YSD clones to the SA-APC marker was observed. This binding explained previously as binding to the APC fluorophore is likely related to the presence of multiple epitopes on this large multimeric protein (Pape, Taylor, Maul, Gearhart, & Jenkins, 2011). The APC binders were eliminated by different strategies such as: replacing the secondary marker to SA-PE or SA-DyLight 633 during the sorting rounds. Selection of hOX40L-targeting antibodies was performed by five sorting rounds starting with 6.3 % YSD binders using 1µM hOX40L. The fifth round resulted with enrichment of YSD binders to 27.7 % using 0.25 µM hOX40L (**cf. Figure 14 and 15**). From 95 enriched picked clones after sequencing and clustering, 13 clones were identified as unique binders (**cf. Table 6**) . Selection of LRP6-targeting antibodies was performed by five sorting rounds starting with 6.7 % YSD binders using 1µM hLRP6, the fifth round

resulted with enrichment of YSD binders to 41.1 % using 0.1 µM hLRP6 **(cf. Figure 16 and 17**). From 20 clones after sequencing and clustering, 2 clones were identified as unique binders (**cf. Table 7**). Selection of hLAG3-targeting antibodies was performed by three sorting rounds starting with 0.5 % YSD binders using 1µM hLAG3. The third round resulted in enrichment of YSD binders to 59.5 % using 0.25 µM hLAG3 (**cf. Figure 18 and 19**). From 95 clones after sequencing and clustering, 18 clones were identified as unique binders (**cf. Table 8**).

The Selection of hCEACAM5-targeting antibodies was performed using a different strategy: here prior to selection with FACS, selection by YSD biopanning was performed (**cf. Figure 20**), applying a YSD biopanning technique which was developed and described previously (Tillotson et al., 2013) (**cf. Figure 3**) .The advantage here is the number of YSD cells that can be taken for the first round of selection, which is grater by one fold (~10^9) compared to the FACS sorting approach. The human gastric cancer derived cell line MKN-45, is known for its high expression of CEACAM5 on the cell surface (Alonso-Camino et al., 2009). For depletion of non CEACAM5 binders, CEACAM5 CRISPR-Cas9 knockout MKN45 cells were constructed at ITL labs (data not shown) using the CRISPR-Cas9 knockout technology (Ran et al., 2013) . Hence, depletion was conducted on cells that are identical to the selection strain, with the elimination of the target itself. After 5 rounds of YSD biopanning only 4.6 % of YSD cells were enriched for CEACAM5 binding indicating for insufficient depletion of non-CEACAM5 binders. The biopanning enriched YSD then was subjected to selection by FACS. Here, selection of hCECAM5-targeting antibodies was performed in four sorting rounds starting with 8.7 % YSD binders using 1µM hCEACAM5, the fifth round resulting in enrichment of YSD binders to 12.1 % when using 0.25 µM hCEACAM5 (**cf. Figure 22**). From 10 clones after sequencing and clustering, 2 clones were identified as unique binders (**cf. Table 9**).

The variable regions of the unique Fab displayed clones from all four campaigns were subcloned into mammalian expression DNA vectors, to obtain soluble expression of full-length IgG1. Using biolayer interferometry (BLI) assay, the full-length IgG1 antibody is first captured on anti-human Fc biosensors followed by association of the corresponding soluble recombinant antigen protein (OX40L, LAG3,LRP6 and CEACAM5) resulted in no wavelength shift at the association step in all campaigns **(cf. Figure 28,30,32 and 34)**. This can be due to loss of binding to the corresponding antigen while reformatting from yeast to mammalian expression, or due to the fact that the antibodies are low affinity antibodies with affinity below the assay's limit of detection. As the full-length IgG1antibody is bivalent, in solution it can potentially interact with two antigen molecules that are immobilized to a surface leading to an "avidity affect" which may result in artificially higher affinity measurements (Tobias & Kumaraswamy, 2013). Therefore, using BLI in a different orientation, where a biotinylated antigen is immobilized to the streptavidin biosensors surface, followed by adding the antibodies in solution, may reveal low affinity antibodies. Using this BLI strategy, a wavelength shift was detected

at the association step when adding the corresponded antibodies to the biotinylated immobilized antigens in all campaigns, indicating specific binding of the antibodies but with low affinity to the antigen that can be estimated in a range of micromolar **(cf. Figure 29,31,33 and 35)**.

As the study confirms specific binding of the isolated reformatted IgG1 antibodies, the reason for their low affinity antibody is interesting. Enrichment of low affinity antibody clones from a yeast display library during selection with FACS was reported previously (Feldhaus et al., 2003). Yeast display library cells can display approximately $10^4 – 10^5$ fusion proteins on each yeast cell surface. Multi-copy display of Fab fragments on yeast surface could enable multivalent interactions, and an increased propensity for multivalent binding by some library clones could lead to recovery of high avidity binders lacking high affinity to the antigen (Boder et al., 2012). While considering the immunoglobulin source in tumor infiltrating B cells, it is still debatable if those autoantibodies against self-antigens (like those screen in this study) can show very high affinity binding and be involved with the killing of tumor cells or their occurrence in the tumor microenvironment is due to antigen presentation but does not lead to generation of high affinity antibodies (Coronella-Wood & Hersh, 2003; Iglesia et al., 2014; Tsou, Katayama, Ostrin, & Hanash, 2016). On the other hand, as specificity was identified with all the isolated antibodies, it may be argued that the low affinity antibodies are a result of the YSD libraries construction strategy. As the heavy and light chains are shuffled in the antibody yeast display libraries, displayed antibodies may not recapitulate the original B cell heavy and light chain combinations. In this study the heavy chain immunoglobulin source for constructing the libraries was restricted to be only IgG isotope by amplifying the variable regions starting from IgG constant regions in order to select the IgG class-switched B cell population. The light chain immunoglobulin source cannot be restricted to IgG class and could be selected with any type of B cell including ones that did not undergo antigen mediated selection. Moreover, before yeast mating, heavy chain libraries from all patients were mixed. This was also done for the light chain libraries, lowering the probability for original paring of heavy and light chains (Marks et al., 1991).

6.3. Evaluation of the YSD TIL-B libraries using biopanning on colon cancer derived cell lines

Evaluation of the YSD TIL-B libraries by target-based screening resulted in isolation of specific but low affinity antibodies to the screened targets. This strategy is limited to the target we select for the screening. Moreover, screening of targets as soluble recombinant proteins when actually they are membrane bound in their native state in the tumor, could lead to missing out on antibodies that only bind effectively to targets expressed on the intact cells in their native conformation (Stern et al., 2016).Therefore, phenotypic screening on intact mammalian cancer cells which present a broad repertoire of cancer associated antigens on their surface in their native confirmation could be a better strategy for evaluation of the TIL-B derived libraries. Due to this, in this study, we also evaluated the

colon cancer patients' TIL-B derived YSD libraries by using the YSD biopanning method on human colon cancer derived cell lines. While previous studies have been reported to isolate successful antibodies from naïve YSD libraries targeting a verity of mammalian cell lines (Dangaj et al., 2013; Wang et al., 2007; Williams et al., 2014; Zorniak et al., 2017), this is the first study to our knowledge to use TIL-B YSD libraries with the biopanning method.

As the immunoglobulin sources of the YSD libraries are derived from tumor infiltrating B cells of colon cancer patients, the strategy for the libraries evaluation was to use the YSD biopanning platform against corresponded colon cancer derived cell lines. For that, 3 distinct colon cancer derived cell lines were chosen: The colorectal carcinoma derived cell line HCT 116, which are a colorectal adenocarcinoma derived cell line HT-29, and SW620 which is colorectal adenocarcinoma derived cell line from a metastatic lymph node site. To isolate antibodies to cancer associated antigens, the CCD-18Co normal colon fibroblast cell line was used as negative cells for depletion of colon normal cell binders. Increased binding of YSD to all HCT 116, HT-29 and SW620 cell surface was microscopically observed after 3 rounds of biopanning **(cf. Figure 36, 37, and 38).** Next, a binding profile analysis of the biopanning enriched YSD clones of the three biopanning approaches was done on a broad panel of 12 distinct cell lines. This included the cell line the YSD cells were panned against, cells from other cancer types, the normal colon cell line and the Chinese hamster ovary derived cell line (CHO-S1). Interestingly, after 4 biopanning rounds the YSD clones that were enriched on the colorectal carcinoma derived cell line HCT116, showed high binding also to the colorectal adenocarcinoma derived cell line HT-29 and to the gastric adenocarcinoma derived cell line MKN45. YSD clones that were enriched on HT-29 cell line showed high binding to the HCT 116 cell line and MKN 45 cell line. In both biopanning schemes, binding to other cancer derived cell lines was negative or low. No binding was observed to the normal colon cell line and the CHO-S1 cell line which is as we expected. These results indicate that the binding profile is selective when clones from the same library were enriched for epitope targets that are expressed only on colorectal cancer derived cell lines (HCT116 and HT-29) and on the gastric cancer derived cell line (MKN45). Moreover, YSD clones that were enriched on the colorectal adenocarcinoma metastatic lymph node site cell line SW620 showed a different profile of binding with high binding observed on all mammary gland adenocarcinoma derived cell lines (MB468 ,MCF7 and SKBR3) and to the HT-29 cell line. As the SW620 colorectal adenocarcinoma are metastatic derived cells they may display a different membrane protein expression. The different binding profile of the enriched YSD that was observed indicates again for selective enrichment.

As the biopanning enriched clones on HCT 116 and HT-29 shared the same binding profile, for further characterization 48 YSD clones were picked and clustered by their VH and VL sequences. The clustering analysis reviled 13 unique YSD clones from the biopanning enriched HCT 116 cell line clones and 10 unique yeast clones from the biopanning enriched HT-29 clones. Interestingly, 3 unique

yeast clones selected from the two distinct biopanning approaches (HCT 116 and HT-29) were found to be the same clones (**cf. Table 10**). Binding analysis of the 20 unique clones resulted in 12 clones that specifically bound to the colorectal carcinoma derived HCT 116 cells. No binding was observed to MCF7, CHO-S1 cells and to normal colon fibroblasts cells **(cf. Figure 42 and Table 11)** .Variable region subcloning of the unique YSD clones resulted in soluble expression of full-length IgG1 antibodies. Cellular binding analysis by flow cytometry resulted in 6 antibodies that bind to the HCT 116 cells **(cf. Figure 43**). When looking at the 12 antibody sequences by multiple alignment analysis **(cf. Figure 44)** the reason for the variation in binding of the antibodies could be hypothesized. The VH sequence multiple alignment reviled that out of 12 antibodies 11 have the same CDR3 and very high identity to each other. On the other hand, multiple alignment of the VL sequences showed high variation in CDR3 and in other segments of the different antibodies variable region (such as framework regions). It has been reported previously, that the heavy chain CDR3 is the region responsible for antigen recognition (Wine et al., 2013) and it is well known from affinity maturation experiments that the affinities of antibodies with identical HCDR3s may differ by up to 100-fold when they have different light chains (Marks et al., 1991; Schier et al., 1996; Yang et al., 1995). Consequently, it can be concluded that probably all selected antibodies share the same epitope binding, directed by the heavy chain, but the binding affinity is determined by the light chain.

As discussed previously, the phenomenon in which binding of antibodies to cells observed in YSD Fab format but not as soluble full-length IgG1 antibodies, is due to an avidity effect of the YSD fab clones (Boder et al., 2012). The multivalent binding resulted in our incapability to differentiate between binding affinity of the selected YSD Fab clones, as all seemed phenotypically to be strong binders under the microscope (**cf. Figure 42**). This aspect should be considered in further studies involving YSD biopanning.

For further characterization, TILB-HCT116-B24 mAb which shows positive binding to HCT 116 cells in crude medium was purified. A cellular binding assay to HCT 116 cells using flow cytometry with a two-fold serial dilution of the mAb (2000 nM-0.98 nM) resulted in a dose response curve with EC50 value of 569 nM (**cf. Figure 44**). A cellular binding assay using fluorescence microscopy with TILB-HCT116-B24 mAb to HCT 116 cells and normal colon fibroblast cells (CCD-18Co) showed specific binding to HCT 116 cells and no binding to the normal cells were observed (**cf. Figure 45**). This result supports the hypothesis of this study, that tumor infiltrating B cells can be a source for selective antibodies to antigens expressed on cancer cells.

6.4. Combining high-throughput sequencing and YSD biopanning screening

In order to comprehensively access the full potential of a given natural or recombinant antibody library usually in the range of 10^6–10^{11} clones, diversity has to be significantly reduced for high-throughput

sequencing to be able to provide a meaningful in-depth view of potential antigen-specific library variants (Glanville et al., 2015). Hence, the YSD biopanning process could be ideal for combining with new generation sequencing (NGS). After few biopanning rounds of the YSD library all antibody sequences based on phenotypic binding to the antigen should ideally be observed multiple times in the sequencing data sets (with ~ 10^6 reads). Therefore, when analyzing by NGS a YSD library after biopanning against antigens presenting on certain cell could revile an accurate selective- binding profile of the enriched VH and VL sequences. This tool can be used for example to compare the binding profile of a YSD library after biopanning against different cancer cell lines. To our knowledge, this is the first study to combine YSD biopanning selection with NGS analysis.

The fourth round biopanning outcome of clones that were enriched on HCT 116, HT-29 and SW620 were NGS analyzed for their VH VL sequences. This analysis revealed a deeper understanding of the biopanning and clone selection process. When we picked 48 YSD clones from each biopanning enrichment on HCT 116 and HT-29 cells and Sanger-sequenced them, we found 10 unique clones for each approach (**cf. Table 15**). This is about 1% of the number of unique sequences diversity obtained from the biopanning enriched libraries (**cf. Table 14**). However, looking at the unique clones that were identified, from 12 clones 11 shared the same VH gene combination with CDR3 in the VH sequences while different VL identified in all clones. This is not surprising as the NGS analysis revealed that the frequency of the HC sequence is 92.6 % while much more diversity in frequency was detected in the VL sequences (<0.5-28%) **(cf. Appendix Figure 55 and 56**). This reinforces the hypothesis of high selective enrichment through the heavy chain antigen recognition site to specific epitopes.

Moreover, a stronger argument to this selective enrichment was revealed by overlapping the unique clones' sequences of the VH and VL sequences between the 3 biopanning approaches **(cf. figure 51 and 52**). Interestingly, the outcome of the 2 independent biopanning selections of the same library on 2 colorectal epithelial derived cell lines HCT116 and HT-29 resulted with very high correlation when overlapping the unique VH genes combined with CDR3 sequences of both biopanning outcome. However, when overlapping the SW620 biopanning sequences, no significant correlation was observed to HCT116 and HT-29 biopanning sequences (**cf. figure 52**). This can be explained by the different source of the cells, as this cell line is derived from the lymph node metastatic site of a colorectal cancer patient and apparently is displaying a distinct antigen surface expression. VL genes sequences revealed some correlation between biopanning HCT116 and HT-29 outcomes in low frequencies but not significant as the VH sequences (**cf. figure 53**). As discussed before, this selective binding through the heavy chain can be a result of the library construction strategy that restricted the heavy chain to the IgG class-switched B cell population.

This study supports the hypothesis that tumor infiltrating B cells (TIL-B) derived libraries contain a repertoire of antibodies that can bind preferentially to cancer cells. These antibodies can help us better understand the innate immunity of cancer and may be a potential source of antibodies for cancer therapy.

6.5. Outlook

Further evaluation is needed for characterization and antigen identification of the isolated TILB-HCT116-B24 mAb. Since the YSD cells expressing multi-copies of Fab fragments bind antigens with high avidity, this technique can be used to capture and isolate target antigens by yeast display immunoprecipitation (Tillotson et al., 2013). The outcome of this study may lead to implementation of new approaches for constructing TIL-B derived display libraries such as utilize tumor infiltrating memory or plasma B cells as the source of antibody immunoglobin of the displayed library. Deep sequencing of the libraries before and after biopanning proved to be a useful tool for understanding the selection process and can be used for establishing new strategies for isolating antibodies by combining NGS with YSD biopanning.

7. References

Alonso-Camino, V., Sánchez-Martín, D., Compte, M., Sanz, L., & Álvarez-Vallina, L. (2009). Lymphocyte display: A novel antibody selection platform based on T cell activation. *PLoS ONE*, *4*(9).

Ayat, H., Burrone, O. R., Sadghizadeh, M., Jahanzad, E., Rastgou, N., Moghadasi, S., & Arbabi, M. (2013). Isolation of scFv antibody fragments against HER2 and CEA tumor antigens from combinatorial antibody libraries derived from cancer patients. *Biologicals*, *41*(6), 345–354.

Ayat, H., Burrone, O. R., Sadghizadeh, M., Jahanzad, E., Rastgou, N., Moghadasi, S., & Arbabi, M. (2013b). Isolation of scFv antibody fragments against HER2 and CEA tumor antigens from combinatorial antibody libraries derived from cancer patients. *Biologicals*, *41*(6), 345–354.

Beck, G., & Habicht, G. S. (1996). Immunity and the invertebrates. *Scientific American*, *275*(5).

Belimezi, M. M., Papanastassiou, D., Merkouri, E., Baxevanis, C. N., & Mamalaki, A. (2006). Growth inhibition of breast cancer cell lines overexpressing Her2/neu by a novel internalized fully human Fab antibody fragment. *Cancer Immunology, Immunotherapy*, *55*(9), 1091–1099.

Benatuil, L., Perez, J. M., Belk, J., & Hsieh, C. M. (2010). An improved yeast transformation method for the generation of very large human antibody libraries. *Protein Engineering, Design and Selection*, *23*(4), 155–159.

Bessa, D., Pereira, F., Moreira, R., Johansson, B., & Queirós, O. (2012). Improved gap repair cloning in yeast: treatment of the gapped vector with Taq DNA polymerase avoids vector self-ligation. *Yeast*, *29*(10), 419–423.

Boder, E. T., Raeeszadeh-Sarmazdeh, M., & Price, J. V. (2012). Engineering antibodies by yeast display. *Archives of Biochemistry and Biophysics*, *526*(2), 99–106.

Boder, E. T., & Wittrup, K. D. (1997). Yeast surface display for screening combinatorial polypeptide libraries. *Nature Biotechnology*, *15*(6), 553–557.

Bowley, D. R., Labrijn, A. F., Zwick, M. B., & Burton, D. R. (2007). Antigen selection from an HIV-1 immune antibody library displayed on yeast yields many novel antibodies compared to selection from the same library displayed on phage. *Protein Engineering, Design and Selection*, *20*(2), 81–90.

Bradbury, A. R. M., Sidhu, S., Dübel, S., & McCafferty, J. (2011). Beyond natural antibodies: The power of in vitro display technologies. *Nature Biotechnology*, *29*(3), 245–254.

Bubeck, P., Winkler, M., & Bautsch, W. (1993). Rapid cloning by homologous recombination in vivo. *Nucleic Acids Research*, *21*(15), 3601–3602.

Carson-Walter, E. B., Watkins, D. N., Nanda, A., Vogelstein, B., Kinzler, K. W., & St Croix, B. (2001). Cell surface tumor endothelial markers are conserved in mice and humans. *Cancer Research*, *61*(18), 6649–6655.

Carter, P. J., & Lazar, G. A. (2018). Next generation antibody drugs: Pursuit of the “high-hanging fruit.” *Nature Reviews Drug Discovery*, *17*(3), 197–223.

Chao, G., Lau, W. L., Hackel, B. J., Sazinsky, S. L., Lippow, S. M., & Wittrup, K. D. (2006). Isolating and engineering human antibodies using yeast surface display. *Nature Protocols*, *1*(2), 755–768.

Coronella-Wood, J. A., & Hersh, E. M. (2003). Naturally occurring B-cell responses to breast cancer. *Cancer Immunology, Immunotherapy*, *52*(12), 715–738.

Coronella, J. A., Spier, C., Welch, M., Trevor, K. T., Stopeck, A. T., Villar, H., & Hersh, E. M. (2002). Antigen-Driven Oligoclonal Expansion of Tumor-Infiltrating B Cells in Infiltrating Ductal Carcinoma of the Breast. *The Journal of Immunology*, *169*(4),

Dangaj, D., Lanitis, E., Zhao, A., Joshi, S., Cheng, Y., Sandaltzopoulos, R., … Scholler, N. (2013). Novel recombinant human b7-h4 antibodies overcome tumoral immune escape to potentiate T-cell antitumor responses. *Cancer Research*, *73*(15), 4820–4829.

Dieu-Nosjean, M. C., Goc, J., Giraldo, N. A., Sautès-Fridman, C., & Fridman, W. H. (2014). Tertiary lymphoid structures in cancer and beyond. *Trends in Immunology*, *35*(11), 571–580.

Doerner, A., Rhiel, L., Zielonka, S., & Kolmar, H. (2014). Therapeutic antibody engineering by high efficiency cell screening. *FEBS Letters*, *588*(2), 278–287.

Dunn, G. P., Bruce, A. T., Ikeda, H., Old, L. J., & Schreiber, R. D. (2002). Immunoediting and immunosurveillance, *3*(11), 991–998.

Emmons, C., & Hunsicker, L. G. (1987). Muromonab-CD3 (Orthoclone OKT3): the first monoclonal antibody approved for therapeutic use. *Iowa Medicine : Journal of the Iowa Medical Society*, *77*(2), 78–82.

Estep, P., Reid, F., Nauman, C., Liu, Y., Sun, T., Sun, J., & Xu, Y. (2013). High throughput solution-based measurement of antibody-antigen affinity and epitope binning. *MAbs*, *5*(2), 270–278.

Fantini, M., Pandolfini, L., Lisi, S., Chirichella, M., Arisi, I., Terrigno, M., … Cattaneo, A. (2017). Assessment of antibody library diversity through next generation sequencing and technical error compensation. *PLOS ONE*, *12*(5).

Feldhaus, M. J., Siegel, R. W., Opresko, L. K., Coleman, J. R., Weaver Feldhaus, J. M., Yeung, Y. A., … Wittrup, K. D. (2003). Flow-cytometric isolation of human antibodies from a nonimmune Saccharomyces cerevisiae surface display library. *Nature Biotechnology*, *21*(2), 163–170.

Flynn, N. J., Somasundaram, R., Arnold, K. M., & Sims-Mourtada, J. (2017). The Multifaceted Roles of B Cells in Solid Tumors: Emerging Treatment Opportunities. *Targeted Oncology*, *12*(2), 139–152.

Fransson, J., Tornberg, U. C., Borrebaeck, C. A. K., Carlsson, R., & Frendéus, B. (2006). Rapid induction of apoptosis in B-cell lymphoma by functionally isolated human antibodies. *International Journal of Cancer*, *119*(2), 349–358.

Frenzel, A., Schirrmann, T., & Hust, M. (2016). Phage display-derived human antibodies in clinical development and therapy. *MAbs*, *8*(7), 1177–1194.

Fridman, W. H., Pagès, F., Sautès-Fridman, C., & Galon, J. (2012). The immune contexture in human tumours: impact on clinical outcome. *Nature Reviews Cancer*, *12*(4), 298–306.

Gera, N., Hussain, M., & Rao, B. M. (2013). Protein selection using yeast surface display. *Methods*, *60*(1), 15–26.

Glanville, J., D'Angelo, S., Khan, T., Reddy, S., Naranjo, L., Ferrara, F., & Bradbury, A. (2015). Deep sequencing in library selection projects: what insight does it bring? *Current Opinion in Structural Biology*, *33*, 146–160.

Gonzalez-Munoz, A. L., Minter, R. R., & Rust, S. J. (2016). Phenotypic screening: The future of antibody discovery. *Drug Discovery Today*, *21*(1), 150–156.

Goodnow, C. C., Vinuesa, C. G., Randall, K. L., MacKay, F., & Brink, R. (2010). Control systems and decision making for antibody production. *Nature Immunology*, *11*(8), 681–688.

Grillo-López, A. J., White, C. A., Varns, C., Shen, D., Wei, A., McClure, A., & Dallaire, B. K. (1999). Overview of the clinical development of rituximab: first monoclonal antibody approved for the treatment of lymphoma. *Seminars in Oncology*, *26*(5 Suppl 14), 66–73. Retrieved from

Grizzle, W. E., Bell, W. C., & Sexton, K. C. (2011). Issues in collecting, processing and storing human tissues and associated information to support biomedical research. *Cancer Biomarkers*, *9*(1–6), 531–549.

Grizzlea, W. E., Bella, W. C., & Sextonb, K. C. (2012). Issues in collecting, processing and storing human tissues and associated information to support biomedical research. *Translational Pathology of Early Cancer*, *9*, 531–549.

Harari, P. M. (2004). Epidermal growth factor receptor inhibition strategies in oncology. *Endocrine-Related Cancer*, *11*(4), 689–708.

Heine, M., Nollau, P., Masslo, C., Nielsen, P., Freund, B., Bruns, O. T., … Schumacher, U. (2011). Investigations on the Usefulness of CEACAMs as Potential Imaging Targets for Molecular Imaging Purposes. *PLoS ONE*, *6*(12).

Hoogenboom, H. R. (2005). Selecting and screening recombinant antibody libraries. *Nature Biotechnology*, *23*(9), 1105–1116.

Hust, M., & Dübel, S. (2010). Human Antibody Gene Libraries. In *Antibody Engineering* (pp. 65–84). Berlin, Heidelberg: Springer Berlin Heidelberg.

Iglesia, M. D., Vincent, B. G., Parker, J. S., Hoadley, K. A., Carey, L. A., Perou, C. M., & Serody, J. S. (2014). Prognostic B-cell Signatures Using mRNA-Seq in Patients with Subtype-Specific Breast and Ovarian Cancer. *Clinical Cancer Research*, (*20*14), 3818–3829.

Janeway, C. (2001). *Immunobiology 5 : the immune system in health and disease*. Garland Pub.

KÖHLER, G., & MILSTEIN, C. (1975). Continuous cultures of fused cells secreting antibody of predefined specificity. *Nature*, *256*(5517), 495–497.

Kotlan, B., Liszkay, G., Blank, M., Csuka, O., Balatoni, T., Toth, L., … Shoenfeld, Y. (2014). The novel panel assay to define tumor-associated antigen-binding antibodies in patients with metastatic melanomas may have diagnostic value. *Immunologic Research*, *61*(1–2), 11–23.

Kotlan, B., Simsa, P., Teillaud, J.-L., Fridman, W. H., Toth, J., McKnight, M., & Glassy, M. C. (2005). Novel ganglioside antigen identified by B cells in human medullary breast carcinomas: the proof of principle concerning the tumor-infiltrating B lymphocytes. *Journal of Immunology (Baltimore, Md. : 1950)*, *175*(4), 2278–2285.

Krah, S., Schröter, C., Eller, C., Rhiel, L., Rasche, N., Beck, J., … Becker, S. (2017). Generation of human bispecific common light chain antibodies by combining animal immunization and yeast display. *Protein Engineering, Design and Selection*, *30*(4), 291–301.

Lee, S. J., Jun, S.-Y., Lee, I. H., Kang, B. W., Park, S. Y., Kim, H. J., … Kim, J. G. (2018). CD274, LAG3, and IDO1 expressions in tumor-infiltrating immune cells as prognostic biomarker for patients with MSI-high colon cancer. *Journal of Cancer Research and Clinical Oncology*, *144*(6), 1005–1014.

Lee, S. J., Lee, J., Park, S. H., Park, J. O., Lim, H. Y., Kang, W. K., … Kim, S. T. (2018). c-MET Overexpression in Colorectal Cancer: A Poor Prognostic Factor for Survival. *Clinical Colorectal Cancer*, *17*(3), 165–169.

Livak, K. J., & Schmittgen, T. D. (2001). Analysis of Relative Gene Expression Data Using Real-Time Quantitative PCR and the 2−ΔΔCT Method. *Methods*, *25*(4), 402–408.

Lonberg, N. (2005). Human antibodies from transgenic animals. *Nature Biotechnology*, *23*(9), 1117–1125.

Lonberg, N. (2008). Fully human antibodies from transgenic mouse and phage display platforms. *Current Opinion in Immunology*, *20*(4), 450–459.

Lu, C. F., Montijn, R. C., Brown, J. L., Klis, F., Kurjan, J., Bussey, H., & Lipke, P. N. (1995). Glycosyl phosphatidylinositol-dependent cross-linking of α-agglutinin and β1,6-glucan in the Saccharomyces cerevisiae cell wall. *Journal of Cell Biology*, *128*(3), 333–340.

Marks, J. D., Hoogenboom, H. R., Bonnert, T. P., McCafferty, J., Griffiths, A. D., & Winter, G. (1991). By-passing immunization: Human antibodies from V-gene libraries displayed on phage. *Journal of Molecular Biology*, *222*(3), 581–597.

Matlock, B. (2015). *Assessment of Nucleic Acid Purity*. Retrieved from www.thermoscientific.com

McCafferty, J., Griffiths, A. D., Winter, G., & Chiswell, D. J. (1990). Phage antibodies: filamentous phage displaying antibody variable domains. *Nature*, *348*(6301), 552–554.

Meeusen, E., Lim, E., & Mathivanan, S. (2017). Secreted Tumor Antigens – Immune Biomarkers for Diagnosis and Therapy. *Proteomics*, *17*(23–24), 1–7.

Minter, R. R., Sandercock, A. M., & Rust, S. J. (2017). Phenotypic screening—the fast track to novel antibody discovery. *Drug Discovery Today: Technologies*, *23*, 83–90.

Mullis, K., Faloona, F., Scharf, S., Saiki, R., Horn, G., & Erlich, H. (1986). Specific enzymatic amplification of DNA in vitro: the polymerase chain reaction. *Cold Spring Harbor Symposia on Quantitative Biology*, *51 Pt 1*, 263–273.

Muramatsu, M., Kinoshita, K., Fagarasan, S., Yamada, S., Shinkai, Y., & Honjo, T. (2000). Class Switch Recombination and Hypermutation Require Activation-Induced Cytidine Deaminase (AID), a Potential RNA Editing Enzyme. *Cell*, *102*(5), 553–563.

Nathanson, D. R., Culliford, A. T., Shia, J., Chen, B., D'Alessio, M., Zeng, Z.-S., … Paty, P. B. (2003). HER 2/neu expression and gene amplification in colon cancer. *International Journal of Cancer*, *105*(6), 796–802.

Nelson, A. L., & Reichert, J. M. (2009). Development trends for therapeutic antibody fragments. *Nature Biotechnology*, *27*(4), 331–337.

Nelson, B. H. (2010). CD20+ B Cells: The Other Tumor-Infiltrating Lymphocytes. *The Journal of Immunology*, *185*(9), 4977–4982.

Ni, M., Zhang, Y., & Lee, A. S. (2011). Beyond the endoplasmic reticulum: atypical GRP78 in cell viability, signalling and therapeutic targeting. *Biochemical Journal*, *434*(2), 181–188.

Novinger, L. J., Ashikaga, T., & Krag, D. N. (2015). Identification of tumor-binding scFv derived from clonally related B cells in tumor and lymph node of a patient with breast cancer. *Cancer Immunology, Immunotherapy*, *64*(1), 29–39.

Pagès, F., Galon, J., Dieu-Nosjean, M. C., Tartour, E., Sautès-Fridman, C., & Fridman, W. H. (2010). Immune infiltration in human tumors: A prognostic factor that should not be ignored. *Oncogene*, *29*(8), 1093–1102.

Pape, K. A., Taylor, J. J., Maul, R. W., Gearhart, P. J., & Jenkins, M. K. (2011). Different B Cell Populations Mediate Early and Late Memory During an Endogenous Immune Response. *Science*, *331*(6021), 1203–1207.

Pardoll, D. M. (2012). The blockade of immune checkpoints in cancer immunotherapy. *Nature Reviews Cancer*, *12*(4), 252–264.

Pavoni, E., Monteriù, G., Santapaola, D., Petronzelli, F., Anastasi, A., Pelliccia, A., … Minenkova, O. (2007). Tumor-infiltrating B lymphocytes as an efficient source of highly specific immunoglobulins recognizing tumor cells. *BMC Biotechnology*, *7*, 1–17.

Punt, C. J., Barbuto, J. A., Zhang, H., Grimes, W. J., Hatch, K. D., & Hersh, E. M. (1994). Anti-tumor antibody produced by human tumor-infiltrating and peripheral blood B lymphocytes. *Cancer Immunology, Immunotherapy : CII*, *38*(4), 225–232.

Rakestraw, J. A., Sazinsky, S. L., Piatesi, A., Antipov, E., & Wittrup, K. D. (2009). Directed evolution of a secretory leader for the improved expression of heterologous proteins and full-length antibodies in Saccharomyces cerevisiae. *Biotechnology and Bioengineering*, *103*(6), 1192–1201.

Ran, F. A., Hsu, P. D., Wright, J., Agarwala, V., Scott, D. A., & Zhang, F. (2013). Genome engineering using the CRISPR-Cas9 system. *Nature Protocols*, *8*(11), 2281–2308.

Ravn, U., Didelot, G., Venet, S., Ng, K. T., Gueneau, F., Rousseau, F., … Fischer, N. (2013). Deep sequencing of phage display libraries to support antibody discovery. *Methods*, *60*(1), 99–110.

Rich, R. L., & Myszka, D. G. (2007). Higher-throughput, label-free, real-time molecular interaction analysis. *Analytical Biochemistry*, *361*(1), 1–6.

Riechmann, L., Clark, M., Waldmann, H., & Winter, G. (1988). Reshaping human antibodies for therapy. *Nature*, *332*(6162), 323–327.

Rismani, E., Fazeli, M. S., Mahmoodzadeh, H., Movassagh, A., Azami, S., Karimipoor, M., & Teimoori-Toolabi, L. (2017). Pattern of LRP6 gene expression in tumoral tissues of colorectal cancer. *Cancer Biomarkers*, *19*(2), 151–159.

Rothe, A., Klimka, A., Tur, M. K., Pfitzner, T., Huhn, M., Sasse, S., … Barth, S. (2004). Construction of phage display libraries from reactive lymph nodes of breast carcinoma patients and selection for specifically binding human single chain Fv on cell lines. *International Journal of Molecular Medicine*, *14*(4), 729–764.

Sánchez-Martín, D., Sørensen, M. D., Lykkemark, S., Sanz, L., Kristensen, P., Ruoslahti, E., & Álvarez-Vallina, L. (2015). Selection strategies for anticancer antibody discovery: searching off the beaten path. *Trends in Biotechnology*, *33*(5), 292–301.

Schier, R., McCall, A., Adams, G. P., Marshall, K. W., Merritt, H., Yim, M., … Marks, J. D. (1996). Isolation of Picomolar Affinity Anti-c-erbB-2 Single-chain Fv by Molecular Evolution of the Complementarity Determining Regions in the Center of the Antibody Binding Site. *Journal of Molecular Biology*, *263*(4), 551–567.

Schroeder, A., Mueller, O., Stocker, S., Salowsky, R., Leiber, M., Gassmann, M., … Ragg, T. (2006). The RIN: An RNA integrity number for assigning integrity values to RNA measurements. *BMC Molecular Biology*, *7*, 1–14.

Schröter, C., Beck, J., Krah, S., Zielonka, S., Doerner, A., Rhiel, L., … Becker, S. (2018). Selection of Antibodies with Tailored Properties by Application of High-Throughput Multiparameter Fluorescence-Activated Cell Sorting of Yeast-Displayed Immune Libraries. *Molecular Biotechnology*, *60*(10), 727–735.

Scott, J. K., & Smith, G. P. (1990). Searching for peptide ligands with an epitope library. *Science (New York, N.Y.)*, *249*(4967), 386–390.

Sgro, C. (1995). Side-effects of a monoclonal antibody, muromonab CD3/orthoclone OKT3: bibliographic review. *Toxicology*, *105*(1), 23–29.

Sheehan, J., & Marasco, W. A. (2015). Phage and Yeast Display. *Microbiology Spectrum*, *3*(1), AID-0028-2014.

Shen, M., Sun, Q., Wang, J., Pan, W., Ren, X., Shen, M., … Ren, X. (2016). Positive and negative functions of B lymphocytes in tumors. *Oncotarget*, *7*(34), 55828–55839.

Sikora, K., Alderson, T., Ellis, J., Phillips, J., & Watson, J. (1983). Human hybridomas from patients with malignant disease. *British Journal of Cancer*, *47*(1), 135–145.

Sikora, K., Alderson, T., Phillips, J., & Watson, J. V. (1982). Human hybridomas from malignant gliomas. *Lancet (London, England)*, *1*(8262), 11–14.

Sistrunk, W. E., & Maccarty, W. C. (1922). Life expectancy following radical amputation for carcinoma of the breast: a clinical and pathologic study of 218 cases. *Annals of Surgery*, *75*(1), 61–69.

Skerra, A., & Plückthun, A. (1988). Assembly of a functional immunoglobulin Fv fragment in Escherichia coli. *Science (New York, N.Y.)*, *240*(4855), 1038–1041. Retrieved from

Smith, G. P. (1985). Filamentous fusion phage: novel expression vectors that display cloned antigens on the virion surface. *Science (New York, N.Y.)*, *228*(4705), 1315–1317.

Starzynska, T., Marsh, P., Schofield, P., Roberts, S., Myers, K., & Stern, P. (1994). Prognostic significance of 5T4 oncofetal antigen expression in colorectal carcinoma. *British Journal of Cancer*, *69*(5), 899–902.

Stern, L. A., Schrack, I. A., Johnson, S. M., Deshpande, A., Bennett, N. R., Harasymiw, L. A., … Hackel, B. J. (2016). Geometry and expression enhance enrichment of functional yeast-displayed ligands via cell panning. *Biotechnology and Bioengineering*, *113*(11), 2328–2341.

Strebhardt, K., & Ullrich, A. (2008). Paul Ehrlich's magic bullet concept: 100 years of progress. *Nature Reviews Cancer*, *8*(6), 473–480.

Suan, D., Sundling, C., & Brink, R. (2017). Plasma cell and memory B cell differentiation from the germinal center. *Current Opinion in Immunology*, *45*, 97–102.

Tillotson, B. J., Cho, Y. K., & Shusta, E. V. (2013). Cells and cell lysates: A direct approach for engineering antibodies against membrane proteins using yeast surface display. *Methods*, *60*(1), 27–37.

Tobias, R., & Kumaraswamy, S. (2013). *Biomolecular Binding Kinetics Assays on the Octet Platform*. Retrieved from http://csbi.mit.edu/instrumentation/ForteBio_App_Note_14.pdf

Tsou, P., Katayama, H., Ostrin, E. J., & Hanash, S. M. (2016). The emerging role of b cells in tumor immunity. *Cancer Research*, *76*(19), 5591–5601.

Underwood, J. C. (1974). Lymphoreticular infiltration in human tumours: prognostic and biological implications: a review. *British Journal of Cancer*, *30*(6), 538–548.

Waldmann, H., & Hale, G. (2005). CAMPATH: From concept to clinic. *Philosophical Transactions of the Royal Society B: Biological Sciences*, *360*(1461), 1707–1711.

Wang, X. X., Cho, Y. K., & Shusta, E. V. (2007). Mining a yeast library for brain endothelial cell-binding antibodies. *Nature Methods*, *4*(2), 143–145.

Weaver-Feldhaus, J. M., Lou, J., Coleman, J. R., Siegel, R. W., Marks, J. D., & Feldhaus, M. J. (2004). Yeast mating for combinatorial Fab library generation and surface display. *FEBS Letters*, *564*(1–2), 24–34.

Webb, G. J., Hirschfield, G. M., & Lane, P. J. L. (2016). OX40, OX40L and Autoimmunity: a Comprehensive Review. *Clinical Reviews in Allergy and Immunology*, *50*(3), 312–332.

Weiner, G. J. (2015). Building better monoclonal antibody-based therapeutics. *Nature Reviews Cancer*, *15*(6), 361–370.

Williams, R. M., Hajiran, C. J., Nayeem, S., & Sooter, L. J. (2014). Identification of an antibody fragment specific for androgen-dependent prostate cancer cells. *BMC Biotechnology*, *14*(1), 1–11.

Wine, Y., Boutz, D. R., Lavinder, J. J., Miklos, A. E., Hughes, R. A., Hoi, K. H., … Georgiou, G. (2013). Molecular deconvolution of the monoclonal antibodies that comprise the polyclonal serum response. *Proceedings of the National Academy of Sciences of the United States of America*, *110*(8), 2993–2998.

Workman, P., Draetta, G. F., Schellens, J. H. M., & Bernards, R. (2017). How Much Longer Will We Put Up With 100,000 Cancer Drugs? *Cell*, *168*(4), 579–583.

Wouters, M. C., & Nelson, B. H. (2018). Prognostic significance of tumor-infiltrating B cells and plasma cells in human cancer. *Clinical Cancer Research*, clincanres.1481.2018.

Xin, X. W., & Shusta, E. V. (2005). The use of scFv-displaying yeast in mammalian cell surface selections. *Journal of Immunological Methods*, *304*(1–2), 30–42.

Yanai, H., Nakamura, K., Hijioka, S., Kamei, A., Ikari, T., Ishikawa, Y., … Miyajima, A. (2010). Dlk-1, a cell surface antigen on foetal hepatic stem/progenitor cells, is expressed in hepatocellular, colon, pancreas and breast carcinomas at a high frequency. *Journal of Biochemistry*, *148*(1), 85–92.

Yang, W.-P., Green, K., Pinz-Sweeney, S., Briones, A. T., Burton, D. R., & Barbas III, C. F. (1995). CDR Walking Mutagenesis for the Affinity Maturation of a Potent Human Anti-HIV-1 Antibody into the Picomolar Range. *Journal of Molecular Biology*, *254*(3), 392–403.

Yasuda, M., Takenoyama, M., Obata, Y., Sugaya, M., So, T., Hanagiri, T., … Yasumoto, K. (2002). Tumor-infiltrating B lymphocytes as a potential source of identifying tumor antigen in human lung cancer. *Cancer Research*, *62*(6), 1751–1756.

Zaenker, P., Gray, E. S., & Ziman, M. R. (2016). Autoantibody Production in Cancer-The Humoral Immune Response toward Autologous Antigens in Cancer Patients. *Autoimmunity Reviews*, *15*(5), 477–483.

Zhang, H., Lake, D. F., Barbuto, J. A., Bernstein, R. M., Grimes, W. J., & Hersh, E. M. (1995). A human monoclonal antimelanoma single-chain Fv antibody derived from tumor-infiltrating lymphocytes. *Cancer Research*, *55*(16), 3584–3591.

Zorniak, M., Clark, P. A., Umlauf, B. J., Cho, Y., Shusta, E. V., & Kuo, J. S. (2017). Yeast display biopanning identifies human antibodies targeting glioblastoma stem-like cells. *Scientific Reports*, *7*(1), 1–12.

8. Appendix

8.1. Supporting Information

The NGS analysis report for TIL-B κ and TIL-B λ libraries and biopanning enriched pools: TIL-B HCT116, TIL-B HT29 and TIL-B SW620 are depicted in **Figure 53-57**. The report includes a table showing the frequency distribution of the top sequences, a graph showing the V gene distribution and a graph showing the CDR3 read length distribution of the VH and VL or VK genes.

A

Library	ChainType	V_Gene	CDR3_AA	TOT	TOT_perc
TIL-B κ	VH	IGHV3-7	ARDLNWNYVFWYFDL	172219	8.698
TIL-B κ	VH	IGHV1-2	ARRSIYNWSHGFDI	135425	6.840
TIL-B κ	VH	IGHV5-51	VRRTYGNIGAYSYDY	127135	6.421
TIL-B κ	VH	IGHV5-51	ARLYDSSGFHSSAEPFDV	67419	3.405
TIL-B κ	VH	IGHV1-8	ARRWYCSSASCRARLKADKQTFYNYYGMDV	51433	2.598
TIL-B κ	VH	IGHV2-70	ARMGLYDFFYGIDV	40057	2.023
TIL-B κ	VH	IGHV5-51	ARRATSDGDYAGWDDIFDM	38392	1.939
TIL-B κ	VH	IGHV4-59	ARDRATVPDSFHT	37273	1.882
TIL-B κ	VH	IGHV6-1	ARDPMVSLGDHHYYYGLDV	28419	1.435
TIL-B κ	VH	IGHV2-5	AHRESYDDTRHFDY	20035	1.012
TIL-B κ	VH	IGHV6-1	ARGGRGTQFDY	19253	0.972
TIL-B κ	VH	IGHV3-21	ARDLLVGASIY	19080	0.964
TIL-B κ	VH	IGHV2-70	ARTNSLRAVAGGGGWFDP	18024	0.910
TIL-B κ	VH	IGHV1-69	ARDQRGYDYYYYYGMDV	16818	0.849
TIL-B κ	VH	IGHV5-51		16580	0.837
TIL-B κ	VH	IGHV1-69	ANKPRGYSGYTRGTLYGLDV	16518	0.834
TIL-B κ	VH	IGHV6-1	ARRNSSSGGMDV	16330	0.825
TIL-B κ	VH	IGHV3-23	ANRDCGGDCPDY	15704	0.793
TIL-B κ	VH	IGHV1-69	ARGGIVVVLAAGPQKNAFDL	14897	0.752
TIL-B κ	VH	IGHV5-51	ARRPGTIYDGALLPTRYSFDL	14402	0.727

B

Library	ChainType	V_Gene	CDR3_AA	TOT	TOT_perc
TIL-B κ	VK	IGKV1-12	QQADSFPPT	207054	7.766
TIL-B κ	VK	IGKV2-30	MQGTHWPFT	86822	3.256
TIL-B κ	VK	IGKV4-1	QQYYSSPLT	39189	1.470
TIL-B κ	VK	IGKV3-20	QQYGMSPRT	37132	1.393
TIL-B κ	VK	IGKV4-1	QQYYGTPFT	29475	1.106
TIL-B κ	VK	IGKV4-1	QQYFGTPYT	26912	1.009
TIL-B κ	VK	IGKV4-1	QQYYETPNT	23005	0.863
TIL-B κ	VK	IGKV4-1	QQYWGPPS	21486	0.806
TIL-B κ	VK	IGKV1-39	QQADSFPPT	18628	0.699
TIL-B κ	VK	IGKV3-11	QQRGTWPPT	16954	0.636
TIL-B κ	VK	IGKV3-20	QQYGTSPLT	16338	0.613
TIL-B κ	VK	IGKV4-1	QQYYSTPYT	16217	0.608
TIL-B κ	VK	IGKV3-15	QEYNNWPPRT	15689	0.588
TIL-B κ	VK	IGKV4-1	HQYYSAPLT	14544	0.546
TIL-B κ	VK	IGKV3-20	QQYGSSPLT	13430	0.504
TIL-B κ	VK	IGKV4-1	QQYYSAPLT	12725	0.477
TIL-B κ	VK	IGKV4-1	QQYYNTPWT	11216	0.421
TIL-B κ	VK	IGKV1-5	QQFKTYPLT	11148	0.418
TIL-B κ	VK	IGKV4-1	QQADSFPPT	11067	0.415
TIL-B κ	VK	IGKV1-12	QQANSFPLA	10795	0.405

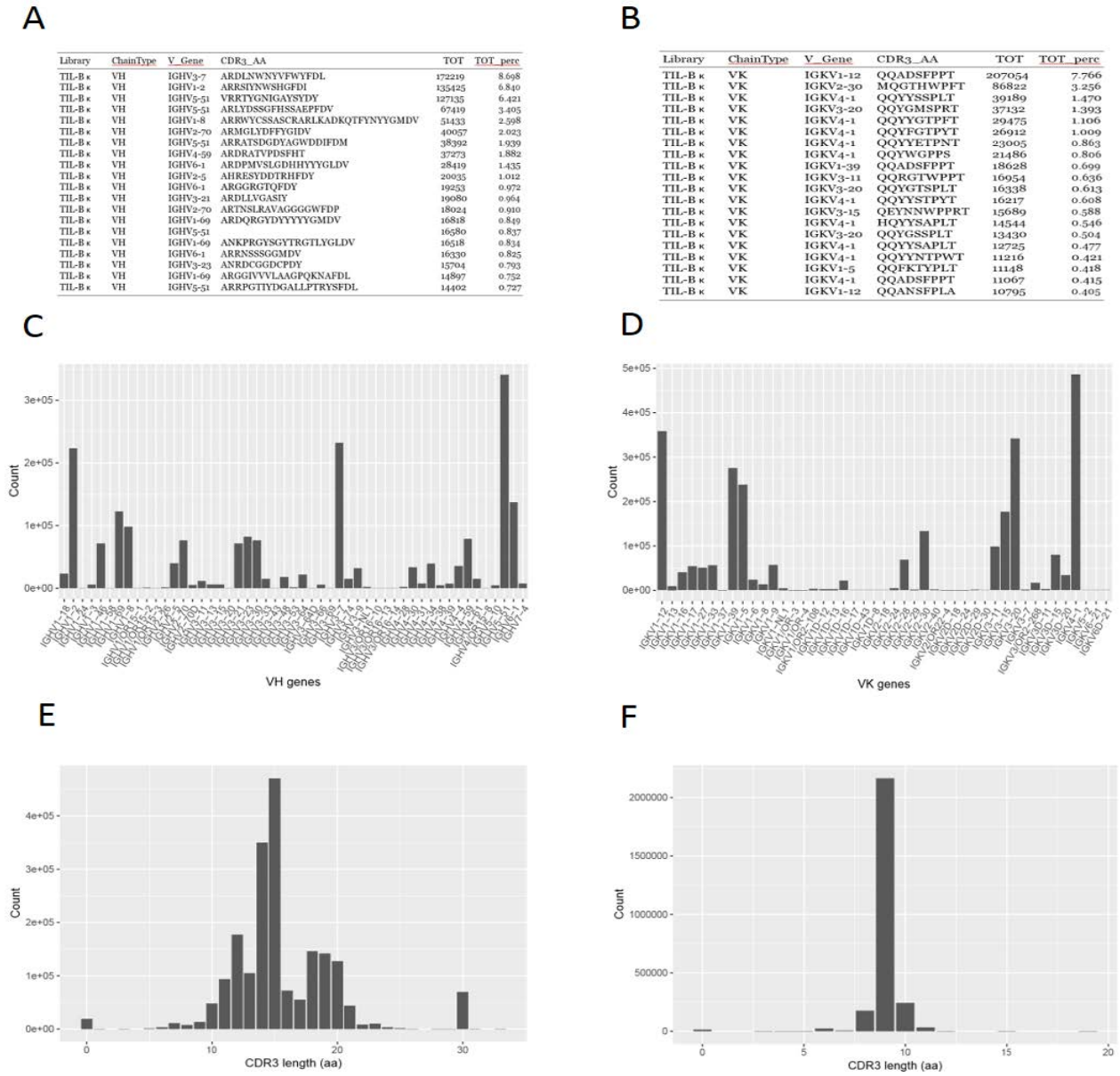

Figure 53: **NGS report summary for the TIL-B κ library**.

(A) Top sequences frequency distribution of VH genes and CDR3 **(B)** Top sequences frequency distribution of VK genes and CDR3 **(C)** VH genes distribution **(D)** VK genes distribution **(E)** CDR3 length distribution of VH genes **(F)** CDR3 length distribution of VK genes

A

Library	ChainType	V_Gene	CDR3_AA	TOT	TOT_perc
TIL-B λ	VH	IGHV5-51	VRRTYGNIGAYSYDY	102996	8.543
TIL-B λ	VH	IGHV1-2	ARRSIYNWSHGFDI	96873	8.035
TIL-B λ	VH	IGHV3-7	ARDLNWNYVFWYFDL	78173	6.484
TIL-B λ	VH	IGHV2-70	ARMGLYDFFYGIDV	34611	2.871
TIL-B λ	VH	IGHV5-51	ARRATSDGDYAGWDDIFDM	24668	2.046
TIL-B λ	VH	IGHV5-51	ARLYDSSGFHSSAEPFDV	22824	1.893
TIL-B λ	VH	IGHV6-1	ARDPMVSLGDHHYYYGLDV	22534	1.869
TIL-B λ	VH	IGHV3-21	ARDLLVGASIY	19197	1.592
TIL-B λ	VH	IGHV2-5	AHRESYDDTRHFDY	17082	1.417
TIL-B λ	VH	IGHV4-34	ARVVMANKMGLYYYYYYMDA	14665	1.216
TIL-B λ	VH	IGHV1-69	ANKPRGYSGYTRGTLYGLDV	14366	1.192
TIL-B λ	VH	IGHV1-69	ARGGIVVVLAAGPQKNAFDL	12869	1.067
TIL-B λ	VH	IGHV4-59	ARDRATVPDSFHT	12434	1.031
TIL-B λ	VH	IGHV5-51		12431	1.031
TIL-B λ	VH	IGHV6-1	ARGGRGTQFDY	12016	0.997
TIL-B λ	VH	IGHV1-8	ARRWYCSSASCRARLKADKQTFYNYYGMDV	11861	0.984
TIL-B λ	VH	IGHV3-64	ARGPDSSSADYYYYYYGMDV	10450	0.867
TIL-B λ	VH	IGHV5-51	ARRPGTIYDGALLPTRYSFDL	10218	0.848
TIL-B λ	VH	IGHV4-4	AKGGYRYVWGRGSYYYALEV	9919	0.823
TIL-B λ	VH	IGHV5-51	ARQYYDSTEGNWFDS	9898	0.821

B

Library	ChainType	V_Gene	CDR3_AA	TOT	TOT_perc
TIL-B λ	VL	IGLV6-57	QSYDSSNHVV	87533	4.673
TIL-B λ	VL	IGLV3-21	QVWDSSSDHWV	82647	4.412
TIL-B λ	VL	IGLV1-44	AAWDDSLHGPV	57413	3.065
TIL-B λ	VL	IGLV8-61	LLFVGSG1SV	42083	2.246
TIL-B λ	VL	IGLV4-69	QTWDRDIVV	39086	2.086
TIL-B λ	VL	IGLV6-57	QSYDIKNPWV	31688	1.692
TIL-B λ	VL	IGLV3-19	NARASGGGHLI	31068	1.658
TIL-B λ	VL	IGLV3-19	NSRDSSGNHPVV	26813	1.431
TIL-B λ	VL	IGLV6-57	QSYDSSNPVV	18956	1.012
TIL-B λ	VL	IGLV3-19	SSRDISGNHVV	17620	0.941
TIL-B λ	VL	IGLV6-57	QSYDSSNWV	17149	0.915
TIL-B λ	VL	IGLV3-21	QVWDSSSNHRV	16989	0.907
TIL-B λ	VL	IGLV2-14	SSYTTTRLCL	16190	0.864
TIL-B λ	VL	IGLV10-54	SSWDSDLTVYF	14390	0.768
TIL-B λ	VL	IGLV10-54	SAWDTSLSAWV	14318	0.764
TIL-B λ	VL	IGLV1-44	ATWEDTVKGWV	12561	0.671
TIL-B λ	VL	IGLV1-44	TAWDGSLSAVV	12270	0.655
TIL-B λ	VL	IGLV3-19	NSRDSSGNHWV	12150	0.649
TIL-B λ	VL	IGLV8-61	ALYVRRDTWV	11602	0.619
TIL-B λ	VL	IGLV7-46	LLSYSGAVV	10833	0.578

C

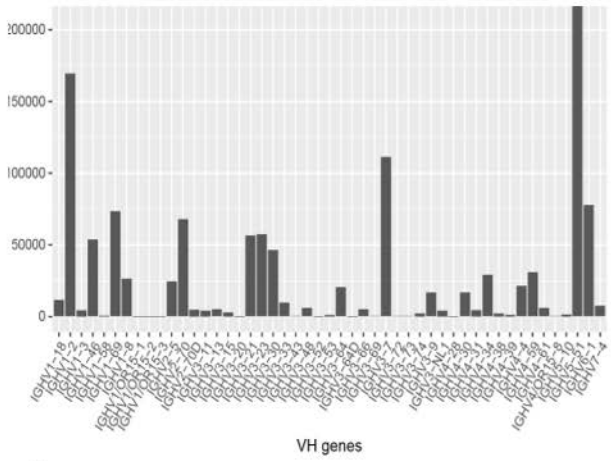

D

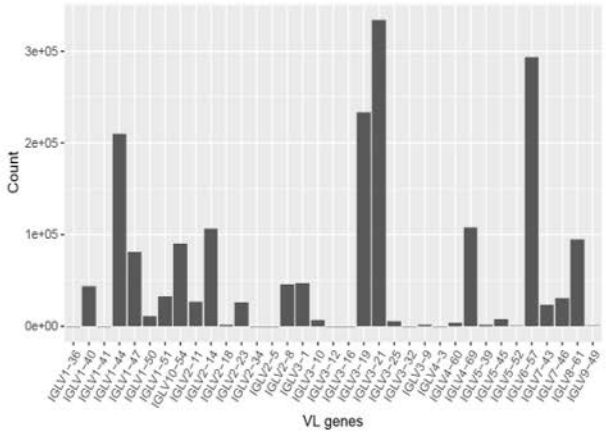

E

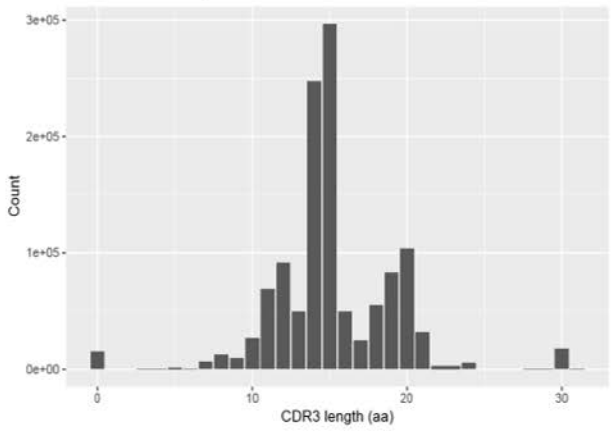

F

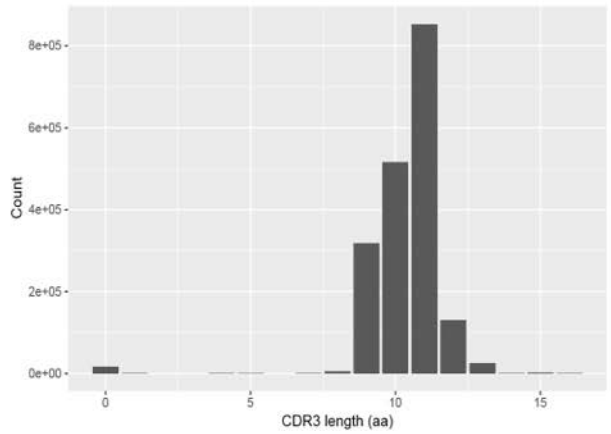

Figure 54: **NGS report summary for the TIL-B λ library.**

(A) Top sequences frequency distribution of VH genes and CDR3 **(B)** Top sequences frequency distribution of VL genes and CDR3 **(C)** VH genes distribution **(D)** VL genes distribution **(E)** CDR3 length distribution of VH genes **(F)** CDR3 length distribution of VL genes

A

Library	ChainType	V_Gene	CDR3_AA	TOT	TOT_perc
HCT116	VH	IGHV3-15	TTGRHYCSGGSCHLSFFDY	742841	92.624
HCT116	VH	IGHV1-2	ARDLGVYSGSPWDY	14552	1.814
HCT116	VH	IGHV1/OR15-3	ARARSGVGATRSLWNFDY	7355	0.917
HCT116	VH	IGHV3-33	ARDLSGAADY	2751	0.343
HCT116	VH	IGHV3-15	TTGRHYCSGGSCHLSFFDD	1243	0.155
HCT116	VH	IGHV3-23	VKDGHDYGYDH	997	0.124
HCT116	VH	IGHV3-15	TTGRHYCSGGSCHLSFVDY	836	0.104
HCT116	VH	IGHV3-15	TTGRHDCSGGSCHLSFFDY	741	0.092
HCT116	VH	IGHV3-15	TTGRHYCSGGSCHLSFLDY	705	0.088
HCT116	VH	IGHV3-21	ARDSSGYLMSGHYYYYYMDV	660	0.082
HCT116	VH	IGHV3-15	TTGRHYCSGGSCHLAFFDY	657	0.082
HCT116	VH	IGHV3-30	ARDLSGAADY	656	0.082
HCT116	VH	IGHV3-15	TTGRHYCSGGSCHLSCFDY	617	0.077
HCT116	VH	IGHV3-15	TTGRHYCRGGSCHLSFFDY	615	0.077
HCT116	VH	IGHV3-49	TPTYQRGSGSYKY	610	0.076
HCT116	VH	IGHV3-15	TTGRHYCSGGSCHLSVFDY	565	0.070
HCT116	VH	IGHV3-15	TTGRHYGSGGSCHLSFFDY	557	0.069
HCT116	VH	IGHV3-15	TTGRHYCSGGSCHLSFFDC	499	0.062
HCT116	VH	IGHV1-2	ARARSGVGATRSLWNFDY	487	0.061
HCT116	VH	IGHV3-15	TTGRHYWSGGSCHLSFFDY	471	0.059

B

Library	ChainType	V_Gene	CDR3_AA	TOT	TOT_perc
HTC116	VK	IGKV3-15	QQYNNWPDT	228970	25.911
HTC116	VK	IGKV4-1	QQYYTTPQT	144037	16.300
HTC116	VK	IGKV1-33	QQYGMSPRT	128701	14.564
HTC116	VK	IGKV3-20	QQYGMSPRT	58247	6.591
HTC116	VK	IGKV4-1	QQYYGTPFT	31731	3.591
HTC116	VK	IGKV3-15	QQYGMSPRT	25480	2.883
HTC116	VK	IGKV3-15	QQYYTTPQT	20198	2.286
HTC116	VK	IGKV4-1	QQYNNWPDT	19239	2.177
HTC116	VK	IGKV3-15	QQYGSWPRT	17432	1.973
HTC116	VK	IGKV1-39	QQSYSSFWT	12115	1.371
HTC116	VK	IGKV3D-15	QQYNNWPDT	9626	1.089
HTC116	VK	IGKV1-6	QQYYNTPWT	9209	1.042
HTC116	VK	IGKV1-12	QQANSFPLT	7317	0.828
HTC116	VK	IGKV1-5	QHLSGYPCT	6825	0.772
HTC116	VK	IGKV1-33	QQYNNWPDT	6779	0.767
HTC116	VK	IGKV3-15	QQHNDWPSS	6581	0.745
HTC116	VK	IGKV1-33	QQYDDLIALT	6231	0.705
HTC116	VK	IGKV4-1	QQYGMSPRT	6130	0.694
HTC116	VK	IGKV1-39	QQYGMSPRT	6005	0.680
HTC116	VK	IGKV1-39	QQSYSAPYT	5685	0.643

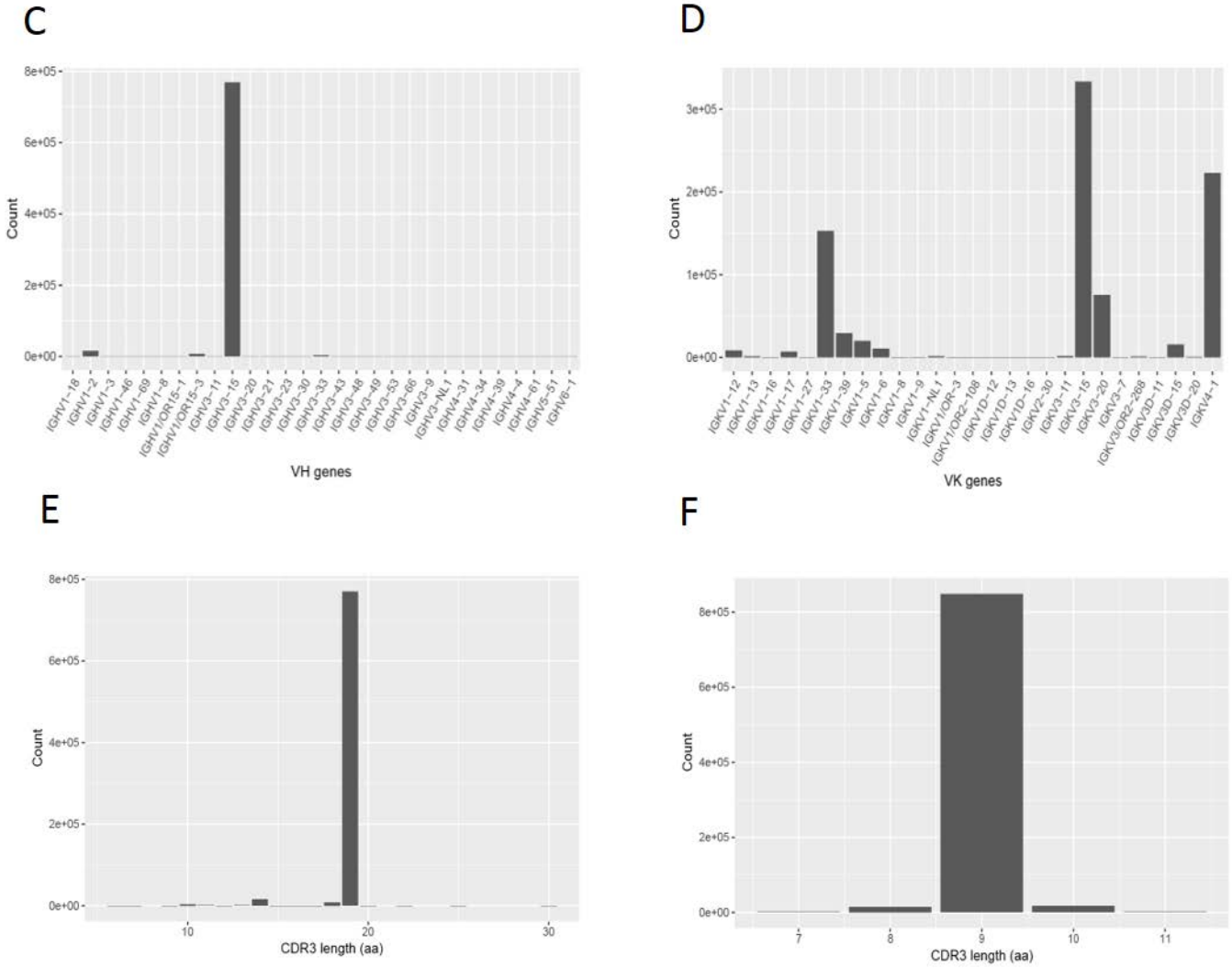

Figure 55: **NGS report summary for the biopanning pool TIL-B HCT 116.**

(A) Top sequences frequency distribution of VH genes and CDR3 **(B)** Top sequences frequency distribution of VK genes and CDR3 **(C)** VH genes distribution **(D)** VK genes distribution **(E)** CDR3 length distribution for VH genes **(F)** CDR3 length distribution of VK genes

A

Library	ChainType	V_Gene	CDR3_AA	TOT	TOT_perc
HT29	VH	IGHV3-15	TTGRHYCSGGSCHLSFFDY	349086	49.953
HT29	VH	IGHV1-2	VRKGDY	143267	20.501
HT29	VH	IGHV1-3	ARRWYCSSASCRARLKADKQTFYNYYGMDV	57820	8.274
HT29	VH	IGHV3-15	ASPGIAAAGIDY	26289	3.762
HT29	VH	IGHV1-46	ANKPRGYSGYTRGTLYGLDV	16457	2.355
HT29	VH	IGHV3-21	ASPGIAAAGIDY	10432	1.493
HT29	VH	IGHV1-3	VRKGDY	7878	1.127
HT29	VH	IGHV1-3	ARRPWSGGYNWFDP	7226	1.034
HT29	VH	IGHV1-2	ARRWYCSSASCRARLKADKQTFYNYYGMDV	5220	0.747
HT29	VH	IGHV1-3	ANKPRGYSGYTRGTLYGLDV	4510	0.645
HT29	VH	IGHV1-2	ANKPRGYSGYTRGTLYGLDV	4097	0.586
HT29	VH	IGHV3-23	ARGRGRLRWGP	2905	0.416
HT29	VH	IGHV1-3	ARRDRSGSYYSLDY	2747	0.393
HT29	VH	IGHV3-23	ASSYSSSWWS	2633	0.377
HT29	VH	IGHV3-11	ARADYGDYGVYFDY	2262	0.324
HT29	VH	IGHV3-48	ASPGIAAAGIDY	2255	0.323
HT29	VH	IGHV1-69	ANKPRGYSGYTRGTLYGLDV	1748	0.250
HT29	VH	IGHV1-46	VRKGDY	1717	0.246
HT29	VH	IGHV1/OR15-3	ARRWYCSSASCRARLKADKQTFYNYYGMDV	1692	0.242
HT29	VH	IGHV1/OR15-1	VRKGDY	1670	0.239

B

Library	ChainType	V_Gene	CDR3_AA	TOT	TOT_perc
HT29	VK	IGKV4-1	QQYYTTPQT	254001	28.496
HT29	VK	IGKV3-20	QQYGMSPRT	163961	18.394
HT29	VK	IGKV4-1	HQYYSAPLT	73841	8.284
HT29	VK	IGKV1-12	QQADSFPPT	34488	3.869
HT29	VK	IGKV3-15	QQYNNWPDT	33785	3.790
HT29	VK	IGKV4-1	QQSSKWPVT	30869	3.463
HT29	VK	IGKV4-1	QQYNNGLWT	27218	3.054
HT29	VK	IGKV3-11	QQRSKWPST	16229	1.821
HT29	VK	IGKV1-5	QQRSYWRT	12031	1.350
HT29	VK	IGKV1-33	QQYGMSPRT	12009	1.347
HT29	VK	IGKV4-1	QQYGMSPRT	10521	1.180
HT29	VK	IGKV4-1	QHYWT	8861	0.994
HT29	VK	IGKV3-15	QQYGSWPRT	8825	0.990
HT29	VK	IGKV4-1	QQYYSSPLT	7428	0.833
HT29	VK	IGKV3-15	QQYYTTPQT	6753	0.758
HT29	VK	IGKV3-15	QQYGMSPRT	6333	0.710
HT29	VK	IGKV4-1	QQYNNWPDT	6268	0.703
HT29	VK	IGKV2-30	MQGTHWPFT	4816	0.540
HT29	VK	IGKV3-11	QQRSTWPPT	4666	0.523
HT29	VK	IGKV4-1	QQYMSTPWT	4600	0.516

C

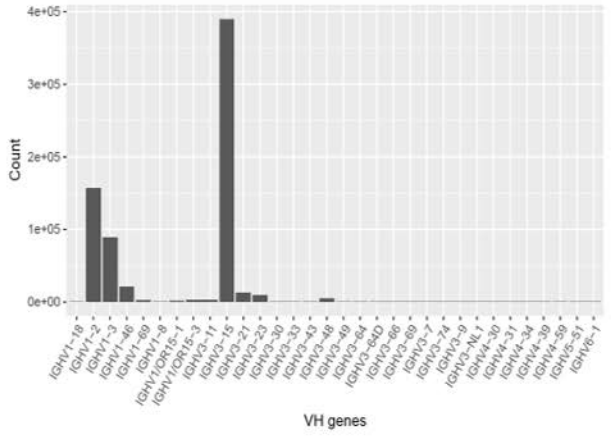

D

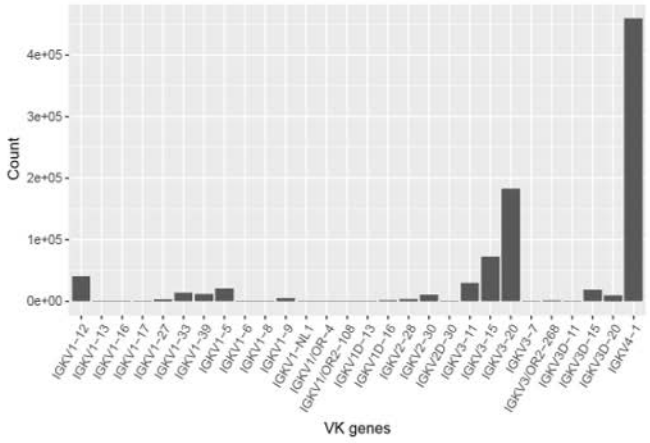

E

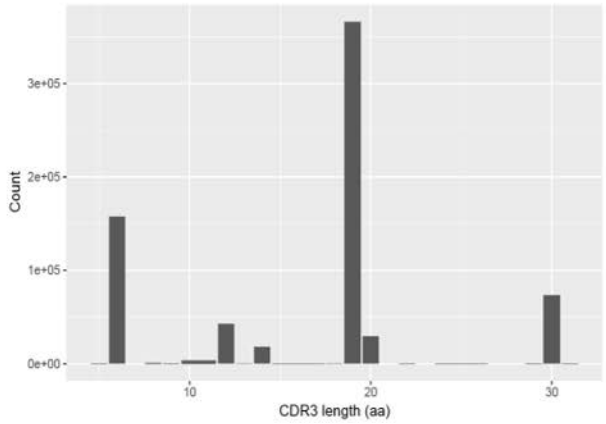

F

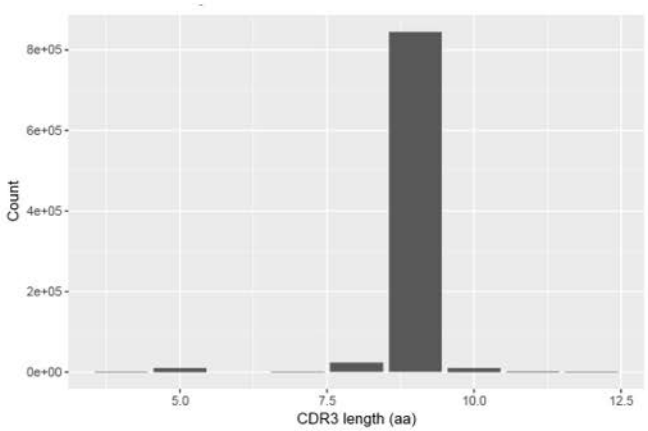

Figure 56: **NGS report summary for the biopanning pool TIL-B HT-29.**

(A) Top sequences frequency distribution of VH genes and CDR3 **(B)** Top sequences frequency distribution of VK genes and CDR3 **(C)** VH genes distribution **(D)** VK genes distribution **(E)** CDR3 length distribution of VH genes **(F)** CDR3 length distribution of VK genes

A

Library	ChainType	V_Gene	CDR3_AA	TOT	TOT_perc
SW620	VH	IGHV3-48	ASPGIAAAGIDY	168383	22.489
SW620	VH	IGHV3-15	ASPGIAAAGIDY	148670	19.856
SW620	VH	IGHV3-21	ASPGIAAAGIDY	148448	19.827
SW620	VH	IGHV1-2	VRKGDY	87109	11.634
SW620	VH	IGHV3-23	ASPGIAAAGIDY	67836	9.060
SW620	VH	IGHV1-46	ARARSGVGATRSLWNFDY	13426	1.793
SW620	VH	IGHV3-NL1	ASPGIAAAGIDY	8765	1.171
SW620	VH	IGHV3-30	ASPGIAAAGIDY	5702	0.762
SW620	VH	IGHV3-23	ASSYSSSWWS	5391	0.720
SW620	VH	IGHV1/OR15-3	ARARSGVGATRSLWNFDY	5390	0.720
SW620	VH	IGHV3-23	VRKGDY	5343	0.714
SW620	VH	IGHV3-30	ATFSRYFDWVPDY	3888	0.519
SW620	VH	IGHV1-2	ARDLGVYSGSPWDY	3505	0.468
SW620	VH	IGHV3-48	VRKGDY	3487	0.466
SW620	VH	IGHV3-33	ARDSSGYLMSGHYYYYMDV	3372	0.450
SW620	VH	IGHV3-15	ARGGGRFLWPYFGMDV	3142	0.420
SW620	VH	IGHV1-2	ARARSGVGATRSLWNFDY	2498	0.334
SW620	VH	IGHV1/OR15-1	ARARSGVGATRSLWNFDY	2239	0.299
SW620	VH	IGHV3-23	AREYCSSTSCYVSADNYYYYYGMDV	2018	0.270
SW620	VH	IGHV1-2	ASPGIAAAGIDY	1863	0.249

B

Library	ChainType	V_Gene	CDR3_AA	TOT	TOT_perc
SW620	VK	IGKV1-12	QQADSFPPT	432767	36.703
SW620	VK	IGKV3D-15	QQYYETPNT	124898	10.593
SW620	VK	IGKV3-11	QQRSKWPST	119878	10.167
SW620	VK	IGKV3-20	QKYNSAPLT	40847	3.464
SW620	VK	IGKV4-1	HQTYNNEWA	30728	2.606
SW620	VK	IGKV3D-15	QKYNSAPLT	29414	2.495
SW620	VK	IGKV3-20	QQYYETPNT	23577	2.000
SW620	VK	IGKV2-30	MQGTHWPFT	20666	1.753
SW620	VK	IGKV3D-20	QQRSKWPST	17058	1.447
SW620	VK	IGKV4-1	QQYYGTPYT	13891	1.178
SW620	VK	IGKV4-1	QHYWT	13846	1.174
SW620	VK	IGKV4-1	QQYFGTPYT	13773	1.168
SW620	VK	IGKV4-1	HQYYSAPLT	13075	1.109
SW620	VK	IGKV3D-15	QQADSFPPT	12881	1.092
SW620	VK	IGKV3-11	QQADSFPPT	11822	1.003
SW620	VK	IGKV4-1	QQSSKWPVT	10781	0.914
SW620	VK	IGKV4-1	QQYYETPNT	9813	0.832
SW620	VK	IGKV3D-15	QQYNNWPPWT	9251	0.785
SW620	VK	IGKV4-1	QQADSFPPT	8565	0.726
SW620	VK	IGKV1D-16	QQYYETPNT	8121	0.689

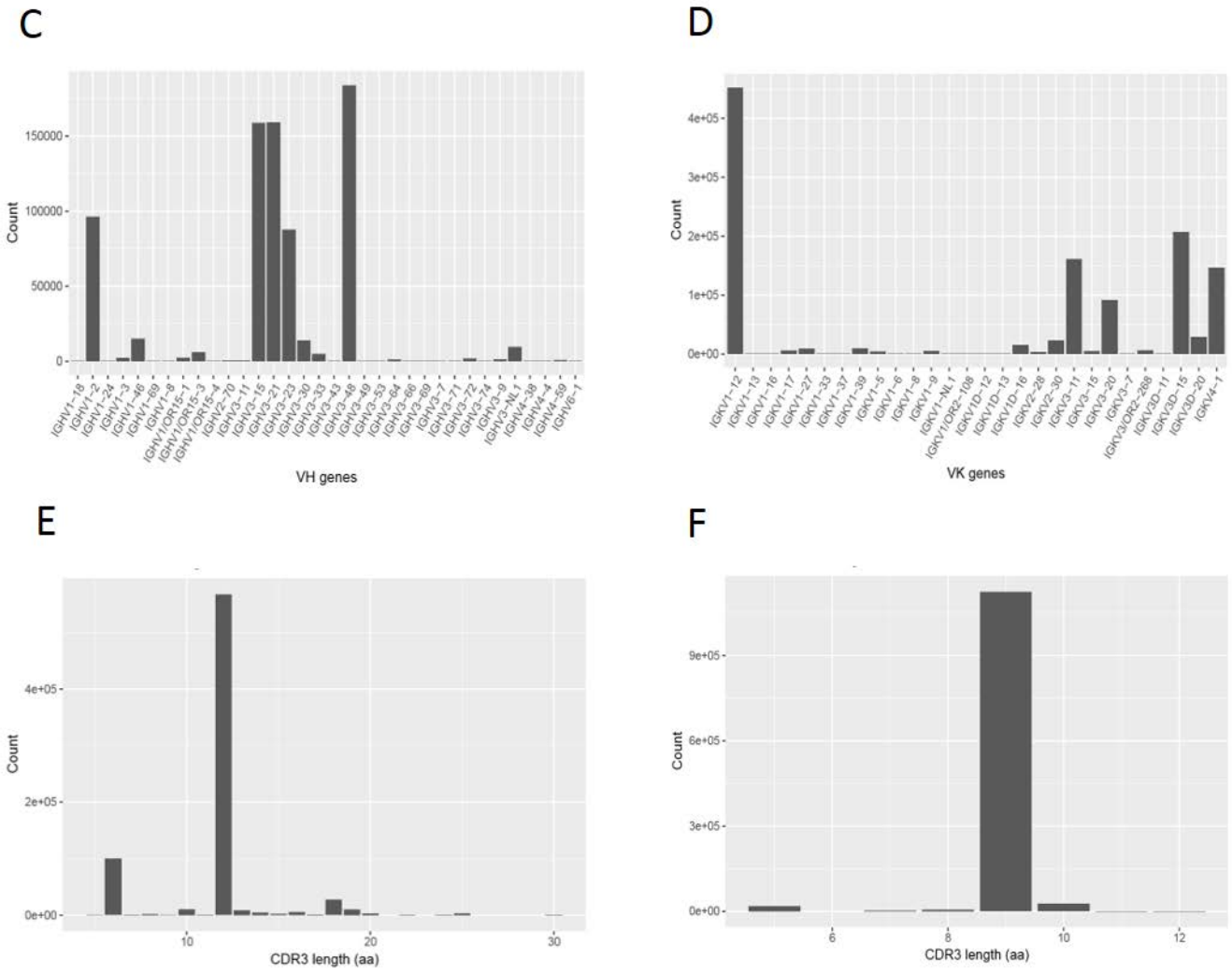

Figure 57: **NGS report summary for the biopanning pool TIL-B SW620.**

(A) Top sequences frequency distribution of VH genes and CDR3 **(B)** Top sequences frequency distribution of VK genes and CDR3 **(C)** VH genes distribution **(D)** VK genes distribution **(E)** CDR3 length distribution of VH genes **(F)** CDR3 length distribution of VK genes

8.2. Abbreviations

aa	Amino acid
ADC	Antibody-drug conjugate
ADCC	antibody-dependent cellular cytotoxicity
AHC	Anti-human Fc biosensor
AID	Activation-induced cytidine deaminase
Amp	Ampicillin
APC	Allophycocyanin
BCR	B cell-receptor
BLI	Biolayer interferometry
bp	Base pair
BSA	Bovine serum albumin
CCR4	CC chemokine receptor 4
CDC	complement-dependent cytotoxicity
cDNA	Complementary DNA
CDR	Complementary determining regions
CEA	Carcinoembryonic antigen
CEACAM1,5,6	Carcinoembryonic antigen-related cell adhesion molecule 1,5,6
CH1, CH2, CH3	Constant domain 1, 2 and 3 of the heavy chain
C-Met	Tyrosine-protein kinase Met
CTL4	Cytotoxic T-lymphocyte-associated protein 4
Da	Dalton
dH20	Distilled water
DLK1	Protein delta homolog 1
DNA	Deoxyribonucleic acid
dNTPs	Deoxyribonucleotide triphosphate
DO	Dropout
E. coli	*Escherichia coli*
EC50	Half maximal effective concentration
ECD	Extracellular domain
EGFR	Epidermal growth factor receptor
Fab	Fragment antigen-binding
FACS	fluorescence-activated cell sorting
FBS	Fetal bovine serum
Fc	Fragment crystallizable

FcγR	Fcγ receptor
FDA	Food and Drug Administration
FDCs	Follicular dendritic cells
FITC	Fluorescein
FR	framework regions
GAL1	Galactose 1 promoter
H	Hour
HC	Heavy chain
HER2	human epidermal growth factor receptor 2
His-tag	Histidine tag, usually composed of six histidines
HIV-1	Human immunodeficiency virus-1
h-	Human
Ig	Immunoglobulin
KB	Kinetics buffer
LAG3	Lymphocyte-activation gene 3
LB medium	Luria-Bertani medium
LC	Light chain
Leu	Leucine
LRP6	Low-density lipoprotein receptor-related protein 6
mAbs	Monoclonal antibodies
MCS	Multiple cloning site
MFI	Mean fluorescence intensity
MoA	Mechanisms of action
mRNA	Messenger ribonucleic acid
MSA	Multiple sequence alignment
MWCO	Molecular weight cut-off
NGS	Next-generation sequencing
NK cells	Natural killer cells
OD	Optic density
OX40L	OX40 ligand
PBMCs	Peripheral blood mononuclear cells
PBS	Phosphate buffered saline
PCR	Polymerase chain reaction
PD1	Programmed cell death protein 1
PDB	Protein Data Bank

PDGFRα	Platelet-derived growth factor receptor α
PDL-1	Programmed death-ligand 1
PE	R-phycoerythrin
RINe	RNA integrity number equivalent
RNA	Ribonucleic acid
RNKL	Receptor activator of nuclear factor kappa-B ligand
rpm	Revolutions per minute
RT	Room temperature
S. cerevisiae	Saccharomyces cerevisiae
SA	Streptavidin
scFv	Single-chain variable fragment
SD	Synthetic defined
sec	second
SLAMF7	SLAM family member 7
SN	Sentinel lymph node
TAA	Tumor-associated antigens
TCR	T-cell receptor
TIL-B	Tumor infiltrating B cells
TILs	Tumor infiltrating lymphocytes
Tim-3	T-cell immunoglobulin and mucin-domain containing-3
TLS	Tertiary lymphoid structures
Tris	Tris(hydroxymethyl)aminomethane
Trp	Tryptophan
v/v	Volume per volume
VEGF	Vascular endothelial growth factor
VH	Variable domain of the heavy chain
VL	Variable domain of the light chain
w/v	Weight per volume
YPD	Yeast extract peptone dextrose
YSD	Yeast surface display

8.3. List of figures

8.4. List of tables

8.5. *Curriculum vitae*

Name:	Ashi Sapir
Date of birth:	August 10th, 1978
Place of birth:	Rehovot, Israel
Nationality:	Israeli
Address:	Kalmn Bialer 4, Rehovot, Israel

Work experience:

04/2009 – 01/2016	Senior Technician, Merck KGaA (Inter-Lab),Yavne, Israel

Education:

01/2016 – today	Doctorate in biochemistry, Merck KGaA and Technische Universität Darmstadt, Germany, supervision Prof Dr. Harald Kolmar
04/2007 – 04/2009	Master of Science in Biochemistry and food science ,The Hebrew University of Jerusalem, Rehovot, Israel. (*Magna cum laude*) - Master thesis: "Development of an enzyme-linked immunosorbent assay and a beta-1 adrenergic receptor-based assay for monitoring the drug atenolol"
10/2003 – 10/2006	Bachelor of Science in Animal Science, The Hebrew University of Jerusalem, Rehovot, Israel
09/1990 – 09/1996	High school diploma "Aharon Katzir " Rehovot, Israel

(Ashi Sapir)

8.6. Acknowledgments

Thanks

First and foremost, I would like to thank Prof. Dr. Harald Kolmar for accepting me to his lab for the doctoral thesis, as well for his support and advice during this work. Likewise, I would like to thank Dr. Arie Zauberman, Dr. Björn Hock, Dr. Andreas Menrad and Regine Shevach who enabled and encouraged this first collaboration between Merck R&D group in Israel and TU Darmstadt to take place. Thank you all for the given opportunity to research this innovative topic.

I would like to thank Dr. Arie Zauberman for his supervision on this challenging project, his advice, support and guidance. Furthermore, I would like to thank everyone in the R&D group in Israel who helped me directly and indirectly. I would like to thank the yeast display team, Benny Cohen, Sasi Otmi, Dr. Nelia Shechter and Roni Haviv who helped and guided me through many assays in this work. Also, I would like to thank Tali Medina for her expertise in molecular biology, Dr. Shira Warszawski for her help with the NGS analysis, Doron Kalimi with the fluorescent microscopy assay and Dr. Mira Toister-Achituv for her help with tissue procurement from hospitals and proof reading of this work. Also, I would like to thank the rest of the group, Dr. Daniel Helman, Dr. Asaf Spiegel, Natalia Zabavnik, Ofer Rotemberg, Nir Berger, Dr. Sagi Barzilai, Dr. Ohad Tarcic, Dr. Sivan Kagan, Dr. Diana Varol and Dr. Bar Nathansohn-Levi who provided advice or helped with many aspects of this work.

I also would like to thank Svea Becker for her help, who traveled all the way from Germany to Israel to do her Master thesis, parts of which are included in this work.

Special thanks to my colleagues at EMD Serono: Dr. Vanita Sood, Dr. Yves Fomekong Nanfack, Dr. Julie Nardone and Dr. Thomas Clarke. All the NGS analyses in this work would not have happened without their great and willing help. I would especially like to thank Dr. Thomas Clarke, who was extremely professional throughout the whole process, from the initial analysis of the samples until the generation of the NGS report.

Many thanks to my colleagues at EMD Serono and Merck Darmstadt for their immense help to obtain great part of the proteins used in this work: Dr. Angela Lim, Dr. Xinyan Zhao, Dr. Vera Sellers and Dirk Mueller-Pompalla.

I would like to thank the Rambam Health Care Campus for the collaboration which allowed the access to the patients' samples, especially to Dr. Ronit Almog for the coordination and Dr. Yaniv Zohar for the tissue immunohistochemistry screening.

Warm thanks also to Barbara Diestelmann and Kineret Dayan for taking care of all the administration related to the dissertation, kindly and always with a smile. And to all employees of Merck in Yavne, Darmstadt and in Billerica sites who helped in different ways with this work.

Lastly, I would like to thank my Mom and my family for their great support and care, throughout the entire process of preparing the dissertation.

9. Affirmations

Ashi Sapir

Kalman Byaler 4

7666114 Rehovot, Israel

(Datum)

Erklärung

Ich erkläre hiermit, dass ich meine Dissertation selbstständig und nur mit den angegebenen Hilfsmitteln angefertigt und noch keinen Promotionsversuch unternommen habe.

(Ashi Sapir)

Ashi Sapir

Kalman Bialer 4

7666114 Rheovot,Israel

(Datum)

Erklärung der Übereinstimmung

Ich erkläre hiermit, dass die elektronishe Version der Doktorarbeit mit der schriftlischen Version übereinstimmt. Die elektronische Version liegt dem Prüfungssekretariat vor.

(Ashi Sapir)